ISSN 1007-9327 (print)
ISSN 2219-2840 (online)

World Journal of *Gastroenterology*

World J Gastroenterol 2024 January 28; 30(4): 286-423

Published by Baishideng Publishing Group Inc

World Journal of Gastroenterology

Contents

Weekly Volume 30 Number 4 January 28, 2024

LETTER TO THE EDITOR

World Journal of Gastroenterology

Weekly Volume 30 Number 4 January 28, 2024

Contents

ABOUT COVER

Editorial Board Member of *World Journal of Gastroenterology*, Giuseppe Sica, MD, PhD, Professor of Surgery, Department of Surgical Science, Tor Vergata University Hospital, Rome 00133, Italy. giuseppe.sica@ptvonline.it

AIMS AND SCOPE

The primary aim of *World Journal of Gastroenterology* (*WJG*, *World J Gastroenterol*) is to provide scholars and readers from various fields of gastroenterology and hepatology with a platform to publish high-quality basic and clinical research articles and communicate their research findings online. *WJG* mainly publishes articles reporting research results and findings obtained in the field of gastroenterology and hepatology and covering a wide range of topics including gastroenterology, hepatology, gastrointestinal endoscopy, gastrointestinal surgery, gastrointestinal oncology, and pediatric gastroenterology.

INDEXING/ABSTRACTING

The *WJG* is now abstracted and indexed in Science Citation Index Expanded (SCIE), MEDLINE, PubMed, PubMed Central, Scopus, Reference Citation Analysis, China Science and Technology Journal Database, and Superstar Journals Database. The 2023 edition of Journal Citation Reports® cites the 2022 impact factor (IF) for *WJG* as 4.3; Quartile category: Q2. The *WJG*'s CiteScore for 2021 is 8.3.

RESPONSIBLE EDITORS FOR THIS ISSUE

Production Editor: *Yu-Xi Chen*; **Production Department Director:** *Xiang Li*; **Editorial Office Director:** *Jia-Ru Fan*.

NAME OF JOURNAL
World Journal of Gastroenterology

ISSN
ISSN 1007-9327 (print) ISSN 2219-2840 (online)

LAUNCH DATE
October 1, 1995

FREQUENCY
Weekly

PUBLICATION DATE
January 28, 2024

PUBLISHING PARTNER
Shanghai Pancreatic Cancer Institute and Pancreatic Cancer Institute, Fudan University
Biliary Tract Disease Institute, Fudan University

INSTRUCTIONS TO AUTHORS
https://www.wjgnet.com/bpg/gerinfo/204

GUIDELINES FOR ETHICS DOCUMENTS
https://www.wjgnet.com/bpg/GerInfo/287

GUIDELINES FOR NON-NATIVE SPEAKERS OF ENGLISH
https://www.wjgnet.com/bpg/gerinfo/240

PUBLICATION ETHICS
https://www.wjgnet.com/bpg/GerInfo/288

PUBLICATION MISCONDUCT
https://www.wjgnet.com/bpg/gerinfo/208

POLICY OF CO-AUTHORS
https://www.wjgnet.com/bpg/GerInfo/310

ARTICLE PROCESSING CHARGE
https://www.wjgnet.com/bpg/gerinfo/242

STEPS FOR SUBMITTING MANUSCRIPTS
https://www.wjgnet.com/bpg/GerInfo/239

ONLINE SUBMISSION
https://www.f6publishing.com

PUBLISHING PARTNER's OFFICIAL WEBSITE
https://www.shca.org.cn
https://www.zs-hospital.sh.cn

World Journal of Gastroenterology

Submit a Manuscript: https://www.f6publishing.com

World J Gastroenterol 2024 January 28; 30(4): 286-289

DOI: 10.3748/wjg.v30.i4.286

ISSN 1007-9327 (print) ISSN 2219-2840 (online)

EDITORIAL

Revolutionizing gastric cancer treatment: The potential of immunotherapy

Grigorios Christodoulidis, Konstantinos Eleftherios Koumarelas, Marina Nektaria Kouliou

Specialty type: Gastroenterology and hepatology

Provenance and peer review: Invited article; Externally peer reviewed.

Peer-review model: Single blind

Peer-review report's scientific quality classification

Grade A (Excellent): A
Grade B (Very good): B, B
Grade C (Good): 0
Grade D (Fair): 0
Grade E (Poor): 0

P-Reviewer: Chatterjee B, India; Mu YP, China; Sun GH, China

Received: November 5, 2023
Peer-review started: November 5, 2023
First decision: December 6, 2023
Revised: December 19, 2023
Accepted: January 15, 2024
Article in press: January 15, 2024
Published online: January 28, 2024

Grigorios Christodoulidis, Konstantinos Eleftherios Koumarelas, Marina Nektaria Kouliou, Department of General Surgery, University Hospital of Larissa, Larissa 41110, Greece

Corresponding author: Grigorios Christodoulidis, MD, PhD, Surgeon, Department of General Surgery, University Hospital of Larissa, Mezourlo, Larissa 41110, Greece. gregsurg@yahoo.gr

Abstract

Gastric cancer, a prevalent malignancy worldwide, ranks sixth in terms of frequency and third in fatality, causing over a million new cases and 769000 annual deaths. Predominant in Eastern Europe and Eastern Asia, risk factors include family medical history, dietary habits, tobacco use, *Helicobacter pylori*, and Epstein-Barr virus infections. Unfortunately, gastric cancer is often diagnosed at an advanced stage, leading to a grim prognosis, with a 5-year overall survival rate below 5%. Surgical intervention, particularly with D2 Lymphadenectomy, is the mainstay for early-stage cases but offers limited success. For advanced cases, the National Comprehensive Cancer Network recommends chemotherapy, radiation, and targeted therapy. Emerging immunotherapy presents promise, especially for unresectable or metastatic cases, with strategies like immune checkpoint inhibitors, tumor vaccines, adoptive immunotherapy, and nonspecific immunomodulators. In this Editorial, with regards to the article "Advances and key focus areas in gastric cancer immunotherapy: A comprehensive scientometric and clinical trial review", we address the advances in the field of immunotherapy in gastric cancer and its future prospects.

Key Words: Immunotherapy; Adaptive immunotherapy; Tumor vaccines; Chimeric antigen receptor therapy; Tumor-infiltrating lymphocytes therapy; Natural killer therapy; Cytokine-induced killer therapy; Engineered T cell receptor therapy; Immune checkpoint inhibitors

Core Tip: Immunotherapy, especially immune checkpoint inhibitors (ICIs), has revolutionized cancer treatment by targeting programmed cell death 1, programmed cell death ligand 1 (PD-L1), and cytotoxic T lymphocyte-associated antigen-4 (CTLA-4), enhancing the immune response. While PD-L1 and CTLA-4's prognostic significance in gastric cancer remains debatable, ICIs like nivolumab and pembrolizumab show promise. Tailored approaches, such as zolbetuximab for CLDN 18.2 or trastuzumab, pembrolizumab, and chemotherapy for human epidermal growth factor receptor 2-positive cases, demonstrate effectiveness. Tumor vaccines and dendritic cell-based vaccines hold potential in personalized therapy. Adoptive Immunotherapy utilizes tumor-infiltrating lymphocytes therapy, engineered T cell receptor therapy, Chimeric antigen receptor T-cell therapy, natural killer cell therapy, and cytokine-induced killer cell therapy, each with distinct benefits and challenges. The immunotherapy landscape continues to evolve, offering hope for improved cancer management.

Citation: Christodoulidis G, Koumarelas KE, Kouliou MN. Revolutionizing gastric cancer treatment: The potential of immunotherapy. *World J Gastroenterol* 2024; 30(4): 286-289
URL: https://www.wjgnet.com/1007-9327/full/v30/i4/286.htm
DOI: https://dx.doi.org/10.3748/wjg.v30.i4.286

INTRODUCTION

Gastric cancer ranks among the most prevalent malignancies worldwide, occupying the sixth position in terms of frequency and the third spot in terms of fatality, accounting for over one million new cases and 769000 annual deaths[1-3]. It is primarily observed in Eastern Europe and Eastern Asia. Noteworthy risk factors include family medical history, dietary practices, tobacco use, *Helicobacter pylori* and Epstein-Barr virus (EBV) infections. Regrettably, the diagnosis of gastric cancer is often delayed, with more than half of patients being diagnosed at the stage of advanced metastatic cancer, leading to a significantly unfavorable prognosis. The 5-year overall survival (OS) rate in such cases remains below 5%, and the life expectancy is limited to merely 8 months[1,2].

Up to this point, surgical intervention remains the sole definitive treatment for early-stage gastric cancer when coupled with a D2 Lymphadenectomy. Nevertheless, even with this approach, the 5-year OS rate does not exceed 50%[4]. For advanced gastric cancer, the recommended management according to the National Comprehensive Cancer Network (NCCN) involves the use of double or triple platinum and fluoropyrimidine-based chemotherapy, combined with radiation therapy and targeted therapy[2].

In recent years, emerging immunotherapy has exhibited promising outcomes, particularly for patients with unresectable, locally advanced, recurrent, or metastatic gastric cancer. There are four principal strategies in immunotherapy: Immune checkpoint inhibitors (ICIs), tumor vaccines, adoptive immunotherapy (ACT), and nonspecific immunomodulators[1,5]. Targeted therapies function by inhibiting cell growth through the blockade of specific molecular pathways and proteins, while immunotherapy stimulates the patient's immune response against cancerous cells. However, owing to the diverse molecular subtypes of gastric cancer and the intricate nature of the tumor microenvironment, immunotherapy proves effective only within specific patient subgroups[1,5]. For human epidermal growth factor receptor 2 (HER2)-positive gastric cancer, tailored regimens encompassing Trastuzumab, Pembrolizumab, and XELOX/PF are employed, while for HER2-negative cases, first-line chemotherapy is combined with nivolumab, cindilimab, or tislelizumab[1,2].

IMMUNOTHERAPEUTIC STRATEGIES

The most commonly employed form of immunotherapy among the various alternatives is ICIs. The introduction of inhibitors targeting programmed cell death 1 (PD-1) and programmed cell death ligand 1 (PD-L1) has profoundly transformed the landscape of cancer management. The interaction between PD-L1 and PD-1 induces T-cell dysfunction, exhaustion, and an elevation in their tolerance levels[1,5]. Consequently, the inhibition of PD-1 and PD-L1, as well as cytotoxic T lymphocyte-associated antigen-4 (CTLA-4), serves to augment the immune response and activate T-cells. Despite the application of immunotherapy, there exist conflicting findings concerning the prognostic implications of PD-L1 or CTLA-4 positivity in gastric cancer[1,4]. ICIs are currently in clinical use and are undergoing extensive research due to their demonstrated lower toxicity, improved tolerability, and potential for yielding superior outcomes when compared to conventional chemotherapy. Nowadays the effectiveness of a PD-L1 inhibitor can be foreseen. The assessment of MSI status, PD-L1 and PD-1 expression levels as well as the EBV status gives insight for the success rate of ICIs utilization. EBV positive tumors, MSI-H tumors, as well as tumors with increased expression of PD-L1 or PD-1 in tumor cells and infiltrating immune cells have a significant better response to ICIs[6]. In a meta-analysis conducted by Liu *et al*[2], various ICIs were evaluated for their efficacy and safety. Nivolumab, pembrolizumab, rilotumumab, Andecaliximab (ADX), and bevacizumab were associated with superior progression-free survival (PFS), while pembrolizumab and nivolumab exhibited improved OS when contrasted with traditional chemotherapy[2]. It is worth noting that these results did not achieve statistical significance. In contrast, nimotuzumab and ipataserib demonstrated less favorable outcomes in terms of both PFS and OS in comparison to chemotherapy. Bavacizumab and ADX were found to be safer and associated with more manageable complications than chemotherapy. Through a subgroup analysis focusing on different types of gastric

cancers, Liu *et al*[2] proposed several regimens deemed most effective:

For patients with CLDN 18.2, the combination of zolbetuximab with chemotherapy led to increased OS and PFS. In HER2-negative cases, the most effective regimen was found to be nivolumab in conjunction with chemotherapy, as suggested by the findings of the Checkmate-649 study. For individuals with HER2-positive gastric cancer, especially those who are untreated, unresectable, or have metastatic disease, the simultaneous use of trastuzumab, pembrolizumab, and chemotherapy emerged as the most effective approach, supported by the NCCN guidelines. In cases of MET-1 positive gastric cancer, no immunotherapy regimen was found to confer significant benefits. Lastly, as a second-line treatment for advanced gastric cancer, the utilization of vamucirumab and paclitaxel was proposed[2].

An additional category of immunotherapy involves the utilization of tumor vaccines. There are 4 types of tumor vaccines: cell-based, protein- or peptide-based, or gene-based (DNA/RNA), predominantly relying on dendritic cells (DCs) as their primary adjuvants. DCs are acknowledged as antigen-presenting cells (APCs) that, through the processing and presentation of antigens to T-cells, evoke and regulate the adaptive immune response in patients. Consequently, the employment of DCs as an immunotherapeutic measure holds the potential to activate and modulate an anti-tumor immune response[1,7]. Notably, DCs vaccines are designed to exclusively target tumor neoantigens, thereby instigating a personalized approach that has demonstrated the capability to induce complete tumor regression, as evidenced in clinical trials, rendering them a prominent subject of contemporary research[1,8]. DCs fused with gastric cancer cells or carrying peptides and RNAs may stimulate effectively the patients immune response. Right now 20 out of 23 trials on tumor vaccines, concern DCs vaccines. M-RNA vaccines are a great alternative, with increased efficacy and a rapid immune response. These vaccines when combined with chemotherapies based on cisplatin and 5-fluorouracil on clinical trials give encouraging results[5]. Nevertheless, the domain of gastric cancer presents a formidable challenge due to increased immunogenicity, antigenic shifts, and immune evasion when attempting to target tumor antigens. The immune system's evasion is principally attributed to the fact that these neoantigens are typically present in other tissues, consequently eluding recognition by APCs[1,7]. According to a bibliometric analysis conducted by Li *et al*[1], there have been 23 clinical trials aimed at elucidating the efficacy of tumor vaccines[1].

One of the most pivotal forms of immunotherapy is ACT. The fundamental concept underlying this technique is to transfer lymphocytes and other immune cells with the purpose of fortifying the anti-tumor response, generating effector T-cells that specifically target tumor antigens, and enhancing the function of regulatory T-cells, ultimately leading to improved outcomes and prognosis[1]. Physicians have at their disposal five distinct types of adaptive immunotherapy:

Tumor-infiltrating lymphocytes (TIL) therapy, which harnesses immune cells from within the tumor, enabling improved recognition of tumor antigens, heightened specificity, and reduced toxicity. The assessment of TIL serves as a valuable biomarker, and the coexistence of PD-1-positive and TIL-positive entities in gastric cancer correlates with superior outcomes in terms of PFS and OS[1,5].

Engineered T cell receptor (TCR) therapy, which operates by presenting antigens with specific Major Histocompatibility Complex (MHC) molecules, resulting in effective tumor regression. However, the use of high-avidity TCRs may give rise to significant toxicity[1,5].

Chimeric antigen receptor T-cell (CAR-T) therapy, sharing a similar principle, employs genetically engineered T cells capable of recognizing tumor antigens independently of MHC molecules. The fourth generation of CAR-T therapy circumvents immunosuppression and mitigates toxicity. Common targets include mesothelin, ANTXR1, MUC3A, and CLDN 18.2, with the latter being a subject of ongoing clinical trials[1,5,9].

Natural killer (NK) cell therapy, the fourth category of immunotherapy, leverages the potential of increased numbers of functional NK cells to enhance patient outcomes. In patients with gastric cancer, NK cells often exhibit an elevated expression of PD-1, exacerbating the prognosis. In animal models, the simultaneous use of interleukin-2 activated NK cells with anti-PD-1 treatment has been shown to impede tumor growth and facilitate immune cell infiltration into the tumor. However, NK cell therapy necessitates substantial quantities of effective NK cells, limiting its applicability[1,5,10].

Lastly, cytokine-induced killer cells represent a viable alternative, combining the cytotoxic and anti-tumor capabilities of CD3+CD56- T cell and CD3+CD56+ T-lymphocytes while operating without the constraints of MHC molecules[1,5].

CONCLUSION

Since the development of the ICIs, the field of immunotherapy is advancing with significant rates. Many novel approaches are under extended research and in clinical trials in order to assess the efficacy of each therapy and the toxicity deriving from their use. Nowadays the use of immunotherapy tends to integrate more and more in order to achieve precision medicine and the detection of novel biomarkers will assist to a better tailored and personalized use of these therapies.

FOOTNOTES

Author contributions: Christodoulidis G, Koumarelas KE and Kouliou MN contributed to this paper; Christodoulidis G designed the overall concept and outline of the manuscript; Christodoulidis G, Koumarelas KE and Kouliou MN contributed to the discussion and design of the manuscript; Christodoulidis G, Koumarelas KE and Kouliou MN contributed to the writing, editing the manuscript, and review of literature.

Conflict-of-interest statement: All the authors report no relevant conflicts of interest for this article.

Country/Territory of origin: Greece

ORCID number: Grigorios Christodoulidis 0000-0003-3413-0666; Konstantinos Eleftherios Koumarelas 0000-0002-5614-4770; Marina Nektaria Kouliou 0000-0002-2055-2297.

S-Editor: Li L
L-Editor: A
P-Editor: Li L

REFERENCES

1 **Li YN**, Xie B, Zhang Y, He MH, Xing Y, Mu DM, Wang H, Guo R. Advances and key focus areas in gastric cancer immunotherapy: A comprehensive scientometric and clinical trial review (1999-2023). *World J Gastroenterol* 2023; **29**: 5593-5617 [PMID: 37970478 DOI: 10.3748/wjg.v29.i40.5593]

2 **Liu S**, Wong HY, Xie L, Kim Y, Shu D, Zheng B, Liu N, Xing C, Chen X, Dong Q. Comparative efficacy and tolerability of targeted and immunotherapy combined with chemotherapy as first-line treatment for advanced gastric cancer: a Bayesian network meta-analysis. *Sci Rep* 2022; **12**: 22024 [PMID: 36539429 DOI: 10.1038/s41598-022-24426-9]

3 **Shah MA**, Kennedy EB, Alarcon-Rozas AE, Alcindor T, Bartley AN, Malowany AB, Bhadkamkar NA, Deighton DC, Janjigian Y, Karippot A, Khan U, King DA, Klute K, Lacy J, Lee JJ, Mehta R, Mukherjee S, Nagarajan A, Park H, Saeed A, Semrad TJ, Shitara K, Smyth E, Uboha NV, Vincelli M, Wainberg Z, Rajdev L. Immunotherapy and Targeted Therapy for Advanced Gastroesophageal Cancer: ASCO Guideline. *J Clin Oncol* 2023; **41**: 1470-1491 [PMID: 36603169 DOI: 10.1200/JCO.22.02331]

4 **Xu H**, Li T, Shao G, Wang W, He Z, Xu J, Qian Y, Liu H, Ge H, Wang L, Zhang D, Yang L, Li F, Xu Z. Evaluation of neoadjuvant immunotherapy plus chemotherapy in Chinese surgically resectable gastric cancer: a pilot study by meta-analysis. *Front Immunol* 2023; **14**: 1193614 [PMID: 37426646 DOI: 10.3389/fimmu.2023.1193614]

5 **Jin X**, Liu Z, Yang D, Yin K, Chang X. Recent Progress and Future Perspectives of Immunotherapy in Advanced Gastric Cancer. *Front Immunol* 2022; **13**: 948647 [PMID: 35844558 DOI: 10.3389/fimmu.2022.948647]

6 **Chang X**, Ge X, Zhang Y, Xue X. The current management and biomarkers of immunotherapy in advanced gastric cancer. *Medicine (Baltimore)* 2022; **101**: e29304 [PMID: 35623069 DOI: 10.1097/MD.0000000000029304]

7 **Guo Z**, Yuan Y, Chen C, Lin J, Ma Q, Liu G, Gao Y, Huang Y, Chen L, Chen LZ, Huang YF, Wang H, Li B, Chen Y, Zhang X. Durable complete response to neoantigen-loaded dendritic-cell vaccine following anti-PD-1 therapy in metastatic gastric cancer. *NPJ Precis Oncol* 2022; **6**: 34 [PMID: 35661819 DOI: 10.1038/s41698-022-00279-3]

8 **Faghfuri E**, Shadbad MA, Faghfouri AH, Soozangar N. Cellular immunotherapy in gastric cancer: adoptive cell therapy and dendritic cell-based vaccination. *Immunotherapy* 2022; **14**: 475-488 [PMID: 35232264 DOI: 10.2217/imt-2021-0285]

9 **Qi C**, Gong J, Li J, Liu D, Qin Y, Ge S, Zhang M, Peng Z, Zhou J, Cao Y, Zhang X, Lu Z, Lu M, Yuan J, Wang Z, Wang Y, Peng X, Gao H, Liu Z, Wang H, Yuan D, Xiao J, Ma H, Wang W, Li Z, Shen L. Claudin18.2-specific CAR T cells in gastrointestinal cancers: phase 1 trial interim results. *Nat Med* 2022; **28**: 1189-1198 [PMID: 35534566 DOI: 10.1038/s41591-022-01800-8]

10 **Ishikawa T**, Okayama T, Sakamoto N, Ideno M, Oka K, Enoki T, Mineno J, Yoshida N, Katada K, Kamada K, Uchiyama K, Handa O, Takagi T, Konishi H, Kokura S, Uno K, Naito Y, Itoh Y. Phase I clinical trial of adoptive transfer of expanded natural killer cells in combination with IgG1 antibody in patients with gastric or colorectal cancer. *Int J Cancer* 2018; **142**: 2599-2609 [PMID: 29388200 DOI: 10.1002/ijc.31285]

World Journal of Gastroenterology

Submit a Manuscript: https://www.f6publishing.com

World J Gastroenterol 2024 January 28; 30(4): 290-307

DOI: 10.3748/wjg.v30.i4.290

ISSN 1007-9327 (print) ISSN 2219-2840 (online)

REVIEW

Portal hypertension in patients with nonalcoholic fatty liver disease: Current knowledge and challenges

Anita Madir, Ivica Grgurevic, Emmanuel A Tsochatzis, Massimo Pinzani

Specialty type: Gastroenterology and Hepatology

Provenance and peer review: Unsolicited article; Externally peer reviewed.

Peer-review model: Single blind

Peer-review report's scientific quality classification

Grade A (Excellent): 0
Grade B (Very good): B
Grade C (Good): C
Grade D (Fair): 0
Grade E (Poor): 0

P-Reviewer: He F, China; Ji G, China

Received: October 5, 2023
Peer-review started: October 5, 2023
First decision: December 6, 2023
Revised: December 19, 2023
Accepted: January 8, 2024
Article in press: January 8, 2024
Published online: January 28, 2024

Anita Madir, Ivica Grgurevic, Department of Gastroenterology, Hepatology and Clinical Nutrition, University Hospital Dubrava, Zagreb 10000, Croatia

Ivica Grgurevic, School of Medicine, University of Zagreb, Zagreb 10000, Croatia

Ivica Grgurevic, Faculty of Pharmacy and Biochemistry, University of Zagreb, Zagreb 10000, Croatia

Emmanuel A Tsochatzis, Massimo Pinzani, UCL Institute for Liver and Digestive Health, Royal Free Hospital and University College London, London NW3 2PF, United Kingdom

Corresponding author: Ivica Grgurevic, DSc, FEBG, FRCP, MD, Professor, Department of Gastroenterology, Hepatology and Clinical Nutrition, University Hospital Dubrava, Gojko Susak Avenue 6, Zagreb 10000, Croatia. ivica.grgurevic@mef.hr

Abstract

Portal hypertension (PH) has traditionally been observed as a consequence of significant fibrosis and cirrhosis in advanced non-alcoholic fatty liver disease (NAFLD). However, recent studies have provided evidence that PH may develop in earlier stages of NAFLD, suggesting that there are additional pathogenetic mechanisms at work in addition to liver fibrosis. The early development of PH in NAFLD is associated with hepatocellular lipid accumulation and ballooning, leading to the compression of liver sinusoids. External compression and intra-luminal obstacles cause mechanical forces such as strain, shear stress and elevated hydrostatic pressure that in turn activate mechanotransduction pathways, resulting in endothelial dysfunction and the development of fibrosis. The spatial distribution of histological and functional changes in the periportal and perisinusoidal areas of the liver lobule are considered responsible for the pre-sinusoidal component of PH in patients with NAFLD. Thus, current diagnostic methods such as hepatic venous pressure gradient (HVPG) measurement tend to underestimate portal pressure (PP) in NAFLD patients, who might decompensate below the HVPG threshold of 10 mmHg, which is traditionally considered the most relevant indicator of clinically significant portal hypertension (CSPH). This creates further challenges in finding a reliable diagnostic method to stratify the prognostic risk in this population of patients. In theory, the measurement of the portal pressure gradient guided by endoscopic ultrasound might overcome the limitations of HVPG measurement by avoiding the influence of the pre-sinusoidal component, but more investigations are needed to test its clinical utility for this indication. Liver and spleen stiffness measurement in combination with platelet

count is currently the best-validated non-invasive approach for diagnosing CSPH and varices needing treatment. Lifestyle change remains the cornerstone of the treatment of PH in NAFLD, together with correcting the components of metabolic syndrome, using nonselective beta blockers, whereas emerging candidate drugs require more robust confirmation from clinical trials.

Key Words: Non-alcoholic fatty liver disease; Portal hypertension; Mechanotransduction; Endothelial dysfunction; Hepatic venous pressure gradient

Core Tip: Portal hypertension (PH) occurs in patients with cirrhosis, but in non-alcoholic fatty liver disease (NAFLD) it is sometimes observed in non-cirrhotic stages due to perisinusoidal fibrosis and damage to liver microcirculation. The severity of PH tends to be underestimated by hepatic venous pressure gradient (HVPG) measurement in NAFLD, potentially due to the presence of pre-sinusoidal component, and some patients decompensate at HVPG < 10 mmHg. Liver elastography needs further validation in obese patients as it might overestimate the severity of PH. While candidate drugs for PH are currently in development, lifestyle changes and modulation of metabolic derangements remain the mainstay of treatment.

Citation: Madir A, Grgurevic I, Tsochatzis EA, Pinzani M. Portal hypertension in patients with nonalcoholic fatty liver disease: Current knowledge and challenges. *World J Gastroenterol* 2024; 30(4): 290-307
URL: https://www.wjgnet.com/1007-9327/full/v30/i4/290.htm
DOI: https://dx.doi.org/10.3748/wjg.v30.i4.290

INTRODUCTION

Portal hypertension (PH) plays a crucial prognostic role in chronic liver disease (CLD), including non-alcoholic fatty liver disease (NAFLD). PH develops during the evolution of CLD as a result of the increased accumulation of extracellular matrix in the liver, leading to elevated resistance to the portal blood flow, further aggravated by the distortion of the liver architecture and vascular network, which is caused by the formation of regenerative nodules. In addition to this static component, a reversible element of the heightened resistance derives from the contraction of hepatic stellate cells (HSCs) around the liver sinusoids, which is activated by the underlying pathogenetic process. This results in the development of PH at the sinusoidal level, which is typical for viral hepatitis and alcohol-related liver disease (ALD).

Current knowledge of the pathophysiology, diagnosis and treatment of PH relies predominantly on the data accumulated from the studies conducted regarding these two aetiologies of CLD. Considering the changing aetiological landscape of CLD, with NAFLD becoming the leading cause of liver-related morbidity, it is important to understand all aspects pertaining to the PH arising in the context of NAFLD. Based on recent reports, the development, diagnosis and prognosis of PH in NAFLD might not completely fit into the existing paradigms and rules established with chronic viral hepatitis and ALD. This article aims to describe the present understanding of the topic, as well as to highlight the unmet needs and controversial issues in the diagnosis and management of PH in patients with NAFLD.

PATHOPHYSIOLOGICAL BACKGROUND

General aspects of the development of portal hypertension in chronic liver diseases

Portal hypertension is defined as a clinical syndrome caused by elevated blood pressure in the portal venous system. Patients who suffer from advanced chronic liver disease (ACLD), especially cirrhosis, have an increased risk of developing PH[1,2]. Liver cirrhosis arises as the result of prolonged liver damage caused by various aetiological agents that finally lead to the replacement of the healthy parenchyma with fibrotic tissue, the formation of regenerative nodules and the distortion of the microarchitecture, including the liver vascular network[3,4]. In the portal tracts located at the periphery of the hepatic lobule (zone 1), terminal branches of both the hepatic artery and portal vein join into liver sinusoids and form a complex capillary network that drains into the centrilobular area of the central vein outflow (zone 3)[5,6]. Arteriolar inflow needs to be efficiently controlled to prevent damage and shear stress to liver sinusoids because of the very high arterial hydrostatic pressure, which is up to 40 times higher relative to that present in terminal branches of the portal vein[6-8]. Vasoregulatory changes in both intrahepatic and systemic circulation have an important role in the development and further aggravation of PH in individuals with cirrhosis. Hepatic causes of PH are essentially classified into three types according to the main location of the blood flow disturbance in the hepatic circulation: pre-sinusoidal, sinusoidal and post-sinusoidal[9,10]. Sinusoidal PH is the most common type, and it typically occurs in cirrhosis patients [11]. The principal causes of intrahepatic PH are depicted in Table 1.

Table 1 Principal intrahepatic causes of portal hypertension (adapted based on references[1,9])

Pre-sinusoidal	Sinusoidal	Post-sinusoidal
Developmental abnormalities:	Fibrosis in the space of Disse:	Granulomatous phlebitis:
Adult polycystic liver disease	Metabolic cause: non-alcohol-associated fatty liver disease, Zellweger syndrome	Mycobacterium avium infection
Congenital hepatic fibrosis	Inflammatory cause: schistosomiasis, viral hepatitis B and C, chronic Q fever, cytomegalovirus	Mycobacterium intracellular infection
Arteriovenous fistulas	Induced by drugs or toxins: amiodarone, methotrexate, alcohol, vinyl chloride, copper	Sarcoidosis
Porto-sinusoidal vascular disease:	Early alcohol-associated liver disease (defenestration)	Primary vascular malignancies:
Idiopathic non-cirrhotic portal hypertension		Epithelioid haemangioendothelioma
		Angiosarcoma
Granulomatous liver disease:	Microvesicular steatosis hypertrophied hepatocytes	Phlebosclerosis of hepatic veins:
Schistosomiasis (bilharzia)		Alcohol-associated liver disease
Mineral oil granuloma		Chronic radiation injury
Sarcoidosis		Hypervitaminosis A
Biliary diseases:	Infiltrative diseases:	Lipogranulomas:
Autoimmune cholangiopathy	Idiopathic myeloid metaplasia	Mineral oil granuloma
Primary sclerosing cholangitis	Gaucher disease	
Toxic biliary injury	Mastocytosis	
Biliary cholangitis		
Neoplastic occlusion of the intrahepatic portal vein	Amyloid or light-chain deposition in the space of Disse	Sinusoidal obstruction syndrome
	Acute hepatic injury	Budd-Chiari syndrome

The impact of lipid accumulation on PH development in early NAFLD

Hepatocyte ballooning occurs early in NAFLD pathogenesis because of the accumulation of cholesterol and fatty acids within the cytoplasm of hepatocytes[5,12]. Lipid-laden hepatocytes cause external sinusoidal compression, leading to increased intrahepatic vascular resistance (IHVR) and shear stress[5,13]. These sinusoids, which are deformed, tortuous and up to 50% narrower, are mostly located in the periportal region of hepatic lobules and impose a heightened resistance to portal blood flow before it enters the sinusoids[14,15]. Another structural change in NAFLD contributing to IHVR development is the formation of lipogranulomas commonly located near terminal hepatic venules, which are dispersed in portal tracts and the hepatic acinus[16,17]. Steatonecrosis, an event caused by the disintegration of hepatocytes due to excessive lipid accumulation[14,18], results in the liberation of lipid droplets which travel through the Disse space and the endothelium and fill the sinusoid as a sinusoidal lipid embolus[14].

The impact of the activation of neutrophils on PH development

The stretching of liver sinusoidal endothelial cells (LSECs) caused by the enlargement of hepatocytes activates Notch-dependent neutrophil chemotaxis[19]. Together with neutrophil chemotactic chemokines, which are produced by hepatocytes and HSCs, these signals have a crucial role in the recruitment of leukocytes and formation of neutrophil extracellular traps (NETs)[19], intraluminal web-like structures composed primarily of deoxyribonucleic acid (DNA)-histone complexes originating from neutrophils, which bind pathogens[20] and impose a barrier that leads to increased fluid shear stress at the level of sinusoids[21]. Thus, lipid accumulation in hepatocytes, with the consequent deformation of sinusoids, combined with the formation of lipogranulomas and NETs, as well as lipid emboli, contributes to sinusoid hypoperfusion[13,22,23], microvascular thrombosis[24] and the development of PH, with heightened presinusoidal resistance in NAFLD[13,25].

The principal mechanisms of portal hypertension development in NAFLD are illustrated in Figure 1.

Animal models supporting the role of liver steatosis in the development of PH

The association between increased portal vein pressure (PVP) and steatosis has been observed in numerous animal experimental models. One of the oldest experiments confirming this connection was carried out almost 50 years ago. Donryu rats were fed a choline-deficient diet for eight to 38 weeks. Two thirds of the rats died during the feeding period and 27 developed a fatty liver (n = 7), some with fibrosis (n = 8) and others with cirrhosis (n = 12)[5,15]. The results showed a decrease in portal blood flow, an increase in PVP and a narrowing of sinusoids without visible abnormalities in

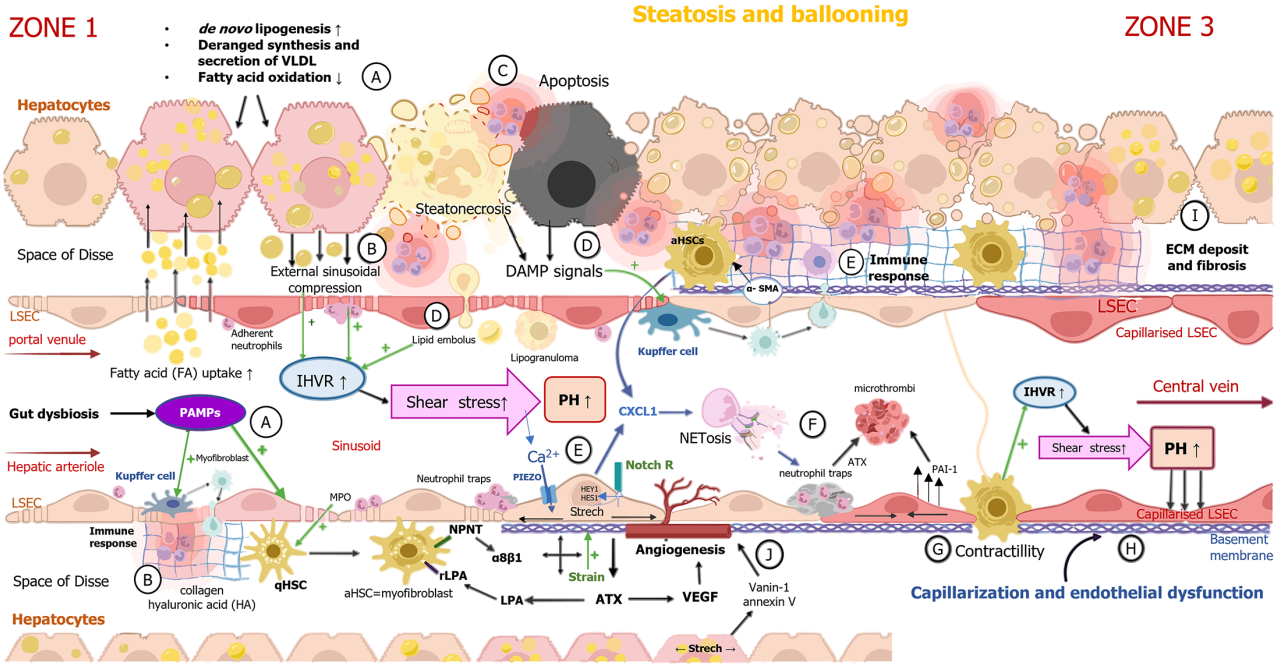

DOI: 10.3748/wjg.v30.i4.290

Figure 1 Development of portal hypertension in non-alcoholic fatty liver disease. A: Ballooning of hepatocytes are caused by excessive lipid uptake. Pathogen-associated molecular patterns (PAMPs), along with other products of intestinal dysbiosis, arrive at the liver *via* the portal blood flow and act on liver sinusoidal endothelial cells (LSECs) and Kupffer cells (KCs) from the luminal side of the sinusoid; B: Excessive lipid accumulation in hepatocytes and PAMPs trigger inflammation by cytokine secretion and immune cell infiltration; C: Immune cell infiltration leads to steatonecrosis, apoptosis and hepatic stellate cells (HSCs) activation; D: Hepatocytes dying by steatonecrosis and apoptosis release damage-associated molecular pattern molecules, causing the activation of KCs and subsequently HSCs. The destruction of lipid-laden hepatocytes incites lipid embolus liberation in the sinusoidal lumen. Lipid droplets participate in lipogranuloma formation, which interferes with sinusoidal blood flow and results in elevated intrahepatic vascular resistance (IHVR); E: Activated HSCs transdifferentiate to proliferative, contractile and collagen-producing myofibroblasts which secrete vascular endothelial growth factor (VEGF) and inflammatory chemokines such as neutrophil chemotactic chemokines and synthesize α-smooth muscle actin. Notch-dependent neutrophil chemotaxis is also activated by the stretching of LSECs caused by the enlargement of hepatocytes and the liver; F: Stretch-activated LSECs promote the creation of neutrophil extracellular traps (NETs), web-like structures composed primarily of DNA-histone complexes originating from neutrophils. NETs contribute to the creation of microthrombi; G: The activation of HSCs is a key event mediating the elevation of IHVR by contracting around the sinusoid. IHVR is also elevated by extrasinusoidal compression caused by swollen steatotic hepatocytes and increased shear stress produced by intraluminal obstacles such as NETs; H: Sinusoid capillarization and the endothelial dysfunction of LSECs are important events that promote the activation of HSCs and KCs, initiating liver fibrosis and inflammation promotion; I: Myofibroblasts and mechanical forces lead to collagen and hyaluronic acid deposition in the space of Disse, causing an excessive increase in extracellular matrix (ECM) stiffness. The cross-linking of ECM proteins and collagen leads to the formation of perisinusoidal fibrosis; J: Angiogenesis occurs as liver fibrosis progresses. Stretched lipid-laden hepatocytes, HSCs, portal myofibroblasts and macrophages stimulate angiogenesis by producing a greater amount of VEGF and other similar mediators as a response to shear stress, hypoxia and inflammation. qHSC: Quiescent hepatic stellate cell; aHSCs: Activated hepatic stellate cells; DAMPs: Damage-associated molecular pattern molecules; αSMA: α-smooth muscle actin; FA: Fatty acid; HA: Hyaluronic acid; CXCL: Chemokine (C-X-C motif) ligand 1; α-SMA: Alpha-smooth muscle actin; MPO: Myeloperoxidase; PAI-1: Plasminogen activator inhibitor-1; ATX: Autotaxin; LPA: Lysophosphatidic acid.

the pre- and post-sinusoidal vessels. All these findings were detected in rats with steatosis without fibrosis, suggesting that steatosis alone is sufficient for the formation of PH[5,10]. In another experimental NAFLD model, obese male Zucker rats with high-grade hepatic steatosis without cirrhosis were studied in comparison with lean rats aged 25 to 30 weeks (n = 7 *vs* 7). Compared to the control animals, an increment in IHVR and reductions of 35% to 38% in the total hepatic blood flow and portal venous flow were observed[5,26]. Francque *et al*[27] conducted a similar study on male Wistar rats given a methionine-choline-deficient (MCD) diet (n = 30) while another group was fed a control diet (n = 30) for four weeks. The two groups were compared through *in vivo* haemodynamic measurements and in situ perfusion experiments, as well as vascular corrosion and liver tissue and serum analysis. In the MCD diet group, the histopathology showed severe steatosis without evidence of inflammation or fibrosis, and the portal pressure gradient was significantly elevated, indicating an increased intrahepatic resistance, while vascular corrosion casts demonstrated a replacement of the regular sinusoidal anatomy by a sinusoidal wall with a disorganized pattern, in addition to vascular extensions and multiple interconnections. An increase in the expression of vasoconstrictor molecules and enzymes [thromboxane synthase and endothelin-1 (ET-1)] was also registered[27].

The impact of endothelial dysfunction on PH development in NAFLD

Endothelial dysfunction is defined as the loss of various key functions of the endothelium[28,29], chiefly characterized by a lower response of LSECs to the endothelium-dependent vasodilator acetylcholine[30] and a decrease in the production and release of endothelium-driven vasodilatory factors such as nitric oxide (NO)[31,32]. In a normal liver, hepatocytes release low levels of vascular endothelial growth factor (VEGF), which helps LSECs to generate NO through a cytosolic

calcium increase, leading to calmodulin binding and the activation of endothelial nitric oxide synthase (eNOS)[33,34]. To maintain physiological pressure in the sinusoids, shear stress induced by blood flow represents a constant stimulus of NO production in LSECs[35]. The first step in the development of endothelial dysfunction is the reduced production of NO [36] supplied by lessened protein kinase B (Akt)-dependent eNOS phosphorylation, causing diminished eNOS activity [30]. A very important molecule in the endothelial production of NO is insulin[37]. Insulin activates NO release through Akt *via* the Ca^{2+}-independent pathway[37,38]. The disruption of insulin signaling observed in insulin resistance impairs the endothelial production of NO[38,39]. Decreased NO bioavailability[40] can also be generated by increased intracellular levels of reactive oxygen species[41] because of excessive lipid accumulation in the liver, endoplasmic reticular stress and mitochondrial dysfunction[10,42,43]. Elevated ROS concentrations reduce the amount of bioactive NO through direct chemical interactions, inducing the formation of toxic peroxynitrite[44]. The latter uncouples eNOS to become a dysfunctional superoxide-generating enzyme, which additionally contributes to vascular oxidative stress[44]. eNOS dysfunction is also caused by the formation of eNOS inhibitors[45] such as asymmetric dimethylarginine[46], a paracrine and a competitive inhibitor of eNOS. The reduced bioavailability of NO can lead to sinusoidal contraction through the activation of perisinusoidal HSCs, resulting in increased IHVR and the elevation of portal pressure[47]. Sinusoidal dysfunction and IHVR in NAFLD pathogenesis are represented in feedback loops and interactions between LSECs, hepatocytes, Kupffer cells, hepatic stellate cells and other immune system cells[10]. The chronology of changes in the structural and functional causes of IHVR is difficult to establish due to the complexity of cell-cell interactions[48].

The impact of vascular dysregulation on PH development in NAFLD

In NAFLD-ballooned hepatocytes, activated HSCs and macrophages stimulate angiogenesis by producing a greater amount of VEGF as a response to shear stress, hypoxia and inflammation[5,49]. Liver steatosis induces hypoxia by both a mechanical pressure on sinusoids and an excessive lipid metabolism which increases oxygen consumption[49]. Increased VEGF levels in NAFLD promote angiogenesis (the formation of new blood vessels)[50] and qualitative changes in liver vessels called vascular remodeling[49,51]. Sinusoidal capillarization, an early morphological feature of endothelial dysfunction, is marked by a dedifferentiation of LSECs, as well as the formation of the basal membrane and loss of fenestration, and represents an example of qualitative vascular remodeling[49,52]. Both angiogenesis and sinusoidal capillarization contribute to the distortion of the normal liver vascular network, blood shunting with consequent tissue hypoxia and deranged metabolic exchange across the endothelial interface[53]. The triggers of sinusoidal capillarization have not been fully elucidated[54], but it is believed that capillarization occurs as a result of the exposure of LSECs to extreme lipid accumulation in parenchymal cells and a surplus amount of circulating lipids in the sinusoidal blood flow [30]. As a response to disproportionate lipid exposure, LSECs express lipid-induced adhesion molecules, integrins (vascular cell adhesion molecule 1, intercellular adhesion molecule, E-selectin and vascular adhesion protein 1), leading to the induction of the recruitment of leukocytes and their translocation into the liver parenchyma[55]. The excessive exposure of LSECs to lipids may cause mitochondrial dysfunction, DNA damage in hepatocytes, endoplasmic reticulum stress and cytoskeleton alterations[56]. A perfusion of hepatic sinusoids can also be aggravated by functional impairments, such as the contracting and swelling of LSECs in response to vasoactive mediators produced by ballooned hepatocytes, *e.g.*, ET-1[23,57]. However, it is important to note that the main liver cells involved in controlling the sinusoidal diameter are perisinusoidal HSCs, also known as liver-specific pericytes[58,59]. Lipid-laden hepatocytes secrete microparticles that promote angiogenesis[60]. Examples of such molecules are vanin-1 and annexin V, which are isolated in the blood of perisinusoidal spaces and produced by stretched and/or compressed centrilobular hepatocytes[5, 60]. Damage in the periportal vascular area may also play an important pathogenic role in NAFLD-dependent PH[5,10]. A high degree of steatosis or periportal fibrosis leads to a poor regulation of arteriolar inflow and creates shear stress in liver sinusoids, which are low-pressure, low-flow vascular channels linking the periportal area of portal inflow (zone 1) to the centrilobular area of central vein outflow (zone 3)[5]. Between zone 1 and zone 3, intralobular arterioles occasionally drain to sinusoids[61]. The influence of "arterial twigs" on sinusoidal flow has not been fully clarified, but they may represent zones of higher pressure[61]. A recently conducted study showed that splanchnic vasodilatation in NAFLD also contributes to the rise in portal pressure long before the development of cirrhosis[62]. Splanchnic vasodilatation and hyperdynamic circulation in NAFLD-dependent PH are characterized by low arterial responsiveness to a vasoconstrictor mediator, a rise in portal venous and mesenteric arterial blood flow and a decrease in main arterial blood pressure[62,63]. Numerous vasoactive mediators (calcitonin gen-related peptide, glucagon, NO, platelet-activating factor, atrial natriuretic peptide and adrenomedullin, as well as bile salts and endocannabinoids) are involved in the arteriolar vasodilatation in the visceral vascular bed that drains into the portal circulation[11,64] and results in an increase in portal inflow and pressure[11,64].

The mechanisms that are important in the development of endothelial dysfunction and capillarization are shown in Figure 2. To summarize the information about early pathophysiological changes in the development of PH in NAFLD, external compression and intraluminal obstacles (*e.g.*, microthrombi, lipid emboli and neutrophil traps) caused by structural changes in NAFLD result in impaired sinusoidal blood flow and may contribute to the development of PH in early NAFLD. Mechanotransduction pathways activated by multiple mechanical forces such as strain, shear stress and hydrostatic pressure result in endothelial dysfunction and fibrosis development, contributing to the maintenance and progression of PH.

The role of increased portal pressure in NAFLD pathogenesis

PH in NAFLD begins to develop as a result of IHVR and the de-differentiation of liver cells[35]. The initial site of IHVR formation is the hepatic sinusoid[65], while the distal segment of the preterminal portal venule serves as a sphincter for blood redistribution[66]. IHVR has two components, which are structural[67] and functional[68], characterized by extrasinusoidal and intrasinusoidal disturbances[35]. Total available space within the liver capsule in NAFLD becomes

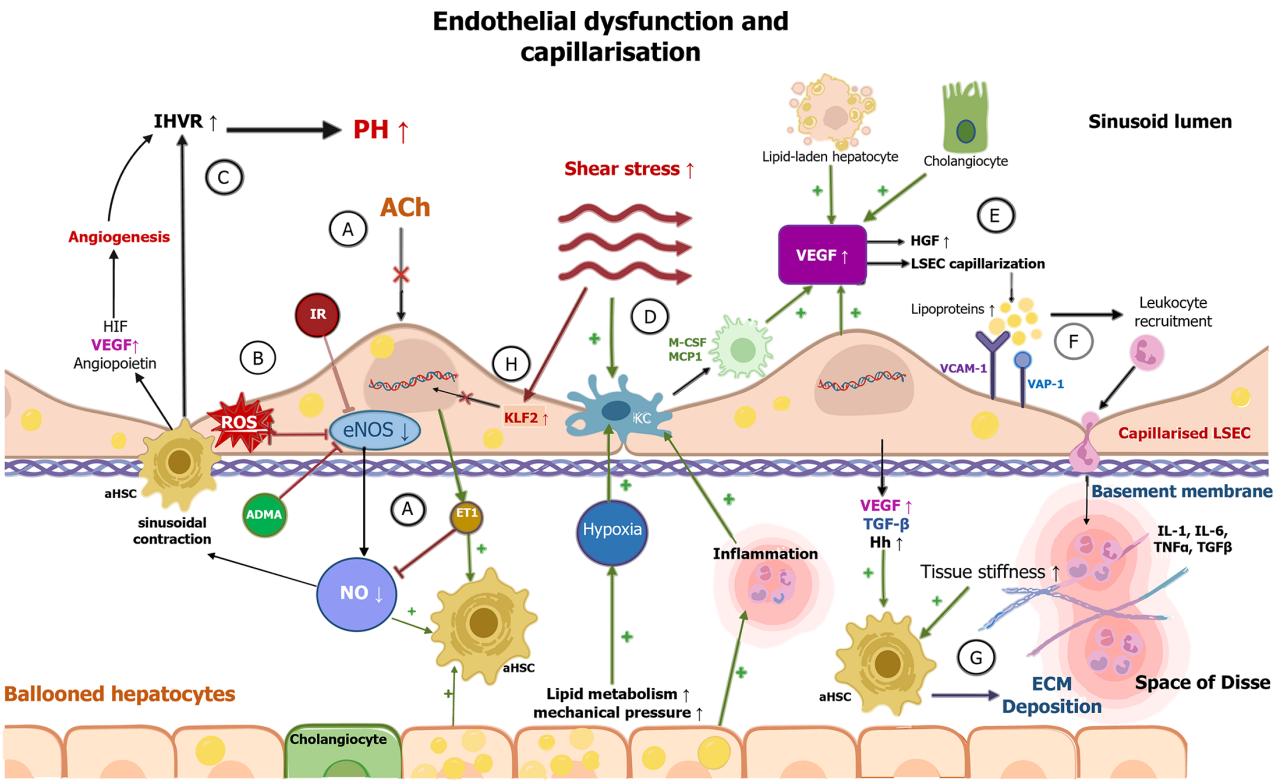

DOI: 10.3748/wjg.v30.i4.290

Figure 2 Development of endothelial dysfunction and capillarization. A: The initial step in the development of endothelial dysfunction is the reduced production of nitric oxide (NO) caused by decreased endothelial nitric-oxide synthase (eNOS) activity and the low response of liver sinusoidal endothelial cells (LSECs) to acetylcholine; B: Reduced NO bioavailability can be caused by insulin resistance, heightened intracellular levels of reactive oxygen species and the formation of eNOS, paracrine and competitive inhibitors such as asymmetric dimethylarginine; C: Low levels of NO paired with increased endothelin 1 (ET-1) synthesis lead to sinusoidal contraction through the activation of perisinusoidal hepatic stellate cells (HSCs), resulting in elevated intrahepatic vascular resistance and the elevation of portal pressure; D: As a response to shear stress, hypoxia and inflammation, lipid-laden hepatocytes, cholangiocytes, LSECs, activated HSCs and Kupffer cells stimulate angiogenesis by producing an excessive amount of vascular endothelial growth factor (VEGF); E: Hypoxia in fatty liver is induced by mechanical pressure on sinusoids and increased lipid metabolism. Elevated VEGF concentrations lead to the promotion of angiogenesis and fibrogenesis by the increased fibrogenic functions of HSC, as well as LSEC capillarization and the secretion of hepatocyte growth factor. Capillarization, marked by the formation of the basal membrane and loss of fenestration, occurs as a result of LSECs exposure to lipid accumulation in parenchymal cells and a great amount of circulating lipids in the blood; F: As a response to excessive lipid exposure, LSECs express lipid-induced adhesion molecules (VCAM-1, VAP-1, *etc.*), activate Kupffer cells through the secretion of pro-inflammatory cytokines and induce leukocyte recruitment and their translocation into the liver parenchyma; G: Capillarized LSECs also activate HSCs through the release of angiocrine signals such as VEGF, transforming growth factor and hedgehog signals. Activated HSCs begin to deposit extracellular matrix, which increases tissue stiffness, further stimulating HSC activation; H: Shear stress downregulates the expression of ET-1 *via* Krüppel-like factors 2 (KLF2) activation. LSECs overexpress KLF2 to maintain HSCs in a quiescent state as a compensatory mechanism to manage vascular dysfunction. Unfortunately, this is an insufficient mechanism for preventing portal hypertension development. ACh: Acetylcholine; aHSC: Activated hepatic stellate cell; KC: Kupffer cell; ROS: Reactive oxygen species; HIF: Hypoxia-inducible factor; M-CSF: Macrophage colony-stimulating factor; MCP1: Monocyte chemoattractant protein-1; IR: Insulin resistance; ADMA: Asymmetric dimethylarginine; HGF: Hepatocyte growth factor; VCAM-1: Vascular cell adhesion molecule 1; VAP-1: Vascular adhesion protein-1; IL-1: Interleukin-1; IL-6: Interleukin-6; TNFα: Tumor necrosis factor α; TGF-β: Transforming growth factor; Hh: Hedgehog signals.

restricted as a result of lipid accumulation and hepatocellular swelling, leading to a volumetric squeeze and consequently to a reduction in the sinusoidal spaces and a drop in blood flow[15,69,70] Mechanical forces taking place in the sinusoidal microenvironment of NAFLD (such as increased hydrostatic pressure, strain and shear stress) cause the deformation of cellular structures such as caveolae and plasma membrane lipid rafts, and result in an excessive extracellular matrix (ECM) deposition in the perisinusoidal space of Disse as well as sinusoidal hypercontractility. They also modify the conductivity of ion channels, expose new protein-binding sites and change the activity of transmembrane receptors[35,71,72]. The increase in ECM stiffness that results from the cross-linking of ECM proteins and collagen[73,74] is detected by integrins, mechanosensitive transmembrane proteins that initiate key biological processes upon stretch-induced conformational changes[74,75]. These are also involved in the binding and recruitment of cytoskeleton linker proteins[76], the activation of the transforming growth factor-β (TGF-β) signaling pathway[77] and the conformational alteration of ion channels[78]. Structural changes caused by steatosis in connection with mechanical forces induced by ECM accumulation and haemodynamic changes, as described previously, lead to the compression and/or stretching of liver cells and stimulation of signaling pathways[35], including the contraction and relaxation of the actin filament of the hepatocyte cytoskeleton that result in increased intracellular tension[35,79,80]. Intracellular tension pulls ECM-bound integrins, which then organize into focal adhesions and, together with adaptor proteins, strengthen the ECM-cytoskeleton connection[35,79,80]. The tension generated in the cytoskeleton is transmitted through the linker of the nucleoskeleton and cytoskeleton complex[35,79,80]. The deformation of the nucleus, which is proportional to the stiffness of the ECM

[81], affects the change in the gene expression by changing the permeability of the nuclear membrane and altering the rheology of chromatin[35]. This causes the translocation of transcription factors and co-factors[79] such as the yes-associated protein (YAP)/transcriptional coactivator with PDZ-binding *motif* (TAZ)[82]. The co-factors YAP/TAZ are mechanosensitive and can detect fluid shear stress, as well as increases in liver cell density and changes in ECM stiffness [83]. YAP/TAZ regulate the biological behavior of liver cells and the profibrotic response through an insufficiently elucidated mechanism[84,85], resulting in the further accumulation of fibrosis[86,87]. Other important transcription factors are myocardin-related transcription factor-A[88] and *zyxin*, part of the mechanosensing FA complex[89]. These factors translocate to the nucleus as a result of cell stretching and regulate the expression of genes related to inflammation, proliferation and cell apoptosis[35,76,89-91].

In conclusion, disrupted mechanical homeostasis in liver sinusoids is the key contributor to the pathogenesis of NAFLD, caused by intracellular lipid accumulation, enhanced ECM stiffness and altered functions in the contractile cytoskeleton that finally lead to further fibrosis accumulation and cellular contractility, representing the positive feedback loop mediated through the mechanotransduction pathways.

The development of fibrosis and its impact on PH

In NAFLD, excessive lipid accumulation triggers inflammation through cytokine secretion and immune cell infiltration [92]. The initiation of the inflammatory response leads to hepatocyte necrosis, apoptosis[93] and HSC activation[94,95] as the characteristic features of non-alcoholic steatohepatitis (NASH), in which a large amount of free fatty acids released from the injured hepatocytes, as well as damage-associated molecular patterns (DAMPs), are removed by Kupffer cells [96-98]. The latter release profibrogenic growth factors (TGF-β and platelet-derived growth factor)[99] that, in conjunction with ROS, pro-inflammatory cytokines (interleukin-6, interleukin-10 and tumor necrosis factor α)[100,101] and products of lipid peroxidation[102], along with endothelin and fibronectin produced by capillarized LSECs, result in HSC activation[5]. Activated HSCs transdifferentiate from the quiescent phenotype to proliferative, contractile and collagen-producing myofibroblasts[103]. These cause the synthesis of ECM through the production of collagen (types I, III and V) and hyaluronic acid[103]. In addition to the ECM products, myofibroblasts also synthesize α-smooth muscle actin[104], a hallmark of HSC activation[105], and release VEGF and chemokines such as macrophage colony-stimulating factor and monocyte chemoattractant protein-1 . Collagen is deposited in the space of Disse as an early phenomenon in NAFLD that generates the formation of perisinusoidal fibrosis and narrowing of the sinusoidal lumen[5]. Fibrosis in NAFLD develops in the pericellular space around the central veins and in the perisinusoidal space of zone 3[106], whereas the fibrosis pattern in other chronic liver diseases initially shows a portal instead of a pericentral distribution[107]. Due to the specific distribution of fibrosis in patients with NAFLD, PH may occur before the development of cirrhosis[107]. Increased ECM stiffness sends a positive feedback signal to HSCs, contributing to the further progression of liver fibrosis[35]. This results in the remodeling of the liver architecture and the formation of cirrhotic nodules with the additional distortion of hepatic microcirculation[108,109]. Both the structural component, represented by accumulated fibrosis with narrowed sinusoids and a distorted microvascular network, and the dynamic one resulting from endothelial dysfunction and myofibroblast contraction (with the latter considered responsible for 20%-30% of the IHVR) contribute to the rise in portal pressure[110, 111].

In conclusion, the development of liver fibrosis has a fundamental influence on the advancement and further aggravation of PH, not only as the structural barrier to the intrahepatic blood flow, but also by inducing the secretion of local vasoactive mediators. This leads to vascular dysregulation and the functional deterioration of endothelial dysfunction that additionally aggravates IHVR[5,35].

PORTAL HYPERTENSION IN RELATION TO THE STAGE OF LIVER FIBROSIS AND GRADE OF STEATOSIS: CLINICAL DATA

Large-scale epidemiological investigations focused on the prevalence of PH among the NAFLD patients are lacking. However, several clinical studies have been conducted to investigate the relationship between the development and severity of PH and the histological and clinical features of NAFLD. In a cohort of 50 overweight patients who underwent transjugular liver biopsy (TJLB) coupled with HVPG measurements, PH (HVPG > 5 mmHg) was diagnosed in 14 (28%) of subjects and the only histological parameter that differed between them and those without PH was a higher grade of steatosis (P = 0.016). In the group with PH, only 21% of patients had advanced fibrosis/cirrhosis. The independent clinical predictors of PH were waist circumference (P = 0.008) and the homeostatic model assessment for insulin resistance (HOMA IR; P = 0.043)[112]. In a prospective cohort study that included 40 obese patients who underwent TJLB (30% with diabetes, 70% with NASH) and HVPG measurements, PH was found in eight (20%) patients, and none had cirrhosis. The presence of PH positively correlated with the proinflammatory blood cytokine profile as well as with microvascular changes in the form of sinusoidal dilatation, previously reported as an early histological change in severe steatosis even in the absence of advanced fibrosis[27,113]. In an observational investigation, in a cohort of 354 subjects with biopsy-confirmed NAFLD, 100 patients exhibited clinical signs of PH (the presence of at least one of esophageal varices (EV), portosystemic encephalopathy, splenomegaly or ascites). Among them, 77 had liver cirrhosis and 11 had bridging fibrosis (stage F3). However, signs of PH were also present even in 12 (12%) patients who had no or only mild fibrosis (stages F0-F2)[107]. PH was increasingly detected in patients at a more advanced stage of fibrosis (r = 0.48, P = 0.006). In the F0-F2 subgroup (n = 204), a comparison between those with PH (n = 12) and those without PH (n = 192) was made, and the only histological feature that was significantly different between the groups was a higher grade of liver steatosis in patients with PH (mean grade 2.3 ± 0.5 *vs* 1.9 ± 0.7, P = 0.03). This work provides evidence that even clinically significant PH may

exist before liver fibrosis enters an advanced stage, which is classically considered the threshold for PH development, and this might be caused by fat overload leading to the progressive enlargement of hepatocytes and reduction of the sinusoidal lumen[10,107].

In another investigation, 14/89 (16%) patients with clinically significant portal hypertension (CSPH) diagnosed by HVPG measurement were found to not have cirrhosis, and seven had stages F0-F2 (five were diagnosed with NASH). All these patients had perisinusoidal fibrosis and 8/14 had hepatocyte ballooning[114]. Based on these results, it becomes clear that patients with NAFLD may have PH and even CSPH without cirrhosis. Somewhat different results came from a study that investigated the prevalence of PH in a cohort of 292 NAFLD patients with metabolic syndrome associated with a liver stiffness measurement (LSM) > 8 kPa and/or liver blood test abnormalities (alanine aminotransferase > upper limit of normal), with no prior liver decompensation events. These patients were referred for TJLB and HVPG measurements, and 75/292 had liver cirrhosis. Among the 217 non-cirrhotic patients, 36 had PH (only one had CSPH), and there was no difference in steatosis or inflammatory grade between the patients with and without PH[115]. The only patient who presented with CSPH in the non-cirrhotic group was a young woman with Alström syndrome, severe type 2 diabetes, arterial hypertension and obesity. To compare, in the group of 75 patients with cirrhosis, PH was present in 53 (71%), CSPH in 38 (51%) and severe PH in 29 (39%). Accordingly, whereas PH might appear even in a non-cirrhotic liver, severe PH was not observed in NAFLD patients in the absence of cirrhosis[115].

Portal hypertension and advanced cirrhosis, regardless of aetiology, are traditionally associated with splenomegaly [116]. Interestingly, the results of a recent retrospective study in a large population of patients with biopsy-proven NAFLD revealed a strong correlation between splenomegaly and increased body weight, whereas none between splenomegaly and the histological degree of the underlying disease could be confirmed[117]. Thus, splenomegaly might be considered a consequence of visceral lipid deposition in the spleen and not necessarily a sign of PH. This view is further supported by the results from some other investigations demonstrating an enlarged spleen size in people with NAFLD with no other signs of PH, as well as in otherwise healthy individuals with a higher body height and weight[118,119].

THE PROGNOSTIC PROPERTIES OF THE HVPG IN NAFLD

In terms of stratifying the risk of hepatic decompensation, the prognostic properties of the HVPG have mostly been derived from investigations conducted in patients with viral and alcoholic aetiologies of chronic liver disease, where they have demonstrated robust predictive values. The normal HVPG value is 1-5 mmHg, and values of 6-9 mmHg are considered subclinical PH, while an HVPG ≥10 mmHg represents CSPH, as from this threshold all major complications related to PH start to develop, including the formation EV, ascites accumulation and portal encephalopathy[120-123]. Esophageal varices bleed at an HVPG ≥ 12 mmHg, and the risk of death increases significantly in patients with an HVPG ≥ 16 mmHg[120,121,123]. Given the complexity of the histological presentation and pathogenesis of PH in NAFLD, the HVPG cut-off values that are used in other aetiologies might not be appropriate for this purpose in NAFLD. To further elucidate this issue, a multicentric cross-sectional study was conducted with a cohort of 548 patients with advanced NAFLD and 444 with advanced hepatitis C (aHCV), who underwent detailed PH evaluation including HVPG measurement, TJLB, gastroscopy and abdominal imaging. Advanced chronic liver disease was defined either clinically by the presence of PH (HVPG > 5 mmHg) or histologically by the presence of stage 3 or 4 of liver fibrosis, and the majority of patients had compensated ACLD (cACLD; 71%). The median HVPG was lower in patients with advanced non-alcoholic fatty liver disease (aNAFLD; 13 mmHg *vs* 15 mmHg), although the indicators of liver function were similar between them and the aHCV group, whereas decompensation rates were higher among aNAFLD patients (32% *vs* 25%, $P = 0.019$), suggesting that NAFLD patients decompensated at lower HVPG levels[124]. According to the classic HVPG thresholds, clinical decompensation appeared in both groups at an HVPG > 10 mmHg, while no signs were detected in aHCV patients with an HVPG < 10 mmHg. Interestingly, some NAFLD patients experienced decompensation even when the HVPG was < 10 mmHg[124]. Further insights into this issue were provided from a study that investigated the agreement between wedge hepatic vein pressure (WHVP) and portal pressure (PP) in patients with decompensated NASH cirrhosis ($n = 40$), as well as those with alcohol-related ($n = 40$) and HCV-related decompensated cirrhosis ($n = 40$). All the patients were treated with a transjugular intrahepatic portosystemic shunt and the results revealed an excellent correlation between WHVP and PP in those with alcohol-related or HCV-related cirrhosis ($r = 0.92$; $P < 0.001$; intraclass correlation coefficient (ICC) 0.96; $P < 0.001$) whereas it was only moderate in the NASH group ($r = 0.61$; $P < 0.001$; ICC 0.74; $P < 0.001$). When the WHVP differed by > 10% from PP, this was regarded as a disagreement between the two, and this occurred more frequently in the NASH group (37.5% *vs* 14%; $P = 0.003$)[125], where WHVP tended to underestimate PP. Data from a simtuzumab trial revealed that 14% of patients with NASH cirrhosis and an HVPG < 10 mmHg developed liver decompensation during a median follow-up of 4.7 mo. Nevertheless, an HVPG ≥ 10 mmHg maintained its prognostic properties in terms of predicting the liver decompensation in the overall group of patients with NASH cirrhosis, in comparison to those who had an HVPG < 10 mmHg (hazard ratio 2.83; 95% confidence interval, 1.33-6.02; $P = 0.007$)[126].

Based on these studies, there is strong evidence for the underestimation of portal pressure in NAFLD patients by HVPG, probably due to the presence of a pre-sinusoidal component. In this line, portal inflammation and ductular reaction in the portal tracts were described in patients with advanced NASH[127,128], and it may be plausible that biliary injury contributes to increased presinusoidal pressure, and therefore favors PP underestimation. Whether periportal fibrosis and/or biliary injury may contribute to increase vascular tone and resistance to blood flow at the level of the portal venules remains to be elucidated.

INNOVATIVE DIAGNOSTIC APPROACHES TO DIAGNOSING PORTAL HYPERTENSION IN NAFLD: A CONCEPT OF ENDO-HEPATOLOGY

The hepatic venous pressure gradient (HVPG) represents the gold standard for diagnosing and grading PH[2,121,123,129]. However, it is invasive, expensive and not widely available[130,131]. Among the most serious drawbacks of the HVPG is its inability to detect pre-sinusoidal PH, which obviously takes place in patients with NAFLD, and thus the HVPG might not reliably rule out CSPH in this group. These objective limitations of the HVPG have influenced the search for other methods to be invented and used for diagnosing PH.

Endoscopic ultrasound-guided portal pressure gradient (EUS-PPG) measurement represents a new diagnostic approach to direct PVP assessment. This new method is currently being tested in correlation to traditional HVPG measurement[10]. Under EUS guidance, a modified 25-gauge fine-needle aspiration needle connected to a digital manometer, a self-calibrating compact pressure transducer, is inserted through the liver parenchyma directly into a hepatic vein branch and the portal vein[10,132]. After three consecutive measurements, the mean value is calculated and recorded as the EUS-PPG. In theory, this method could overcome limitations from the HVPG as it measures EUS-PPG, and thus it might more reliably assess the PH grade even in the presence of a pre-sinusoidal component. The first EUS-guided portal vein puncture with portography and pressure measurement was performed on a pig model in 2004[133]. In further animal models, an excellent correlation between EUS-PPG and HVPG measurements (r = 0.99) was demonstrated [132]. In a human pilot study conducted in 28 patients with chronic liver disease, EUS-PPG demonstrated a 100% feasibility of accessing all targeted vessels, with no adverse events. In addition, the EUS-PPG results were highly correlated with the presence of clinical signs of PH (no HVPG measurements were available)[134]. Although it has exhibited promising results, this method needs to be further tested over a larger cohort of patients with different aetiologies of chronic liver disease. Moreover, the issue of how to validate its accuracy in patients with presinusoidal PH, in the absence of a gold diagnostic standard (because the HVPG might not be considered as such in this scenario), still remains. Another limitation of EUS-PPG is that sedation must be used to achieve reliable EUS-PPG measurements, but this heavily influences the hepato-portal haemodynamic and thus probably the results of EUS-PPG measurements as well. The direct measurement of portal pressure is also possible through a surgical approach, which is obviously not acceptable for wider clinical use[10,135].

THE NON-INVASIVE DIAGNOSIS OF PORTAL HYPERTENSION IN NAFLD

In addition to the HVPG as an invasive assessment of PVP, numerous non-invasive diagnostic methods have been investigated, and some of them are currently utilized in clinical practice. Ultrasound-based methods have been the most frequently evaluated and are widely implemented in hepatology practices, as they are harmless, with no ionizing radiation, easy to use and supported by a large body of scientific evidence. By employing conventional ultrasound, it is possible to detect morphological signs of PH, such as splenomegaly, the presence of ascites or portosystemic collaterals, which is also achievable through other imaging methods such as computed tomography (CT) or magnetic resonance imaging (MRI). The last two are either ionizing (CT), or not that readily available (MRI). However, morphological signs of PH detected by imaging methods indicate the presence of CSPH, whereas the goal should be to detect the existence of CSPH as early as possible before the signs of the advanced stage develop. In this line, elastography represents one of the most promising candidates, and has become probably the most influential non-invasive diagnostic tool applied in everyday hepatology practice, including the assessment of PH. Most data have been accumulated with the use of transient elastography (TE), but significant evidence also exists for other ultrasound-based methods such as point shear wave elastography and two-dimensional shear wave elastography[136,137]. The pivotal study testing the diagnostic performance of TE for CSPH was published in 2021 and included an international cohort of 836 patients with CLD of mixed aetiology (including 248 with NAFLD), paired LSM and HVPG measurements and no history of liver decompensation. All patients had an LSM ≥ 10 kPa, and the overall prevalence of PH and CSPH was 83% and 59%, respectively. At the LSM cut-off ≥ 25 kPa, TE had a ≥ 90% positive predictive value (PPV) for ruling in CSPH in all aetiologies except for NAFLD, where only 77% of patients with an LSM over this threshold had CSPH according to the HVPG measurements. For non-obese NAFLD patients, the PPV of LSM over 25 kPa was better, with 91.7% of these patients having CSPH. The PPV for obese patients with NAFLD was lower, but the specificity was similar, and the reduced PPV was due to a lower prevalence of CSPH. For ruling CSPH out, a combination of LSM ≤ 15 kPa and platelet count ≥ 150 × 10^9/L had a ≥ 90% negative predictive value for all aetiologies of CLD including NAFLD, except for hepatitis B, due to the very low number of tested participants. In an attempt to improve the prediction of CSPH in NAFLD patients, the authors constructed a nomogram by using LSM, body mass index (BMI) and platelet count, and demonstrated that at a certain LSM the probability of CSPH is much lower in obese patients compared to their non-obese counterparts[138]. These results were considered by the Baveno VII consensus, which issued recommendations for the non-invasive evaluation of PH utilizing the cut-off values of LSM and platelet count as obtained in this work[139]. To validate these non-invasive criteria for diagnosing CSPH, a retrospective cohort study on 76 cACLD patients (23 with NAFLD) was conducted, and the results revealed that the LSM ≥ 25 kPa criterion had 88.9% specificity and 87.1% PPV for ruling in CSPH, whereas the LSM ≤ 15 kPa and Plt ≥ 150 criterion had 100% sensitivity and a negative predictive value (NPV) for ruling out CSPH. This paper also confirmed that with an increasing BMI, for any given level of platelet count, higher LSM values were needed for a certain probability of having CSPH[140]. According to the Baveno criteria, patients with platelet count > 150 × 10^9 cells/L and LSM < 20 kPa exhibit a very low risk of having high-risk varices and can safely avoid screening endoscopy[139,141].

A spleen stiffness measurement (SSM) that demonstrated high accuracy in classifying patients according to the presence of varices needing treatment (VNT) and CSPH might be helpful in borderline cases, as it reflects an increased resistance to portal blood flow, and the SSM is not affected by liver steatosis[142-145]. Accordingly, the Baveno VII consensus issued recommendations that an SSM > 50 kPa measured by TE might be applied to rule in CSPH, and an SSM < 21 kPa to exclude it in patients with viral hepatitis[139]. A combined approach in which two out of three criteria (LSM ≥ 25 kPa, SSM > 40 kPa and Plt < 150 × 10^9/L) were employed in cACLD patients to non-invasively identify those with CSPH correctly classified 88% of patients in a recent individual patient data meta-analysis[146]. Whereas the respective PPVs were 91% and 93% in the subgroups with obesity and a non-viral aetiology, the corresponding specificities were 71% and 85%. The combination of two criteria (LSM ≤ 15 kPa, SSM ≤ 40 kPa and Plt count ≥ 150 × 10^9/L) demonstrated a suboptimal NPV (67%) for ruling out CSPH in non-viral aetiology, whereas the NPV was 91% if SSM < 21 kPa was utilized instead. Whether the performance of these cut-offs is limited to patients with NAFLD remains to be further validated. Some promising initial results were published using contrast-enhanced ultrasound, specifically the subharmonic aided pressure estimation method[147], but these results require further validation.

Beside imaging methods, biomarker(s) from blood or stool would be welcome for early detection of PH in NAFLD patients, as this approach could potentially have wider applicability. Given that NAFLD is closely related to type 2 diabetes, postprandial blood glucose (PPG) has been studied as an important blood biomarker for assessing the progression of liver disease from steatosis to fibrosis[148-150]. Elevated PPG during NAFLD occurs prior to fibrosis, indicating a bidirectional relationship between postprandial dysfunction in NAFLD and fibrosis development[149,150]. The results of a recent study on a Chinese NAFLD population showed an independent association between elevated PPG and progression of liver fibrosis[148]. Whereas some investigations described distinctive metabolomic blood/stool signature of advanced fibrosis/cirrhosis in comparison to simple steatosis or mild fibrosis, they still have not revealed reliable single biomarker or biomarker combination specific for PH, and thus further research in this regard is warrantied [151,152].

NON-INVASIVE DIAGNOSIS OF HIGH-RISK ESOPHAGEAL VARICES IN NAFLD

Progression of liver cirrhosis and PH leads to the development of CSPH and its complications in the form of EV, ascites accumulation, portal encephalopathy and EV[9,11,153,154]. Esophago-gastro-duodenoscopy (EGD) represents the gold standard method for diagnosing and assessing the degree of EV, and it offers the possibility of treating EV at the same time[155,156]. However, EGD is an invasive procedure, associated with some risks, including damage to the gut wall, bleeding and perforation, and it is not very well accepted by some patients. Therefore, non-invasive approaches to the diagnosing of EV have been extensively investigated during the last decade. By using non-invasive methods, such as TE in the first place, liver disease is more frequently detected at an early stage, which significantly increases the number of unnecessary endoscopies[157]. Non-invasive Baveno VI (LSM < 20 kPa, Plt > 150 × 10^9/L) and expanded Baveno VI criteria (LSM < 25 kPa, Plt > 110 × 10^9/L) have proven to be efficient in ruling out high-risk VNT[141,158]. According to the original report, it was possible to safely avoid 40% of EGDs at the cost of missing only 1.6% of VNT by applying expanded Baveno VI criteria[159]. However, only a minority of patients included in these investigations had NAFLD, whereas the data referred mostly to patients with alcohol-related cirrhosis and viral cirrhosis. Therefore, NAFLD cirrhosis criteria were proposed by Petta *et al*[160] based on a multicentric international study that included 790 patients with compensated NAFLD cirrhosis who underwent EGD and LSM by TE no more than six months apart. Accordingly, the best performing criteria for ruling out VNT by utilizing an M probe were an LSM < 30 kPa and platelet count > 110000/mm^3, whereas the corresponding values if an XL probe was employed were an LSM < 25 kPa and platelet count > 110000/mm^3, the latter identical to the expanded Baveno VI criteria[160].

Based on these data, an algorithmic approach to ruling out VNT in patients with NAFLD cirrhosis was finally proposed: if LSM could be reliably assessed by an M probe, then Baveno VI criteria should be applied to non-obese subjects, and NAFLD cirrhosis criteria to obese ones. If the XL probe had to be used, again Baveno VI criteria should be applied to non-obese subjects, and NAFLD cirrhosis criteria (extended Baveno VI) to obese ones[160,161]. In a retrospective cohort study from China, the authors investigated the diagnostic performance of Baveno VI and extended the Baveno VI criteria for ruling out VNT in a cohort of 224 patients with biopsy- or clinically proven compensated NAFLD cirrhosis. It should be highlighted that 60.7% patients had coexisting hepatitis B, 15.6% hepatitis C and 8.9% alcohol-related chronic liver disease. The mean LSM was 18.1 ± 13.9 kPa and the authors did not declare which probe(s) they utilized. By employing Baveno VI and expanded Baveno VI criteria, it was possible to avoid endoscopy in 37.5% and 56.7% patients, with the respective risk of missing VNT in 1.19% and 3.15% patients[162]. Obviously, the dilemma regarding the steatosis influence on LSM is still an open issue, in terms of both its impact on the accuracy of non-invasive staging of liver fibrosis in NAFLD patients, as well as in assessing the severity and complications of PH[138,163,164]. Measuring spleen stiffness might also be helpful in this clinical scenario, as it was demonstrated that in patients who were outside Baveno VI criteria based on LSM and platelet count assessment, an SSM ≤ 46 kPa had a 98% NPV for ruling out VNT[165]. Accordingly, the Baveno VII consensus issued a recommendation that endoscopy could be safely avoided in patients who do not meet LSM/platelet criteria if their SSM is ≤ 40 kPa[139]. Again, this recommendation relies on the data obtained mostly from patients with viral hepatitis and thus should be further validated in those with NAFLD.

A SPECIFIC TREATMENT FOR PH IN PATIENTS WITH NAFLD: NOT THERE YET

The numerous molecular and cellular pathophysiological processes that contribute to IHVR in patients with NAFLD represent potential therapeutic targets for PH[5,10,166] Nonselective beta blockers like carvedilol and propranolol are utilized for the prevention of clinical decompensation in patients with compensated cirrhosis and CSPH[167]. Statins have been demonstrated to stimulate the eNOS-NO-soluble guanylate cyclase (sGC)-cyclic guanosine monophosphate pathway with increased intrahepatic NO production, the upregulation of a transcription factor (Krüppel-like transcription factor) and the inhibition of the RhoA/Rho-associated coiled-coil-containing kinase pathway that is important for the development of LSEC capillarization and vasoconstrictive effects[166,168] Multikinase inhibitors (sorafenib) were investigated for attenuating pathological angiogenesis in the course of chronic liver disease[166,169,170]. Immunomodulatory drugs (thalidomide), caspase inhibitors (emricasan), antioxidative drugs, radical scavengers, cyclooxygenase inhibitors and antibiotics (rifaximin)[166] were used to reduce hepatic inflammation and bacterial translocation as important steps in preventing the progression of PH. Farnesoid X receptor agonists were demonstrated to decrease IHVR by stimulating eNOS[171] activity in a rat model of cirrhotic PH[172].

However, despite ongoing research efforts, there are still no specific agents approved for the treatment of PH caused by NAFLD[173]. Therefore, general guidelines for PH should be followed in patients with NAFLD, while lifestyle changes (reduction in caloric intake, weight loss and daily exercise) remain the mainstay of the treatment approach[10].

CONCLUSION

The development of clinically significant portal hypertension mostly occurs in patients with cirrhotic NAFLD. Despite this fact, multiple lines of evidence confirm the early elevation of portal vein pressure and onset of PH in non-cirrhotic NAFLD patients. Increased IHVR is the main cause of PH in NAFLD and arises because of perisinusoidal fibrosis and microcirculation damage. HVPG as an invasive diagnostic method underestimates portal pressure in patients with NAFLD and some patients develop liver decompensation below an HVPG of 10 mmHg, which is traditionally considered the threshold for CSPH. Obesity seems to reduce the diagnostic accuracy of LSM, leading to the overestimation of PH severity. Baveno VII criteria might be used for non-invasive ruling out, but they have suboptimal diagnostic performance for ruling in CSPH in obese NAFLD patients. Similarly, Baveno criteria are reliable for ruling out VNT in non-obese NAFLD patients, whereas in obese patients NAFLD cirrhosis criteria might work better. Recent advances in understanding the pathophysiological background of NAFLD and related PH have resulted in several candidate molecules and pathways that might serve as the targets for pharmacological compounds, but this is still an area of ongoing research, and currently we still lack specific drugs for PH in NAFLD. Nevertheless, it is unrealistic to expect that a single medication could reverse all pathological changes taking place along the complex pathways of PH development in NAFLD, and thus a combination of lifestyle changes, liver-targeted therapies and modulation of metabolic derangements would probably represent the solution to this problem.

FOOTNOTES

Author contributions: All authors contributed to the conception and design of the study and acquisition, analysis and interpretation of the data; Madir A and Grgurevic I drafted the article; Tsochatzis EA and Pinzani M made critical revisions related to important intellectual content; and all the authors approved the final version of the manuscript.

Conflict-of-interest statement: Dr. Madir and Dr. Grgurevic have nothing to disclose. Dr. Tsochatzis reports personal fees from NovoNordisk, personal fees from Boehringer, personal fees from Pfizer, personal fees from Siemens, personal fees from NovoNordisk, personal fees from Echosens, personal fees from Abbvie, outside the submitted work. Dr. Pinzani reports personal fees from Chemomab (Israel); Takeda (USA); Astra Zeneca (UK); Dicerna (USA); Galecto (Sweden); Resolution Therapeutics (UK); Novo Nordisk (DK); Boehringer Ingelheim (Germany), personal fees from Engitix Therapeutics Ltd (UCL Spin-out) (UK), personal fees from Aculive Therapeutics Ltd (Cambridge University Spin-out) (UK), outside the submitted work.

Country/Territory of origin: Croatia

ORCID number: Anita Madir 0000-0001-5789-1869; Ivica Grgurevic 0000-0003-0520-3483; Emmanuel A Tsochatzis 0000-0001-5069-2461.

S-Editor: Gong ZM
L-Editor: A
P-Editor: Chen YX

REFERENCES

1 **Tsochatzis EA**, Bosch J, Burroughs AK. Liver cirrhosis. *Lancet* 2014; **383**: 1749-1761 [PMID: 24480518 DOI: 10.1016/S0140-6736(14)60121-5]

2 **Kumar M**, Sakhuja P, Kumar A, Manglik N, Choudhury A, Hissar S, Rastogi A, Sarin SK. Histological subclassification of cirrhosis based on histological-haemodynamic correlation. *Aliment Pharmacol Ther* 2008; **27**: 771-779 [PMID: 18284653 DOI: 10.1111/j.1365-2036.2008.03653.x]

3 **Pinzani M**, Rosselli M, Zuckermann M. Liver cirrhosis. *Best Pract Res Clin Gastroenterol* 2011; **25**: 281-290 [PMID: 21497745 DOI: 10.1016/j.bpg.2011.02.009]

4 **Sarin SK**, Kapoor D. Non-cirrhotic portal fibrosis: current concepts and management. *J Gastroenterol Hepatol* 2002; **17**: 526-534 [PMID: 12084024 DOI: 10.1046/j.1440-1746.2002.02764.x]

5 **Baffy G**. Origins of Portal Hypertension in Nonalcoholic Fatty Liver Disease. *Dig Dis Sci* 2018; **63**: 563-576 [PMID: 29368124 DOI: 10.1007/s10620-017-4903-5]

6 **Vollmar B**, Menger MD. The hepatic microcirculation: mechanistic contributions and therapeutic targets in liver injury and repair. *Physiol Rev* 2009; **89**: 1269-1339 [PMID: 19789382 DOI: 10.1152/physrev.00027.2008]

7 **NAKATA K**, LEONG GF, BRAUER RW. Direct measurement of blood pressures in minute vessels of the liver. *Am J Physiol* 1960; **199**: 1181-1188 [PMID: 13727666 DOI: 10.1152/ajplegacy.1960.199.6.1181]

8 **Oda M**, Yokomori H, Han JY. Regulatory mechanisms of hepatic microcirculation. *Clin Hemorheol Microcirc* 2003; **29**: 167-182 [PMID: 14724338]

9 **Bosch J**, Iwakiri Y. The portal hypertension syndrome: etiology, classification, relevance, and animal models. *Hepatol Int* 2018; **12**: 1-10 [PMID: 29064029 DOI: 10.1007/s12072-017-9827-9]

10 **Ryou M**, Stylopoulos N, Baffy G. Nonalcoholic fatty liver disease and portal hypertension. *Explor Med* 2020; **1**: 149-169 [PMID: 32685936 DOI: 10.37349/emed.2020.00011]

11 **Bosch J**, García-Pagán JC. Complications of cirrhosis. I. Portal hypertension. *J Hepatol* 2000; **32**: 141-156 [PMID: 10728801 DOI: 10.1016/S0168-8278(00)80422-5]

12 **Ijaz S**, Yang W, Winslet MC, Seifalian AM. Impairment of hepatic microcirculation in fatty liver. *Microcirculation* 2003; **10**: 447-456 [PMID: 14745457 DOI: 10.1038/sj.mn.7800206]

13 **Mitten EK**, Portincasa P, Baffy G. Portal Hypertension in Nonalcoholic Fatty Liver Disease: Challenges and Paradigms. *J Clin Transl Hepatol* 2023; **11**: 1201-1211 [PMID: 37577237 DOI: 10.14218/jcth.2023.00029]

14 **Wisse E**, Braet F, Shami GJ, Zapotoczny B, Vreuls C, Verhaegh P, Frederik P, Peters PJ, Olde Damink S, Koek G. Fat causes necrosis and inflammation in parenchymal cells in human steatotic liver. *Histochem Cell Biol* 2022; **157**: 27-38 [PMID: 34524512 DOI: 10.1007/s00418-021-02030-8]

15 **Wada K**, Fujimoto K, Fujikawa Y, Shibayama Y, Mitsui H, Nakata K. Sinusoidal stenosis as the cause of portal hypertension in choline deficient diet induced fatty cirrhosis of the rat liver. *Acta Pathol Jpn* 1974; **24**: 207-217 [PMID: 4407748 DOI: 10.1111/j.1440-1827.1974.tb00818.x]

16 **Kleiner DE**, Brunt EM, Van Natta M, Behling C, Contos MJ, Cummings OW, Ferrell LD, Liu YC, Torbenson MS, Unalp-Arida A, Yeh M, McCullough AJ, Sanyal AJ; Nonalcoholic Steatohepatitis Clinical Research Network. Design and validation of a histological scoring system for nonalcoholic fatty liver disease. *Hepatology* 2005; **41**: 1313-1321 [PMID: 15915461 DOI: 10.1002/hep.20701]

17 **Hübscher SG**. Histological assessment of non-alcoholic fatty liver disease. *Histopathology* 2006; **49**: 450-465 [PMID: 17064291 DOI: 10.1111/j.1365-2559.2006.02416.x]

18 **Wanless IR**, Bargman JM, Oreopoulos DG, Vas SI. Subcapsular steatonecrosis in response to peritoneal insulin delivery: a clue to the pathogenesis of steatonecrosis in obesity. *Mod Pathol* 1989; **2**: 69-74 [PMID: 2657721]

19 **Hilscher MB**, Sehrawat T, Arab JP, Zeng Z, Gao J, Liu M, Kostallari E, Gao Y, Simonetto DA, Yaqoob U, Cao S, Revzin A, Beyder A, Wang RA, Kamath PS, Kubes P, Shah VH. Mechanical Stretch Increases Expression of CXCL1 in Liver Sinusoidal Endothelial Cells to Recruit Neutrophils, Generate Sinusoidal Microthombi, and Promote Portal Hypertension. *Gastroenterology* 2019; **157**: 193-209.e9 [PMID: 30872106 DOI: 10.1053/j.gastro.2019.03.013]

20 **Manda A**, Pruchniak MP, Araźna M, Demkow UA. Neutrophil extracellular traps in physiology and pathology. *Cent Eur J Immunol* 2014; **39**: 116-121 [PMID: 26155111 DOI: 10.5114/ceji.2014.42136]

21 **Mitten EK**, Baffy G. Mechanotransduction in the pathogenesis of non-alcoholic fatty liver disease. *J Hepatol* 2022; **77**: 1642-1656 [PMID: 36063966 DOI: 10.1016/j.jhep.2022.08.028]

22 **Yoshihara H**, Hijioka T, Eguchi H, Fukui H, Goto M, Inoue A, Kawano S, Sato N, Kamada T. Hepatic microcirculatory disturbance in fatty liver as a cause of portal hypertension. *J Gastroenterol Hepatol* 1989; **4** Suppl 1: 279-281 [PMID: 2519076]

23 **McCuskey RS**. Morphological mechanisms for regulating blood flow through hepatic sinusoids. *Liver* 2000; **20**: 3-7 [PMID: 10726955 DOI: 10.1034/j.1600-0676.2000.020001003.x]

24 **Hilscher MB**, Shah VH. Neutrophil Extracellular Traps and Liver Disease. *Semin Liver Dis* 2020; **40**: 171-179 [PMID: 31726473 DOI: 10.1055/s-0039-3399562]

25 **Baffy G**, Bosch J. Overlooked subclinical portal hypertension in non-cirrhotic NAFLD: Is it real and how to measure it? *J Hepatol* 2022; **76**: 458-463 [PMID: 34606912 DOI: 10.1016/j.jhep.2021.09.029]

26 **Sun CK**, Zhang XY, Wheatley AM. Increased NAD(P)H fluorescence with decreased blood flow in the steatotic liver of the obese Zucker rat. *Microvasc Res* 2003; **66**: 15-21 [PMID: 12826070 DOI: 10.1016/S0026-2862(03)00021-9]

27 **Francque S**, Laleman W, Verbeke L, Van Steenkiste C, Casteleyn C, Kwanten W, Van Dyck C, D'Hondt M, Ramon A, Vermeulen W, De Winter B, Van Marck E, Van Marck V, Pelckmans P, Michielsen P. Increased intrahepatic resistance in severe steatosis: endothelial dysfunction, vasoconstrictor overproduction and altered microvascular architecture. *Lab Invest* 2012; **92**: 1428-1439 [PMID: 22890552 DOI: 10.1038/Labinvest.2012.103]

28 **Galle J**, Quaschning T, Seibold S, Wanner C. Endothelial dysfunction and inflammation: what is the link? *Kidney Int Suppl* 2003; S45-S49 [PMID: 12694307 DOI: 10.1046/j.1523-1755.63.s84.12.x]

29 **Vairappan B**. Endothelial dysfunction in cirrhosis: Role of inflammation and oxidative stress. *World J Hepatol* 2015; **7**: 443-459 [PMID: 25848469 DOI: 10.4254/wjh.v7.i3.443]

30 **Pasarín M**, La Mura V, Gracia-Sancho J, García-Calderó H, Rodríguez-Vilarrupla A, García-Pagán JC, Bosch J, Abraldes JG. Sinusoidal

endothelial dysfunction precedes inflammation and fibrosis in a model of NAFLD. *PLoS One* 2012; **7**: e32785 [PMID: 22509248 DOI: 10.1371/journal.pone.0032785]

31 **Ganz P**, Vita JA. Testing endothelial vasomotor function: nitric oxide, a multipotent molecule. *Circulation* 2003; **108**: 2049-2053 [PMID: 14581383 DOI: 10.1161/01.CIR.0000089507.19675.F9]

32 **Gupta TK**, Toruner M, Chung MK, Groszmann RJ. Endothelial dysfunction and decreased production of nitric oxide in the intrahepatic microcirculation of cirrhotic rats. *Hepatology* 1998; **28**: 926-931 [PMID: 9755227 DOI: 10.1002/hep.510280405]

33 **Papapetropoulos A**, García-Cardeña G, Madri JA, Sessa WC. Nitric oxide production contributes to the angiogenic properties of vascular endothelial growth factor in human endothelial cells. *J Clin Invest* 1997; **100**: 3131-3139 [PMID: 9399960 DOI: 10.1172/JCI119868]

34 **Moncada S**, Palmer RM, Higgs EA. Nitric oxide: physiology, pathophysiology, and pharmacology. *Pharmacol Rev* 1991; **43**: 109-142 [PMID: 1852778]

35 **Felli E**, Selicean S, Guixé-Muntet S, Wang C, Bosch J, Berzigotti A, Gracia-Sancho J. Mechanobiology of portal hypertension. *JHEP Rep* 2023; **5**: 100869 [PMID: 37841641 DOI: 10.1016/j.jhepr.2023.100869]

36 **Picchi A**, Gao X, Belmadani S, Potter BJ, Focardi M, Chilian WM, Zhang C. Tumor necrosis factor-alpha induces endothelial dysfunction in the prediabetic metabolic syndrome. *Circ Res* 2006; **99**: 69-77 [PMID: 16741160 DOI: 10.1161/01.RES.0000229685.37402.80]

37 **Montagnani M**, Chen H, Barr VA, Quon MJ. Insulin-stimulated activation of eNOS is independent of Ca2+ but requires phosphorylation by Akt at Ser(1179). *J Biol Chem* 2001; **276**: 30392-30398 [PMID: 11402048 DOI: 10.1074/jbc.M103702200]

38 **Duncan ER**, Crossey PA, Walker S, Anilkumar N, Poston L, Douglas G, Ezzat VA, Wheatcroft SB, Shah AM, Kearney MT. Effect of endothelium-specific insulin resistance on endothelial function in vivo. *Diabetes* 2008; **57**: 3307-3314 [PMID: 18835939 DOI: 10.2337/db07-1111]

39 **Duncan ER**, Walker SJ, Ezzat VA, Wheatcroft SB, Li JM, Shah AM, Kearney MT. Accelerated endothelial dysfunction in mild prediabetic insulin resistance: the early role of reactive oxygen species. *Am J Physiol Endocrinol Metab* 2007; **293**: E1311-E1319 [PMID: 17711985 DOI: 10.1152/ajpendo.00299.2007]

40 **Tyagi N**, Sedoris KC, Steed M, Ovechkin AV, Moshal KS, Tyagi SC. Mechanisms of homocysteine-induced oxidative stress. *Am J Physiol Heart Circ Physiol* 2005; **289**: H2649-H2656 [PMID: 16085680 DOI: 10.1152/ajpheart.00548.2005]

41 **Schieber M**, Chandel NS. ROS function in redox signaling and oxidative stress. *Curr Biol* 2014; **24**: R453-R462 [PMID: 24845678 DOI: 10.1016/j.cub.2014.03.034]

42 **Clare K**, Dillon JF, Brennan PN. Reactive Oxygen Species and Oxidative Stress in the Pathogenesis of MAFLD. *J Clin Transl Hepatol* 2022; **10**: 939-946 [PMID: 36304513 DOI: 10.14218/JCTH.2022.00067]

43 **Parker KJ**, Ormachea J, Drage MG, Kim H, Hah Z. The biomechanics of simple steatosis and steatohepatitis. *Phys Med Biol* 2018; **63**: 105013 [PMID: 29701180 DOI: 10.1088/1361-6560/aac09a]

44 **Förstermann U**. Nitric oxide and oxidative stress in vascular disease. *Pflugers Arch* 2010; **459**: 923-939 [PMID: 20306272 DOI: 10.1007/s00424-010-0808-2]

45 **Mookerjee RP**, Mehta G, Balasubramaniyan V, Mohamed Fel Z, Davies N, Sharma V, Iwakiri Y, Jalan R. Hepatic dimethylarginine-dimethylaminohydrolase1 is reduced in cirrhosis and is a target for therapy in portal hypertension. *J Hepatol* 2015; **62**: 325-331 [PMID: 25152204 DOI: 10.1016/j.jhep.2014.08.024]

46 **Németh B**, Kustán P, Németh Á, Lenkey Z, Cziráki A, Kiss I, Sulyok E, Ajtay Z. [Asymmetric dimethylarginine: predictor of cardiovascular diseases?]. *Orv Hetil* 2016; **157**: 483-487 [PMID: 26996894 DOI: 10.1556/650.2016.30396]

47 **Fernandez M**. Molecular pathophysiology of portal hypertension. *Hepatology* 2015; **61**: 1406-1415 [PMID: 25092403 DOI: 10.1002/hep.27343]

48 **Swain SM**, Liddle RA. Piezo1 acts upstream of TRPV4 to induce pathological changes in endothelial cells due to shear stress. *J Biol Chem* 2021; **296**: 100171 [PMID: 33298523 DOI: 10.1074/jbc.RA120.015059]

49 **Lei L**, Ei Mourabit H, Housset C, Cadoret A, Lemoinne S. Role of Angiogenesis in the Pathogenesis of NAFLD. *J Clin Med* 2021; **10** [PMID: 33804956 DOI: 10.3390/jcm10071338]

50 **Carmeliet P**, Jain RK. Molecular mechanisms and clinical applications of angiogenesis. *Nature* 2011; **473**: 298-307 [PMID: 21593862 DOI: 10.1038/nature10144]

51 **Poisson J**, Lemoinne S, Boulanger C, Durand F, Moreau R, Valla D, Rautou PE. Liver sinusoidal endothelial cells: Physiology and role in liver diseases. *J Hepatol* 2017; **66**: 212-227 [PMID: 27423426 DOI: 10.1016/j.jhep.2016.07.009]

52 **Orlandi P**, Solini A, Banchi M, Brunetto MR, Cioni D, Ghiadoni L, Bocci G. Antiangiogenic Drugs in NASH: Evidence of a Possible New Therapeutic Approach. *Pharmaceuticals (Basel)* 2021; **14** [PMID: 34681219 DOI: 10.3390/ph14100995]

53 **Verhaegh P**, Wisse E, de Munck T, Greve JW, Verheij J, Riedl R, Duimel H, Masclee A, Jonkers D, Koek G. Electron microscopic observations in perfusion-fixed human non-alcoholic fatty liver disease biopsies. *Pathology* 2021; **53**: 220-228 [PMID: 33143903 DOI: 10.1016/j.pathol.2020.07.018]

54 **Hammoutene A**, Rautou PE. Role of liver sinusoidal endothelial cells in non-alcoholic fatty liver disease. *J Hepatol* 2019; **70**: 1278-1291 [PMID: 30797053 DOI: 10.1016/j.jhep.2019.02.012]

55 **Nasiri-Ansari N**, Androutsakos T, Flessa CM, Kyrou I, Siasos G, Randeva HS, Kassi E, Papavassiliou AG. Endothelial Cell Dysfunction and Nonalcoholic Fatty Liver Disease (NAFLD): A Concise Review. *Cells* 2022; **11** [PMID: 36010588 DOI: 10.3390/cells11162511]

56 **Yuzefovych LV**, Musiyenko SI, Wilson GL, Rachek LI. Mitochondrial DNA damage and dysfunction, and oxidative stress are associated with endoplasmic reticulum stress, protein degradation and apoptosis in high fat diet-induced insulin resistance mice. *PLoS One* 2013; **8**: e54059 [PMID: 23342074 DOI: 10.1371/journal.pone.0054059]

57 **Reynaert H**, Urbain D, Geerts A. Regulation of sinusoidal perfusion in portal hypertension. *Anat Rec (Hoboken)* 2008; **291**: 693-698 [PMID: 18484616 DOI: 10.1002/ar.20669]

58 **Pinzani M**, Failli P, Ruocco C, Casini A, Milani S, Baldi E, Giotti A, Gentilini P. Fat-storing cells as liver-specific pericytes. Spatial dynamics of agonist-stimulated intracellular calcium transients. *J Clin Invest* 1992; **90**: 642-646 [PMID: 1644929 DOI: 10.1172/JCI115905]

59 **Pinzani M**. Hepatic stellate (ITO) cells: expanding roles for a liver-specific pericyte. *J Hepatol* 1995; **22**: 700-706 [PMID: 7560865 DOI: 10.1016/0168-8278(95)80227-4]

60 **Povero D**, Eguchi A, Niesman IR, Andronikou N, de Mollerat du Jeu X, Mulya A, Berk M, Lazic M, Thapaliya S, Parola M, Patel HH, Feldstein AE. Lipid-induced toxicity stimulates hepatocytes to release angiogenic microparticles that require Vanin-1 for uptake by endothelial cells. *Sci Signal* 2013; **6**: ra88 [PMID: 24106341 DOI: 10.1126/scisignal.2004512]

61 **McCuskey RS**. A dynamic and static study of hepatic arterioles and hepatic sphincters. *Am J Anat* 1966; **119**: 455-477 [PMID: 5972732 DOI:

10.1002/aja.1001190307]
62 **Francque S**, Wamutu S, Chatterjee S, Van Marck E, Herman A, Ramon A, Jung A, Vermeulen W, De Winter B, Pelckmans P, Michielsen P. Non-alcoholic steatohepatitis induces non-fibrosis-related portal hypertension associated with splanchnic vasodilation and signs of a hyperdynamic circulation in vitro and in vivo in a rat model. *Liver Int* 2010; **30**: 365-375 [PMID: 19840249 DOI: 10.1111/j.1478-3231.2009.02136.x]
63 **Nababan SHH**, Lesmana CRA. Portal Hypertension in Nonalcoholic Fatty Liver Disease: From Pathogenesis to Clinical Practice. *J Clin Transl Hepatol* 2022; **10**: 979-985 [PMID: 36304507 DOI: 10.14218/JCTH.2021.00593]
64 **Iwakiri Y**, Shah V, Rockey DC. Vascular pathobiology in chronic liver disease and cirrhosis - current status and future directions. *J Hepatol* 2014; **61**: 912-924 [PMID: 24911462 DOI: 10.1016/j.jhep.2014.05.047]
65 **Rockey DC**, Weisiger RA. Endothelin induced contractility of stellate cells from normal and cirrhotic rat liver: implications for regulation of portal pressure and resistance. *Hepatology* 1996; **24**: 233-240 [PMID: 8707268 DOI: 10.1002/hep.510240137]
66 **Kaneda K**, Ekataksin W, Sogawa M, Matsumura A, Cho A, Kawada N. Endothelin-1-induced vasoconstriction causes a significant increase in portal pressure of rat liver: localized constrictive effect on the distal segment of preterminal portal venules as revealed by light and electron microscopy and serial reconstruction. *Hepatology* 1998; **27**: 735-747 [PMID: 9500702 DOI: 10.1002/hep.510270315]
67 **Wanless IR**. The Role of Vascular Injury and Congestion in the Pathogenesis of Cirrhosis: the Congestive Escalator and the Parenchymal Extinction Sequence. *Curr Hepatol Rep* 2020; **19**: 40-53 [DOI: 10.1007/s11901-020-00508-y]
68 **García-Pagán JC**, Gracia-Sancho J, Bosch J. Functional aspects on the pathophysiology of portal hypertension in cirrhosis. *J Hepatol* 2012; **57**: 458-461 [PMID: 22504334 DOI: 10.1016/j.jhep.2012.03.007]
69 **Selzner M**, Clavien PA. Fatty liver in liver transplantation and surgery. *Semin Liver Dis* 2001; **21**: 105-113 [PMID: 11296690 DOI: 10.1055/s-2001-12933]
70 **Watson CJ**, Calne RY, Padhani AR, Dixon AK. Surgical restraint in the management of liver trauma. *Br J Surg* 1991; **78**: 1071-1075 [PMID: 1933188 DOI: 10.1002/bjs.1800780913]
71 **Chatterjee S**. Endothelial Mechanotransduction, Redox Signaling and the Regulation of Vascular Inflammatory Pathways. *Front Physiol* 2018; **9**: 524 [PMID: 29930512 DOI: 10.3389/fphys.2018.00524]
72 **Tanaka K**, Joshi D, Timalsina S, Schwartz MA. Early events in endothelial flow sensing. *Cytoskeleton (Hoboken)* 2021; **78**: 217-231 [PMID: 33543538 DOI: 10.1002/cm.21652]
73 **Deng B**, Zhao Z, Kong W, Han C, Shen X, Zhou C. Biological role of matrix stiffness in tumor growth and treatment. *J Transl Med* 2022; **20**: 540 [PMID: 36419159 DOI: 10.1186/s12967-022-03768-y]
74 **Duscher D**, Maan ZN, Wong VW, Rennert RC, Januszyk M, Rodrigues M, Hu M, Whitmore AJ, Whittam AJ, Longaker MT, Gurtner GC. Mechanotransduction and fibrosis. *J Biomech* 2014; **47**: 1997-2005 [PMID: 24709567 DOI: 10.1016/j.jbiomech.2014.03.031]
75 **Martino F**, Perestrelo AR, Vinarský V, Pagliari S, Forte G. Cellular Mechanotransduction: From Tension to Function. *Front Physiol* 2018; **9**: 824 [PMID: 30026699 DOI: 10.3389/fphys.2018.00824]
76 **Elosegui-Artola A**, Oria R, Chen Y, Kosmalska A, Pérez-González C, Castro N, Zhu C, Trepat X, Roca-Cusachs P. Mechanical regulation of a molecular clutch defines force transmission and transduction in response to matrix rigidity. *Nat Cell Biol* 2016; **18**: 540-548 [PMID: 27065098 DOI: 10.1038/ncb3336]
77 **Buscemi L**, Ramonet D, Klingberg F, Formey A, Smith-Clerc J, Meister JJ, Hinz B. The single-molecule mechanics of the latent TGF-β1 complex. *Curr Biol* 2011; **21**: 2046-2054 [PMID: 22169532 DOI: 10.1016/j.cub.2011.11.037]
78 **Le Roux AL**, Quiroga X, Walani N, Arroyo M, Roca-Cusachs P. The plasma membrane as a mechanochemical transducer. *Philos Trans R Soc Lond B Biol Sci* 2019; **374**: 20180221 [PMID: 31431176 DOI: 10.1098/rstb.2018.0221]
79 **Maurer M**, Lammerding J. The Driving Force: Nuclear Mechanotransduction in Cellular Function, Fate, and Disease. *Annu Rev Biomed Eng* 2019; **21**: 443-468 [PMID: 30916994 DOI: 10.1146/annurev-bioeng-060418-052139]
80 **Maniotis AJ**, Chen CS, Ingber DE. Demonstration of mechanical connections between integrins, cytoskeletal filaments, and nucleoplasm that stabilize nuclear structure. *Proc Natl Acad Sci U S A* 1997; **94**: 849-854 [PMID: 9023345 DOI: 10.1073/pnas.94.3.849]
81 **Gupta M**, Sarangi BR, Deschamps J, Nematbakhsh Y, Callan-Jones A, Margadant F, Mège RM, Lim CT, Voituriez R, Ladoux B. Adaptive rheology and ordering of cell cytoskeleton govern matrix rigidity sensing. *Nat Commun* 2015; **6**: 7525 [PMID: 26109233 DOI: 10.1038/ncomms8525]
82 **Elosegui-Artola A**, Andreu I, Beedle AEM, Lezamiz A, Uroz M, Kosmalska AJ, Oria R, Kechagia JZ, Rico-Lastres P, Le Roux AL, Shanahan CM, Trepat X, Navajas D, Garcia-Manyes S, Roca-Cusachs P. Force Triggers YAP Nuclear Entry by Regulating Transport across Nuclear Pores. *Cell* 2017; **171**: 1397-1410.e14 [PMID: 29107331 DOI: 10.1016/j.cell.2017.10.008]
83 **Pocaterra A**, Romani P, Dupont S. YAP/TAZ functions and their regulation at a glance. *J Cell Sci* 2020; **133** [PMID: 31996398 DOI: 10.1242/jcs.230425]
84 **Yamashiro Y**, Thang BQ, Ramirez K, Shin SJ, Kohata T, Ohata S, Nguyen TAV, Ohtsuki S, Nagayama K, Yanagisawa H. Matrix mechanotransduction mediated by thrombospondin-1/integrin/YAP in the vascular remodeling. *Proc Natl Acad Sci U S A* 2020; **117**: 9896-9905 [PMID: 32321834 DOI: 10.1073/pnas.1919702117]
85 **Mannaerts I**, Leite SB, Verhulst S, Claerhout S, Eysackers N, Thoen LF, Hoorens A, Reynaert H, Halder G, van Grunsven LA. The Hippo pathway effector YAP controls mouse hepatic stellate cell activation. *J Hepatol* 2015; **63**: 679-688 [PMID: 25908270 DOI: 10.1016/j.jhep.2015.04.011]
86 **Wang X**, Zheng Z, Caviglia JM, Corey KE, Herfel TM, Cai B, Masia R, Chung RT, Lefkowitch JH, Schwabe RF, Tabas I. Hepatocyte TAZ/WWTR1 Promotes Inflammation and Fibrosis in Nonalcoholic Steatohepatitis. *Cell Metab* 2016; **24**: 848-862 [PMID: 28068223 DOI: 10.1016/j.cmet.2016.09.016]
87 **Qing J**, Ren Y, Zhang Y, Yan M, Zhang H, Wu D, Ma Y, Chen Y, Huang X, Wu Q, Mazhar M, Wang L, Liu J, Ding BS, Cao Z. Dopamine receptor D2 antagonism normalizes profibrotic macrophage-endothelial crosstalk in non-alcoholic steatohepatitis. *J Hepatol* 2022; **76**: 394-406 [PMID: 34648896 DOI: 10.1016/j.jhep.2021.09.032]
88 **Miralles F**, Posern G, Zaromytidou AI, Treisman R. Actin dynamics control SRF activity by regulation of its coactivator MAL. *Cell* 2003; **113**: 329-342 [PMID: 12732141 DOI: 10.1016/S0092-8674(03)00278-2]
89 **Wójtowicz A**, Babu SS, Li L, Gretz N, Hecker M, Cattaruzza M. Zyxin mediation of stretch-induced gene expression in human endothelial cells. *Circ Res* 2010; **107**: 898-902 [PMID: 20705921 DOI: 10.1161/CIRCRESAHA.110.227850]
90 **Huveneers S**, Danen EH. Adhesion signaling - crosstalk between integrins, Src and Rho. *J Cell Sci* 2009; **122**: 1059-1069 [PMID: 19339545 DOI: 10.1242/jcs.039446]

91 **Kechagia JZ**, Ivaska J, Roca-Cusachs P. Integrins as biomechanical sensors of the microenvironment. *Nat Rev Mol Cell Biol* 2019; **20**: 457-473 [PMID: 31182865 DOI: 10.1038/s41580-019-0134-2]

92 **Musso G**, Cassader M, Paschetta E, Gambino R. Bioactive Lipid Species and Metabolic Pathways in Progression and Resolution of Nonalcoholic Steatohepatitis. *Gastroenterology* 2018; **155**: 282-302.e8 [PMID: 29906416 DOI: 10.1053/j.gastro.2018.06.031]

93 **Mihm S**. Danger-Associated Molecular Patterns (DAMPs): Molecular Triggers for Sterile Inflammation in the Liver. *Int J Mol Sci* 2018; **19** [PMID: 30309020 DOI: 10.3390/ijms19103104]

94 **Heyens LJM**, Busschots D, Koek GH, Robaeys G, Francque S. Liver Fibrosis in Non-alcoholic Fatty Liver Disease: From Liver Biopsy to Non-invasive Biomarkers in Diagnosis and Treatment. *Front Med (Lausanne)* 2021; **8**: 615978 [PMID: 33937277 DOI: 10.3389/fmed.2021.615978]

95 **Affo S**, Yu LX, Schwabe RF. The Role of Cancer-Associated Fibroblasts and Fibrosis in Liver Cancer. *Annu Rev Pathol* 2017; **12**: 153-186 [PMID: 27959632 DOI: 10.1146/annurev-pathol-052016-100322]

96 **Guicciardi ME**, Malhi H, Mott JL, Gores GJ. Apoptosis and necrosis in the liver. *Compr Physiol* 2013; **3**: 977-1010 [PMID: 23720337 DOI: 10.1002/cphy.c120020]

97 **Malhi H**, Bronk SF, Werneburg NW, Gores GJ. Free fatty acids induce JNK-dependent hepatocyte lipoapoptosis. *J Biol Chem* 2006; **281**: 12093-12101 [PMID: 16505490 DOI: 10.1074/jbc.M510660200]

98 **Bilzer M**, Roggel F, Gerbes AL. Role of Kupffer cells in host defense and liver disease. *Liver Int* 2006; **26**: 1175-1186 [PMID: 17105582 DOI: 10.1111/j.1478-3231.2006.01342.x]

99 **Nguyen-Lefebvre AT**, Horuzsko A. Kupffer Cell Metabolism and Function. *J Enzymol Metab* 2015; **1** [PMID: 26937490]

100 **Tomita K**, Tamiya G, Ando S, Ohsumi K, Chiyo T, Mizutani A, Kitamura N, Toda K, Kaneko T, Horie Y, Han JY, Kato S, Shimoda M, Oike Y, Tomizawa M, Makino S, Ohkura T, Saito H, Kumagai N, Nagata H, Ishii H, Hibi T. Tumour necrosis factor alpha signalling through activation of Kupffer cells plays an essential role in liver fibrosis of non-alcoholic steatohepatitis in mice. *Gut* 2006; **55**: 415-424 [PMID: 16174657 DOI: 10.1136/gut.2005.071118]

101 **Van Herck MA**, Weyler J, Kwanten WJ, Dirinck EL, De Winter BY, Francque SM, Vonghia L. The Differential Roles of T Cells in Non-alcoholic Fatty Liver Disease and Obesity. *Front Immunol* 2019; **10**: 82 [PMID: 30787925 DOI: 10.3389/fimmu.2019.00082]

102 **Slevin E**, Baiocchi L, Wu N, Ekser B, Sato K, Lin E, Ceci L, Chen L, Lorenzo SR, Xu W, Kyritsi K, Meadows V, Zhou T, Kundu D, Han Y, Kennedy L, Glaser S, Francis H, Alpini G, Meng F. Kupffer Cells: Inflammation Pathways and Cell-Cell Interactions in Alcohol-Associated Liver Disease. *Am J Pathol* 2020; **190**: 2185-2193 [PMID: 32919978 DOI: 10.1016/j.ajpath.2020.08.014]

103 **Rojkind M**, Giambrone MA, Biempica L. Collagen types in normal and cirrhotic liver. *Gastroenterology* 1979; **76**: 710-719 [PMID: 421999]

104 **Miao CG**, Yang YY, He X, Huang C, Huang Y, Zhang L, Lv XW, Jin Y, Li J. Wnt signaling in liver fibrosis: progress, challenges and potential directions. *Biochimie* 2013; **95**: 2326-2335 [PMID: 24036368 DOI: 10.1016/j.biochi.2013.09.003]

105 **Ramzy MM**, Abdelghany HM, Zenhom NM, El-Tahawy NF. Effect of histone deacetylase inhibitor on epithelial-mesenchymal transition of liver fibrosis. *IUBMB Life* 2018; **70**: 511-518 [PMID: 29601129 DOI: 10.1002/iub.1742]

106 **Orrego H**, Blendis LM, Crossley IR, Medline A, Macdonald A, Ritchie S, Israel Y. Correlation of intrahepatic pressure with collagen in the Disse space and hepatomegaly in humans and in the rat. *Gastroenterology* 1981; **80**: 546-556 [PMID: 7450445]

107 **Mendes FD**, Suzuki A, Sanderson SO, Lindor KD, Angulo P. Prevalence and indicators of portal hypertension in patients with nonalcoholic fatty liver disease. *Clin Gastroenterol Hepatol* 2012; **10**: 1028-33.e2 [PMID: 22610002 DOI: 10.1016/j.cgh.2012.05.008]

108 **Yeh MM**, Brunt EM. Pathology of nonalcoholic fatty liver disease. *Am J Clin Pathol* 2007; **128**: 837-847 [PMID: 17951208 DOI: 10.1309/RTPM1PY6YGBL2G2R]

109 **Friedman SL**. Hepatic stellate cells: protean, multifunctional, and enigmatic cells of the liver. *Physiol Rev* 2008; **88**: 125-172 [PMID: 18195085 DOI: 10.1152/physrev.00013.2007]

110 **Shah V**. Molecular mechanisms of increased intrahepatic resistance in portal hypertension. *J Clin Gastroenterol* 2007; **41** Suppl 3: S259-S261 [PMID: 17975474 DOI: 10.1097/MCG.0b013e318150d0e1]

111 **Gracia-Sancho J**, Marrone G, Fernández-Iglesias A. Hepatic microcirculation and mechanisms of portal hypertension. *Nat Rev Gastroenterol Hepatol* 2019; **16**: 221-234 [PMID: 30568278 DOI: 10.1038/s41575-018-0097-3]

112 **Francque S**, Verrijken A, Mertens I, Hubens G, Van Marck E, Pelckmans P, Michielsen P, Van Gaal L. Visceral adiposity and insulin resistance are independent predictors of the presence of non-cirrhotic NAFLD-related portal hypertension. *Int J Obes (Lond)* 2011; **35**: 270-278 [PMID: 20661251 DOI: 10.1038/ijo.2010.134]

113 **Vonghia L**, Magrone T, Verrijken A, Michielsen P, Van Gaal L, Jirillo E, Francque S. Peripheral and Hepatic Vein Cytokine Levels in Correlation with Non-Alcoholic Fatty Liver Disease (NAFLD)-Related Metabolic, Histological, and Haemodynamic Features. *PLoS One* 2015; **10**: e0143380 [PMID: 26599575 DOI: 10.1371/journal.pone.0143380]

114 **Rodrigues SG**, Montani M, Guixé-Muntet S, De Gottardi A, Berzigotti A, Bosch J. Patients With Signs of Advanced Liver Disease and Clinically Significant Portal Hypertension Do Not Necessarily Have Cirrhosis. *Clin Gastroenterol Hepatol* 2019; **17**: 2101-2109.e1 [PMID: 30625404 DOI: 10.1016/j.cgh.2018.12.038]

115 **Moga L**, Laroyenne A, Larrue H, Bureau C, Rautou PE. Patients with NAFLD do not have severe portal hypertension in the absence of cirrhosis. *J Hepatol* 2021; **74**: 1269-1270 [PMID: 33340573 DOI: 10.1016/j.jhep.2020.10.011]

116 **Berzigotti A**, Seijo S, Arena U, Abraldes JG, Vizzutti F, García-Pagán JC, Pinzani M, Bosch J. Elastography, spleen size, and platelet count identify portal hypertension in patients with compensated cirrhosis. *Gastroenterology* 2013; **144**: 102-111.e1 [PMID: 23058320 DOI: 10.1053/j.gastro.2012.10.001]

117 **Cacciottolo TM**, Kumar A, Godfrey EM, Davies SE, Allison M. Spleen Size Does Not Correlate With Histological Stage of Liver Disease in People With Nonalcoholic Fatty Liver Disease. *Clin Gastroenterol Hepatol* 2023; **21**: 535-537.e1 [PMID: 35032633 DOI: 10.1016/j.cgh.2022.01.007]

118 **Tsushima Y**, Endo K. Spleen enlargement in patients with nonalcoholic fatty liver: correlation between degree of fatty infiltration in liver and size of spleen. *Dig Dis Sci* 2000; **45**: 196-200 [PMID: 10695635 DOI: 10.1023/A:1005446418589]

119 **Chow KU**, Luxembourg B, Seifried E, Bonig H. Spleen Size Is Significantly Influenced by Body Height and Sex: Establishment of Normal Values for Spleen Size at US with a Cohort of 1200 Healthy Individuals. *Radiology* 2016; **279**: 306-313 [PMID: 26509293 DOI: 10.1148/radiol.2015150887]

120 **Abraldes JG**, Sarlieve P, Tandon P. Measurement of portal pressure. *Clin Liver Dis* 2014; **18**: 779-792 [PMID: 25438283 DOI: 10.1016/j.cld.2014.07.002]

121 **Silva-Junior G**, Baiges A, Turon F, Torres F, Hernández-Gea V, Bosch J, García-Pagán JC. The prognostic value of hepatic venous pressure

gradient in patients with cirrhosis is highly dependent on the accuracy of the technique. *Hepatology* 2015; **62**: 1584-1592 [PMID: 26238376 DOI: 10.1002/hep.28031]

122 **Ripoll C**, Groszmann R, Garcia-Tsao G, Grace N, Burroughs A, Planas R, Escorsell A, Garcia-Pagan JC, Makuch R, Patch D, Matloff DS, Bosch J; Portal Hypertension Collaborative Group. Hepatic venous pressure gradient predicts clinical decompensation in patients with compensated cirrhosis. *Gastroenterology* 2007; **133**: 481-488 [PMID: 17681169 DOI: 10.1053/j.gastro.2007.05.024]

123 **Bosch J**, Abraldes JG, Berzigotti A, García-Pagan JC. The clinical use of HVPG measurements in chronic liver disease. *Nat Rev Gastroenterol Hepatol* 2009; **6**: 573-582 [PMID: 19724251 DOI: 10.1038/nrgastro.2009.149]

124 **Bassegoda O**, Olivas P, Turco L, Mandorfer M, Serra-Burriel M, Tellez L, Kwanten W, Laroyenne A, Farcau O, Alvarado E, Moga L, Vuille-Lessard E, Fortea JI, Ibañez L, Tosetti G, Vanwolleghem T, Larrue H, Burgos-Santamaría D, Stefanescu H, Paternostro R, Cippitelli A, Lens S, Augustin S, Llop E, Laleman W, Trebicka J, Chang J, Masnou H, Zipprich A, Miceli F, Semmler G, Forns X, Primignani M, Bañares R, Puente A, Berzigotti A, Rautou PE, Villanueva C, Ginès P, Garcia-Pagan JC, Procopet B, Bureau C, Albillos A, Francque S, Reiberger T, Schepis F, Graupera I, Hernandez-Gea V. Decompensation in Advanced Nonalcoholic Fatty Liver Disease May Occur at Lower Hepatic Venous Pressure Gradient Levels Than in Patients With Viral Disease. *Clin Gastroenterol Hepatol* 2022; **20**: 2276-2286.e6 [PMID: 34688952 DOI: 10.1016/j.cgh.2021.10.023]

125 **Ferrusquía-Acosta J**, Bassegoda O, Turco L, Reverter E, Pellone M, Bianchini M, Pérez-Campuzano V, Ripoll E, García-Criado Á, Graupera I, García-Pagán JC, Schepis F, Senzolo M, Hernández-Gea V. Agreement between wedged hepatic venous pressure and portal pressure in non-alcoholic steatohepatitis-related cirrhosis. *J Hepatol* 2021; **74**: 811-818 [PMID: 33068638 DOI: 10.1016/j.jhep.2020.10.003]

126 **Sanyal AJ**, Harrison SA, Ratziu V, Abdelmalek MF, Diehl AM, Caldwell S, Shiffman ML, Aguilar Schall R, Jia C, McColgan B, Djedjos CS, McHutchison JG, Subramanian GM, Myers RP, Younossi Z, Muir AJ, Afdhal NH, Bosch J, Goodman Z. The Natural History of Advanced Fibrosis Due to Nonalcoholic Steatohepatitis: Data From the Simtuzumab Trials. *Hepatology* 2019; **70**: 1913-1927 [PMID: 30993748 DOI: 10.1002/hep.30664/suppinfo]

127 **Gadd VL**, Skoien R, Powell EE, Fagan KJ, Winterford C, Horsfall L, Irvine K, Clouston AD. The portal inflammatory infiltrate and ductular reaction in human nonalcoholic fatty liver disease. *Hepatology* 2014; **59**: 1393-1405 [PMID: 24254368 DOI: 10.1002/hep.26937]

128 **Bedossa P**, Patel K. Biopsy and Noninvasive Methods to Assess Progression of Nonalcoholic Fatty Liver Disease. *Gastroenterology* 2016; **150**: 1811-1822.e4 [PMID: 27003601 DOI: 10.1053/j.gastro.2016.03.008]

129 **PATON A**, REYNOLDS TB, SHERLOCK S. Assessment of portal venous hypertension by catheterisation of hepatic vein. *Lancet* 1953; **1**: 918-921 [PMID: 13045450 DOI: 10.1016/S0140-6736(53)92060-1]

130 **Bosch J**, Garcia-Pagán JC, Berzigotti A, Abraldes JG. Measurement of portal pressure and its role in the management of chronic liver disease. *Semin Liver Dis* 2006; **26**: 348-362 [PMID: 17051449 DOI: 10.1055/s-2006-951603]

131 **Groszmann RJ**, Wongcharatrawee S. The hepatic venous pressure gradient: anything worth doing should be done right. *Hepatology* 2004; **39**: 280-282 [PMID: 14767976 DOI: 10.1002/hep.20062]

132 **Huang JY**, Samarasena JB, Tsujino T, Chang KJ. EUS-guided portal pressure gradient measurement with a novel 25-gauge needle device versus standard transjugular approach: a comparison animal study. *Gastrointest Endosc* 2016; **84**: 358-362 [PMID: 26945557 DOI: 10.1016/j.gie.2016.02.032]

133 **Lai L**, Poneros J, Santilli J, Brugge W. EUS-guided portal vein catheterization and pressure measurement in an animal model: a pilot study of feasibility. *Gastrointest Endosc* 2004; **59**: 280-283 [PMID: 14745408 DOI: 10.1016/S0016-5107(03)02544-6]

134 **Huang JY**, Samarasena JB, Tsujino T, Lee J, Hu KQ, McLaren CE, Chen WP, Chang KJ. EUS-guided portal pressure gradient measurement with a simple novel device: a human pilot study. *Gastrointest Endosc* 2017; **85**: 996-1001 [PMID: 27693644 DOI: 10.1016/j.gie.2016.09.026]

135 **Boyer TD**, Triger DR, Horisawa M, Redeker AG, Reynolds TB. Direct transhepatic measurement of portal vein pressure using a thin needle. Comparison with wedged hepatic vein pressure. *Gastroenterology* 1977; **72**: 584-589 [PMID: 838210]

136 **Grgurevic I**, Madir A, Trkulja V, Bozin T, Aralica G, Podrug K, Mikolaševic I, Tsochatzis E, O'Beirne J, Pinzani M. Assessment of clinically significant portal hypertension by two-dimensional shear wave elastography. *Eur J Clin Invest* 2022; **52**: e13750 [PMID: 35040495 DOI: 10.1111/eci.13750]

137 **Thiele M**, Hugger MB, Kim Y, Rautou PE, Elkrief L, Jansen C, Verlinden W, Allegretti G, Israelsen M, Stefanescu H, Piscaglia F, García-Pagán JC, Franque S, Berzigotti A, Castera L, Jeong WK, Trebicka J, Krag A. 2D shear wave liver elastography by Aixplorer to detect portal hypertension in cirrhosis: An individual patient data meta-analysis. *Liver Int* 2020; **40**: 1435-1446 [PMID: 32180327 DOI: 10.1111/Liv.14439]

138 **Pons M**, Augustin S, Scheiner B, Guillaume M, Rosselli M, Rodrigues SG, Stefanescu H, Ma MM, Mandorfer M, Mergeay-Fabre M, Procopet B, Schwabl P, Ferlitsch A, Semmler G, Berzigotti A, Tsochatzis E, Bureau C, Reiberger T, Bosch J, Abraldes JG, Genescà J. Noninvasive Diagnosis of Portal Hypertension in Patients With Compensated Advanced Chronic Liver Disease. *Am J Gastroenterol* 2021; **116**: 723-732 [PMID: 33982942 DOI: 10.14309/ajg.0000000000000994]

139 **de Franchis R**, Bosch J, Garcia-Tsao G, Reiberger T, Ripoll C; Baveno VII Faculty. Baveno VII - Renewing consensus in portal hypertension. *J Hepatol* 2022; **76**: 959-974 [PMID: 35120736 DOI: 10.1016/j.jhep.2021.12.022]

140 **Podrug K**, Trkulja V, Zelenika M, Bokun T, Madir A, Kanizaj TF, O'Beirne J, Grgurevic I. Validation of the New Diagnostic Criteria for Clinically Significant Portal Hypertension by Platelets and Elastography. *Dig Dis Sci* 2022; **67**: 3327-3332 [PMID: 34739624 DOI: 10.1007/s10620-021-07277-8]

141 **de Franchis R**; Baveno VI Faculty. Expanding consensus in portal hypertension: Report of the Baveno VI Consensus Workshop: Stratifying risk and individualizing care for portal hypertension. *J Hepatol* 2015; **63**: 743-752 [PMID: 26047908 DOI: 10.1016/j.jhep.2015.05.022]

142 **Colecchia A**, Montrone L, Scaioli E, Bacchi-Reggiani ML, Colli A, Casazza G, Schiumerini R, Turco L, Di Biase AR, Mazzella G, Marzi L, Arena U, Pinzani M, Festi D. Measurement of spleen stiffness to evaluate portal hypertension and the presence of esophageal varices in patients with HCV-related cirrhosis. *Gastroenterology* 2012; **143**: 646-654 [PMID: 22643348 DOI: 10.1053/j.gastro.2012.05.035]

143 **Colecchia A**, Colli A, Casazza G, Mandolesi D, Schiumerini R, Reggiani LB, Marasco G, Taddia M, Lisotti A, Mazzella G, Di Biase AR, Golfieri R, Pinzani M, Festi D. Spleen stiffness measurement can predict clinical complications in compensated HCV-related cirrhosis: a prospective study. *J Hepatol* 2014; **60**: 1158-1164 [PMID: 24607624 DOI: 10.1016/j.jhep.2014.02.024]

144 **Elkrief L**, Rautou PE, Ronot M, Lambert S, Dioguardi Burgio M, Francoz C, Plessier A, Durand F, Valla D, Lebrec D, Vilgrain V, Castéra L. Prospective comparison of spleen and liver stiffness by using shear-wave and transient elastography for detection of portal hypertension in cirrhosis. *Radiology* 2015; **275**: 589-598 [PMID: 25469784 DOI: 10.1148/radiol.14141210]

145 **Song J**, Huang J, Huang H, Liu S, Luo Y. Performance of spleen stiffness measurement in prediction of clinical significant portal hypertension: A meta-analysis. *Clin Res Hepatol Gastroenterol* 2018; **42**: 216-226 [PMID: 29223365 DOI: 10.1016/j.clinre.2017.11.002]

146 **Dajti E**, Ravaioli F, Zykus R, Rautou PE, Elkrief L, Grgurevic I, Stefanescu H, Hirooka M, Fraquelli M, Rosselli M, Chang PEJ, Piscaglia F,

Reiberger T, Llop E, Mueller S, Marasco G, Berzigotti A, Colli A, Festi D, Colecchia A; Spleen Stiffness—IPD-MA Study Group. Accuracy of spleen stiffness measurement for the diagnosis of clinically significant portal hypertension in patients with compensated advanced chronic liver disease: a systematic review and individual patient data meta-analysis. *Lancet Gastroenterol Hepatol* 2023; **8**: 816-828 [PMID: 37478880 DOI: 10.1016/S2468-1253(23)00150-4]

147 **Eisenbrey JR**, Dave JK, Halldorsdottir VG, Merton DA, Miller C, Gonzalez JM, Machado P, Park S, Dianis S, Chalek CL, Kim CE, Baliff JP, Thomenius KE, Brown DB, Navarro V, Forsberg F. Chronic liver disease: noninvasive subharmonic aided pressure estimation of hepatic venous pressure gradient. *Radiology* 2013; **268**: 581-588 [PMID: 23525208 DOI: 10.1148/radiol.13121769]

148 **Chang X**, Bian H, Xia M, Zhu X, Sun X, Yang X, Gao J, Lin H, Yan H, Gao X. Postprandial glucose is correlated with an increasing risk of liver fibrosis in Chinese patients with nonalcoholic fatty liver disease. *Diabetes Metab* 2022; **48**: 101377 [PMID: 35858659 DOI: 10.1016/j.diabet.2022.101377]

149 **Grandt J**, Jensen AH, Werge MP, Rashu EB, Møller A, Junker AE, Hobolth L, Mortensen C, Johansen CD, Vyberg M, Serizawa RR, Møller S, Gluud LL, Wewer Albrechtsen NJ. Postprandial dysfunction in fatty liver disease. *Physiol Rep* 2023; **11**: e15653 [PMID: 37078380 DOI: 10.14814/phy2.15653]

150 **Jesrani G**, Gupta M, Kaur J, Kaur N, Lehl SS, Singh R. One-Hour Postload Plasma Glucose in Obese Indian Adults with Nonalcoholic Fatty Liver Disease: An Observational Study from North India. *Indian J Endocrinol Metab* 2021; **25**: 450-455 [PMID: 35300452 DOI: 10.4103/ijem.ijem_357_21]

151 **Ganesan R**, Gupta H, Jeong JJ, Sharma SP, Won SM, Oh KK, Yoon SJ, Kim DJ, Suk KT. A metabolomics approach to the validation of predictive metabolites and phenotypic expression in non-alcoholic fatty liver disease. *Life Sci* 2023; **322**: 121626 [PMID: 37003543 DOI: 10.1016/j.lfs.2023.121626]

152 **McGlinchey AJ**, Govaere O, Geng D, Ratziu V, Allison M, Bousier J, Petta S, de Oliviera C, Bugianesi E, Schattenberg JM, Daly AK, Hyötyläinen T, Anstee QM, Orešič M. Metabolic signatures across the full spectrum of non-alcoholic fatty liver disease. *JHEP Rep* 2022; **4**: 100477 [PMID: 35434590 DOI: 10.1016/j.jhepr.2022.100477]

153 **D'Amico G**, Pasta L, Morabito A, D'Amico M, Caltagirone M, Malizia G, Tinè F, Giannuoli G, Traina M, Vizzini G, Politi F, Luca A, Virdone R, Licata A, Pagliaro L. Competing risks and prognostic stages of cirrhosis: a 25-year inception cohort study of 494 patients. *Aliment Pharmacol Ther* 2014; **39**: 1180-1193 [PMID: 24654740 DOI: 10.1111/apt.12721]

154 **Wongcharatrawee S**, Groszmann R. Hemodynamic assessment in clinical practice in portal hypertensive cirrhotics. *Ann Gastroenterol* 2001; **14**: 158-165

155 **North Italian Endoscopic Club for the Study and Treatment of Esophageal Varices**. Prediction of the first variceal hemorrhage in patients with cirrhosis of the liver and esophageal varices. A prospective multicenter study. *N Engl J Med* 1988; **319**: 983-989 [PMID: 3262200 DOI: 10.1056/NEJM198810133191505]

156 **de Franchis R**; Baveno V Faculty. Revising consensus in portal hypertension: report of the Baveno V consensus workshop on methodology of diagnosis and therapy in portal hypertension. *J Hepatol* 2010; **53**: 762-768 [PMID: 20638742 DOI: 10.1016/j.jhep.2010.06.004]

157 **Garcia-Tsao G**, Abraldes JG, Berzigotti A, Bosch J. Portal hypertensive bleeding in cirrhosis: Risk stratification, diagnosis, and management: 2016 practice guidance by the American Association for the study of liver diseases. *Hepatology* 2017; **65**: 310-335 [PMID: 27786365 DOI: 10.1002/hep.28906]

158 **European Association for Study of Liver**; Asociacion Latinoamericana para el Estudio del Higado. EASL-ALEH Clinical Practice Guidelines: Non-invasive tests for evaluation of liver disease severity and prognosis. *J Hepatol* 2015; **63**: 237-264 [PMID: 25911335 DOI: 10.1016/j.jhep.2015.04.006]

159 **Augustin S**, Pons M, Maurice JB, Bureau C, Stefanescu H, Ney M, Blasco H, Procopet B, Tsochatzis E, Westbrook RH, Bosch J, Berzigotti A, Abraldes JG, Genescà J. Expanding the Baveno VI criteria for the screening of varices in patients with compensated advanced chronic liver disease. *Hepatology* 2017; **66**: 1980-1988 [PMID: 28696510 DOI: 10.1002/hep.29363]

160 **Petta S**, Sebastiani G, Bugianesi E, Viganò M, Wong VW, Berzigotti A, Fracanzani AL, Anstee QM, Marra F, Barbara M, Calvaruso V, Cammà C, Di Marco V, Craxì A, de Ledinghen V. Non-invasive prediction of esophageal varices by stiffness and platelet in non-alcoholic fatty liver disease cirrhosis. *J Hepatol* 2018; **69**: 878-885 [PMID: 29802949 DOI: 10.1016/j.jhep.2018.05.019]

161 **de Franchis R**, Krag A. Ruling out esophageal varices in NAFLD cirrhosis: Can we do without endoscopy? *J Hepatol* 2018; **69**: 769-771 [PMID: 30227915 DOI: 10.1016/j.jhep.2018.06.013]

162 **Zheng KI**, Liu C, Li J, Zhao L, Zheng MH, Wang F, Qi X. Validation of Baveno VI and expanded Baveno VI criteria to identify high-risk varices in patients with MAFLD-related compensated cirrhosis. *J Hepatol* 2020; **73**: 1571-1573 [PMID: 32972730 DOI: 10.1016/j.jhep.2020.06.042]

163 **Petta S**, Wong VW, Cammà C, Hiriart JB, Wong GL, Marra F, Vergniol J, Chan AW, Di Marco V, Merrouche W, Chan HL, Barbara M, Le-Bail B, Arena U, Craxì A, de Ledinghen V. Improved noninvasive prediction of liver fibrosis by liver stiffness measurement in patients with nonalcoholic fatty liver disease accounting for controlled attenuation parameter values. *Hepatology* 2017; **65**: 1145-1155 [PMID: 27639088 DOI: 10.1002/hep.28843]

164 **Eddowes PJ**, Sasso M, Allison M, Tsochatzis E, Anstee QM, Sheridan D, Guha IN, Cobbold JF, Deeks JJ, Paradis V, Bedossa P, Newsome PN. Accuracy of FibroScan Controlled Attenuation Parameter and Liver Stiffness Measurement in Assessing Steatosis and Fibrosis in Patients With Nonalcoholic Fatty Liver Disease. *Gastroenterology* 2019; **156**: 1717-1730 [PMID: 30689971 DOI: 10.1053/j.gastro.2019.01.042]

165 **Colecchia A**, Ravaioli F, Marasco G, Colli A, Dajti E, Di Biase AR, Bacchi Reggiani ML, Berzigotti A, Pinzani M, Festi D. A combined model based on spleen stiffness measurement and Baveno VI criteria to rule out high-risk varices in advanced chronic liver disease. *J Hepatol* 2018; **69**: 308-317 [PMID: 29729368 DOI: 10.1016/j.jhep.2018.04.023]

166 **Schierwagen R**, Klein S, Uschner F, Trebicka J. Novel Targets and Drug Development in Portal Hypertension. *Curr Hepatol Rep* 2019; **18**: 187-196 [DOI: 10.1007/s11901-019-00462-4]

167 **Reiberger T**, Ulbrich G, Ferlitsch A, Payer BA, Schwabl P, Pinter M, Heinisch BB, Trauner M, Kramer L, Peck-Radosavljevic M; Vienna Hepatic Hemodynamic Lab. Carvedilol for primary prophylaxis of variceal bleeding in cirrhotic patients with haemodynamic non-response to propranolol. *Gut* 2013; **62**: 1634-1641 [PMID: 23250049 DOI: 10.1136/gutjnl-2012-304038]

168 **Brusilovskaya K**, Königshofer P, Schwabl P, Reiberger T. Vascular Targets for the Treatment of Portal Hypertension. *Semin Liver Dis* 2019; **39**: 483-501 [PMID: 31315135 DOI: 10.1055/s-0039-1693115]

169 **Coriat R**, Gouya H, Mir O, Ropert S, Vignaux O, Chaussade S, Sogni P, Pol S, Blanchet B, Legmann P, Goldwasser F. Reversible decrease of portal venous flow in cirrhotic patients: a positive side effect of sorafenib. *PLoS One* 2011; **6**: e16978 [PMID: 21340026 DOI: 10.1371/journal.pone.0016978]

170 **Pinter M**, Sieghart W, Reiberger T, Rohr-Udilova N, Ferlitsch A, Peck-Radosavljevic M. The effects of sorafenib on the portal hypertensive syndrome in patients with liver cirrhosis and hepatocellular carcinoma--a pilot study. *Aliment Pharmacol Ther* 2012; **35**: 83-91 [PMID: 22032637 DOI: 10.1111/j.1365-2036.2011.04896.x]

171 **Li J**, Kuruba R, Wilson A, Gao X, Zhang Y, Li S. Inhibition of endothelin-1-mediated contraction of hepatic stellate cells by FXR ligand. *PLoS One* 2010; **5**: e13955 [PMID: 21085652 DOI: 10.1371/journal.pone.0013955]

172 **Verbeke L**, Farre R, Trebicka J, Komuta M, Roskams T, Klein S, Elst IV, Windmolders P, Vanuytsel T, Nevens F, Laleman W. Obeticholic acid, a farnesoid X receptor agonist, improves portal hypertension by two distinct pathways in cirrhotic rats. *Hepatology* 2014; **59**: 2286-2298 [PMID: 24259407 DOI: 10.1002/hep.26939]

173 **Mantovani A**, Dalbeni A. Treatments for NAFLD: State of Art. *Int J Mol Sci* 2021; **22** [PMID: 33652942 DOI: 10.3390/ijms22052350]

World Journal of Gastroenterology

Submit a Manuscript: https://www.f6publishing.com

World J Gastroenterol 2024 January 28; 30(4): 308-317

DOI: 10.3748/wjg.v30.i4.308

ISSN 1007-9327 (print) ISSN 2219-2840 (online)

ORIGINAL ARTICLE

Retrospective Study

Value of multiple models of diffusion-weighted imaging to predict hepatic lymph node metastases in colorectal liver metastases patients

Hai-Bin Zhu, Bo Zhao, Xiao-Ting Li, Xiao-Yan Zhang, Qian Yao, Ying-Shi Sun

Specialty type: Gastroenterology and hepatology

Provenance and peer review: Unsolicited article; Externally peer reviewed.

Peer-review model: Single blind

Peer-review report's scientific quality classification

Grade A (Excellent): 0
Grade B (Very good): B, B
Grade C (Good): 0
Grade D (Fair): 0
Grade E (Poor): 0

P-Reviewer: Koehler H, Germany; Padilla M, Latvia

Received: November 6, 2023
Peer-review started: November 6, 2023
First decision: November 30, 2023
Revised: December 15, 2023
Accepted: January 10, 2024
Article in press: January 10, 2024
Published online: January 28, 2024

Hai-Bin Zhu, Bo Zhao, Xiao-Ting Li, Xiao-Yan Zhang, Ying-Shi Sun, Key Laboratory of Carcinogenesis and Translational Research (Ministry of Education/Beijing), Department of Radiology, Peking University Cancer Hospital and Institute, Beijing 100142, China

Qian Yao, Key Laboratory of Carcinogenesis and Translational Research (Ministry of Education/Beijing), Department of Pathology, Peking University Cancer Hospital and Institute, Beijing 100142, China

Corresponding author: Ying-Shi Sun, MD, Chief Physician, Professor, Key Laboratory of Carcinogenesis and Translational Research (Ministry of Education/Beijing), Department of Radiology, Peking University Cancer Hospital and Institute, No. 52 Fucheng Road, Haidian District, Beijing 100142, China. sys27@163.com

Abstract

BACKGROUND

About 10%-31% of colorectal liver metastases (CRLM) patients would concomitantly show hepatic lymph node metastases (LNM), which was considered as sign of poor biological behavior and a relative contraindication for liver resection. Up to now, there's still lack of reliable preoperative methods to assess the status of hepatic lymph nodes in patients with CRLM, except for pathology examination of lymph node after resection.

AIM

To compare the ability of mono-exponential, bi-exponential, and stretched-exponential diffusion-weighted imaging (DWI) models in distinguishing between benign and malignant hepatic lymph nodes in patients with CRLM who received neoadjuvant chemotherapy prior to surgery.

METHODS

In this retrospective study, 97 CRLM patients with pathologically confirmed hepatic lymph node status underwent magnetic resonance imaging, including DWI with ten b values before and after chemotherapy. Various parameters, such as the apparent diffusion coefficient from the mono-exponential model, and the true diffusion coefficient, the pseudo-diffusion coefficient, and the perfusion fraction derived from the intravoxel incoherent motion model, along with distributed diffusion coefficient (DDC) and α from the stretched-exponential

model (SEM), were measured. The parameters before and after chemotherapy were compared between positive and negative hepatic lymph node groups. A nomogram was constructed to predict the hepatic lymph node status. The reliability and agreement of the measurements were assessed using the coefficient of variation and intraclass correlation coefficient.

RESULTS

Multivariate analysis revealed that the pre-treatment DDC value and the short diameter of the largest lymph node after treatment were independent predictors of metastatic hepatic lymph nodes. A nomogram combining these two factors demonstrated excellent performance in distinguishing between benign and malignant lymph nodes in CRLM patients, with an area under the curve of 0.873. Furthermore, parameters from SEM showed substantial repeatability.

CONCLUSION

The developed nomogram, incorporating the pre-treatment DDC and the short axis of the largest lymph node, can be used to predict the presence of hepatic LNM in CRLM patients undergoing chemotherapy before surgery. This nomogram was proven to be more valuable, exhibiting superior diagnostic performance compared to quantitative parameters derived from multiple b values of DWI. The nomogram can serve as a preoperative assessment tool for determining the status of hepatic lymph nodes and aiding in the decision-making process for surgical treatment in CRLM patients.

Key Words: Colorectal cancer; Individualized treatment; Diffusion magnetic resonance imaging; Intravoxel incoherent motion; Liver

Core Tip: This study compared the diagnostic effectiveness of mono-exponential, bi-exponential, and stretched exponential Diffusion-weighted magnetic resonance imaging in predicting hepatic lymph node metastases (LNM) in patients with colorectal liver metastases after chemotherapy. Our finding indicated that only the pre-treatment distributed diffusion coefficient value and the short diameter of the largest lymph node after treatment were independent predictors of hepatic LNM. We developed a nomogram incorporating these two factors to non-invasively and individually predict the status of hepatic lymph nodes, demonstrating significant potential in surgical planning and assessing high-risk patients.

Citation: Zhu HB, Zhao B, Li XT, Zhang XY, Yao Q, Sun YS. Value of multiple models of diffusion-weighted imaging to predict hepatic lymph node metastases in colorectal liver metastases patients. *World J Gastroenterol* 2024; 30(4): 308-317
URL: https://www.wjgnet.com/1007-9327/full/v30/i4/308.htm
DOI: https://dx.doi.org/10.3748/wjg.v30.i4.308

INTRODUCTION

Colorectal carcinoma ranks as the most prevalent digestive tumors globally, with over 50% of patients developing colorectal liver metastases (CRLM) either at diagnosis (synchronous metastases) or during follow-up (metachronous metastases)[1]. Currently, the preferred approach in standard treatment guidelines involves perioperative chemotherapy combined with surgical resection, particularly when achieving complete resection with sufficient residual liver parenchyma is feasible[2,3]. Approximately 10%-31% of CRLM patients exhibit hepatic lymph node metastases (LNM), representing an adverse prognostic factor with significant impact on outcomes[4,5]. Surgery remains the sole potentially curative therapy if LNM are confined to the hepatic pedicle, although this procedure may be associated with potential postoperative complications, such as bleeding, lymphatic leakage, and ischemic bile duct stricture[6,7].

The gold standard for evaluating LNM still relies on histopathological assessment post-operation. Currently, there is inconsistency in the indications for lymphadenectomy in CRLM, partly due to the challenge of preoperatively predicting LNM. For instance, Grobmyer *et al*[8] examined 100 patients with hepatic lymph nodes undergoing resection for primary and metastatic hepatic malignancies. They found that both CT and intraoperative clinical palpation had a high negative predictive value (NPV = 95% and 99%, respectively) with a low positive predictive value (PPV = 30% and 39%, respectively). Similarly, Rau *et al*[9] discovered that a short diameter of lymph nodes larger than 15 mm and a morphologically round shape on computed tomography (CT) had a high NPV of 85% but a relatively low PPV of 43% for LNM. Intriguingly, up to 27% of patients with confirmed pathological LNM were not initially suspected using a combination of CT and intraoperative examination. Therefore, there is a crucial need for reliable predictors of LNM in CRLM before surgery to precisely guide individual decision-making and prevent overtreatment in low-risk patients.

Diffusion-weighted imaging (DWI) has undergone extensive investigation for its utility in cancer detection, treatment response assessment, and prognosis evaluation[10-12]. The apparent diffusion coefficient (ADC), derived from DWI,

exhibits promising capabilities in distinguishing lymph nodes, providing a noninvasive assessment of the microscopic random Brownian motion of water molecules in biological tissues. For instance, Sumi *et al*[13] observed higher ADC values in metastatic lymph nodes compared to benign non-metastatic lymph nodes, whereas Abdel Razek *et al*[14] and Eiber *et al*[15] reported lower ADC values in metastatic lymph nodes. This inconsistency may arise from the mono-exponential decay formula used to calculate ADC values, assuming tissue homogeneity and water molecule movement with a Gaussian distribution. Intravoxel incoherent motion (IVIM) is a technique capable of potentially differentiating perfusion components from the pure diffusion of water molecules using a biexponential model. This model allows for the quantification of three parameters: The true diffusion coefficient (D), the pseudo-diffusion coefficient (D*), and the perfusion fraction (f). Consequently, parameters obtained from the IVIM model have demonstrated superior diagnostic performance compared to traditional ADC in differentiating hepatic lesions in previous studies[16,17]. More recently, Bennett *et al*[18] introduced the stretched-exponential model (SEM), providing an alternative approach to quantify intravoxel heterogeneity. The SEM employs two parameters: The distributed diffusion coefficient (DDC) and the intravoxel water diffusion heterogeneity (α). However, to date, there remains a paucity of studies comparing functional magnetic resonance imaging (MRI) parameters derived from different models to determine the status of hepatic lymph nodes in CRLM patients.

The objective of this study was to assess the diagnostic accuracy of three mathematical models of DWI in distinguishing between benign and malignant hepatic lymph nodes in CRLM patients who underwent chemotherapy prior to surgery.

MATERIALS AND METHODS

Study participants

This retrospective study protocol received approval from the Medical Ethics Committee of Beijing Cancer Hospital, and informed consent was waived.

CRLM patients with a pathologic diagnosis of hepatic lymph nodes in our hospital between January 2015 and January 2023 were included in this study. Patients had to undergo at least two cycles of neoadjuvant chemotherapy and undergo MRI examinations before neoadjuvant chemotherapy (pre-treatment point) and within 1 mo before surgery (post-treatment point). Exclusion criteria were: (1) Patients who underwent hepatectomy without hepatic lymph node resection; (2) Patients without measurable hepatic lymph nodes > 5 mm on the baseline MRI; and (3) Patients without multiple b-values of DWI sequence or insufficient quality of DWI for analysis. A total of 97 patients were enrolled in this study.

MRI protocol

All patients underwent MRI examinations using a 1.5T MRI device (Signa Excite II; GE Healthcare, Milwaukee, WI, United States) equipped with an 8-channel phased array body coil. The imaging protocol included axial T2-weighted imaging (T2WI) with fat saturation, multiple b-values of DWI, and dynamic contrast-enhanced (DCE) MRI sequences. A respiratory-triggered single-shot echo planar imaging sequence was employed for DWI, with b-values of 0, 20, 50, 100, 200, 600, 800, 1000, 1200, and 1500 s/mm^2, respectively. The DWI sequence parameters were: Repetition time (TR)/echo time (TE) = 3000/80; slice thickness = 6 mm; slice gap = 1 mm; matrix = 128 × 90. The total acquisition time for the DWI sequence was approximately 6 min and 19 s. The corresponding parameters for T2WI were: TR/TE = 12630/70 ms; slice thickness = 6 mm; slice gap = 1 mm; matrix = 228 × 224.

MRI image analysis

Images were independently analyzed by two radiologists (B.Z., with 6 years of experience, and H.B.Z with 12 years of experience), utilizing the FuncTool Software implemented in GE Workstation 4.6. The radiologists were blinded to clinical information, pathological results, and each other's findings. To determine the regions of interest (ROI), the radiologists manually drew the ROI on the DWI image with a b-value of 800 s/mm^2 at the maximum transverse diameter of the hepatic lymph node, avoiding areas containing adjacent vessels and artifacts. T2WI and DCE-MRI images served as references. Additionally, the mean value of parameters obtained from the two observers for each ROI was calculated for further analysis.

The signal intensity (SI) of each ROI was fitted using the following mathematical models, where S(b) is the SI at a particular b value, and S(0) is the SI with b = 0 s/mm^2:

(1) ADC was calculated using the mono-exponential model:

$S(b)/S(0) = \exp(-b \times ADC)$

(2) Three parameters were calculated using biexponential IVIM model according to the following equation:

$S(b)/S(0) = f \times \exp(-b \times D^*) + (1-f) \times (-b \times D)$

D: The true diffusion coefficient; D*: Pseudo-diffusion coefficient; f: The fraction of pseudo-diffusion.

(3) DDC and α were acquired from SEM using the following mathematical equation:

$S(b)/S(0) = \exp\{-(b \times DDC)\}^{\alpha}$

DDC: The distributed diffusion coefficient, characterizing the distribution of diffusion rates within a voxel; α: Ranging from 0 to 1, represents intravoxel diffusion heterogeneity.

Surgical technique and clinical information

Hepatic lymph nodes were delineated based on specific criteria, encompassing nodes along the hepatoduodenal ligament, which includes structures like the proper hepatic artery, portal vein, bile duct, and retro-pancreatic head. Nodes along the common hepatic artery and coeliac artery, covering the coeliac, common hepatic, and left gastric arteries, were also considered. Since hepatic lymph nodes were not routinely dissected, only suspected nodes on preoperative imaging and/or intraoperative examination were removed. Hematoxylin and eosin stained specimens of the surgically removed lymph nodes were examined by specialized pathologists, and all pathological results were obtained from final pathological reports.

Clinical information of CRLM patients was collected retrospectively, encompassing age, sex, location (left half colon *vs* right half colon), T and N stage of the primary tumor, synchronous or metachronous liver metastases, number of liver metastases (single *vs* multiple), RAS gene status (mutation type *vs* wild type), treatment response based on RECIST1.1 standard, disappearing lesions (identified when no visible lesion is observed on all imaging sequences after chemotherapy), and levels of carcinoembryonic antigen (CEA) and carbohydrate antigen 19-9 (CA19-9). Serum tumor markers were categorized into two groups: Those within normal limits and those exceeding normal limits, defined as 5 ng/mL for CEA and 40 ng/mL for CA19-9.

Statistical analysis

Continuous variables are presented as mean ± SD, while categorical variables are expressed as numbers and percentages. To compare characteristics between the two groups, independent-samples *t*/Mann-Whitney or chi-square tests were employed. To identify independent factors associated with hepatic LNM, multivariable logistic regression was conducted using a forward stepwise approach. The diagnostic performance of the predictive model was assessed using the receiver operating characteristic (ROC) curve, and the area under the ROC curve (AUC) with its 95% confidence interval (CI) was calculated. The model's cutoffs were determined using the maximum Youden's method. Sensitivity, specificity, PPV and NPV were also computed to evaluate the model's performance. Inter-observer agreements of quantitative metrics were tested using intraclass correlation coefficients (ICC), with ICC > 0.75 indicating good agreement, 0.40 to 0.75 suggesting moderate agreement, and ≤ 0.40 indicating poor agreement. All statistical analyses were performed using SPSS 25.0 (IBM Corporation, Armonk, NY, United States). A two-sided *P* value less than 0.05 was considered statistically significant, indicating a significant difference or association between variables.

RESULTS

Clinicopathologic characteristics

Among the 97 enrolled patients, 40 patients (41.2%; mean ± age = 57.53 ± 9.43 years) exhibited hepatic LNM, while the other 57 patients (58.8%; mean ± age = 52.91 ± 10.48 years) did not.

Univariate and multivariate analyses for factors associated with hepatic LNM

In univariate analysis, the short and long axes of the largest lymph node before treatment, short and long axes of the largest lymph node after treatment, pre-treatment D, pre-treatment DDC, post-treatment ADC, post-treatment DDC, and post-treatment α were found to be statistically significant with hepatic LNM ($P < 0.05$).

In multivariate analysis, only pre-treatment DDC (OR < 0.001; $P = 0.002$) and the short axis of the largest lymph node after treatment (OR = 1.509; $P < 0.001$) were identified as independent risk factors for the status of hepatic LNM. The detailed results of the univariate and multivariate analyses are presented in Table 1.

Comparison of parameters from models for prediction hepatic LNM

Table 2 summarizes the results of ROC analysis for quantitative parameters from all three models for predicting hepatic LNM. Pre-DDC had the largest AUC (AUC = 0.770; 95%CI: 0.676-0.865), followed by post-DDC (AUC = 0.739; 95%CI: 0.641-0.838) and post-ADC (AUC = 0.664; 95%CI: 0.553-0.774). The sensitivity, specificity, PPV, NPV, and accuracy of pre-DDC for differentiating malignant and benign hepatic lymph nodes were 85.0%, 59.6%, 59.6%, 85.0%, and 70.1%, respectively, with an optimal cutoff value of 1.92×10^{-3} mm^2/s.

Furthermore, the short axis of the largest lymph node before and after treatment also exhibited good performance in predicting hepatic LNM. The highest accuracy (77.3%) was achieved at a cutoff value of 10 mm (the best cut off value = 9.5 mm) for the short axis of the largest hepatic lymph node after treatment, which had 52.5% sensitivity and 94.7% specificity for differentiating the status of hepatic lymph nodes.

Development the nomogram for prediction hepatic LNM

The nomogram, incorporating pre-treatment DDC and the short axis of the largest lymph node after treatment, exhibited effective performance in predicting hepatic LNM. The AUC of the nomogram was 0.873 (95%CI: 0.803-0.943) (Figure 1), with sensitivity, specificity, PPV, NPV, and accuracy at 82.5%, 82.5%, 87.0%, 76.7%, and 82.5%, respectively. The nomogram for predicting hepatic LNM is presented in Figure 2.

Interobserver agreement for radiologic parameters

Moderate or good interobserver agreement was achieved for quantitative parameters (ICC range: 0.47-0.83). The ICCs of DDC before and after treatment were 0.52 and 0.81, respectively.

Table 1 Univariate and multivariate analysis of clinical and magnetic resonance imaging factors for prediction of hepatic lymph nodes metastases

		Univariate analysis			Multivariate analysis	
		Non-hepatic LNM (*n* = 57)	hepatic LNM HLN (*n* = 40)	*P* value	OR (95%CI)	*P* value
Gender	Male/female	44/13	27/13	0.029[a]		
Age		52.91 ± 10.48	57.53 ± 9.43	0.054		
BMI		24.63 ± 3.04	24.50 ± 3.04	0.842		
Primary location	Right/left-side	15/42	6/34	0.944		
Differentiation	Low to moderate/High	55/2	40/0	0.510		
T stage of primary tumor	T1+2/T3+4	3/54	4/36	0.650		
N stage of primary tumor	N0/N+	9/48	5/35	0.149		
Gene	RAS-wild/mutation	38/19	28/12	0.729		
Simultaneous liver metastases	No/Yes	13/44	12/28	0.425		
Distribution	Solitary/Bilateral	20/37	15/25	0.808		
Number of CRLM	≤ 3/> 3	17/40	15/25	0.429		
Size (mm)		38.25 ± 27.69	37.88 ± 22.11	0.944		
RECIST	Response/Non-response	33/24	21/19	0.599		
Disappearing lesion	No/Yes	46/11	34/6	0.584		
pre-CEA	≤ 5/> 5 ng/mL	15/42	11/29	0.897		
pre-CA199	≤ 40/> 40 U/mL	26/31	17/23	0.761		
post-CEA	≤ 5/> 5 ng/mL	27/30	17/23	0.635		
post-CA199	≤ 40/> 40 U/mL	33/24	25/15	0.649		
Short axis of largest lymph node before treatment	mm	7.39 ± 2.65	11.88 ± 5.35	< 0.001[a]		
Long axis of largest lymph node before treatment	mm	14.25 ± 6.41	18.28 ± 7.28	0.005[a]		
Pre-ADC	mm^2/s	1.54 ± 0.35	1.49 ± 0.30	0.394		
Pre-D	mm^2/s	1.21 ± 0.43	1.02 ± 0.25	0.005[a]		
Pre-D*	mm^2/s	3.33 ± 2.37	2.70 ± 2.38	0.200		
Pre-f		0.49 ± 0.17	0.45 ± 0.14	0.330		
Pre-DDC	mm^2/s	3.21 ± 1.69	2.01 ± 0.83	< 0.001[a]	< 0.001	0.002[a]
Pre-α		0.59 ± 0.17	0.62 ± 0.16	0.363		
Short axis of largest lymph node after treatment	mm	6.74 ± 2.13	10.43 ± 3.62	< 0.001[a]	1.509 (1.235-1.845)	< 0.001[a]
Long axis of largest lymph node after treatment	mm	13.46 ± 5.78	17.08 ± 6.82	0.006[a]		
Post-ADC	mm^2/s	1.64 ± 0.32	1.45 ± 0.32	0.006[a]		
Post-D	mm^2/s	1.35 ± 0.86	1.24 ± 0.78	0.529		
Post-D*	mm^2/s	3.69 ± 2.96	3.48 ± 3.38	0.751		
Post-f		0.51 ± 0.18	0.52 ± 0.18	0.732		
Post-DDC		3.46 ± 1.48	2.37 ± 0.91	< 0.001[a]		
Post-α		0.61 ± 0.13	0.67 ± 0.13	0.035[a]		

[a]*P* values that are significantly different between metastatic and non-metastatic HLN group.

HLN: Hemolymph node; OR: Odds ratio; BMI: Body mass indices; CRLM: Colorectal liver metastases; RECIST: Response Evaluation Criteria In Solid Tumors; CEA: Carcinoembryonic antigen; CA19-9: Carbohydrate antigen 19-9; ADC: Apparent diffusion coefficient; CI: Confidence interval; DDC: Distributed diffusion coefficient; LNM: Lymph node metastases; D: True diffusion coefficient; D*: Pseudo-diffusion coefficient; f: The perfusion fraction; α: Intravoxel water diffusion heterogeneity.

Table 2 Diagnostic performance of quantitative parameters and nomogram in predicting hepatic lymph node metastases in colorectal liver metastases patient

	AUC	Cut off value	Sensitivity (%)	Specificity (%)	PPV (%)	NPV (%)	Accuracy (%)
Pre-ADC	0.551 (0.436-0.666)	1.70	32.5	82.5	56.5	63.5	61.5
Pre-D	0.648 (0.538-0.758)	1.15	55.0	77.2	62.9	58.1	68.0
Pre-D*	0.592 (0.477-0.707)	2.51	55.0	66.7	53.7	71.0	62.1
Pre-f	0.577 (0.462-0.692)	3.98	70.0	47.5	48.3	64.3	56.7
Pre-DDC	0.770 (0.676-0.865)	1.92	85.0	59.6	59.6	85.0	70.1
Pre-α	0.573 (0.456-0.689)	0.59	62.5	59.6	52.1	69.4	60.8
Post-ADC	0.664 (0.553-0.774)	1.46	75.0	52.6	52.6	75.0	61.9
Post-D	0.581 (0.447-0.681)	1.21	50.0	70.2	54.1	66.7	62.1
Post-D*	0.558 (0.438-0.678)	1.27	85.0	33.3	47.2	76.0	54.6
Post-f	0.521 (0.403-0.638)	3.98	77.5	31.6	44.3	66.7	50.5
Post-DDC	0.739 (0.641-0.838)	2.26	82.5	52.5	55.0	81.1	64.9
Post-α	0.623 (0.509-0.737)	0.65	57.5	70.2	57.5	70.2	65.0
Short axis of largest lymph node before treatment (mm)	0.773 (0.674-0.872)	12	50.0	94.7	87.0	73.0	76.3
Short axis of largest lymph node after treatment (mm)	0.811 (0.724-0.899)	10	52.5	94.7	38.9	74.0	77.3
Nomogram	0.873 (0.803, 0.943)	1.03	82.5	82.5	87.0	76.7	82.5

AUC: Area under the receiver operating characteristic curve; ADC: Apparent diffusion coefficient; NPV: Negative predictive value; PPV: Positive predictive value; DDC: Distributed diffusion coefficient; D: True diffusion coefficient; D*: Pseudo-diffusion coefficient; f: The perfusion fraction; α: Intravoxel water diffusion heterogeneity.

DISCUSSION

In this study, our goal was to assess the diagnostic potential of DWI parameters using three models to differentiate between benign hepatic lymph nodes and metastatic lymph nodes in patients with initially resectable CRLM. Our findings indicate that the DDC values obtained from the SEM were significantly lower in metastatic lymph nodes compared to non-metastatic lymph nodes, both before and after treatment. Notably, the baseline DDC value exhibited the highest accuracy for preoperative lymph node status diagnosis in CRLM patients, outperforming the accuracy of ADC from the mono-exponential model, as well as D, D*, and f from the IVIM model. Furthermore, there was substantial agreement between two independent readers in assessing DDC, suggesting that DDC, along with the short diameter of the largest lymph node, may serve as a reliable, non-invasive, and promising technique in clinical practice for distinguishing between metastatic and non-metastatic lymph nodes before surgery.

Our results show that the baseline DDC from the SEM demonstrated the highest diagnostic performance in distinguishing metastatic from benign hepatic lymph nodes, followed by post-DDC and post-ADC, although the differences among them were not statistically significant. The DDC value is considered a weighted sum of continuous distributions

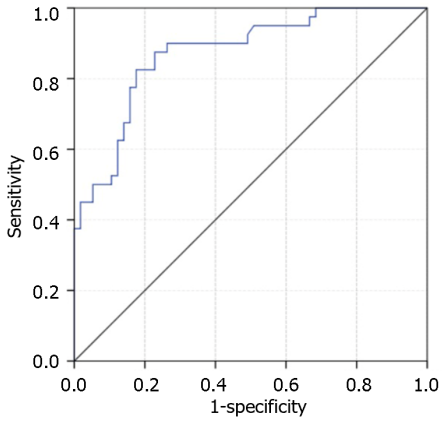

DOI: 10.3748/wjg.v30.i4.308 **Copyright** ©The Author(s) 2024.

Figure 1 The receiver operating characteristic curve of nomogram to predict hepatic lymph node metastases in colorectal liver metastases patients receiving chemotherapy. The area under the curve of the nomogram was 0.873.

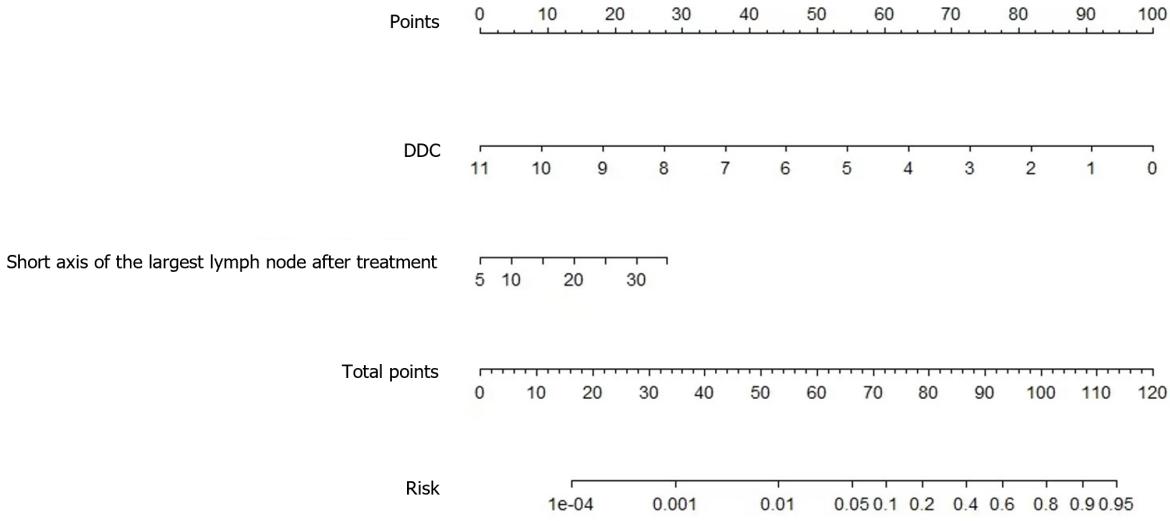

DOI: 10.3748/wjg.v30.i4.308 **Copyright** ©The Author(s) 2024.

Figure 2 Nomogram of model for predicting hepatic lymph node metastases in colorectal liver metastases patients receiving chemotherapy. DDC: Distributed diffusion coefficient.

of ADCs and can offer more information on non-Gaussian distribution. These results can be attributed to increased cellularity, higher nucleus-to-cytoplasm ratios, and more limited extracellular space in malignant lymph nodes, leading to greater intravoxel diffusion heterogeneity[19,20]. Therefore, DDC may have a superior ability to differentiate between benign and malignant liver lesions with minimal overlap compared to ADC calculated from the mono-exponential model, consistent with previous studies on gliomas, ovarian cancer, bladder cancer, and hepatic lesions[21-24]. Additionally, our findings suggest that DDC values calculated from the SEM are more reliable than those from the mono-exponential and IVIM models, aligning with previous studies[25-27].

On the contrary, while quantitative parameters obtained from the IVIM model, except for post-f of benign hepatic lesions, were higher in malignant lymph nodes, the difference was not statistically significant. Several factors may contribute to these results. Firstly, the predictive value of the IVIM model for lymph node status has not been consistently supported in previous literature. For instance, in a study on rectal adenocarcinoma patients, Jia *et al*[28] found that the group with positive lymph nodes exhibited a significantly lower D* value and a higher f value. Conversely, another study on rectal cancer patients showed that the metastatic group had significantly lower D and D* values compared to the nonmetastatic group[29]. Various factors, such as the setting of b-values (especially b-values < 200 s/mm^2), TR, and scan techniques, may influence the results of IVIM parameters. Secondly, the heterogeneity of hepatic lesions can impact the quantitative parameters of the IVIM model. Malignant lesions typically demonstrate more heterogeneity in terms of cellularity, vascularity, and perfusion compared to benign lesions. This inherent heterogeneity can lead to variations in the IVIM parameters, making it challenging to differentiate between benign and malignant lesions based solely on IVIM parameters. Additionally, the limited sample size in our study may introduce selection bias.

Our study also revealed that the short diameter of the largest lymph node after treatment was useful in predicting the status of hepatic lymph nodes in CRLM patients. This finding aligns with a previous study indicating tumor size as an independent predictor of lymph node metastases[30]. We identified the optimal diagnostic threshold for the short diameter of lymph nodes as 10 mm, with a sensitivity of 52.5%, specificity of 94.7%, and accuracy of 77.3%. The nomogram, combining DDC and the short diameter of the largest lymph node, can quantitatively evaluate lymph node metastases with enhanced diagnostic efficacy. The nomogram's diagnostic efficiency, with an AUC of 0.873, demonstrated superior performance compared to using either IVIM or SEM alone. Furthermore, the nomogram exhibited improved sensitivity, specificity, and accuracy. These results suggest that the nomogram can effectively prevent unnecessary lymph node dissection in CRLM patients.

The current study has several limitations. Firstly, it was a retrospective, single-center study with a relatively small sample size. Therefore, further studies with a larger sample size and external validation are needed to validate the findings. Secondly, there may be selection bias because we only included patients with clinically suspected lymph node metastasis who underwent surgical resection. This could potentially underestimate the severity of the condition, as most CRLM patients were excluded if they did not have clinically suspicious metastatic lymph nodes. Thirdly, there may be uncertainty regarding the alignment between the lymph node evaluated by the pathologist and the image slices where the DWI parameters were obtained. Additionally, the setting of b-values in DWI remains controversial. While using too many b-values would result in prolonged scan time, further research is required to determine the optimal number and interval of b-values for accurate assessment, considering the trade-off between scan time and accuracy. Lastly, the study did not analyze the relationship between the models and the survival outcome of the patients.

CONCLUSION

In conclusion, our results suggest that a nomogram incorporating the pre-DDC value calculated from SEM-DWI along with the short diameter of the largest lymph node after treatment may have the potential to predict lymph node metastasis noninvasively in CRLM patients after chemotherapy. This nomogram can be used for individualized, noninvasive high-risk assessment and surgical planning for CRLM patients with suspected metastatic hepatic lymph nodes, thereby reducing unnecessary surgical procedures and the occurrence of complications.

ARTICLE HIGHLIGHTS

Research background

More than 50% of patients with colorectal cancer develop colorectal liver metastases (CRLM), and the presence of metastatic hepatic lymph nodes can greatly influence treatment decisions and patient outcomes. Precise preoperative prediction of hepatic lymph node status is beneficial for individualized treatment and reducing complications.

Research motivation

However, there is currently a lack of reliable radiological tools for predicting the presence of metastatic hepatic lymph nodes in CRLM prior to surgery.

Research objectives

The study aimed to assess the predictive ability of different diffusion-weighted imaging (DWI) models (mono-exponential, bi-exponential, and stretched-exponential) in distinguishing between benign and malignant hepatic lymph nodes in CRLM patients who underwent neoadjuvant chemotherapy.

Research methods

A retrospective study was conducted involving 97 CRLM patients with pathologically confirmed hepatic lymph node status who underwent magnetic resonance imaging, including DWI with ten b values before and after chemotherapy. Various parameters, including apparent diffusion coefficient, the true diffusion coefficient, the pseudo-diffusion coefficient, the perfusion fraction, distributed diffusion coefficient (DDC), and α, derived from different DWI models, were measured and compared between positive and negative hepatic lymph node groups. A nomogram was constructed, and the reliability and agreement of the measurements were assessed using appropriate statistical analyses.

Research results

Multivariate analysis revealed that the pre-treatment DDC value and the short diameter of the largest lymph node after treatment were independent predictors of metastatic hepatic lymph nodes. A nomogram combining these factors demonstrated excellent performance in distinguishing between benign and malignant lymph nodes in CRLM patients, with area under the receiver operating characteristic curve of 0.873. Furthermore, parameters from the stretched-exponential model showed substantial repeatability.

Research conclusions

The developed nomogram, incorporating the pre-treatment DDC and the short axis of the largest lymph node, can be

utilized to predict the presence of hepatic lymph node metastases in CRLM patients who undergo chemotherapy prior to surgery. This nomogram was found to be more valuable than quantitative parameters derived from multiple b values of DWI, exhibiting superior diagnostic performance.

Research perspectives

In the future, the nomogram can serve as a preoperative assessment tool for determining the status of hepatic lymph nodes and aiding in the decision-making process for surgical treatment in CRLM patients.

FOOTNOTES

Co-first authors: Hai-Bin Zhu and Bo Zhao.

Author contributions: Zhu HB and Zhao B contributed equally to this work; Zhu HB, Zhao B, Li XT, Zhang XY and Sun YS designed the research study; Zhu HB, Zhao B, Li XT, Zhang XY and Sun YS performed the research; Li XT and Yao Q contributed new reagents and analytic tools; Zhu HB, Zhao B, Li XT and Yao Q analyzed the data and wrote the manuscript; All authors have read and approve the final manuscript.

Supported by Beijing Hospitals Authority Youth Program, No. QML20231103; Beijing Hospitals Authority Ascent Plan, No. DFL20191103; and National Key R&D Program of China, No. 2023YFC3402805.

Institutional review board statement: This study was conducted in accordance with the regulations and guidelines established by the Medical Ethics Committee (IRB) of Beijing Cancer Hospital. All studies involving human subjects were conducted with IRB approval.

Informed consent statement: Informed consent was waived due to the retrospective study.

Conflict-of-interest statement: The authors declared no conflicts of interest.

Data sharing statement: No additional data are available.

Country/Territory of origin: China

ORCID number: Hai-Bin Zhu 0000-0002-6239-6333; Xiao-Ting Li 0000-0003-2758-3843; Xiao-Yan Zhang 0000-0003-2700-7627; Ying-Shi Sun 0000-0001-9424-1910.

S-Editor: Fan JR
L-Editor: A
P-Editor: Chen YX

REFERENCES

1 **Ferlay J**, Soerjomataram I, Dikshit R, Eser S, Mathers C, Rebelo M, Parkin DM, Forman D, Bray F. Cancer incidence and mortality worldwide: sources, methods and major patterns in GLOBOCAN 2012. *Int J Cancer* 2015; **136**: E359-E386 [PMID: 25220842 DOI: 10.1002/ijc.29210]

2 **Nieuwenhuizen S**, Puijk RS, van den Bemd B, Aldrighetti L, Arntz M, van den Boezem PB, Bruynzeel AME, Burgmans MC, de Cobelli F, Coolsen MME, Dejong CHC, Derks S, Diederik A, van Duijvendijk P, Eker HH, Engelsman AF, Erdmann JI, Fütterer JJ, Geboers B, Groot G, Haasbeek CJA, Janssen JJ, de Jong KP, Kater GM, Kazemier G, Kruimer JWH, Leclercq WKG, van der Leij C, Manusama ER, Meier MAJ, van der Meijs BB, Melenhorst MCAM, Nielsen K, Nijkamp MW, Potters FH, Prevoo W, Rietema FJ, Ruarus AH, Ruiter SJS, Schouten EAC, Serafino GP, Sietses C, Swijnenburg RJ, Timmer FEF, Versteeg KS, Vink T, de Vries JJJ, de Wilt JHW, Zonderhuis BM, Scheffer HJ, van den Tol PMP, Meijerink MR. Resectability and Ablatability Criteria for the Treatment of Liver Only Colorectal Metastases: Multidisciplinary Consensus Document from the COLLISION Trial Group. *Cancers (Basel)* 2020; **12** [PMID: 32635230 DOI: 10.3390/cancers12071779]

3 **Morris VK**, Kennedy EB, Baxter NN, Benson AB 3rd, Cercek A, Cho M, Ciombor KK, Cremolini C, Davis A, Deming DA, Fakih MG, Gholami S, Hong TS, Jaiyesimi I, Klute K, Lieu C, Sanoff H, Strickler JH, White S, Willis JA, Eng C. Treatment of Metastatic Colorectal Cancer: ASCO Guideline. *J Clin Oncol* 2023; **41**: 678-700 [PMID: 36252154 DOI: 10.1200/JCO.22.01690]

4 **Liu W**, Yan XL, Wang K, Bao Q, Sun Y, Xing BC. The outcome of liver resection and lymphadenectomy for hilar lymph node involvement in colorectal cancer liver metastases. *Int J Colorectal Dis* 2014; **29**: 737-745 [PMID: 24743847 DOI: 10.1007/s00384-014-1863-5]

5 **Elias D**, Saric J, Jaeck D, Arnaud JP, Gayet B, Rivoire M, Lorimier G, Carles J, Lasser P. Prospective study of microscopic lymph node involvement of the hepatic pedicle during curative hepatectomy for colorectal metastases. *Br J Surg* 1996; **83**: 942-945 [PMID: 8813780 DOI: 10.1002/bjs.1800830717]

6 **Ercolani G**, Grazi GL, Ravaioli M, Grigioni WF, Cescon M, Gardini A, Del Gaudio M, Cavallari A. The role of lymphadenectomy for liver tumors: further considerations on the appropriateness of treatment strategy. *Ann Surg* 2004; **239**: 202-209 [PMID: 14745328 DOI:

10.1097/01.sla.0000109154.00020.e0]
7 **Ishizuka D**, Shirai Y, Hatakeyama K. Ischemic biliary stricture due to lymph node dissection in the hepatoduodenal ligament. *Hepatogastroenterology* 1998; **45**: 2048-2050 [PMID: 9951863]
8 **Grobmyer SR**, Wang L, Gonen M, Fong Y, Klimstra D, D'Angelica M, DeMatteo RP, Schwartz L, Blumgart LH, Jarnagin WR. Perihepatic lymph node assessment in patients undergoing partial hepatectomy for malignancy. *Ann Surg* 2006; **244**: 260-264 [PMID: 16858189 DOI: 10.1097/01.sla.0000217606.59625.9d]
9 **Rau C**, Blanc B, Ronot M, Dokmak S, Aussilhou B, Faivre S, Vilgrain V, Paradis V, Belghiti J. Neither preoperative computed tomography nor intra-operative examination can predict metastatic lymph node in the hepatic pedicle in patients with colorectal liver metastasis. *Ann Surg Oncol* 2012; **19**: 163-168 [PMID: 21837526 DOI: 10.1245/s10434-011-1994-7]
10 **Ko CC**, Yeh LR, Kuo YT, Chen JH. Imaging biomarkers for evaluating tumor response: RECIST and beyond. *Biomark Res* 2021; **9**: 52 [PMID: 34215324 DOI: 10.1186/s40364-021-00306-8]
11 **Messina C**, Bignone R, Bruno A, Bruno F, Calandri M, Caruso D, Coppolino P, Robertis R, Gentili F, Grazzini I, Natella R, Scalise P, Barile A, Grassi R, Albano D. Diffusion-Weighted Imaging in Oncology: An Update. *Cancers (Basel)* 2020; **12** [PMID: 32521645 DOI: 10.3390/cancers12061493]
12 **Bonekamp S**, Corona-Villalobos CP, Kamel IR. Oncologic applications of diffusion-weighted MRI in the body. *J Magn Reson Imaging* 2012; **35**: 257-279 [PMID: 22271274 DOI: 10.1002/jmri.22786]
13 **Sumi M**, Sakihama N, Sumi T, Morikawa M, Uetani M, Kabasawa H, Shigeno K, Hayashi K, Takahashi H, Nakamura T. Discrimination of metastatic cervical lymph nodes with diffusion-weighted MR imaging in patients with head and neck cancer. *AJNR Am J Neuroradiol* 2003; **24**: 1627-1634 [PMID: 13679283]
14 **Abdel Razek AA**, Soliman NY, Elkhamary S, Alsharaway MK, Tawfik A. Role of diffusion-weighted MR imaging in cervical lymphadenopathy. *Eur Radiol* 2006; **16**: 1468-1477 [PMID: 16557366 DOI: 10.1007/s00330-005-0133-x]
15 **Eiber M**, Beer AJ, Holzapfel K, Tauber R, Ganter C, Weirich G, Krause BJ, Rummeny EJ, Gaa J. Preliminary results for characterization of pelvic lymph nodes in patients with prostate cancer by diffusion-weighted MR-imaging. *Invest Radiol* 2010; **45**: 15-23 [PMID: 19996762 DOI: 10.1097/RLI.0b013e3181bbdc2f]
16 **Zhou XJ**, Gao Q, Abdullah O, Magin RL. Studies of anomalous diffusion in the human brain using fractional order calculus. *Magn Reson Med* 2010; **63**: 562-569 [PMID: 20187164 DOI: 10.1002/mrm.22285]
17 **Ai Z**, Han Q, Huang Z, Wu J, Xiang Z. The value of multiparametric histogram features based on intravoxel incoherent motion diffusion-weighted imaging (IVIM-DWI) for the differential diagnosis of liver lesions. *Ann Transl Med* 2020; **8**: 1128 [PMID: 33240977 DOI: 10.21037/atm-20-5109]
18 **Bennett KM**, Schmainda KM, Bennett RT, Rowe DB, Lu H, Hyde JS. Characterization of continuously distributed cortical water diffusion rates with a stretched-exponential model. *Magn Reson Med* 2003; **50**: 727-734 [PMID: 14523958 DOI: 10.1002/mrm.10581]
19 **Liu C**, Wang K, Li X, Zhang J, Ding J, Spuhler K, Duong T, Liang C, Huang C. Breast lesion characterization using whole-lesion histogram analysis with stretched-exponential diffusion model. *J Magn Reson Imaging* 2018; **47**: 1701-1710 [PMID: 29165847 DOI: 10.1002/jmri.25904]
20 **Seo N**, Chung YE, Park YN, Kim E, Hwang J, Kim MJ. Liver fibrosis: stretched exponential model outperforms mono-exponential and bi-exponential models of diffusion-weighted MRI. *Eur Radiol* 2018; **28**: 2812-2822 [PMID: 29404771 DOI: 10.1007/s00330-017-5292-z]
21 **Bai Y**, Lin Y, Tian J, Shi D, Cheng J, Haacke EM, Hong X, Ma B, Zhou J, Wang M. Grading of Gliomas by Using Monoexponential, Biexponential, and Stretched Exponential Diffusion-weighted MR Imaging and Diffusion Kurtosis MR Imaging. *Radiology* 2016; **278**: 496-504 [PMID: 26230975 DOI: 10.1148/radiol.2015142173]
22 **Wang F**, Wang Y, Zhou Y, Liu C, Xie L, Zhou Z, Liang D, Shen Y, Yao Z, Liu J. Comparison between types I and II epithelial ovarian cancer using histogram analysis of monoexponential, biexponential, and stretched-exponential diffusion models. *J Magn Reson Imaging* 2017; **46**: 1797-1809 [PMID: 28379611 DOI: 10.1002/jmri.25722]
23 **Wang Y**, Hu D, Yu H, Shen Y, Tang H, Kamel IR, Li Z. Comparison of the Diagnostic Value of Monoexponential, Biexponential, and Stretched Exponential Diffusion-weighted MRI in Differentiating Tumor Stage and Histological Grade of Bladder Cancer. *Acad Radiol* 2019; **26**: 239-246 [PMID: 29753491 DOI: 10.1016/j.acra.2018.04.016]
24 **Hu Y**, Tang H, Li H, Li A, Li J, Hu D, Li Z, Kamel IR. Assessment of different mathematical models for diffusion-weighted imaging as quantitative biomarkers for differentiating benign from malignant solid hepatic lesions. *Cancer Med* 2018; **7**: 3501-3509 [PMID: 29733515 DOI: 10.1002/cam4.1535]
25 **Li H**, Liang L, Li A, Hu Y, Hu D, Li Z, Kamel IR. Monoexponential, biexponential, and stretched exponential diffusion-weighted imaging models: Quantitative biomarkers for differentiating renal clear cell carcinoma and minimal fat angiomyolipoma. *J Magn Reson Imaging* 2017; **46**: 240-247 [PMID: 27859853 DOI: 10.1002/jmri.25524]
26 **Kim HC**, Seo N, Chung YE, Park MS, Choi JY, Kim MJ. Characterization of focal liver lesions using the stretched exponential model: comparison with monoexponential and biexponential diffusion-weighted magnetic resonance imaging. *Eur Radiol* 2019; **29**: 5111-5120 [PMID: 30796578 DOI: 10.1007/s00330-019-06048-4]
27 **Jerome NP**, Miyazaki K, Collins DJ, Orton MR, d'Arcy JA, Wallace T, Moreno L, Pearson AD, Marshall LV, Carceller F, Leach MO, Zacharoulis S, Koh DM. Repeatability of derived parameters from histograms following non-Gaussian diffusion modelling of diffusion-weighted imaging in a paediatric oncological cohort. *Eur Radiol* 2017; **27**: 345-353 [PMID: 27003140 DOI: 10.1007/s00330-016-4318-2]
28 **Jia H**, Jiang X, Zhang K, Shang J, Zhang Y, Fang X, Gao F, Li N, Dong J. A Nomogram of Combining IVIM-DWI and MRI Radiomics From the Primary Lesion of Rectal Adenocarcinoma to Assess Nonenlarged Lymph Node Metastasis Preoperatively. *J Magn Reson Imaging* 2022; **56**: 658-667 [PMID: 35090079 DOI: 10.1002/jmri.28068]
29 **Wang C**, Yu J, Lu M, Li Y, Shi H, Xu Q. Diagnostic Efficiency of Diffusion Sequences and a Clinical Nomogram for Detecting Lymph Node Metastases from Rectal Cancer. *Acad Radiol* 2022; **29**: 1287-1295 [PMID: 34802905 DOI: 10.1016/j.acra.2021.10.009]
30 **Zhu HB**, Xu D, Sun XF, Li XT, Zhang XY, Wang K, Xing BC, Sun YS. Prediction of hepatic lymph node metastases based on magnetic resonance imaging before and after preoperative chemotherapy in patients with colorectal liver metastases underwent surgical resection. *Cancer Imaging* 2023; **23**: 18 [PMID: 36810192 DOI: 10.1186/s40644-023-00529-y]

World Journal of Gastroenterology

Submit a Manuscript: https://www.f6publishing.com

World J Gastroenterol 2024 January 28; 30(4): 318-331

DOI: 10.3748/wjg.v30.i4.318

ISSN 1007-9327 (print) ISSN 2219-2840 (online)

ORIGINAL ARTICLE

Retrospective Study

Hepatic arterial infusion chemotherapy with anti-angiogenesis agents and immune checkpoint inhibitors for unresectable hepatocellular carcinoma and meta-analysis

Yu-Zhe Cao, Guang-Lei Zheng, Tian-Qi Zhang, Hong-Yan Shao, Jia-Yu Pan, Zi-Lin Huang, Meng-Xuan Zuo

Specialty type: Gastroenterology and hepatology

Provenance and peer review: Unsolicited article; Externally peer reviewed.

Peer-review model: Single blind

Peer-review report's scientific quality classification

Grade A (Excellent): A
Grade B (Very good): 0
Grade C (Good): 0
Grade D (Fair): 0
Grade E (Poor): 0

P-Reviewer: Saadi S, United States

Received: November 1, 2023
Peer-review started: November 1, 2023
First decision: December 4, 2023
Revised: December 11, 2023
Accepted: January 8, 2024
Article in press: January 8, 2024
Published online: January 28, 2024

Yu-Zhe Cao, Guang-Lei Zheng, Tian-Qi Zhang, Hong-Yan Shao, Jia-Yu Pan, Zi-Lin Huang, Meng-Xuan Zuo, Department of Minimally Invasive Interventional Therapy, Sun Yat-sen University Cancer Center, Guangzhou 510060, Guangdong Province, China

Yu-Zhe Cao, Guang-Lei Zheng, Tian-Qi Zhang, Hong-Yan Shao, Jia-Yu Pan, Zi-Lin Huang, Meng-Xuan Zuo, Department of Minimally Invasive Interventional Therapy, State Key Laboratory of Oncology in South China, Guangzhou 510060, Guangdong Province, China

Yu-Zhe Cao, Guang-Lei Zheng, Tian-Qi Zhang, Hong-Yan Shao, Jia-Yu Pan, Zi-Lin Huang, Meng-Xuan Zuo, Department of Minimally Invasive Interventional Therapy, Guangdong Provincial Clinical Research Center for Cancer, Guangzhou 510060, Guangdong Province, China

Corresponding author: Meng-Xuan Zuo, MD, Attending Doctor, Department of Minimally Invasive Interventional Therapy, Sun Yat-sen University Cancer Center, No. 651 Dongfeng Road East, Yuexiu District, Guangzhou 510060, Guangdong Province, China.
zuomx@sysucc.org.cn

Abstract

BACKGROUND

Hepatic arterial infusion chemotherapy (HAIC) has been proven to be an ideal choice for treating unresectable hepatocellular carcinoma (uHCC). HAIC-based treatment showed great potential for treating uHCC. However, large-scale studies on HAIC-based treatments and meta-analyses of first-line treatments for uHCC are lacking.

AIM

To investigate better first-line treatment options for uHCC and to assess the safety and efficacy of HAIC combined with angiogenesis inhibitors, programmed cell death of protein 1 (PD-1) and its ligand (PD-L1) blockers (triple therapy) under real-world conditions.

METHODS

Several electronic databases were searched to identify eligible randomized controlled trials for this meta-analysis. Study-level pooled analyses of hazard ratios (HRs) and odds ratios (ORs) were performed. This was a retrospective single-center study involving 442 patients with uHCC who received triple therapy

or angiogenesis inhibitors plus PD-1/PD-L1 blockades (AIPB) at Sun Yat-sen University Cancer Center from January 2018 to April 2023. Propensity score matching (PSM) was performed to balance the bias between the groups. The Kaplan-Meier method and cox regression were used to analyse the survival data, and the log-rank test was used to compare the suvival time between the groups.

RESULTS

A total of 13 randomized controlled trials were included. HAIC alone and in combination with sorafenib were found to be effective treatments (*P* values for ORs: HAIC, 0.95; for HRs: HAIC + sorafenib, 0.04). After PSM, 176 HCC patients were included in the analysis. The triple therapy group (n = 88) had a longer median overall survival than the AIPB group (n = 88) (31.6 months *vs* 14.6 months, $P < 0.001$) and a greater incidence of adverse events (94.3% *vs* 75.4%, $P < 0.001$).

CONCLUSION

This meta-analysis suggests that HAIC-based treatments are likely to be the best choice for uHCC. Our findings confirm that triple therapy is more effective for uHCC patients than AIPB.

Key Words: Unresectable hepatocellular carcinoma; Hepatic arterial infusion chemotherapy; Angiogenesis inhibitors; Programmed cell death protein 1; Programmed death ligand 1

Core Tip: The network meta-analysis showed the treatment based on hepatic arterial infusion chemotherapy (HAIC) had the best efficacy on unresectable hepatocellular carcinoma (uHCC). The retrospective, relatively large-scale study suggested HAIC combined with angiogenesis inhibitors and programmed cell death protein 1 (PD-1)/programmed death ligand 1 (PD-L1) blockers could improve the uHCC patients' prognosis. After propensity score matching, it demonstrated that triple therapy was able to prolong the uHCC patients' survival than angiogenesis inhibitors and PD-1/PD-L1 blockers.

Citation: Cao YZ, Zheng GL, Zhang TQ, Shao HY, Pan JY, Huang ZL, Zuo MX. Hepatic arterial infusion chemotherapy with anti-angiogenesis agents and immune checkpoint inhibitors for unresectable hepatocellular carcinoma and meta-analysis. *World J Gastroenterol* 2024; 30(4): 318-331

URL: https://www.wjgnet.com/1007-9327/full/v30/i4/318.htm

DOI: https://dx.doi.org/10.3748/wjg.v30.i4.318

INTRODUCTION

Primary liver cancer is a malignant tumor of the digestive system that is common worldwide. China has a particularly high incidence of liver cancer, with approximately 410000 new cases and 391000 deaths annually; liver cancer is the second largest cause of cancer-related death in the country[1]. Among primary liver cancers, hepatocellular carcinoma (HCC) is the main pathological type. In the subclinical phase, patients tend to be asymptomatic. Therefore, at the time of diagnosis, most patients have already reached advanced stages of the disease. Therefore, fewer than 30% of patients are candidates for surgical resection[2,3].

According to several clinical trials, sorafenib and lenvatinib have been recommended by multiple authoritative guidelines as first-line treatment options for advanced HCC for some time[4-6]. The results of the IMbrave150 trial ushered in a new era in HCC therapy, in which angiogenesis inhibitors were combined with programmed cell death protein 1/programmed cell death ligand 1 (PD-1/PD-L1) blockees, which is now becoming the new standard first-line therapy[7]. Researchers have conducted several clinical studies on various immune-related drugs, angiogenesis inhibitors, and various combination regimens for unresectable HCC (uHCC). The FOHAIC study also revealed that hepatic arterial perfusion chemotherapy (HAIC) using the FOLFOX regimen was more effective than sorafenib in patients with uHCC[8]. Several studies have suggested that triple therapy has the potential to further improve the prognosis in patients with uHCC[9-12]. As the results of multiple clinical studies have been published, several questions remain surrounding this type of therapy, such as which treatment approach has the best therapeutic effect on uHCC? How effective is triple therapy when used in large-scale real-world clinical applications?

In this study, we attempted to identify the optimal treatment for uHCC based on data from phase III randomized controlled trials (RCTs) through a network meta-analysis. We also investigated the safety and efficacy of triple therapy in patients with HCC from a Chinese population under real-world conditions. We then performed propensity score matching (PSM) to compare triple therapy to angiogenesis inhibitors plus PD1/PDL1 blockers (AIPB), which has been recommended as a first-line treatment for uHCC by some guidelines[13,14]. This study also confirmed the safety of triple therapy under real-world conditions.

MATERIALS AND METHODS

Literature search, data extraction, and network meta-analysis

We performed an extensive literature search of the PubMed, Embase, and Cochrane Library databases for RCTs published from January 1, 2018, to January 1, 2023. The Supplementary material details the search strategy and inclusion criteria. Two authors independently screened the trials for eligibility and extracted information from each one. The included RCTs were then assessed for risk of bias using the Cochrane risk of bias 2 tool, which showed low risk levels for all the included studies (Supplementary Figure 1).

Triple therapy real-world study

Patients who were treated with triple therapy or AIPB as a first-line treatment for advanced HCC between January 2018 and April 2023 at the Department of Minimally Invasive Interventional Therapy, Sun Yat-sen University Cancer Center in Guangzhou, China, were screened for eligibility. HCC was diagnosed histologically or radiologically in accordance with the latest international guidelines[15]. The inclusion criteria were as follows: (1) Stage B (not applicable for surgery or progressed on locoregional therapy) or stage C HCC according to the Barcelona Clinic Liver Cancer (BCLC) staging system; (2) Child–Pugh score of A–C; (3) Eastern cooperative oncology group performance status (ECOG PS) of 0–2; (4) Age ≥ 18 years; and (5) At least one available follow-up data point. The exclusion criteria were as follows: (1) History of receiving any systemic chemotherapy, angiogenesis inhibitors, or immunotherapy; (2) Lack of medical imaging data; and (3) History of a second primary malignant tumor. The details are shown in the Supplementary materials. This study was reviewed and approved by the Sun Yat-sen University Cancer Center Ethics Committee. Informed consent was waived due to the retrospective nature of the analysis.

Treatment regimens: Small-molecule tyrosine kinase inhibitors such as sorafenib, a type of angiogenesis inhibitor, were administered orally, and the doses were determined based on the manufacturers' instructions. Bevacizumab, another type of angiogenesis inhibitor, was administered intravenously at a dose of 15 mg/kg body weight every 3 wk. Atezolizumab, a type of programmed cell death ligand 1 blocker, was administered intravenously at a dose of 1200 mg every 3 wk. Programmed cell death protein 1 (PD-1) blockers, including pembrolizumab, camrelizumab, tislelizumab, and sintilimab, were administered intravenously at 200 mg every 3 wk. Toripalimab, another PD-1 blocker, was injected through an intravenous drip of 240 mg every 3 wk following the instructions. The HAIC regimen was based on FOLFOX and consisted of 85 mg/m^2 oxaliplatin, 200 mg/m^2 calcium folinate, and 2.5 g/m^2 5-fluorouracil every 3 wk. HAIC was performed under the guidance of digital subtraction angiography by interventional radiologists. The celiac axis, superior mesenteric artery, inferior phrenic artery and right renal artery were selectively catheterized for angiography. If angiography revealed that the HCC blood supply originated from different vessels, the main feeding artery was reserved for super selective catheterization, and an indwelling microcatheter was inserted into the HAIC while the other feeding vessels were embolized. During the study period, dose modifications and treatment interruptions were sometimes initiated according to drug-related toxicity grades, as recommended relative to the physiological condition of each patient. HAIC was performed for 4–6 rounds in the absence of disease progression. Patients received angiogenesis inhibitors and PD-1/PD-L1 blockers during and after HAIC treatment to consolidate the therapeutic effects in the long-term.

Assessment of clinical outcomes: The patients involved in the study were followed up every 6–12 wk to assess treatment response. Radiological response was assessed according to the modified Response Evaluation Criteria in Solid Tumors (mRECIST) criteria based on liver dynamic computed tomography or magnetic resonance imaging data. The primary endpoint that was assessed was overall survival (OS), which was defined as the time from the start date of systemic chemotherapy or HAIC to death. progression-free survival (PFS) (the time from the start date of systemic chemotherapy or HAIC to the date of disease progression or death from any cause). The secondary endpoints that were determined included PFS and 6-, 12- and 24-mo OS rates; objective response rate (ORR); and adverse events (AEs). The ORR was defined as the proportion of patients who achieved a complete response (CR) or partial response (PR), and the disease control rate was defined as the proportion of patients who achieved CR, PR, or stable disease. AEs during treatment were identified using patient-reported symptom data, examination-based findings, and clinical laboratory test results. The National Cancer Institute Common Terminology Criteria for AEs, version 5.0, was used to classify AEs from any cause according to type and severity.

Statistical analysis

Unstratified hazard ratios (HRs) with 95%CI and odds ratios (ORs) with the number of responders and sample sizes that compared the different treatment regimens for treating uHCC were retrieved and synthesized to determine the overall treatment effects. Potential heterogeneity among the studies was assessed using I^2 statistics. Random effects models were used to calculate pooled ORR or HR in the presence of significant heterogeneity ($I^2 > 50\%$); otherwise, the fixed effects model was used.

To account for the different distributions of covariates between the two groups, we performed PSM. Then, 1:1 matching was performed using nearest-neighbor matching based on the performance status data. In this study, the caliper of the match was 0.03. OS, PFS and survival rates were calculated using the Kaplan–Meier method and were compared between the groups using the log-rank test. Cox regression was used to explore the potential risk factors associated with survival time. All real-world clinical data are expressed as the mean ± SD, median (range), or number (%), as appropriate. Continuous variables were compared using Student's *t* test (or the Mann–Whitney U test, if appropriate), and categorical variables were compared using the chi-square test (or Fisher's exact test, if appropriate).

Table 1 *P* value of different interventions

Intervention	OR	Intervention	HR
HAIC	0.9520107	HAIC + Sorafenib	0.03757857
HAIC + Sorafenib	0.9420071	HAIC	0.09333929
SIRT	0.8131607	TACE + Lenvatinib	0.098075
TACE + Lenvatinib	0.8014429	Sintilimab + Bevacizumabbiosimila	0.24973929
Sintilimab + Bevacizumabbiosimila	0.6559643	Camrelizumab + Rivoceranib	0.30909286
Lenvatinib + Pembrolizumab	0.5922857	Atezolizumab + Bevacizumab	0.35838929
Camrelizumab + Rivoceranib	0.5853643	Lenvatinib + Pembrolizumab	0.51200714
Durvalumab + Tremelimumab	0.523425	Durvalumab + Tremelimumab	0.52634286
Durvalumab	0.3891893	Donafenib	0.62278571
Atezolizumab + Bevacizumab	0.3369036	Tislelizumab	0.66164643
Lenvatinib	0.3254286	Nivolumab	0.67260357
Tislelizumab	0.2732107	Durvalumab	0.68975714
Nivolumab	0.1859964	Lenvatinib	0.78121071
Donafenib	0.1165357	Sorafenib	0.9135
Sorafenib	0.007075	SIRT	0.97393214

HAIC: Hepatic arterial infusion chemotherapy; TACE: Transcatheter arterial chemoembolization; SIRT: Selective internal radiation therapy; HR: Hazard ratio; OR: Odds ratio.

Statistical analyses were conducted using R v4.2.2 (R Core Team, Vienna, Austria). https://www.R-project.org/). Two-sided *P* values < 0.05 were considered to indicate statistical significance.

RESULTS

Network meta-analysis on first-line treatment of uHCC

Literature search and screening results: Our initial literature search resulted 1735 articles. After deleting duplicate publications, 1079 articles remained. After screening the titles and abstracts, 68 articles were excluded. Our full-text review resulted in the removal of an additional seven articles. Ultimately, 13 studies involving 7817 patients were included in this network meta-analysis[6,8,16-25]. The literature selection process is described in Supplementary Figure 2, and the characteristics of the included patient population are shown in Supplementary Table 1.

Results of network-meta-analysis: ORRs per Response Evaluation Criteria in Solid Tumors 1.1 and HRs were reported in all 13 studies and included 15 different interventions. There was no significant heterogeneity between the studies (ORR: I^2 = 5%; HR: I^2 = 7%), so the fixed-effects model was adopted. The P scores for ORR showed that the best ORR outcomes were obtained with HAIC compared to sorafenib (OR: 35.66; 95%CI: 9.94–249.91; P: 0.952; Table 1, Supplementary Figure 3, Supplementary Table 2). The *P* values for HRs showed that the lowest HRs were obtained with HAIC plus sorafenib compared to those with sorafenib alone (HR: 0.36; 95%CI: 0.25–0.52; *P* = 0.891; Table 1, Supplementary Figure 4, Supplementary Table 3).

Retrospective study

Baseline characteristics of the patients: A total of 442 patients with uHCC were enrolled in the study; 324 patients underwent triple therapy, and 118 patients underwent AIPB. The median follow-up times were 14.6 months and 16.8 ± 10.3 months in the triple therapy group and 8.25 months and 11.7 ± 10.2 months in the AIPB group. The algorithm used for case enrollment is shown in Supplementary Figure 5. The average number of patients who received 5.08 ± 1.61 rounds of HAIC in the triple therapy group. Based on our multivariable logistic regression model, baseline characteristics, including age, ECOG PS, Child–Pugh class, maximum tumor diameter, AFP level, tumor number, and vascular invasion and extrahepatic metastasis conditions, which were significantly different between the groups, were matched (Table 2). After PSM, 88 patients in the triple therapy group were matched to 88 patients in the AIPB group (Table 2). The median age in both groups was 55.0 years, and all the patients were evaluated as having an ECOG PS ranging from 0-1. Notably, some patients in the AIPB group were diagnosed at an earlier stage. In other words, the proportion of BCLC C patients in the AIPB cohort was lower (87.5% *vs* 92%).

Table 2 Baseline characteristics before or after propensity score matching, *n* (%)

Variable	Prior to PSM			Following PSM		
	Triple therapy (*n* = 324)	AIPB (*n* = 118)	*P* value	Triple therapy (*n* = 88)	AIPB (*n* = 88)	*P* value
Age						
Mean (SD)	50.2 (11.2)	55.4 (11.6)	< 0.001	54.2 (10.8)	53.9 (11.2)	0.859
Median [Min, Max]	51.0 [23.0, 80.0]	56.5 [23.0, 82.0]		55.0 [26.0, 78.0]	55.0 [23.0, 74.0]	
Sex						
Female	36 (11.1)	8 (6.8)	0.244	11 (12.5)	6 (6.8)	0.307
Male	288 (88.9)	110 (93.2)		77 (87.5)	82 (93.2)	
ECOG PS						
0	318 (98.1)	106 (89.8)	< 0.001	85 (96.6)	85 (96.6)	1
1	6 (1.9)	11 (9.3)		3 (3.4)	3 (3.4)	
2	0 (0)	1 (0.8)		0 (0)	0 (0)	
Hepatitis virus						
Negative	27 (8.3)	15 (12.7)	0.228	11 (12.5)	12 (13.6)	1
Positive	297 (91.7)	103 (87.3)		77 (87.5)	76 (86.4)	
ALT						
mean (SD)	62.4 (72.8)	53.6 (34.9)	0.0894	58.4 (60.5)	53.2 (36.1)	0.489
Median [Min, Max]	44.6 [8.90, 930]	45.4 [6.10, 196]		41.1 [8.90, 448]	44.6 [6.10, 196]	
AST						
mean (SD)	92.5 (83.1)	88.3 (78.5)	0.627	82.0 (65.3)	87.1 (84.9)	0.657
Median [Min, Max]	66.2 [13.5, 702]	66.8 [11.1, 470]		58.7 [13.5, 327]	63.7 [11.1, 470]	
Child-Pugh class						
A	296 (91.4)	94 (79.7)	0.00133	75 (85.2)	77 (87.5)	0.826
B	28 (8.6)	24 (20.3)		13 (14.8)	11 (12.5)	
AFP > 400 ng/mL						
No	142 (43.8)	60 (50.8)	0.229	45 (51.1)	42 (47.7)	0.763
Yes	182 (56.2)	58 (49.2)		43 (48.9)	46 (52.3)	
Maximum diameter of tumor/cm						
mean (SD)	10.5 (4.25)	9.38 (4.75)	0.0291	9.86 (4.07)	9.57 (4.83)	0.668
Median [Min, Max]	10.3 [1.90, 23.5]	9.25 [1.10, 21.0]		10.0 [2.10, 19.2]	9.10 [1.10, 20.5]	
Tumor number						
Single	122 (37.7)	19 (16.1)	< 0.001	21 (23.9)	19 (21.6)	0.857
Multiple	202 (62.3)	99 (83.9)		67 (76.1)	69 (78.4)	
Vascular invasion						
No	78 (24.1)	42 (35.6)	0.0221	25 (28.4)	30 (34.1)	0.515
Yes	246 (75.9)	76 (64.4)		63 (71.6)	58 (65.9)	
Extrahepatic metastasis						
No	171 (52.8)	45 (38.1)	0.00888	34 (38.6)	38 (43.2)	0.646
Yes	153 (47.2)	73 (61.9)		54 (61.4)	50 (56.8)	
BCLC						

A	0 (0)	2 (1.7)	0.0632	0 (0)	2 (2.3)	0.309
B	30 (9.3)	11 (9.3)		7 (8.0)	9 (10.2)	
C	294 (90.7)	105 (89.0)		81 (92.0)	77 (87.5)	

AFP: Alpha-fetoprotein; ALT: Alanine aminotransferase; AST: Aspartate aminotransferase; AIPB: Angiogenesis inhibitors and programmed cell death protein 1/programmed cell death ligand 1 blockers; triple therapy: Hepatic arterial infusion chemotherapy plus angiogenesis inhibitors and programmed cell death protein 1/programmed cell death ligand 1 blockers; PSM: Propensity score matching; BCLC: Barcelona Clinic Liver Cancer; ECOG PS: Eastern Cooperative Oncology Group performance status.

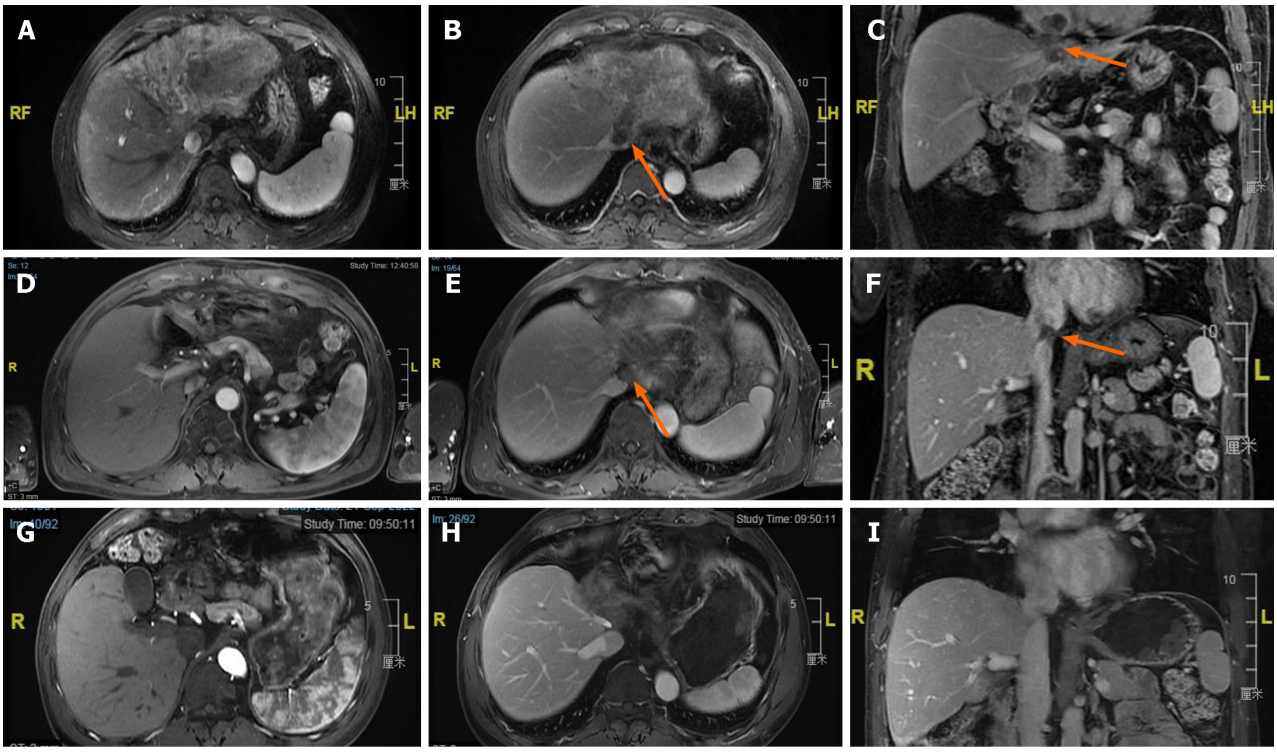

DOI: 10.3748/wjg.v30.i4.318 **Copyright** ©The Author(s) 2024.

Figure 1 A patients with unresectable hepatocellular carcinoma and inferior vena cava tumor thrombus who has received triple therapy and reached complete response according to modified Response Evaluation Criteria in Solid Tumors and the tumor thrombus has shrank completely. A-C: Images taken before treatment; D-F: Images taken at 1 month after hepatic arterial infusion chemotherapy; G-I: Images taken at the latest follow-up. A, D and G is arterial phase in the axial view. B, E and H is venous phase in the axial view. C, F and I is venous phase in the coronal view. The arrow denotes the tumor thrombus. R: Right; RF: Right foot; L: Left; LH: Left head.

Efficacy of different treatments: The ORR was 62.9% (n = 204) in the triple group and 29.7% (n = 35) in the AIPB group in the primary database. After PSM, the ORR of the triple therapy group was still greater (55.7% *vs* 35.2%, P = 0.032) (Supplementary Table 4). CR was observed in 21 patients prior to PSM and in 6 patients following PSM in the triple therapy group (an example can be seen in Figure 1). According to the Kaplan–Meier analysis, the primary data showed longer median PFS (11.1 months *vs* 6.0 months, P < 0.001) and median OS (not reached *vs* 11.8 months, P < 0.001) with triple therapy. After PSM, the median PFSs were estimated to be 12.5 months and 7.8 months (P = 0.036), and the median OS were 31.6 months and 14.6 months (HR = 2.42, 95%CI = 1.49-3.92, P < 0.001) in the triple therapy group and AIPB group, respectively (Figure 2). The 6-months, 12-months, and 24-months survival rates of the patients receiving triple therapy were 96.5%, 82.2% and 57.0%, respectively, while they were 73.5%, 54.3% and 37.7%, respectively, in the AIPB group.

Univariate analysis revealed that four factors had effects on OS in the triple therapy group: Larger tumor diameter, multiple foci, extrahepatic metastasis, Child–Pugh grade B and number of rounds of HAIC (Figure 3A). Cox multivariate regression analysis revealed that Child–Pugh grade B (HR: 1.74, P < 0.001; Figure 3B) and multiple foci (HR: 2.17, P < 0.001; Figure 3B) were risk factors for poor long-term survival, and > 4 rounds of HAIC was a protective factor for survival (HR: 0.43, P < 0.001; Figure 3B). Survival analysis also revealed that patients who received > 4 rounds of HAIC (not reached *vs* 18.2 months; P < 0.001; Supplementary Figure 6A) or who were diagnosed with a single disease focus (not reached *vs* 24.6 months; P < 0.001; Supplementary Figure 6B) had longer OS. Subgroup analysis of OS using forest plots revealed that triple therapy was more effective in most patients, especially for males, Child-Pugh A patients, patients aged < 60 years, and patients diagnosed with multiple tumors or extrahepatic metastasis (Figure 3C).

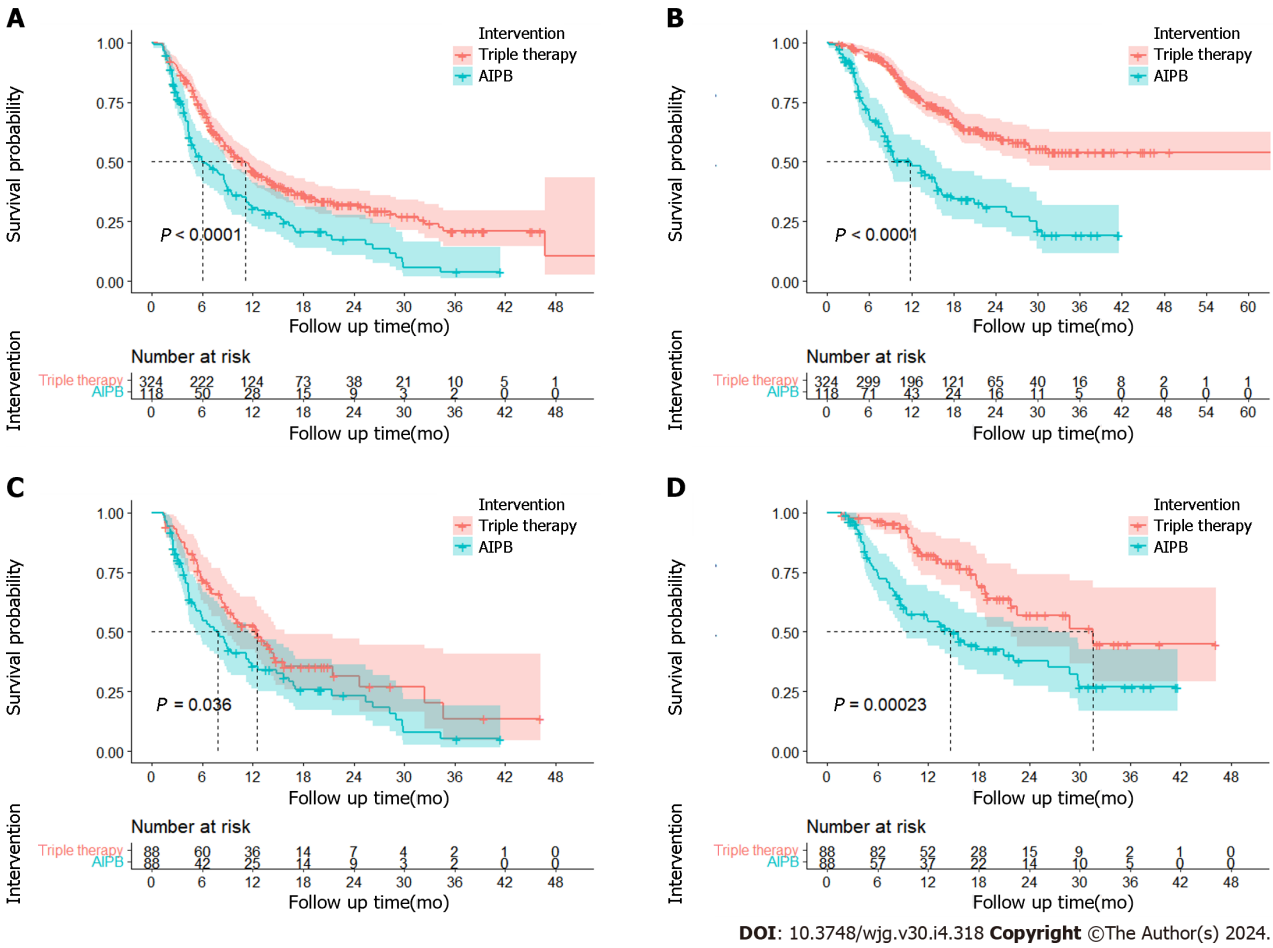

DOI: 10.3748/wjg.v30.i4.318

Figure 2 Kaplan-Meier curves of progression-free survival and overall survival in the triple therapy group and angiogenesis inhibitors and programmed cell death protein 1/programmed cell death ligand 1 blockers group. A: Prior to propensity score matching (PSM), median progression-free survival (PFS) was 11.1 *vs* 6.0 mo, $P < 0.001$; B: Prior to PSM, median overall survival (OS) was not reached *vs* 11.8 mo, $P < 0.001$; C: Following PSM, median PFS was 12.5 *vs* 7.8 mo, $P = 0.036$; D: Following PSM, median OS was 31.6 *vs* 14.6 mo, $P < 0.001$. triple therapy: Hepatic arterial infusion chemotherapy plus angiogenesis inhibitors and programmed cell death protein 1/programmed cell death ligand 1 blockers; AIPB: Angiogenesis inhibitors and programmed cell death protein 1/programmed cell death ligand 1 blockers.

Safety of different treatments: After PSM, the incidence of AEs in the triple therapy group was greater than that in the AIPB group (94.3% *vs* 75.4%, $P < 0.001$). Although more Grade 3-4 AEs occurred in the triple therapy group, there was no significant difference in the incidence of Grade 3-4 AEs (56.8% *vs* 43.2%, $P = 0.097$), and there were no Grade 5 AEs (Table 3). The most common AE was abdominal pain in the triple therapy group, for which the incidence was 79.8% (259/324). When they started HAIC treatment, many patients had varying degrees of abdominal pain during the infusion of oxaliplatin. This was typically managed by slowing the speed of infusion or temporarily stopping it. In some cases of particularly severe and acute abdominal pain, anisodamine or lidocaine was administered through intravenous injection or an arterial catheter to relieve the pain. Two patients developed hepatic comas following HAIC but fully recovered during treatment. In addition, liver dysfunction, including increases in aminotransferases and/or bilirubin, was relatively common in both groups, not only because of drug-related side effects but also because of their own background of liver cirrhosis.

DISCUSSION

Although the first-line treatment recommended by authoritative clinical guidelines for uHCC is AIPB, such as atezolizumab plus bevacizumab, these treatments have a number of limitations in clinical applications. The default anti-inflammatory or immunotolerant immune status of the liver may interfere with the drugs that act on it[26], which may lead to a relatively low ORR. The main cause of death among patients with uHCC is liver tumor progression[27,28]. Although there are a number of different protocols for administering AIPB, the median patient survival time using this approach has remained less than 24 months[17,19,20,29]. In addition, the IMbrave150 studies suggested that the effects of AIPB treatment are likely to be severely diminished if patients are diagnosed with high-risk factors, such as tumor invasion of the main trunk of the portal vein (Vp4), bile duct invasion, or/or tumor occupancy of ≥ 50% of the liver[17,30].

Table 3 Summary of adverse events, *n* (%)

	Before PSM				After PSM			
	Triple therapy group (*n* = 324)		AIPB group (*n* = 118)		Triple therapy group (*n* = 88)		AIPB group (*n* = 88)	
	Grade 1-2	Grade 3-4	Grade 1-2	Grade 3-4	Grade 1-2	Grade 3-4	Grade 1-2	Grade 3-4
Fever	67 (20.7)	23 (7.1)	4 (3.4)	2 (1.7)	20 (22.7)	8 (9.1)	4 (4.5)	0 (0)
Nausea	100 (30.9)	0 (0)	6 (5.1)	0 (0)	24 (27.3)	0 (0)	5 (5.7)	0 (0)
Vomit	32 (9.9)	15 (4.6)	7 (5.9)	6 (5.1)	7 (8.0)	3 (3.4)	6 (6.8)	4 (4.5)
Abdominal pain	97 (29.9)	162 (50.0)	18 (15.3)	18 (15.3)	24 (27.3)	44 (50.0)	15 (17.0)	13 (14.8)
ALT increased	79 (24.4)	125 (38.6)	32 (27.1)	39 (33.1)	27 (30.4)	33 (37.5)	22 (25.0)	29 (33.0)
AST increased	130 (40.1)	161 (49.7)	36 (30.5)	44 (37.3)	40 (45.5)	49 (55.7)	26 (29.5)	34 (38.6)
Hyperbilirubinemia	37 (11.4)	7 (2.2)	7 (5.9)	11 (9.3)	10 (11.4)	0 (0)	4 (4.5)	8 (9.1)
Anemia	37 (11.4)	8 (2.5)	7 (5.9)	4 (3.4)	11 (12.5)	1 (1.1)	5 (5.7)	3 (3.4)
Neutropenia	86 (26.5)	20 (6.2)	9 (7.6)	12 (10.2)	29 (33.0)	5 (5.7)	5 (5.7)	9 (10.2)
Thrombocytopenia	103 (31.8)	90 (27.8)	27 (22.9)	20 (16.9)	24 (27.3)	16 (18.2)	20 (22.7)	13 (14.8)
Bleeding	48 (14.8)	3 (0.9)	1 (0.8)	1 (0.8)	12 (13.6)	1 (1.1)	1 (1.1)	1 (1.1)
Diarrhea	62 (19.1)	60 (18.5)	22 (18.6)	3 (2.5)	17 (19.3)	5 (5.7)	17 (19.3)	3 (3.4)
Hoarseness	80 (24.7)	0 (0)	13 (11.0)	0 (0)	21 (23.9)	0 (0)	10 (11.4)	0 (0)
Rash	92 (28.4)	4 (1.2)	28 (23.7)	4 (3.4)	24 (27.3)	0 (0)	20 (22.7)	3 (3.4)
HFS	69 (21.3)	9 (2.8)	19 (16.1)	18 (15.3)	18 (20.5)	1 (1.1)	14 (15.9)	11 (12.5)
Hypertension	76 (23.5)	11 (3.4)	31 (26.3)	34 (28.8)	22 (25.0)	3 (3.4)	23 (26.1)	27 (30.7)
RCCEP	42 (13.0)	14 (4.3)	16 (13.6)	6 (5.1)	11 (12.5)	5 (5.7)	13 (14.8)	6 (6.8)
Hypothyroidism	64 (19.8)	8 (2.5)	2 (1.7)	0 (0)	18 (20.5)	2 (2.3)	0 (0)	0 (0)
Fatigue	32 (9.9)	31 (9.6)	4 (3.4)	4 (3.4)	6 (6.8)	8 (9.1)	3 (3.4)	2 (2.3)
Hepatitis	10 (3.1)	1 (0.3)	0 (0)	0 (0)	5 (5.7)	1 (1.1)	0 (0)	0 (0)
Coma	0 (0)	2 (0.6)	0 (0)	0 (0)	0 (0)	0 (0)	0 (0)	0 (0)

AFP: Alpha-fetoprotein; AIPB: Angiogenesis inhibitors and programmed cell death protein 1/programmed cell death ligand 1 blockers; triple therapy: Hepatic arterial infusion chemotherapy plus angiogenesis inhibitors and programmed cell death protein 1/programmed cell death ligand 1 blockers; ALT: Alanine aminotransferase; AST: Aspartate aminotransferase; HFS: Hand-foot syndrome; RCCEP: Reactive cutaneous capillary endothelial proliferation.

Many uHCC patients in some areas, especially in China, are diagnosed with vascular invasion or/or a high tumor burden. The most effective way to prolong survival is to control liver lesions. In terms of local hepatic treatment for uHCC, the most popular choice for most physicians is transcatheter arterial chemoembolization (TACE). Nonetheless, if the tumor burden is high, there is a very high probability of "TACE failure/refractoriness"[31-33]. If patients are diagnosed with reduced or absent portal vein blood supplies caused by portal vein tumor thrombi or severe cirrhosis, the use of TACE will be limited. Several studies have revealed that HAIC is more effective than TACE for large HCCs[34]. The FOHAIC study suggested that FOLFOX-HAIC had a significant effect on patients with uHCC and that HAIC could be used as an additional local hepatic treatment for uHCC[8]. According to our meta-analysis, HAIC plus sorafenib or HAIC alone was able to prolong the survival time of patients with uHCC more than AIPB regimens. Unfortunately, there is a scarcity of prospective or retrospective studies with large sample sizes on triple therapy.

Our retrospective data revealed that triple therapy was effective and safe. The ORR, PFS, and OS of patients receiving triple therapy (ORR: 33.2% per mRECIST; PFS: 6.9 months; OS: 19.2 months) outperformed those of patients receiving most AIPB regimens. For example, this was true for atezolizumab plus bevacizumab (ORR: 33.2% per mRECIST; PFS: 6.9 months; OS: 19.2 months) in the IMbrave150 trial; pembrolizumab plus lenvatinib (ORR: 40.8% per mRECIST; PFS: 8.2 months; OS: 21.2 months) in the LEAP002 trial; and camrelizumab plus rivoceranib (ORR: 33.1% per mRECIST; PFS: 5.6 months; OS: 22.1 months) in the CARES 310 study[7,17,19,29]. The survival benefit observed in this study may be due to the synergistic antitumor effects of these chemical agents. Transarterial chemotherapy can induce immunogenic cell death by releasing tumor-related antigens and supporting the evolution of tumor-specific CD8+ T cells, which may synergize with angiogenesis inhibitors to enhance the effect of PD-1/PD-L1 blockers[35-37]. Increased concentrations of drugs in the liver can cause liver lesions to shrink directly and slow the deterioration of liver function caused by disease progression. According to our survival analysis, the patients in the AIPB subgroup had shorter survival times than those

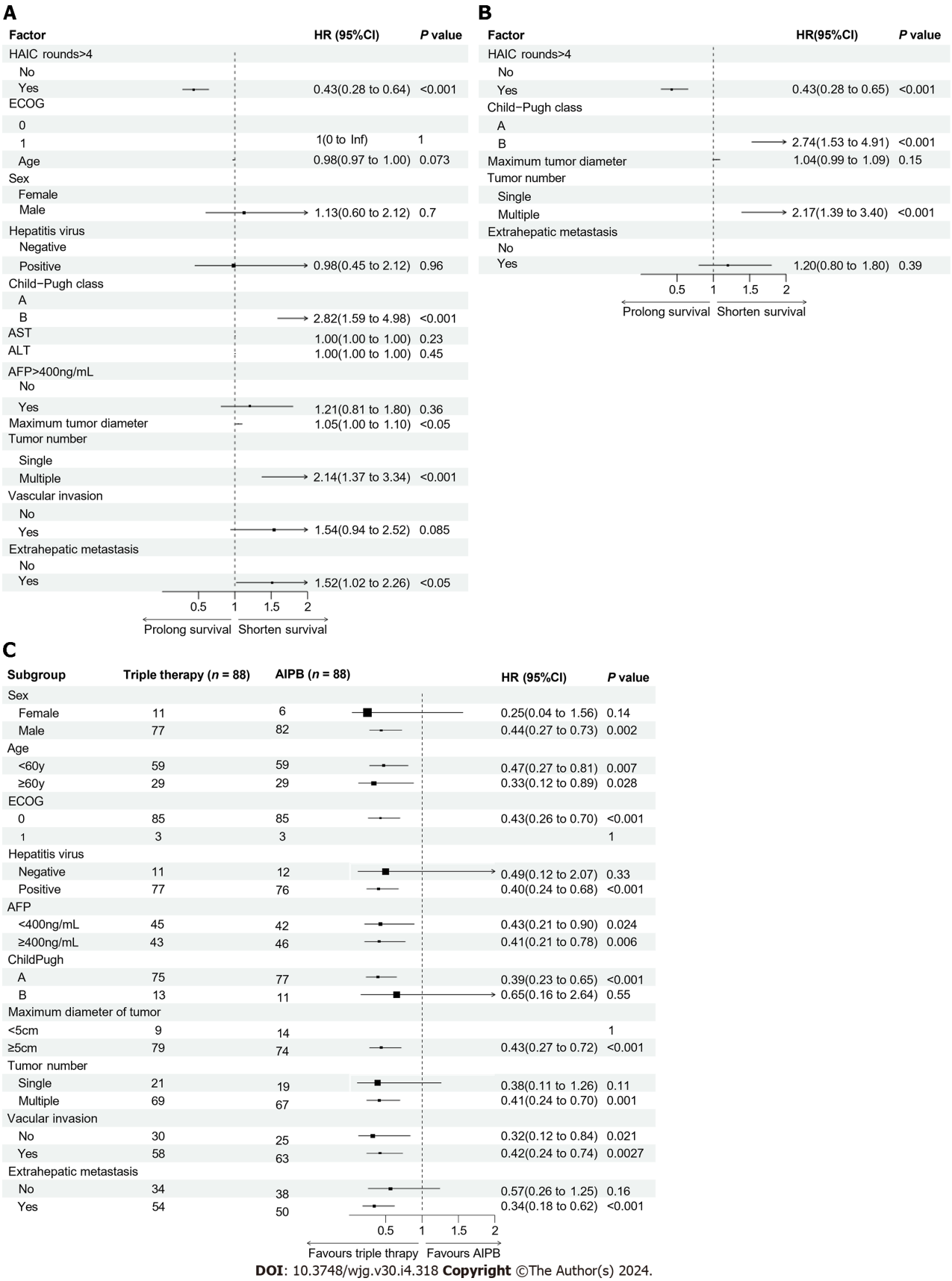

DOI: 10.3748/wjg.v30.i4.318

Figure 3 Forest plots of Cox regression analysis. A: The results of univariatable Cox regression in the triple therapy group prior to propensity score matching (PSM); B: The results of multivariable Cox regression in the triple therapy group prior to PSM; C: Subgroup analysis of overall survival after PSM. HR: Hazard ratio; ECOG: Eastern Cooperative Oncology Group; Inf: Infinite; EHM: Extrahepatic metastasis; AFP: Alpha-fetoprotein; ALT: Alanine aminotransferase; AST: Aspartate aminotransferase; triple therapy: Hepatic arterial infusion chemotherapy plus angiogenesis inhibitors and programmed cell death protein 1/programmed cell death ligand 1 blockers; AIPB: Angiogenesis inhibitors and programmed cell death protein 1/programmed cell death ligand 1 blockers; HAIC: Hepatic arterial infusion

chemotherapy.

in the other trials on AIPB regimens, likely due to their poor baseline conditions prior to treatment. More than half of the patients (n = 58) in the AIBP group were diagnosed with major vein tumor thrombus, and the mean maximum tumor diameter was more than 9 cm, suggesting that the patients in this group had high tumor burdens. The median OS of similar patients in the IMbrave150 study was only 7.8 months, which is consistent with the results of our study[30].

We also attempted to identify which factors could influence the effect of triple therapy and found that > 4 rounds of HAIC were a protective factor. Four rounds of HAIC represent a regimen similar to the median number of HAIC rounds reported in several other studies[8,38-40]. The number of HAIC rounds performed was strongly affected by each patient's response to triple therapy because if tumors progress after the first few HAIC cycles, the HAIC cycles will be discontinued. Multiple liver lesions have also been recognized as risk factors because the presence of multiple lesions often implies the presence of multiple feeding vessels. Therefore, even if attempts are made to embolize other arteries until there is only a single blood supply, there is a high probability that some small arteries may be missed. To ensure that all lesions can be treated by HAIC, a microcatheter should be placed in a larger blood vessel branch, which implies that more normal liver tissue is likely to be damaged by the administered drugs, potentially harming liver function.

Overall, the incidence of adverse reactions to triple therapy was greater than that reported in the AIPB group. The combination of HAIC and systematic treatments was able to increase the incidence of AEs; another reasonable explanation is that most AIBP patients were treated and followed up as outpatients so that some AEs, especially some slight AEs, were ignored. Notably, abnormal liver function was the common AE in the triple therapy group. However, unlike many other local treatments, the effects of HAIC on liver function appear to be largely short-term, with few apparent adverse effects on long-term survival. However, we believe that the limitation of triple therapy in the Child-Pugh B population with poor hepatic functional reserve may result from irreversible liver injury secondary to chemotherapy. Another common AE, thrombocytopenia, is caused not only by myelosuppression due to chemotherapy but also by hypersplenism secondary to cirrhosis. A substantial proportion of the patients recovered from thrombocytopenia following splenic embolization.

A substantial amount of information was lost due to the limitations of this retrospective study. Our sample included only patients from China, so the study was inevitably affected by some degree of sampling bias. It remains unclear exactly which biomarkers can be used to judge patients' prognoses. Studies at the cellular or molecular level could not be carried out due to a lack of tumor biopsy samples. To prove the efficacy and safety of triple therapy, additional large-scale prospective RCTs on this topic are warranted.

CONCLUSION

This meta-analysis suggested that HAIC-based treatment regimens were able to effectively improve the prognosis in patients with uHCC. Our findings confirmed that even though the triple therapy protocol increased the incidence and severity of AEs, it yielded a higher ORR and longer PFS and OS than AIPB.

ARTICLE HIGHLIGHTS

Research background

Unresectable hepatocellular carcinoma had been difficult to be treated in the past, hepatic arterial chemotherapy infusion chemotherapy (HAIC) as well as angiogenesis inhibitors plus programmed cell death protein 1/programmed cell death ligand 1 (PD-1/PD-L1) blockers were proved to prolong the unresectable hepatocellular carcinoma (uHCC) patients' survival, respectively. Meanwhile, some phase II single arm suggested that the combination of HAIC and angiogenesis inhibitors and PD-1/PD-L1 blockers (AIPB) (triple therapy) was effective in treating uHCC. But which treatment is the best choice was still confused. The study was designed to answer the question.

Research motivation

The best first-line treatment for uHCC was unclear and there was lack of studies to compare the efficacy and safety between triple therapy and AIPB. There were so many choices that clinical staff may be confused when they need to treat uHCC patients. If we can find the relatively better regimen, it is helpful for the standardization of the uHCC treatment to improve the patients' prognosis.

Research objectives

The study aimed to identified the HAIC and HAIC-based treatments was the best choice for uHCC. Based on the result, we explored the efficacy and safety of one of HAIC-based treatment, triple therapy in the real-world condition compared to AIPB. The results of the study could be the evidence to guide clinical reasonable treatment and prospective clinical study.

Research methods
We have tried to perform a network meta-analysis to find the first choice to uHCC and identified the efficacy and safety of triple therapy compared to AIPB through a retrospective cohort study.

Research results
The network meta-analysis including 13 phase randomized controlled trials (RCTs) showed HAIC and HAIC-based treatments were likely to be the first choice to treat uHCC. HAIC plus camrelizumab plus AIPB (triple therapy) had better progression-free survival and overall survival than AIPB without HAIC for uHCC. Even though the incidence of adverse events in the triple therapy group was higher than the AIPB group, the safety of triple therapy was still acceptable.

Research conclusions
HAIC-based treatments were better than other regimens for treating uHCC. Triple therapy was more effective than AIPB in the Chinese uHCC population. All of the above results proved the significance of local treatments in the uHCC treating.

Research perspectives
There is absolutely a need for studies at the cellular or molecular level and additional large-scale prospective RCTs on this topic.

ACKNOWLEDGEMENTS

We are thankful for the support of the patients in this study. We are grateful to Dr. Fei Cao and Ms. Xiao-Ting Bei for their assistance with the clinical management of the patients.

FOOTNOTES

Co-first authors: Yu-Zhe Cao and Guang-Lei Zheng.

Co-corresponding authors: Zi-Lin Huang and Meng-Xuan Zuo.

Author contributions: Cao YZ, Zheng GL, Zuo MX and Huang ZL participated equally in conceptualization; Cao YZ, Zuo MX and Zheng GL made great contribution in the in the data curation, formal analysis, methodology and investigation; Zhang TQ, Shao HY and Pan JY has participated in the investigation and the validation; The project administration and supervision were accomplished by Huang ZL and Zuo MX; Cao YZ and Zheng GL had finished the original draft; Zuo MX and Huang ZL has been responsible for the review and editing; All authors have provided final approval of the manuscript version to be submitted for publication. Cao YZ and Zheng GL, contributed equally to this work and share first authorship for their contribution in conceptualization, data curation, formal analysis, methodology, investigation and draft writing. Huang ZL and Zuo MX, contributed equally to this work and are co-corresponding authors for their contribution in conceptualization, project administration, supervision, revision and approvement for final edition of the manuscript.

Supported by Natural Science Foundation of Guangdong Province, No. 2020A1515011539.

Institutional review board statement: This study was reviewed and approved by the Sun Yat-sen University Cancer Center Ethics Committee. Informed consent was waived due to the retrospective nature of the analysis.

Informed consent statement: Informed consent was waived due to the retrospective nature of the analysis, which has been approved by Ethic Committee of Sun Yat-sen University Cancer Center.

Conflict-of-interest statement: All the authors report no relevant conflicts of interest for this article.

Data sharing statement: The datasets of the manuscript is available from the corresponding authors at Sun Yat-sen University Cancer Center Research Data Deposit repository (https://www.researchdata.org.cn/). Consent was not obtained but the presented data are anonymized and risk of identification is low.

Country/Territory of origin: China

ORCID number: Tian-Qi Zhang 0000-0002-1528-5323; Zi-Lin Huang 0000-0002-1643-1994; Meng-Xuan Zuo 0000-0003-3589-7316.

S-Editor: Li L

L-Editor: A
P-Editor: Chen YX

REFERENCES

1 **Sung H**, Ferlay J, Siegel RL, Laversanne M, Soerjomataram I, Jemal A, Bray F. Global Cancer Statistics 2020: GLOBOCAN Estimates of Incidence and Mortality Worldwide for 36 Cancers in 185 Countries. *CA Cancer J Clin* 2021; **71**: 209-249 [PMID: 33538338 DOI: 10.3322/caac.21660]

2 **Thomas MB**, Jaffe D, Choti MM, Belghiti J, Curley S, Fong Y, Gores G, Kerlan R, Merle P, O'Neil B, Poon R, Schwartz L, Tepper J, Yao F, Haller D, Mooney M, Venook A. Hepatocellular carcinoma: consensus recommendations of the National Cancer Institute Clinical Trials Planning Meeting. *J Clin Oncol* 2010; **28**: 3994-4005 [PMID: 20679622 DOI: 10.1200/JCO.2010.28.7805]

3 **Villanueva A**. Hepatocellular Carcinoma. *N Engl J Med* 2019; **380**: 1450-1462 [PMID: 30970190 DOI: 10.1056/NEJMra1713263]

4 **Kudo M**, Arizumi T. Transarterial Chemoembolization in Combination with a Molecular Targeted Agent: Lessons Learned from Negative Trials (Post-TACE, BRISK-TA, SPACE, ORIENTAL, and TACE-2). *Oncology* 2017; **93**: 127-134 [PMID: 29258086 DOI: 10.1159/000481243]

5 **Llovet JM**, Ricci S, Mazzaferro V, Hilgard P, Gane E, Blanc JF, de Oliveira AC, Santoro A, Raoul JL, Forner A, Schwartz M, Porta C, Zeuzem S, Bolondi L, Greten TF, Galle PR, Seitz JF, Borbath I, Häussinger D, Giannaris T, Shan M, Moscovici M, Voliotis D, Bruix J; SHARP Investigators Study Group. Sorafenib in advanced hepatocellular carcinoma. *N Engl J Med* 2008; **359**: 378-390 [PMID: 18650514 DOI: 10.1056/NEJMoa0708857]

6 **Kudo M**, Finn RS, Qin S, Han KH, Ikeda K, Piscaglia F, Baron A, Park JW, Han G, Jassem J, Blanc JF, Vogel A, Komov D, Evans TRJ, Lopez C, Dutcus C, Guo M, Saito K, Kraljevic S, Tamai T, Ren M, Cheng AL. Lenvatinib *vs* sorafenib in first-line treatment of patients with unresectable hepatocellular carcinoma: a randomised phase 3 non-inferiority trial. *Lancet* 2018; **391**: 1163-1173 [PMID: 29433850 DOI: 10.1016/S0140-6736(18)30207-1]

7 **Finn RS**, Qin S, Ikeda M, Galle PR, Ducreux M, Kim TY, Kudo M, Breder V, Merle P, Kaseb AO, Li D, Verret W, Xu DZ, Hernandez S, Liu J, Huang C, Mulla S, Wang Y, Lim HY, Zhu AX, Cheng AL; IMbrave150 Investigators. Atezolizumab plus Bevacizumab in Unresectable Hepatocellular Carcinoma. *N Engl J Med* 2020; **382**: 1894-1905 [PMID: 32402160 DOI: 10.1056/NEJMoa1915745]

8 **Lyu N**, Wang X, Li JB, Lai JF, Chen QF, Li SL, Deng HJ, He M, Mu LW, Zhao M. Arterial Chemotherapy of Oxaliplatin Plus Fluorouracil Versus Sorafenib in Advanced Hepatocellular Carcinoma: A Biomolecular Exploratory, Randomized, Phase III Trial (FOHAIC-1). *J Clin Oncol* 2022; **40**: 468-480 [PMID: 34905388 DOI: 10.1200/JCO.21.01963]

9 **Gu YK**, Zhang TQ, Zuo MX, Geng ZJ, Li JB, Huang ZL, Wu PH. Hepatic artery infusion chemotherapy (HAIC) combined with apatinib and camrelizumab for hepatocellular carcinoma (HCC) in BCLC stage c: A prospective, single-arm, phase II trial (TRIPLET study). Conference Abstract. *Journal of Clinical Oncology***40** [DOI: 10.1200/JCO.2022.40.16_suppl.4106]

10 **Lai Z**, He M, Bu X, Xu Y, Huang Y, Wen D, Li Q, Xu L, Zhang Y, Wei W, Chen M, Kan A, Shi M. Lenvatinib, toripalimab plus hepatic arterial infusion chemotherapy in patients with high-risk advanced hepatocellular carcinoma: A biomolecular exploratory, phase II trial. *Eur J Cancer* 2022; **174**: 68-77 [PMID: 35981413 DOI: 10.1016/j.ejca.2022.07.005]

11 **Liu BJ**, Gao S, Zhu X, Guo JH, Kou FX, Liu SX, Zhang X, Wang XD, Cao G, Chen H, Liu P, Xu HF, Gao QZ, Yang RJ. Real-world study of hepatic artery infusion chemotherapy combined with anti-PD-1 immunotherapy and tyrosine kinase inhibitors for advanced hepatocellular carcinoma. *Immunotherapy* 2021; **13**: 1395-1405 [PMID: 34607482 DOI: 10.2217/imt-2021-0192]

12 **Xu Y**, Fu S, Mao Y, Huang S, Li D, Wu J. Efficacy and safety of hepatic arterial infusion chemotherapy combined with programmed cell death protein-1 antibody and lenvatinib for advanced hepatocellular carcinoma. *Front Med (Lausanne)* 2022; **9**: 919069 [PMID: 36117969 DOI: 10.3389/fmed.2022.919069]

13 **Chen LT**, Martinelli E, Cheng AL, Pentheroudakis G, Qin S, Bhattacharyya GS, Ikeda M, Lim HY, Ho GF, Choo SP, Ren Z, Malhotra H, Ueno M, Ryoo BY, Kiang TC, Tai D, Vogel A, Cervantes A, Lu SN, Yen CJ, Huang YH, Chen SC, Hsu C, Shen YC, Tabernero J, Yen Y, Hsu CH, Yoshino T, Douillard JY. Pan-Asian adapted ESMO Clinical Practice Guidelines for the management of patients with intermediate and advanced/relapsed hepatocellular carcinoma: a TOS-ESMO initiative endorsed by CSCO, ISMPO, JSMO, KSMO, MOS and SSO. *Ann Oncol* 2020; **31**: 334-351 [PMID: 32067677 DOI: 10.1016/j.annonc.2019.12.001]

14 **Reig M**, Forner A, Rimola J, Ferrer-Fàbrega J, Burrel M, Garcia-Criado Á, Kelley RK, Galle PR, Mazzaferro V, Salem R, Sangro B, Singal AG, Vogel A, Fuster J, Ayuso C, Bruix J. BCLC strategy for prognosis prediction and treatment recommendation: The 2022 update. *J Hepatol* 2022; **76**: 681-693 [PMID: 34801630 DOI: 10.1016/j.jhep.2021.11.018]

15 **Rinella ME**, Neuschwander-Tetri BA, Siddiqui MS, Abdelmalek MF, Caldwell S, Barb D, Kleiner DE, Loomba R. AASLD Practice Guidance on the clinical assessment and management of nonalcoholic fatty liver disease. *Hepatology* 2023; **77**: 1797-1835 [PMID: 36727674 DOI: 10.1097/HEP.0000000000000323]

16 **He M**, Li Q, Zou R, Shen J, Fang W, Tan G, Zhou Y, Wu X, Xu L, Wei W, Le Y, Zhou Z, Zhao M, Guo Y, Guo R, Chen M, Shi M. Sorafenib Plus Hepatic Arterial Infusion of Oxaliplatin, Fluorouracil, and Leucovorin *vs* Sorafenib Alone for Hepatocellular Carcinoma With Portal Vein Invasion: A Randomized Clinical Trial. *JAMA Oncol* 2019; **5**: 953-960 [PMID: 31070690 DOI: 10.1001/jamaoncol.2019.0250]

17 **Cheng AL**, Qin S, Ikeda M, Galle PR, Ducreux M, Kim TY, Lim HY, Kudo M, Breder V, Merle P, Kaseb AO, Li D, Verret W, Ma N, Nicholas A, Wang Y, Li L, Zhu AX, Finn RS. Updated efficacy and safety data from IMbrave150: Atezolizumab plus bevacizumab *vs* sorafenib for unresectable hepatocellular carcinoma. *J Hepatol* 2022; **76**: 862-873 [PMID: 34902530 DOI: 10.1016/j.jhep.2021.11.030]

18 **Qin S**, Chan LS, Gu S, Bai Y, Ren Z, Lin X, Chen Z, Jia W, Jin Y, Guo Y, Sultanbaev AV, Pazgan-Simon M, Pisetska M, Liang X, Chen C, Nie Z, Wang L, Cheng AL, Kaseb A, Vogel A. LBA35 Camrelizumab (C) plus rivoceranib (R) *vs* sorafenib (S) as first-line therapy for unresectable hepatocellular carcinoma (uHCC): A randomized, phase III trial. Conference Abstract. *Annals of Oncology* 2022; **33**: S1401-S1402 [DOI: 10.1016/j.annonc.2022.08.032]

19 **Finn RS**, Kudo M, Merle P, Meyer T, Qin S, Ikeda M, Xu R, Edeline J, Ryoo BY, Ren Z, Cheng AL, Galle PR, Kaneko S, Kumada H, Wang A, Mody K, Dubrovsky L, Siegel AB, Llovet J. LBA34 Primary results from the phase III LEAP-002 study: Lenvatinib plus pembrolizumab *vs* lenvatinib as first-line (1L) therapy for advanced hepatocellular carcinoma (aHCC). Conference Abstract. *Annals of Oncology* 2022; **33**: S1401 [DOI: 10.1016/j.annonc.2022.08.031]

20 **Ren Z**, Xu J, Bai Y, Xu A, Cang S, Du C, Li Q, Lu Y, Chen Y, Guo Y, Chen Z, Liu B, Jia W, Wu J, Wang J, Shao G, Zhang B, Shan Y, Meng Z, Gu S, Yang W, Liu C, Shi X, Gao Z, Yin T, Cui J, Huang M, Xing B, Mao Y, Teng G, Qin Y, Xia F, Yin G, Yang Y, Chen M, Wang Y, Zhou H, Fan J; ORIENT-32 study group. Sintilimab plus a bevacizumab biosimilar (IBI305) *vs* sorafenib in unresectable hepatocellular carcinoma (ORIENT-32): a randomised, open-label, phase 2-3 study. *Lancet Oncol* 2021; **22**: 977-990 [PMID: 34143971 DOI: 10.1016/S1470-2045(21)00252-7]

21 **Yau T**, Park JW, Finn RS, Cheng AL, Mathurin P, Edeline J, Kudo M, Harding JJ, Merle P, Rosmorduc O, Wyrwicz L, Schott E, Choo SP, Kelley RK, Sieghart W, Assenat E, Zaucha R, Furuse J, Abou-Alfa GK, El-Khoueiry AB, Melero I, Begic D, Chen G, Neely J, Wisniewski T, Tschaika M, Sangro B. Nivolumab *vs* sorafenib in advanced hepatocellular carcinoma (CheckMate 459): a randomised, multicentre, open-label, phase 3 trial. *Lancet Oncol* 2022; **23**: 77-90 [PMID: 34914889 DOI: 10.1016/S1470-2045(21)00604-5]

22 **Chow PKH**, Gandhi M, Tan SB, Khin MW, Khasbazar A, Ong J, Choo SP, Cheow PC, Chotipanich C, Lim K, Lesmana LA, Manuaba TW, Yoong BK, Raj A, Law CS, Cua IHY, Lobo RR, Teh CSC, Kim YH, Jong YW, Han HS, Bae SH, Yoon HK, Lee RC, Hung CF, Peng CY, Liang PC, Bartlett A, Kok KYY, Thng CH, Low AS, Goh ASW, Tay KH, Lo RHG, Goh BKP, Ng DCE, Lekurwale G, Liew WM, Gebski V, Mak KSW, Soo KC; Asia-Pacific Hepatocellular Carcinoma Trials Group. SIRveNIB: Selective Internal Radiation Therapy Versus Sorafenib in Asia-Pacific Patients With Hepatocellular Carcinoma. *J Clin Oncol* 2018; **36**: 1913-1921 [PMID: 29498924 DOI: 10.1200/JCO.2017.76.0892]

23 **Peng Z**, Fan W, Zhu B, Wang G, Sun J, Xiao C, Huang F, Tang R, Cheng Y, Huang Z, Liang Y, Fan H, Qiao L, Li F, Zhuang W, Peng B, Wang J, Li J, Kuang M. Lenvatinib Combined With Transarterial Chemoembolization as First-Line Treatment for Advanced Hepatocellular Carcinoma: A Phase III, Randomized Clinical Trial (LAUNCH). *J Clin Oncol* 2023; **41**: 117-127 [PMID: 35921605 DOI: 10.1200/JCO.22.00392]

24 **Qin S**, Bi F, Gu S, Bai Y, Chen Z, Wang Z, Ying J, Lu Y, Meng Z, Pan H, Yang P, Zhang H, Chen X, Xu A, Cui C, Zhu B, Wu J, Xin X, Wang J, Shan J, Chen J, Zheng Z, Xu L, Wen X, You Z, Ren Z, Liu X, Qiu M, Wu L, Chen F. Donafenib Versus Sorafenib in First-Line Treatment of Unresectable or Metastatic Hepatocellular Carcinoma: A Randomized, Open-Label, Parallel-Controlled Phase II-III Trial. *J Clin Oncol* 2021; **39**: 3002-3011 [PMID: 34185551 DOI: 10.1200/JCO.21.00163]

25 **Qin S**, Kudo M, Meyer T, Finn RS, Vogel A, Bai Y, Guo Y, Meng Z, Zhang T, Satoh T, Hiraoka A, Marino D, Assenat E, Wyrwicz L, Campos MC, Hsing-Tao K, Boisserie F, Li S, Chen Y, Zhu AX. LBA36 Final analysis of RATIONALE-301: Randomized, phase III study of tislelizumab *vs* sorafenib as first-line treatment for unresectable hepatocellular carcinoma. Conference Abstract. *Annals of Oncology***33**: S1402-S1403 [DOI: 10.1016/j.annonc.2022.08.033]

26 **Kubes P**, Jenne C. Immune Responses in the Liver. *Annu Rev Immunol* 2018; **36**: 247-277 [PMID: 29328785 DOI: 10.1146/annurev-immunol-051116-052415]

27 **Zhu AX**, Finn RS, Edeline J, Cattan S, Ogasawara S, Palmer D, Verslype C, Zagonel V, Fartoux L, Vogel A, Sarker D, Verset G, Chan SL, Knox J, Daniele B, Webber AL, Ebbinghaus SW, Ma J, Siegel AB, Cheng AL, Kudo M; KEYNOTE-224 investigators. Pembrolizumab in patients with advanced hepatocellular carcinoma previously treated with sorafenib (KEYNOTE-224): a non-randomised, open-label phase 2 trial. *Lancet Oncol* 2018; **19**: 940-952 [PMID: 29875066 DOI: 10.1016/S1470-2045(18)30351-6]

28 **Gauci ML**, Lanoy E, Champiat S, Caramella C, Ammari S, Aspeslagh S, Varga A, Baldini C, Bahleda R, Gazzah A, Michot JM, Postel-Vinay S, Angevin E, Ribrag V, Hollebecque A, Soria JC, Robert C, Massard C, Marabelle A. Long-Term Survival in Patients Responding to Anti-PD-1/PD-L1 Therapy and Disease Outcome upon Treatment Discontinuation. *Clin Cancer Res* 2019; **25**: 946-956 [PMID: 30297458 DOI: 10.1158/1078-0432.CCR-18-0793]

29 **Qin S**, Chan SL, Gu S, Bai Y, Ren Z, Lin X, Chen Z, Jia W, Jin Y, Guo Y, Hu X, Meng Z, Liang J, Cheng Y, Xiong J, Ren H, Yang F, Li W, Chen Y, Zeng Y, Sultanbaev A, Pazgan-Simon M, Pisetska M, Melisi D, Ponomarenko D, Osypchuk Y, Sinielnikov I, Yang TS, Liang X, Chen C, Wang L, Cheng AL, Kaseb A, Vogel A; CARES-310 Study Group. Camrelizumab plus rivoceranib *vs* sorafenib as first-line therapy for unresectable hepatocellular carcinoma (CARES-310): a randomised, open-label, international phase 3 study. *Lancet* 2023; **402**: 1133-1146 [PMID: 37499670 DOI: 10.1016/S0140-6736(23)00961-3]

30 **Finn RS**, Qin S, Ikeda M, Galle PR, Ducreux M, Kim TY, Kudo M, Lim HY, Breder V, Merle P, Kaseb A, Li D, Feng YH, Verret W, Nicholas A, Li L, Ma N, Zhu AX, Cheng AL. IMbrave150: Updated efficacy and safety by risk status in patients (pts) receiving atezolizumab (atezo) + bevacizumab (bev) *vs* sorafenib (sor) as first-line treatment for unresectable hepatocellular carcinoma (HCC). Conference Abstract. *Cancer Research* 2021; **81** [DOI: 10.1158/1538-7445.AM2021-CT009]

31 **Mazzaferro V**, Llovet JM, Miceli R, Bhoori S, Schiavo M, Mariani L, Camerini T, Roayaie S, Schwartz ME, Grazi GL, Adam R, Neuhaus P, Salizzoni M, Bruix J, Forner A, De Carlis L, Cillo U, Burroughs AK, Troisi R, Rossi M, Gerunda GE, Lerut J, Belghiti J, Boin I, Gugenheim J, Rochling F, Van Hoek B, Majno P; Metroticket Investigator Study Group. Predicting survival after liver transplantation in patients with hepatocellular carcinoma beyond the Milan criteria: a retrospective, exploratory analysis. *Lancet Oncol* 2009; **10**: 35-43 [PMID: 19058754 DOI: 10.1016/S1470-2045(08)70284-5]

32 **Yasui Y**, Tsuchiya K, Kurosaki M, Takeguchi T, Takeguchi Y, Okada M, Wang W, Kubota Y, Goto T, Komiyama Y, Higuchi M, Takaura K, Hayashi T, Takada H, Tamaki N, Nakanishi H, Itakura J, Takahashi Y, Asahina Y, Enomoto N, Himeno Y, Izumi N. Up-to-seven criteria as a useful predictor for tumor downstaging to within Milan criteria and Child-Pugh grade deterioration after initial conventional transarterial chemoembolization. *Hepatol Res* 2018; **48**: 442-450 [PMID: 29278654 DOI: 10.1111/hepr.13048]

33 **Wang Q**, Xia D, Bai W, Wang E, Sun J, Huang M, Mu W, Yin G, Li H, Zhao H, Li J, Zhang C, Zhu X, Wu J, Gong W, Li Z, Lin Z, Pan X, Shi H, Shao G, Liu J, Yang S, Zheng Y, Xu J, Song J, Wang W, Wang Z, Zhang Y, Ding R, Zhang H, Yu H, Zheng L, Gu W, You N, Wang G, Zhang S, Feng L, Liu L, Zhang P, Li X, Chen J, Xu T, Zhou W, Zeng H, Huang W, Jiang W, Zhang W, Shao W, Li L, Niu J, Yuan J, Lv Y, Li K, Yin Z, Xia J, Fan D, Han G; China HCC-TACE Study Group. Development of a prognostic score for recommended TACE candidates with hepatocellular carcinoma: A multicentre observational study. *J Hepatol* 2019; **70**: 893-903 [PMID: 30660709 DOI: 10.1016/j.jhep.2019.01.013]

34 **Li QJ**, He MK, Chen HW, Fang WQ, Zhou YM, Xu L, Wei W, Zhang YJ, Guo Y, Guo RP, Chen MS, Shi M. Hepatic Arterial Infusion of Oxaliplatin, Fluorouracil, and Leucovorin Versus Transarterial Chemoembolization for Large Hepatocellular Carcinoma: A Randomized Phase III Trial. *J Clin Oncol* 2022; **40**: 150-160 [PMID: 34648352 DOI: 10.1200/JCO.21.00608]

35 **Yi M**, Jiao D, Qin S, Chu Q, Wu K, Li A. Synergistic effect of immune checkpoint blockade and anti-angiogenesis in cancer treatment. *Mol Cancer* 2019; **18**: 60 [PMID: 30925919 DOI: 10.1186/s12943-019-0974-6]

36 **Zhu H**, Shan Y, Ge K, Lu J, Kong W, Jia C. Oxaliplatin induces immunogenic cell death in hepatocellular carcinoma cells and synergizes with immune checkpoint blockade therapy. *Cell Oncol (Dordr)* 2020; **43**: 1203-1214 [PMID: 32797385 DOI: 10.1007/s13402-020-00552-2]

37 **Tesniere A**, Schlemmer F, Boige V, Kepp O, Martins I, Ghiringhelli F, Aymeric L, Michaud M, Apetoh L, Barault L, Mendiboure J, Pignon

JP, Jooste V, van Endert P, Ducreux M, Zitvogel L, Piard F, Kroemer G. Immunogenic death of colon cancer cells treated with oxaliplatin. *Oncogene* 2010; **29**: 482-491 [PMID: 19881547 DOI: 10.1038/onc.2009.356]

38 **Lyu N**, Kong Y, Mu L, Lin Y, Li J, Liu Y, Zhang Z, Zheng L, Deng H, Li S, Xie Q, Guo R, Shi M, Xu L, Cai X, Wu P, Zhao M. Hepatic arterial infusion of oxaliplatin plus fluorouracil/Leucovorin *vs* sorafenib for advanced hepatocellular carcinoma. *J Hepatol* 2018; **69**: 60-69 [PMID: 29471013 DOI: 10.1016/j.jhep.2018.02.008]

39 **Liang RB**, Zhao Y, He MK, Wen DS, Bu XY, Huang YX, Lai ZC, Xu YJ, Kan A, Wei W, Zhang YJ, Chen MS, Guo RP, Li QJ, Shi M. Hepatic Arterial Infusion Chemotherapy of Oxaliplatin, Fluorouracil, and Leucovorin With or Without Sorafenib as Initial Treatment for Advanced Hepatocellular Carcinoma. *Front Oncol* 2021; **11**: 619461 [PMID: 34055599 DOI: 10.3389/fonc.2021.619461]

40 **Zheng K**, Zhu X, Fu S, Cao G, Li WQ, Xu L, Chen H, Wu D, Yang R, Wang K, Liu W, Wang H, Bao Q, Liu M, Hao C, Shen L, Xing B, Wang X. Sorafenib Plus Hepatic Arterial Infusion Chemotherapy *vs* Sorafenib for Hepatocellular Carcinoma with Major Portal Vein Tumor Thrombosis: A Randomized Trial. *Radiology* 2022; **303**: 455-464 [PMID: 35103539 DOI: 10.1148/radiol.211545]

World Journal of Gastroenterology

Submit a Manuscript: https://www.f6publishing.com

World J Gastroenterol 2024 January 28; 30(4): 332-345

DOI: 10.3748/wjg.v30.i4.332

ISSN 1007-9327 (print) ISSN 2219-2840 (online)

ORIGINAL ARTICLE

Observational Study

Circulating microRNA expression and nonalcoholic fatty liver disease in adolescents with severe obesity

Yi-Jie Li, Brittney O Baumert, Nikos Stratakis, Jesse A Goodrich, Hao-Tian Wu, Jing-Xuan He, Yin-Qi Zhao, Max T Aung, Hong-Xu Wang, Sandrah P Eckel, Douglas I Walker, Damaskini Valvi, Michele A La Merrill, Justin R Ryder, Thomas H Inge, Todd Jenkins, Stephanie Sisley, Rohit Kohli, Stavra A Xanthakos, Andrea A Baccarelli, Rob McConnell, David V Conti, Lida Chatzi

Specialty type: Gastroenterology and hepatology

Provenance and peer review: Invited article; Externally peer reviewed.

Peer-review model: Single blind

Peer-review report's scientific quality classification

Grade A (Excellent): 0
Grade B (Very good): B, B
Grade C (Good): C
Grade D (Fair): 0
Grade E (Poor): 0

P-Reviewer: Gao YT, China; Niu CY, China; Zhou B, China

Received: September 29, 2023
Peer-review started: September 29, 2023
First decision: November 6, 2023
Revised: December 4, 2023
Accepted: January 9, 2024
Article in press: January 9, 2024
Published online: January 28, 2024

Yi-Jie Li, Brittney O Baumert, Jesse A Goodrich, Jing-Xuan He, Yin-Qi Zhao, Max T Aung, Hong-Xu Wang, Sandrah P Eckel, Rob McConnell, David V Conti, Lida Chatzi, Department of Population and Public Health Sciences, Keck School of Medicine, University of Southern California, Los Angeles, CA 90032, United States

Nikos Stratakis, Barcelona Institute of Global Health, Barcelona Institute of Global Health, Barcelona 08036, Spain

Hao-Tian Wu, Andrea A Baccarelli, Department of Environmental Health Sciences, Mailman School of Public Health, Columbia University, New York, NY 10032, United States

Douglas I Walker, Gangarosa Department of Environmental Health, Rollins School of Public Health, Emory University, Atlanta, GA 30329, United States

Damaskini Valvi, Department of Environmental Medicine and Public Health, Icahn School of Medicine at Mount Sinai, New York, NY 10029, United States

Michele A La Merrill, Department of Environmental Toxicology, University of California, Davis, CA 95616, United States

Justin R Ryder, Thomas H Inge, Department of Surgery, Lurie Children's Hospital of Chicago, Chicago, IL 60611, United States

Justin R Ryder, Thomas H Inge, Northwestern University Feinberg School of Medicine, Northwestern University, Chicago, IL 60611, United States

Todd Jenkins, Division of Biostatistics and Epidemiology, Cincinnati Children's Hospital Medical Center, Cincinnati, OH 45229, United States

Todd Jenkins, Stavra A Xanthakos, Department of Pediatrics, University of Cincinnati College of Medicine, Cincinnati, OH 45229, United States

Stephanie Sisley, Department of Pediatrics, Children's Nutrition Research Center USDA/ARS, Baylor College of Medicine, Houston, TX 77030, United States

Rohit Kohli, Department of Gastroenterology, Children's Hospital Los Angeles, Los Angeles, CA 90027, United States

Stavra A Xanthakos, Division of Gastroenterology, Hepatology and Nutrition, Cincinnati Children's Hospital Medical Center, Cincinnati, OH 45229, United States

Corresponding author: Lida Chatzi, MD, PhD, Professor, Department of Population and Public Health Sciences, Keck School of Medicine, University of Southern California, 1845 N. Soto Street, Los Angeles, CA 90032, United States. chatzi@usc.edu

Abstract

BACKGROUND

Nonalcoholic fatty liver disease (NAFLD) is one of the most common chronic liver diseases in children and adolescents. NAFLD ranges in severity from isolated hepatic steatosis to nonalcoholic steatohepatitis (NASH), wherein hepatocellular inflammation and/or fibrosis coexist with steatosis. Circulating microRNA (miRNA) levels have been suggested to be altered in NAFLD, but the extent to which miRNA are related to NAFLD features remains unknown. This analysis tested the hypothesis that plasma miRNAs are significantly associated with histological features of NAFLD in adolescents.

AIM

To investigate the relationship between plasma miRNA expression and NAFLD features among adolescents with NAFLD.

METHODS

This study included 81 adolescents diagnosed with NAFLD and 54 adolescents without NAFLD from the Teen-Longitudinal Assessment of Bariatric Surgery study. Intra-operative core liver biopsies were collected from participants and used to characterize histological features of NAFLD. Plasma samples were collected during surgery for miRNA profiling. A total of 843 plasma miRNAs were profiled using the HTG EdgeSeq platform. We examined associations of plasma miRNAs and NAFLD features using logistic regression after adjusting for age, sex, race, and other key covariates. Ingenuity Pathways Analysis was used to identify biological functions of miRNAs that were associated with multiple histological features of NAFLD.

RESULTS

We identified 16 upregulated plasma miRNAs, including miR-193a-5p and miR-193b-5p, and 22 downregulated plasma miRNAs, including miR-1282 and miR-6734-5p, in adolescents with NAFLD. Moreover, 52, 16, 15, and 9 plasma miRNAs were associated with NASH, fibrosis, ballooning degeneration, and lobular inflammation, respectively. Collectively, 16 miRNAs were associated with two or more histological features of NAFLD. Among those miRNAs, miR-411-5p was downregulated in NASH, ballooning, and fibrosis, while miR-122-5p, miR-1343-5p, miR-193a-5p, miR-193b-5p, and miR-7845-5p were consistently and positively associated with all histological features of NAFLD. Pathway analysis revealed that most common pathways of miRNAs associated with multiple NAFLD features have been associated with tumor progression, while we also identified linkages between miR-122-5p and hepatitis C virus and between miR-199b-5p and chronic hepatitis B.

CONCLUSION

Plasma miRNAs were associated with NAFLD features in adolescent with severe obesity. Larger studies with more heterogeneous NAFLD phenotypes are needed to evaluate miRNAs as potential biomarkers of NAFLD.

Key Words: MicroRNA; Nonalcoholic fatty liver disease; Non-alcoholic steatohepatitis; Liver fibrosis; Lobular inflammation; Ballooning degeneration

Core Tip: Nonalcoholic fatty liver disease (NAFLD) is the most common chronic liver disease in the world, and its prevalence in adolescents is increasing. Studies suggest plasma microRNAs (miRNAs) are dysregulated in NAFLD, but relevant observational studies are scarce. In this study, we analyzed the expression of plasma miRNA in adolescents diagnosed with NAFLD by liver biopsy. We identified associations between histological features of NAFLD and plasma miRNA expression. Further, we found consistent expression of miRNA across different features of NAFLD. Although these results need further testing and validation, our findings suggest these miRNAs could be diagnostic and prognostic biomarkers of NAFLD.

Citation: Li YJ, Baumert BO, Stratakis N, Goodrich JA, Wu HT, He JX, Zhao YQ, Aung MT, Wang HX, Eckel SP, Walker DI, Valvi D, La Merrill MA, Ryder JR, Inge TH, Jenkins T, Sisley S, Kohli R, Xanthakos SA, Baccarelli AA, McConnell R, Conti DV, Chatzi L. Circulating microRNA expression and nonalcoholic fatty liver disease in adolescents with severe obesity. *World J Gastroenterol* 2024; 30(4): 332-345
URL: https://www.wjgnet.com/1007-9327/full/v30/i4/332.htm
DOI: https://dx.doi.org/10.3748/wjg.v30.i4.332

INTRODUCTION

Nonalcoholic fatty liver disease (NAFLD) is defined by excessive fat accumulation in the liver and the presence of steatosis without heavy alcohol use[1,2]. NAFLD is comprised of two conditions: Nonalcoholic fatty liver (NAFL) and nonalcoholic steatohepatitis (NASH). Although both NAFL and NASH include accumulation of fat in hepatocytes, the histopathological abnormality in NASH involves further hepatocellular ballooning, fibrosis, and lobular inflammation[3-6]. In the United States, the overall estimated prevalence of NAFL and NASH are approximately 30% and 5%, respectively[7]. The prevalence of NAFLD in adolescents is 18.5%[8] and has more than doubled over the past 20 years to affect approximately one-half of adolescents with obesity[9,10]. Studies suggest that histopathological features of pediatric NAFLD are different from adult NAFLD[11,12], and children with NAFLD may experience increased risk of severe liver disease and higher liver-related mortality in adulthood[13].

Thus, early diagnosis and prevention of NAFLD among adolescents are crucial. Liver biopsy is the gold standard to diagnose NAFLD[14] yet is invasive and costly[15]. Alternately, noninvasive assessments for NAFLD such as blood tests of aspartate aminotransferase and alanine aminotransferase are commonly used[15,16], but are less predictive of more advanced NAFLD features such as NASH and fibrosis[17,18]. Nonetheless, more robust, noninvasive diagnostic biomarkers of the full spectrum of NAFLD disease severity, are needed.

MicroRNAs (miRNAs) are non-coding RNA that regulate gene expression[19]. In addition to intracellular activities, miRNA can be encapsulated in circulating extracellular vesicles that can convey biological information to recipient cells [20]. Hence, miRNAs play crucial roles in various aspects of metabolism and are frequently dysregulated in the context of diseases[21]. Evidence suggests that dysregulation of miRNA is associated with NAFLD pathogenesis[22-26], *via* multiple pathways, including lipid metabolism, insulin signaling, hepatocyte apoptosis, hepatic inflammation, and liver fibrosis [22,23]. To date, NAFLD–miRNA association studies in humans are scarce and have presented inconsistent results[25-39], and only two studies included adolescents[38,39]. Moreover, only one study measured associations between lobular inflammation and ballooning degeneration with miRNA expression[32], and it focused solely on the expression of miR-34a, miR-122, miR-191, miR-192, and miR-200a. Therefore, it is critical to further investigate the relationship between NAFLD and miRNA expression in adolescents.

The objectives of this study were to: (1) Examine the associations between circulating miRNA levels and histological characteristics of NAFLD in adolescents with obesity; and (2) investigate the pathways of identified NAFLD-related miRNA.

MATERIALS AND METHODS

Study population and design

This study was based on data from the Teen-Longitudinal Assessment of Bariatric Surgery (Teen-LABS study, ClinicalTrials.gov NCT00465829), a prospective, multicenter, observational study of adolescents (≤ 19 years of age) with severe obesity who underwent bariatric surgery in 2007-2012 and enrolled at participating clinical centers in the United States: Cincinnati Children's Hospital Medical Center (Cincinnati, Ohio), Nationwide Children's Hospital (Columbus, Ohio), University of Pittsburgh Medical Center (Pittsburgh, Pennsylvania), Texas Children's Hospital (Houston, Texas), and Children's Hospital of Alabama (Birmingham, Alabama)[10,40-42]. The protocol, assent/consent forms, and monitoring plans for data and safety were approved by the institutional review boards of each institution, the independent data and safety monitoring board prior to study initiation, and the University of Southern California review board[10,40-42]. Detailed cohort information is described in previous studies[10,40-42].

Outcome measurement

Liver biopsies were obtained by a laparoscopically controlled, transabdominal core needle biopsy technique after induction of anesthesia and before performing the bariatric procedure[10,40-42]. Biopsies were evaluated by an experienced hepatopathologist using the NASH Clinical Research Network scoring system[43]. NAFLD features were categorized as definite NASH, borderline NASH, NAFLD not NASH (NAFL), and no NAFLD[10,44]. Other histological features of NAFLD were also categorized, including ballooning, lobular inflammation, and fibrosis[10].

MiRNA profile

Plasma samples were collected at baseline, typically within 30 days of bariatric surgery and stored at -70 °C. Analyses were performed at HTG Molecular Diagnostics, Inc. (Tucson, AZ) for HTG EdgeSeq miRNA sequencing. HTG EdgeSeq

uses EdgeSeq miRNA Whole Transcriptome Assay and Illumina HiSeq 4000 to quantify 2083 mature miRNA. For quality control, triplicate internal human brain tissue controls were sequenced. HTG EdgeSeq Parser software (version 5.0.535.3181) was used for alignment to a priori defined target sequences. The following quality control measures were implemented: (1) Percentage of bases with a quality score 30 ≥ 87%; (2) percentage of clusters passing filter ≥ 75%; (3) cluster density of 180-290 k/mm^2; and (4) all samples passing HTG-defined criteria, including > 500000 reads, < 14% reads aligned to positive control probes, and > 0.08 relative standard deviation of reads allocated to each probe with each sample. To correct technical batch effects, we used the ComBat_seq function of the *sva package* in R[45]. Sequencing reads were normalized within and across plates using relative log expression[46]. The reliability of each probe was determined by calculating the coefficient of variation for each miRNA across human brain tissue control samples. Analysis included a total of 843 miRNAs with coefficient of variation ≤ 0.25 in replicate control samples. All final counts were converted to counts per million and log2-transformed prior to analysis.

Confounders and covariate data

Standardized methods for Teen-LABS data collection have been described previously[10,40-42]. We included participant characteristics as important confounders, including: Age[47-49], body mass index (BMI)[49-51], sex[49,52,53], weight loss prior to surgery[54,55], and covariates, such as race[56,57], parents' income[58,59] and clinical site of surgery. Data were collected within 30 days of bariatric surgery at in-person visits with trained study personnel. Detailed descriptions of methods, comorbidities, data definitions, medical record data, and laboratory testing can be found in previous publications[10,40-42].

Statistical analysis

Due to the low frequency of borderline NASH (n = 22, 16.3%) and definite NASH (n = 8, 5.9%) in the study population, these two categories were combined and referred to as general NASH (n = 30, 22%). Similarly, we grouped the two ballooning degeneration conditions, which were prominent (n = 5, 3.7%) and less characteristics (n = 16, 11.9%), to create a general ballooning group (n = 21, 15.6%). These groupings ensured an adequate sample size for meaningful analysis and interpretation of results. To investigate associations between histological features of NAFLD and miRNA, we used multivariate logistic regression to investigate miRNA expression in participants with NAFLD (NAFL and NASH). Additional comparisons between each histological grouping, including NASH (NASH *vs*. NAFL), fibrosis, lobular inflammation, and ballooning, were performed using independent logistic regression models for each comparison. Coefficient estimates of miRNA expression change (log odds ratio), standard errors, and P value for each miRNA relationship were calculated. To account for multiple comparisons, we applied the false discovery rate (FDR) approach with a threshold of 0.05 to adjust P values from each regression analysis. All models were adjusted by covariates. All statistical analysis was conducted in RStudio version 1.0.143 (RStudio: Integrated Development for R. RStudio, Inc., Boston, MA, United States, http://www.rstudio.com/).

Pathway analysis

We investigated pathways of NAFLD-related miRNA in both miRbase and the Kyoto Encyclopedia for Genes and Genomes from Ingenuity Pathway Analysis (IPA) (Qiagen Inc., https://www.qiagenbioinformatics.com/products/ingenuitypathway-analysis)[60-62]. Given that an individual miRNA can participate in numerous pathways, we used the miRNA Target Filter tool from IPA and selected experimentally observed diseases and functions of NAFLD-related miRNA in humans.

RESULTS

Characteristics of the study population

The analysis consisted of 135 study participants with complete data. The mean age was 16.9 years (SD = 1.5), mean BMI was 53.8 kg/m^2 (SD = 9.8), and 73.3% were female. Because more than half of study participants were recruited from a single clinical site, we re-categorized study site as a binary variable for subsequent regression models. Study population characteristics are summarized in Table 1.

Prevalence of histological features of NAFLD

By histological analysis, 40% of participants did not have NAFLD, while 37.8% were diagnosed with NAFL, 16.3% with borderline NASH, and 5.9% with definite NASH at the time of surgery. Notably, a high proportion of participants from the Teen-LABS cohort exhibited progressive histopathological features associated with NAFLD-19.3% were diagnosed with fibrosis, and 71.9% were diagnosed with lobular inflammation. Furthermore, 3.7% of participants were diagnosed with prominent ballooning degeneration, while 11.9% exhibited ballooning with fewer characteristics. Distribution of NAFLD features is summarized in Table 1.

Associations of plasma miRNA expression with histological features of NAFLD

The distribution of NAFLD–miRNA associations is shown in Supplementary Table 1, Figure 1A. We found 38 associations between NAFLD and plasma miRNA expression levels. A subset of 16 miRNA displayed upregulation, while a subset of 22 miRNAs demonstrated downregulation. There was dysregulation of 17 downregulated miRNAs and 35 upregulated miRNAs in patients with NASH relative to those with NAFL (Supplementary Table 2, Figure 1B). However,

Table 1 Baseline characteristics of teen-longitudinal assessment of bariatric surgery participants, *n* = 135

Characteristics	Mean (SD)/*n* (%)
Age (yr)	16.86 (1.53)
BMI (kg/m^2)	53.80 (9.81)
Weight loss prior to surgery (kg)	0.69 (8.36)
Sex	
Female	99 (73.33)
Male	36 (26.67)
Race (binary)	
White or Caucasian	93 (68.89)
Others	42 (31.11)
Parents' income	
< $25000	53 (39.26)
$25000-$74999	57 (42.22)
≥ $75000	25 (18.52)
NAFLD	
NAFL	51 (37.78)
Borderline NASH	22 (16.30)
Definite NASH	8 (5.93)
No NAFLD	54 (40.00)
Fibrosis	
Presence	26 (19.26)
None	109 (80.74)
Ballooning degeneration	
Many, prominent	5 (3.70)
Less characteristics	16 (11.86)
None	114 (84.44)
Lobular inflammation	
Presence	97 (71.85)
None	38 (28.15)

BMI: Body mass index; NAFL: Nonalcoholic fatty liver; NAFLD: Nonalcoholic fatty liver disease; NASH: Nonalcoholic steatohepatitis.

these findings did not retain significance after applying multiple comparison adjustments (FDR > 0.05).

Within the group of participants with fibrosis (*n* = 26), we observed downregulation of 8 miRNAs and upregulation of 8 miRNAs compared to participants without fibrosis (*n* = 109). Additionally, in participants with ballooning (*n* = 21), we identified 15 altered miRNAs, including downregulation of miR-1224-5p, miR-369-5p, miR-411-5p, and miR-500b-5p. Among participants diagnosed with lobular inflammation (*n* = 97), we identified downregulation of 6 miRNAs and upregulation of miR-1244, miR-125b-2-3p, and miR-365b-5p compared to individuals without lobular inflammation. Associations among ballooning, fibrosis, and lobular inflammation with plasma miRNA levels are depicted in Supplementary Tables 3-5 and Figure 1C-E. However, no associations met statistical significance after multiple comparison adjustment (FDR > 0.05).

Integration of miRNA profiles associated with multiple histological features of NAFLD

A total of 16 miRNAs exhibited differences in expression across two or more histological features of NAFLD (Figure 2). MiR-193a-5p was consistently upregulated in NASH, ballooning and fibrosis; miR-193b-5p was consistently upregulated in NAFLD, NASH, and fibrosis; expression of miR-411-5p was downregulated in NASH, ballooning, and fibrosis. Additionally, we observed inconsistent expression patterns of miR-1301-5p and miR-1296-5p between NAFLD and NASH-miR-1301-5p and miR-1296-5p were upregulated in NAFLD yet downregulated in NASH. Additionally, we

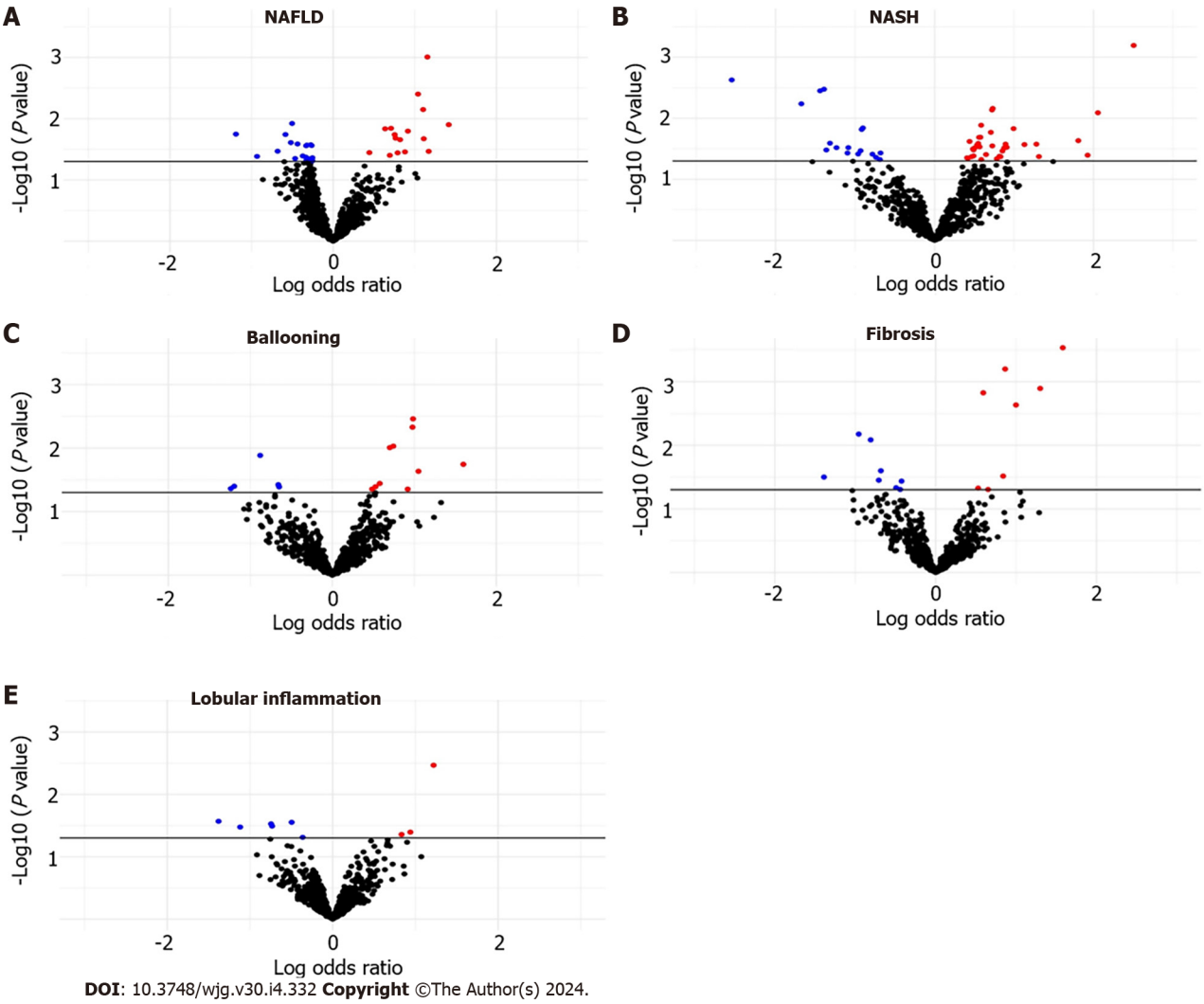

DOI: 10.3748/wjg.v30.i4.332 **Copyright** ©The Author(s) 2024.

Figure 1 Volcano plots of associations between histological features of nonalcoholic fatty liver disease and microRNA expression. A: MicroRNAs (miRNAs) associated with nonalcoholic fatty liver disease (NAFLD); B: MiRNAs associated with nonalcoholic steatohepatitis (NASH) relative to nonalcoholic fatty liver; C: MiRNAs associated with ballooning; D: MiRNAs associated with fibrosis; E: MiRNAs associated with lobular inflammation. Solid horizonal line represents $P = 0.05$, and any dots above the line indicate miRNAs with significant associations. Negative associations are in blue; positive associations are in red; black dots below the solid line represent insignificant miRNAs; higher absolute x-value of a dot indicates greater magnitude of change in miRNA expression in patients with histological progression of NAFLD, either increased ($x > 0$) or decreased ($x < 0$); higher y-value of a dot indicates smaller P value of associations. NAFLD: Nonalcoholic fatty liver disease; NASH: Nonalcoholic steatohepatitis.

observed downregulation of miR-7150 in NAFLD, and this miRNA was conversely upregulated in individuals with ballooning.

The 16 miRNAs associated with two or more histological features of NAFLD were subsequently subjected to scaling and grouped into two distinct clusters using the k-means clustering algorithm and the elbow method[63-66]. Cluster 1 comprised 6 miRNAs, the majority of which were upregulated in individuals with NAFLD. However, these miRNAs were mostly downregulated in patients with NASH, fibrosis, lobular inflammation, and ballooning. Cluster 2 encompassed 10 miRNAs, most of which were upregulated in NASH, fibrosis, and ballooning. In addition to overall inconsistency between the clusters, we noted consistent upregulation of miR-122-5p, miR-1343-5p, miR-193a-5p, miR-193b-5p, and miR-7845-5p across histological features of NAFLD. Figure 2 shows a graphical representation of associations between multiple histological features of NAFLD and miRNA expression.

Pathway analysis of miRNA associated with multiple histological features of NAFLD

We conducted pathway analysis on the 16 miRNAs associated with two or more histological features of NAFLD. Analysis revealed 16 experimentally confirmed pathways predominantly involving 6 overlapping NAFLD-related miRNAs in humans (Table 2). Specifically, miR-122-5p, miR-193b-5p, miR-199b-5p, and miR-323-3p were associated with apoptosis of tumor cell lines, while miR-122-5p, miR-193a-5p, and miR-199b-5p were associated with cell migration. Notably, miR-122-5p and miR-199b-5p were associated with multiple pathways in humans. For example, miR-122-5p was associated with production of hepatitis C virus, RNA decay, metastatic hepatocellular carcinoma, replication of viral replicon, and invasion of hepatoma cell lines. Similarly, miR-199b-5p was associated with congenital adrenal hyperplasia, chronic hepatitis B, early-stage invasive cervical squamous cell carcinoma, and proliferation of myeloma cell lines.

Table 2 Pathway analysis for miRNA associated with multiple histological features of non-alcoholic fatty liver disease in teen-longitudinal assessment of bariatric surgery participants

Disease and functions	miRNA
Apoptosis of tumor cell lines	miR-122-5p, miR-193b-5p, miR-199b-5p, miR-323-3p
Migration of cells	miR-122-5p, miR-193a-5p, miR-199b-5p
Apoptosis of myeloma cell lines	miR-122-5p, miR-193a-5p
Dedifferentiated liposarcoma	miR-193a-5p, miR-199b-5p
Production of hepatitis C virus	miR-122-5p
Decay of RNA	miR-122-5p
Metastatic hepatocellular carcinoma	miR-122-5p
Replication of viral replicon	miR-122-5p
Invasion of hepatoma cell lines	miR-122-5p
Chemosensitivity of squamous cell carcinoma cell lines	miR-193a-5p
Epithelial-mesenchymal transition of adenocarcinoma cell lines	miR-193a-5p
Migration of adenocarcinoma cell lines	miR-193a-5p
Congenital adrenal hyperplasia	miR-199b-5p
Chronic hepatitis B	miR-199b-5p
Early-stage invasive cervical squamous cell carcinoma	miR-199b-5p
Proliferation of myeloma cell lines	miR-199b-5p

A total of 16 miRNA were included as input for independent practice association. To ensure reliability and relevance of results, we specifically extracted pathways that were experimentally confirmed in human studies, considering only those with $P < 0.05$.

DISCUSSION

Our study is the first to show associations between histological features of NAFLD and expression of plasma miRNA in adolescents with severe obesity. The IPA results revealed that miRNAs associated with multiple NAFLD features were linked to cancer, hepatitis B and hepatitis C. Our findings have several important implications. First, our findings were consistent with previous epidemiological studies[26]. Additionally, we identified novel NAFLD-miRNA associations. Moreover, our findings revealed consistent patterns of miRNA expression across various histological features of NAFLD, diagnosed using gold standard methods. The consistency of miRNA expression trends across different NAFLD features strengthen their potential utility as valuable diagnostic and prognostic markers for NAFLD.

Associations between histological features of NAFLD and miRNA expression

Among the 38 NAFLD-related miRNAs identified in our study, several associations are comparable to published epidemiological studies. Our findings demonstrating positive associations between NAFLD and expression of miR-193a-5p, and miR-7150 align with current epidemiological studies[26]. However, it is noteworthy that Soronen *et al*[67] reported increased expression of hepatic miR-584-5p in those with NAFLD, while we found a negative association between NAFLD and plasma miR-584-5p levels. However, this differential expression may be attributed to variation in miRNA measurement sites, as contrasting expression patterns between hepatic miR-122[30] and serum miR-122[36] have been reported in those with NASH.

Additionally, NASH-related miRNA findings from our study align with current research findings. For example, we identified increased expression of miR-2861, miR-3940-5p, miR-6727-5p, miR-6771-5p, miR-6780b-5p, miR-6845-5p, and miR-7114-3p in participants with NASH, consistent with reported positive associations between these miRNAs in the setting of NAFLD and/or NASH[26]. However, it is important to note that this previous study also demonstrated downregulation of miR-6741-5p, miR-6782-5p, and miR-7108-5p in individuals with NAFLD and/or NASH[26], which contrasts with our observation of positive associations between these miRNA and NASH. We also observed a negative association between NASH and miR-182-5p, while mouse studies suggest this miRNA attenuates NASH[68]. In addition, Katsura *et al*[69] reported downregulation of miR-301b in mice with NASH, which is consistent with our findings.

We identified more miRNAs specifically associated with ballooning degeneration, fibrosis, and lobular inflammation, respectively. Among these miRNAs, we identified increased levels of plasma miR-34a-5p in participants with liver fibrosis, while epidemiological studies also show upregulation of miR-34a in NAFLD and NASH patients[29].

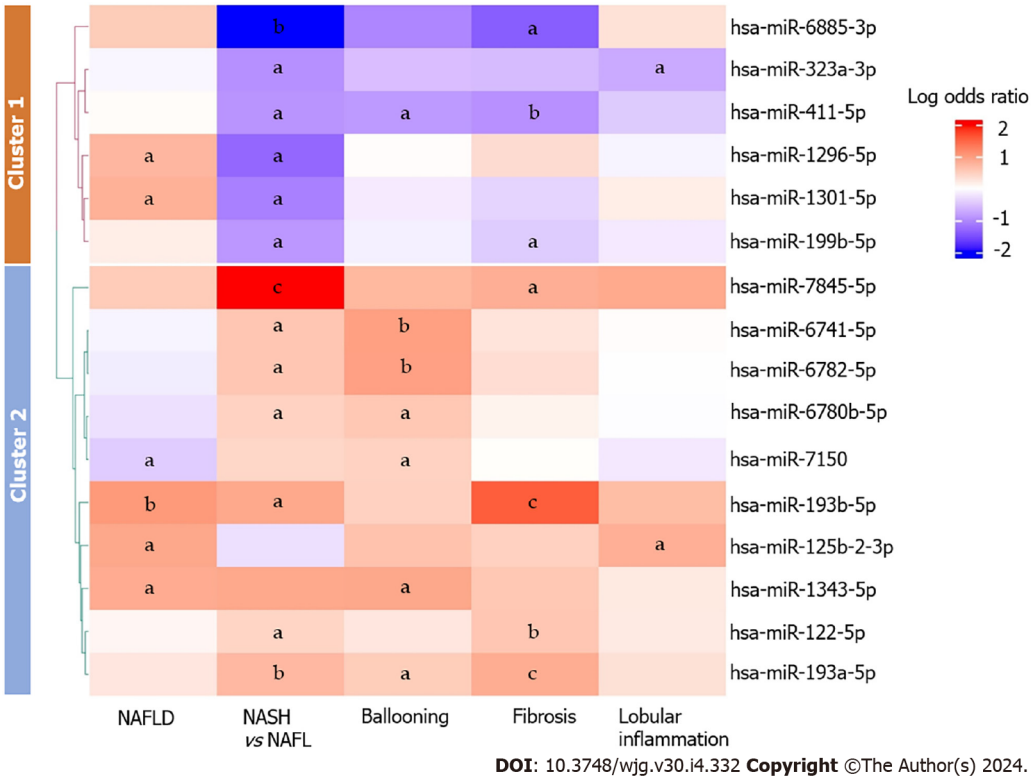

DOI: 10.3748/wjg.v30.i4.332

Figure 2 Heatmap of microRNA associated with two or more histological features of nonalcoholic fatty liver disease. Heatmap for association between microRNA (miRNA) expression and histological features of nonalcoholic fatty liver disease (NAFLD) in Teen-Longitudinal Assessment of Bariatric Surgery participants. Red indicates positive association, and purple indicates negative association. 16 miRNAs were associated with two or more histological features and were assigned into two clusters by k-means clustering. Cluster 1 (red bar on left) includes 6 miRNAs that are mostly upregulated in patients with NAFLD, but downregulated in patients with nonalcoholic steatohepatitis (NASH) (relative to nonalcoholic fatty liver), ballooning, fibrosis, and lobular inflammation. Cluster 2 (green bar on left) includes 10 miRNAs that are mostly upregulated in the presence of NASH, ballooning and fibrosis. $^{a}P < 0.05$, $^{b}P < 0.01$, $^{c}P < 0.001$. NAFLD: Nonalcoholic fatty liver disease; NASH: Nonalcoholic steatohepatitis.

Integration of miRNA expression across NAFLD features

We identified several miRNAs associated with two or more NAFLD features. Interestingly, plasma levels of miR-122-5p, miR-1343-5p, miR-193a-5p, miR-193b-5p, and miR-7845-5p exhibited consistent increases across all histological features of NAFLD. Similarly, previous studies reported that miR-122-5p and miR-193a-5p were upregulated in individuals with NAFLD[26,33]. Moreover, Johnson *et al*[26] found strong associations between increased miR-193a-5p levels and NAFLD activity grade and fibrosis stage. Furthermore, Pirola *et al*[36] reported increased expression of serum miR-125b in individuals with NAFLD. Similarly, we found upregulated plasma miR-125b-2-3p expression with NAFLD and lobular inflammation.

Additionally, our analysis revealed decreased levels of miR-1296-5p, miR-1301-5p, miR-199b-5p, miR-411-5p, and miR-6885-3p in NASH compared to NAFL, while these levels were elevated in NAFLD compared to individuals without NAFLD. These miRNAs also demonstrated predominantly negative associations with fibrosis, lobular inflammation, and ballooning (Figure 2). Notably, the downregulation of miR-411-5p aligned with a recent study by Wan *et al*[70], which reported decreased expression of serum miR-411-5p in persons with NASH. Collectively, the distinct expression patterns observed across various NAFLD features suggest that these miRNAs may serve as potential biomarkers for NAFLD progression.

Pathway analysis of miRNA associated with histological features of NAFLD

An increasing body of research have investigated the associations between NAFLD and miRNA expression, yet little is known about mechanisms underlying the dysregulation of circulating miRNA in NAFLD patients. We first conducted pathway analysis by IPA, and the results revealed that most overlapping miRNA were associated with tumorigenesis. Analysis also highlighted linkage between miR-122-5p and production of hepatitis C virus and between miR-199b-5p and chronic hepatitis B. Given the high prevalence of NAFLD in those with hepatitis C virus and the reported associations among miR-122, hepatitis C virus, and NAFLD[34], the relationship among miR-122-5p, hepatitis C virus, and NAFLD warrants further attention[71]. Furthermore, meta-analyses suggest an inverse association between hepatitis B virus infection and risk of developing NAFLD[72], offering potential insights into the mechanisms involving miR-199b-5p in NAFLD in the context of hepatitis B virus infection.

Experimental studies provide valuable insights into the molecular mechanisms underlying associations between NAFLD and miRNA expression while minimizing confounding variables intrinsic to human observational studies. Particularly, miR-122, a highly expressed hepatic miRNA in hepatocytes, is associated with NAFLD progression by

Table 3 Molecular pathways of non-alcoholic fatty liver disease-associated miRNA in teen-longitudinal assessment of bariatric surgery participants

miRNA	Target	Function
miR-122	SIRT-1[73]; FOXO3[74]	miR-122 downregulates SIRT-1 and induces steatosis and hepatic lipogenesis in NAFLD[73]; miR-122-5p inhibits FOXO3 to attenuate inflammatory response and oxidative stress damage in NAFLD[74]
miR-125b	TNFAIP3[79]	miR-125b targets TNFAIP3 and promotes the NF-κB-mediated inflammatory response in NAFLD [79]
miR-146a	MED1[75]	miR-146a targets MED1 and improves hepatic lipid and glucose metabolism in NAFLD[75]
miR-181a	PPARα[76]	miR-181a inhibits PPARα and aggravates lipid accumulation in hepatocytes[76]
miR-22	SIRT-1[78]	miR-22 targets SIRT-1 and inhibits gluconeogenesis[78]
miR-34a	TGF-β1/Smad3[80]	miR-34a-5p targets TGF-β1/Smad3 and inhibits liver fibrosis in hepatic stellate cells[80]
miR-375	RAC1[81]	miR-375 inhibits RAC1 and alleviates liver fibrosis[81]

FOXO3: Forkhead box O 3; SIRT-1: Sirtuin 1; TNFAIP3: Tumor necrosis factor alpha-induced protein 3; MED1: Mediator complex subunit 1; PPARα: Peroxisome proliferator-activated receptor-α; TGF-β1: Transforming growth factor-β1; Smad3: Mothers against decapentaplegic family 3; RAC1: Rac family small GTPase 1; NAFLD: Non-alcoholic fatty liver disease.

regulating lipid metabolism[23]. For example, Long *et al*[73] revealed that miR-122 inhibited liver kinase B1/AMP-activated protein kinase signaling pathway, which further induced hepatic lipogenesis and steatosis in NAFLD. Additionally, the inhibition of miR-122-5p may suppress the inflammation and oxidative stress damage in NAFLD[74]. Given the observed upregulation of circulating miR-122 and downregulation of hepatic miR-122 in NASH patients[30,36], the elevated circulating miR-122-5p across NAFLD features in our study might be released by hepatocytes. Furthermore, we identified downregulation of plasma miR-146a-5p, miR-181a-5p, and miR-22-3p in individuals with NAFLD, which is supported by experimental studies of miRNA. For example, miR-146a targeted complex subunit 1 to attenuate lipid accumulation and alleviate NAFLD progression in mice[75]. Additionally, miR-181a was found to downregulate peroxisome proliferator-activated receptor-α and mediate lipid metabolisms in NAFLD in human liver cells[76]. Moreover, miR-22 is a pivotal regulator of lipid and glucose metabolism, playing a crucial role in mitigating NAFLD progression in mice[77]. For example, miR-22 inhibited sirtuin-1 and regulated gluconeogenesis in NAFLD[78]. We also observed increased expression of miR-125b-2-3p in both NAFLD and lobular inflammation, while studies indicated that miR-125b promoted the nuclear factor kappa-light-chain-enhancer of activated B cells-mediated inflammatory response in NAFLD[79]. Furthermore, we observed positive associations between liver fibrosis and expression of miR-34a-5p and miR-375, while experimental research suggested that both miR-34a-5p and miR-375 could alleviate liver fibrosis[80,81]. Together these experimental data support a plausible biological mechanism of NAFLD-miRNA association (Table 3).

Strength, limitations, and recommendations for future research

Our study has several strengths. Liver biopsies are considered the gold standard in NAFLD assessment, thus ensuring robust and accurate diagnoses of our study. Besides, the consistency of our NAFLD–miRNA associations with epidemiological studies further reinforced the importance of circulating miRNA in NAFLD, supporting their potential use as diagnostic markers. Additionally, our study revealed NAFLD-miRNA associations that have only been previously recognized in experimental research, enhancing the translational value of our findings. By bridging the gap between experimental research and clinical observations, our study helps unravel the complexities of NAFLD and its potential management strategies. Furthermore, our study provides comprehensive characterization of more severe NAFLD features through liver biopsies. Previous studies only profiled specific miRNAs, namely miR-34a, miR-122, miR-191, miR-192, and miR-200a, in patients with ballooning and lobular inflammation[32], while our study conducted an analysis of 843 miRNAs across various histological features of NAFLD. By integrating miRNA expression across these histological features of NAFLD, we uncovered consistent expression patterns of plasma miRNA that hold promise as potential NAFLD biomarkers. Conversely, miRNAs that exhibit differential expression across histological features also warrant further investigation to understand their specific roles and mechanisms in NAFLD pathogenesis.

However, this study was not without limitations. The miRNAs were profiled at baseline, limiting the ability to establish a straightforward causal relationship between NAFLD and plasma miRNA expression. Investigations incorporating longitudinal cohort study designs could better elucidate the temporal relationship and causal associations between NAFLD and plasma miRNA expression. Given our specific focus on adolescents with obesity, who are at high risk of developing NAFLD[10,50,51], and the limitations arising from our small sample size, a validation for generalizability is imperative. The limitation in sample size is an inherent consequence of our methodological choice to employ liver biopsy for NAFLD diagnosis. While liver biopsy ensures accurate and definitive diagnosis, its invasiveness and cost present challenges in expanding the participant pool[82]. Studies with larger and more diverse populations would facilitate more robust and conclusive findings regarding NAFLD–miRNA associations.

CONCLUSION

Our study provides valuable insights into differential miRNA expression in adolescents with NAFLD. In addition to the previously reported miR-122-5p, miR-193a-5p, and miR-34a, our findings reveal the presence of novel NAFLD-associated miRNAs, namely miR-125b-2-3p and miR-193b-5p. Furthermore, our research underscores similar expression trend of specific miRNAs, such as miR-122-5p, miR-1343-5p, miR-193a-5p, miR-193b-5p, and miR-7845-5p, across all histological features of NAFLD, highlighting their potential roles in pathogenesis and promise as diagnostic and prognostic biomarkers for NAFLD. Plasma miRNAs hold potential to distinguish different stages and phenotypes of NAFLD, allowing for more precise clinical disease classification and targeted management strategies.

ARTICLE HIGHLIGHTS

Research background

Nonalcoholic fatty liver disease (NAFLD) is the most prevalent chronic liver diseases in the world, impacting approximately 25% of the population. The gold standard for NAFLD diagnosis is liver biopsy, yet it is invasive and expensive. Therefore, it is essential to provide alternative methods for NAFLD diagnosis. Recent studies propose that plasma microRNAs (miRNAs) are potential biomarkers for NAFLD, though research in this area remains limited.

Research motivation

This study is motivated by the current gaps of concerning associations between plasma miRNAs and NAFLD. This study aims to identify potential biomarkers for NAFLD diagnosis and NAFLD progression.

Research objectives

The objective of this study is to investigate associations between histological features of NAFLD and plasma miRNAs in adolescents with severe obesity.

Research methods

A total of 135 participants from the Teen Longitudinal Assessment of Bariatric Surgery (Teen-LABS) study were included in this study. Within Teen-LABS, the histological features of NAFLD, including NAFLD, nonalcoholic steatohepatitis (NASH), ballooning degeneration, fibrosis, and lobular inflammation, are characterized based on liver biopsy. Multivariate logistic regression was employed to investigates associations between NAFLD features and 843 plasma miRNAs. Pathway analysis was performed for identified NAFLD-associated miRNA by Ingenuity Pathway Analysis (IPA).

Research results

In the present study, we identified 38, 52, 16, 15, and 9 plasma miRNAs associated with NAFLD, NASH, fibrosis, ballooning, and lobular inflammation, respectively. Among these miRNA, miR-122-5p, miR-1343-5p, miR-193a-5p, miR-193b-5p, and miR-7845-5p were consistently upregulated across NAFLD features. In contrast, miR-1296-5p, miR-1301-5p, miR-199b-5p, miR-411-5p, and miR-6885-3p were positively associated with NAFLD, yet displayed predominant decreasing in NASH, fibrosis, ballooning, and lobular inflammation. IPA results suggested that most of NAFLD-associated miRNAs were related to cancer.

Research conclusions

Positive and consistent associations were observed between miR-122-5p, miR-1343-5p, miR-193a-5p, miR-193b-5p, and miR-7845-5p and NAFLD features, indicating their potential as biomarkers for NAFLD diagnosis. Additionally, miR-1296-5p, miR-1301-5p, miR-199b-5p, miR-411-5p, and miR-6885-3p showed different patterns of expression in response to NAFLD severity, indicating they had potential for characterizing NAFLD progression.

Research perspectives

Conducting studies with larger and more diverse populations would contribute to more conclusive findings regarding NAFLD–miRNA associations. Furthermore, experimental research is imperative to understand the underlying molecular mechanisms of NAFLD-miRNA associations.

FOOTNOTES

Author contributions: Li YJ and Chatzi L designed the research study; Li YJ performed the research; Conti DV, Stratakis N, Goodrich JA, Zhao YQ, Wang HX, and He JX contributed new analytic tools; Ryder JR, Inge TH, Jenkins T, Sisley S, Kohli R and Xanthakos SA contributed data collection; Li YJ wrote the manuscript; Baumert BO, Stratakis N, Goodrich JA, Wu HT, Aung MT, Eckel SP, Walker DI, Valvi D, La Merrill MA, Ryder JR, Inge TH, Jenkins T, Sisley S, Kohli R, Xanthakos SA, Baccarelli AA, McConnell R, Conti DV and Chatzi L reviewed and revised manuscript; all authors have read and approve the final manuscript.

Supported by National Institute of Environmental Health, No. R01ES030691; No. R01ES030364, No. R01ES029944, No. U01HG013288,

No. T32-ES013678, No. P30ES007048, No. U2CES030859, No. R01ES032831, No. R01ES033688, No. P30ES023515, and No. P2CES033433; National Human Genome Research Institute and National Institute of Environmental Health, No. U01HG013288; California Environmental Protection Agency, No. 20-E0017; National Cancer Institute and National Institute of Environmental Health, No. P01CA196569; Ministry of Science and Innovation and State Research Agency, No. CEX2018-000806-S; European Union ("NextGenerationEU/PRTR"), No. IJC2020-043630-I; European Union's Horizon Europe Research And Innovation Programme Under the Marie Skłodowska-Curie Actions Postdoctoral Fellowships, No. 101059245; United States Department of Agriculture, No. 6250-51000-053; National Institutes of Health, No. R01DK128117−01A1; and The Teen-LABS Consortium: National Institute of Diabetes and Digestive and Kidney Diseases, No. UM1DK072493 and No. UM1DK095710.

Institutional review board statement: This study used data from the Teen-LABS study (ClinicalTrials.gov NCT00465829), under a protocol approved by the institutional review boards of the participating institutions: Cincinnati Children's Hospital Medical Center (Cincinnati, Ohio), Nationwide Children's Hospital (Columbus, Ohio), University of Pittsburgh Medical Center (Pittsburgh, Pennsylvania), Texas Children's Hospital (Houston, Texas), and Children's Hospital of Alabama (Birmingham, Alabama).

Informed consent statement: This is a secondary data analysis, which means we do not have informed consent nor any private information of participants.

Conflict-of-interest statement: There are no conflicts of interest to report.

Data sharing statement: Technical appendix, statistical code, and dataset available from the corresponding author at chatzi@usc.edu.

STROBE statement: The authors have read the STROBE Statement-checklist of items, and the manuscript was prepared and revised according to the STROBE Statement-checklist of items.

Country/Territory of origin: United States

ORCID number: Yi-Jie Li 0000-0001-7551-117X; Brittney O Baumert 0000-0003-1220-8557; Nikos Stratakis 0000-0003-4613-0989; Jesse A Goodrich 0000-0001-6615-0472; Hao-Tian Wu 0000-0002-6271-0249; Jing-Xuan He 0000-0002-4524-4928; Yin-Qi Zhao 0000-0003-2413-732X; Max T Aung 0000-0001-5541-5447; Hong-Xu Wang 0000-0002-4980-219X; Sandrah P Eckel 0000-0001-6050-7880; Douglas I Walker 0000-0003-2912-398X; Damaskini Valvi 0000-0003-4633-229X; Michele A La Merrill 0000-0002-5720-5862; Justin R Ryder 0000-0002-7506-9497; Thomas H Inge 0000-0001-7782-1112; Stephanie Sisley 0000-0003-2900-7014; Rohit Kohli 0000-0002-0198-7703; Stavra A Xanthakos 0000-0001-9179-005X; Andrea A Baccarelli 0000-0002-3436-0640; Rob McConnell 0000-0001-5243-6410; Lida Chatzi 0000-0002-3319-2438.

S-Editor: Qu XL
L-Editor: A
P-Editor: Yu HG

REFERENCES

1 **Abd El-Kader SM**, El-Den Ashmawy EM. Non-alcoholic fatty liver disease: The diagnosis and management. *World J Hepatol* 2015; **7**: 846-858 [PMID: 25937862 DOI: 10.4254/wjh.v7.i6.846]
2 **Anstee QM**, Targher G, Day CP. Progression of NAFLD to diabetes mellitus, cardiovascular disease or cirrhosis. *Nat Rev Gastroenterol Hepatol* 2013; **10**: 330-344 [PMID: 23507799 DOI: 10.1038/nrgastro.2013.41]
3 **Machado MV**, Diehl AM. Pathogenesis of Nonalcoholic Steatohepatitis. *Gastroenterology* 2016; **150**: 1769-1777 [PMID: 26928243 DOI: 10.1053/j.gastro.2016.02.066]
4 **Takahashi Y**, Fukusato T. Histopathology of nonalcoholic fatty liver disease/nonalcoholic steatohepatitis. *World J Gastroenterol* 2014; **20**: 15539-15548 [PMID: 25400438 DOI: 10.3748/wjg.v20.i42.15539]
5 **Pais R**, Pascale A, Fedchuck L, Charlotte F, Poynard T, Ratziu V. Progression from isolated steatosis to steatohepatitis and fibrosis in nonalcoholic fatty liver disease. *Clin Res Hepatol Gastroenterol* 2011; **35**: 23-28 [PMID: 21634051 DOI: 10.1016/j.gcb.2010.06.004]
6 **Ong JP**, Younossi ZM. Epidemiology and natural history of NAFLD and NASH. *Clin Liver Dis* 2007; **11**: 1-16, vii [PMID: 17544968 DOI: 10.1016/j.cld.2007.02.009]
7 **Cotter TG**, Rinella M. Nonalcoholic Fatty Liver Disease 2020: The State of the Disease. *Gastroenterology* 2020; **158**: 1851-1864 [PMID: 32061595 DOI: 10.1053/j.gastro.2020.01.052]
8 **Arshad T**, Paik JM, Biswas R, Alqahtani SA, Henry L, Younossi ZM. Nonalcoholic Fatty Liver Disease Prevalence Trends Among Adolescents and Young Adults in the United States, 2007-2016. *Hepatol Commun* 2021; **5**: 1676-1688 [PMID: 34558817 DOI: 10.1002/hep4.1760]
9 **Welsh JA**, Karpen S, Vos MB. Increasing prevalence of nonalcoholic fatty liver disease among United States adolescents, 1988-1994 to 2007-2010. *J Pediatr* 2013; **162**: 496-500.e1 [PMID: 23084707 DOI: 10.1016/j.jpeds.2012.08.043]
10 **Xanthakos SA**, Jenkins TM, Kleiner DE, Boyce TW, Mourya R, Karns R, Brandt ML, Harmon CM, Helmrath MA, Michalsky MP, Courcoulas AP, Zeller MH, Inge TH; Teen-LABS Consortium. High Prevalence of Nonalcoholic Fatty Liver Disease in Adolescents

Undergoing Bariatric Surgery. *Gastroenterology* 2015; **149**: 623-34.e8 [PMID: 26026390 DOI: 10.1053/j.gastro.2015.05.039]
11 **Takahashi Y**, Inui A, Fujisawa T, Takikawa H, Fukusato T. Histopathological characteristics of non-alcoholic fatty liver disease in children: Comparison with adult cases. *Hepatol Res* 2011; **41**: 1066-1074 [PMID: 22035383 DOI: 10.1111/j.1872-034X.2011.00855.x]
12 **Nobili V**, Alisi A, Newton KP, Schwimmer JB. Comparison of the Phenotype and Approach to Pediatric vs Adult Patients With Nonalcoholic Fatty Liver Disease. *Gastroenterology* 2016; **150**: 1798-1810 [PMID: 27003600 DOI: 10.1053/j.gastro.2016.03.009]
13 **Feldstein AE**, Charatcharoenwitthaya P, Treeprasertsuk S, Benson JT, Enders FB, Angulo P. The natural history of non-alcoholic fatty liver disease in children: a follow-up study for up to 20 years. *Gut* 2009; **58**: 1538-1544 [PMID: 19625277 DOI: 10.1136/gut.2008.171280]
14 **Perumpail BJ**, Khan MA, Yoo ER, Cholankeril G, Kim D, Ahmed A. Clinical epidemiology and disease burden of nonalcoholic fatty liver disease. *World J Gastroenterol* 2017; **23**: 8263-8276 [PMID: 29307986 DOI: 10.3748/wjg.v23.i47.8263]
15 **Vilar-Gomez E**, Chalasani N. Non-invasive assessment of non-alcoholic fatty liver disease: Clinical prediction rules and blood-based biomarkers. *J Hepatol* 2018; **68**: 305-315 [PMID: 29154965 DOI: 10.1016/j.jhep.2017.11.013]
16 **Ferraioli G**, Wong VW, Castera L, Berzigotti A, Sporea I, Dietrich CF, Choi BI, Wilson SR, Kudo M, Barr RG. Liver Ultrasound Elastography: An Update to the World Federation for Ultrasound in Medicine and Biology Guidelines and Recommendations. *Ultrasound Med Biol* 2018; **44**: 2419-2440 [PMID: 30209008 DOI: 10.1016/j.ultrasmedbio.2018.07.008]
17 **Amernia B**, Moosavy SH, Banookh F, Zoghi G. FIB-4, APRI, and AST/ALT ratio compared to FibroScan for the assessment of hepatic fibrosis in patients with non-alcoholic fatty liver disease in Bandar Abbas, Iran. *BMC Gastroenterol* 2021; **21**: 453 [PMID: 34861841 DOI: 10.1186/s12876-021-02038-3]
18 **Nallagangula KS**, Nagaraj SK, Venkataswamy L, Chandrappa M. Liver fibrosis: a compilation on the biomarkers status and their significance during disease progression. *Future Sci OA* 2018; **4**: FSO250 [PMID: 29255622 DOI: 10.4155/fsoa-2017-0083]
19 **Ha M**, Kim VN. Regulation of microRNA biogenesis. *Nat Rev Mol Cell Biol* 2014; **15**: 509-524 [PMID: 25027649 DOI: 10.1038/nrm3838]
20 **Creemers EE**, Tijsen AJ, Pinto YM. Circulating microRNAs: novel biomarkers and extracellular communicators in cardiovascular disease? *Circ Res* 2012; **110**: 483-495 [PMID: 22302755 DOI: 10.1161/CIRCRESAHA.111.247452]
21 **Cui M**, Wang H, Yao X, Zhang D, Xie Y, Cui R, Zhang X. Circulating MicroRNAs in Cancer: Potential and Challenge. *Front Genet* 2019; **10**: 626 [PMID: 31379918 DOI: 10.3389/fgene.2019.00626]
22 **Gjorgjieva M**, Sobolewski C, Dolicka D, Correia de Sousa M, Foti M. miRNAs and NAFLD: from pathophysiology to therapy. *Gut* 2019; **68**: 2065-2079 [PMID: 31300518 DOI: 10.1136/gutjnl-2018-318146]
23 **Fang Z**, Dou G, Wang L. MicroRNAs in the Pathogenesis of Nonalcoholic Fatty Liver Disease. *Int J Biol Sci* 2021; **17**: 1851-1863 [PMID: 33994867 DOI: 10.7150/ijbs.59588]
24 **Pek SL**, Tavintharan S, Woon K, Lin L, Ong CN, Lim SC, Sum CF. MicroRNAs as biomarkers of hepatotoxicity in a randomized placebo-controlled study of simvastatin and ubiquinol supplementation. *Exp Biol Med (Maywood)* 2016; **241**: 317-330 [PMID: 26429200 DOI: 10.1177/1535370215605588]
25 **Auguet T**, Aragonès G, Berlanga A, Guiu-Jurado E, Martí A, Martínez S, Sabench F, Hernández M, Aguilar C, Sirvent JJ, Del Castillo D, Richart C. miR33a/miR33b* and miR122 as Possible Contributors to Hepatic Lipid Metabolism in Obese Women with Nonalcoholic Fatty Liver Disease. *Int J Mol Sci* 2016; **17** [PMID: 27669236 DOI: 10.3390/ijms17101620]
26 **Johnson K**, Leary PJ, Govaere O, Barter MJ, Charlton SH, Cockell SJ, Tiniakos D, Zatorska M, Bedossa P, Brosnan MJ, Cobbold JF, Ekstedt M, Aithal GP, Clément K, Schattenberg JM, Boursier J, Ratziu V, Bugianesi E, Anstee QM, Daly AK; LITMUS Consortium Investigators§; LITMUS Consortium Investigators. Increased serum miR-193a-5p during non-alcoholic fatty liver disease progression: Diagnostic and mechanistic relevance. *JHEP Rep* 2022; **4**: 100409 [PMID: 35072021 DOI: 10.1016/j.jhepr.2021.100409]
27 **Becker PP**, Rau M, Schmitt J, Malsch C, Hammer C, Bantel H, Müllhaupt B, Geier A. Performance of Serum microRNAs -122, -192 and -21 as Biomarkers in Patients with Non-Alcoholic Steatohepatitis. *PLoS One* 2015; **10**: e0142661 [PMID: 26565986 DOI: 10.1371/journal.pone.0142661]
28 **Chai C**, Rivkin M, Berkovits L, Simerzin A, Zorde-Khvalevsky E, Rosenberg N, Klein S, Yaish D, Durst R, Shpitzen S, Udi S, Tam J, Heeren J, Worthmann A, Schramm C, Kluwe J, Ravid R, Hornstein E, Giladi H, Galun E. Metabolic Circuit Involving Free Fatty Acids, microRNA 122, and Triglyceride Synthesis in Liver and Muscle Tissues. *Gastroenterology* 2017; **153**: 1404-1415 [PMID: 28802563 DOI: 10.1053/j.gastro.2017.08.013]
29 **Liu XL**, Pan Q, Zhang RN, Shen F, Yan SY, Sun C, Xu ZJ, Chen YW, Fan JG. Disease-specific miR-34a as diagnostic marker of non-alcoholic steatohepatitis in a Chinese population. *World J Gastroenterol* 2016; **22**: 9844-9852 [PMID: 27956809 DOI: 10.3748/wjg.v22.i44.9844]
30 **Cheung O**, Puri P, Eicken C, Contos MJ, Mirshahi F, Maher JW, Kellum JM, Min H, Luketic VA, Sanyal AJ. Nonalcoholic steatohepatitis is associated with altered hepatic MicroRNA expression. *Hepatology* 2008; **48**: 1810-1820 [PMID: 19030170 DOI: 10.1002/hep.22569]
31 **Kim TH**, Lee Y, Lee YS, Gim JA, Ko E, Yim SY, Jung YK, Kang S, Kim MY, Kim H, Kim BH, Kim JH, Seo YS, Yim HJ, Yeon JE, Um SH, Byun KS. Circulating miRNA is a useful diagnostic biomarker for nonalcoholic steatohepatitis in nonalcoholic fatty liver disease. *Sci Rep* 2021; **11**: 14639 [PMID: 34282172 DOI: 10.1038/s41598-021-94115-6]
32 **Ezaz G**, Trivedi HD, Connelly MA, Filozof C, Howard K, L Parrish M, Kim M, Herman MA, Nasser I, Afdhal NH, Jiang ZG, Lai M. Differential Associations of Circulating MicroRNAs With Pathogenic Factors in NAFLD. *Hepatol Commun* 2020; **4**: 670-680 [PMID: 32363318 DOI: 10.1002/hep4.1501]
33 **Tan Y**, Ge G, Pan T, Wen D, Gan J. A pilot study of serum microRNAs panel as potential biomarkers for diagnosis of nonalcoholic fatty liver disease. *PLoS One* 2014; **9**: e105192 [PMID: 25141008 DOI: 10.1371/journal.pone.0105192]
34 **Cermelli S**, Ruggieri A, Marrero JA, Ioannou GN, Beretta L. Circulating microRNAs in patients with chronic hepatitis C and non-alcoholic fatty liver disease. *PLoS One* 2011; **6**: e23937 [PMID: 21886843 DOI: 10.1371/journal.pone.0023937]
35 **Celikbilek M**, Baskol M, Taheri S, Deniz K, Dogan S, Zararsiz G, Gursoy S, Guven K, Ozbakır O, Dundar M, Yucesoy M. Circulating microRNAs in patients with non-alcoholic fatty liver disease. *World J Hepatol* 2014; **6**: 613-620 [PMID: 25232454 DOI: 10.4254/wjh.v6.i8.613]
36 **Pirola CJ**, Fernández Gianotti T, Castaño GO, Mallardi P, San Martino J, Mora Gonzalez Lopez Ledesma M, Flichman D, Mirshahi F, Sanyal AJ, Sookoian S. Circulating microRNA signature in non-alcoholic fatty liver disease: from serum non-coding RNAs to liver histology and disease pathogenesis. *Gut* 2015; **64**: 800-812 [PMID: 24973316 DOI: 10.1136/gutjnl-2014-306996]
37 **Yamada H**, Suzuki K, Ichino N, Ando Y, Sawada A, Osakabe K, Sugimoto K, Ohashi K, Teradaira R, Inoue T, Hamajima N, Hashimoto S. Associations between circulating microRNAs (miR-21, miR-34a, miR-122 and miR-451) and non-alcoholic fatty liver. *Clin Chim Acta* 2013;

424: 99-103 [PMID: 23727030 DOI: 10.1016/j.cca.2013.05.021]
38 **Lin H**, Mercer KE, Ou X, Mansfield K, Buchmann R, Børsheim E, Tas E. Circulating microRNAs Are Associated With Metabolic Markers in Adolescents With Hepatosteatosis. *Front Endocrinol (Lausanne)* 2022; **13**: 856973 [PMID: 35498403 DOI: 10.3389/fendo.2022.856973]
39 **Zhou X**, Huang K, Jia J, Ni Y, Yuan J, Liang X, Lin H, Peng W, Wu W, Dong G, Fu J. Exosomal miRNAs Profile in Children's Nonalcoholic Fatty Liver Disease and the Correlation with Transaminase and Uric Acid. *Ann Nutr Metab* 2020; **76**: 44-53 [PMID: 32172249 DOI: 10.1159/000506665]
40 **Inge TH**, Zeller M, Harmon C, Helmrath M, Bean J, Modi A, Horlick M, Kalra M, Xanthakos S, Miller R, Akers R, Courcoulas A. Teen-Longitudinal Assessment of Bariatric Surgery: methodological features of the first prospective multicenter study of adolescent bariatric surgery. *J Pediatr Surg* 2007; **42**: 1969-1971 [PMID: 18022459 DOI: 10.1016/j.jpedsurg.2007.08.010]
41 **Inge TH**, Zeller MH, Jenkins TM, Helmrath M, Brandt ML, Michalsky MP, Harmon CM, Courcoulas A, Horlick M, Xanthakos SA, Dolan L, Mitsnefes M, Barnett SJ, Buncher R; Teen-LABS Consortium. Perioperative outcomes of adolescents undergoing bariatric surgery: the Teen-Longitudinal Assessment of Bariatric Surgery (Teen-LABS) study. *JAMA Pediatr* 2014; **168**: 47-53 [PMID: 24189578 DOI: 10.1001/jamapediatrics.2013.4296]
42 **Inge TH**, Courcoulas AP, Jenkins TM, Michalsky MP, Helmrath MA, Brandt ML, Harmon CM, Zeller MH, Chen MK, Xanthakos SA, Horlick M, Buncher CR; Teen-LABS Consortium. Weight Loss and Health Status 3 Years after Bariatric Surgery in Adolescents. *N Engl J Med* 2016; **374**: 113-123 [PMID: 26544725 DOI: 10.1056/NEJMoa1506699]
43 **Kleiner DE**, Brunt EM, Van Natta M, Behling C, Contos MJ, Cummings OW, Ferrell LD, Liu YC, Torbenson MS, Unalp-Arida A, Yeh M, McCullough AJ, Sanyal AJ; Nonalcoholic Steatohepatitis Clinical Research Network. Design and validation of a histological scoring system for nonalcoholic fatty liver disease. *Hepatology* 2005; **41**: 1313-1321 [PMID: 15915461 DOI: 10.1002/hep.20701]
44 **Brunt EM**, Kleiner DE, Wilson LA, Belt P, Neuschwander-Tetri BA; NASH Clinical Research Network (CRN). Nonalcoholic fatty liver disease (NAFLD) activity score and the histopathologic diagnosis in NAFLD: distinct clinicopathologic meanings. *Hepatology* 2011; **53**: 810-820 [PMID: 21319198 DOI: 10.1002/hep.24127]
45 **Leek JT**, Johnson WE, Parker HS, Jaffe AE, Storey JD. The sva package for removing batch effects and other unwanted variation in high-throughput experiments. *Bioinformatics* 2012; **28**: 882-883 [PMID: 22257669 DOI: 10.1093/bioinformatics/bts034]
46 **Anders S**, Huber W. Differential expression analysis for sequence count data. *Genome Biol* 2010; **11**: R106 [PMID: 20979621 DOI: 10.1186/gb-2010-11-10-r106]
47 **McPherson S**, Hardy T, Dufour JF, Petta S, Romero-Gomez M, Allison M, Oliveira CP, Francque S, Van Gaal L, Schattenberg JM, Tiniakos D, Burt A, Bugianesi E, Ratziu V, Day CP, Anstee QM. Age as a Confounding Factor for the Accurate Non-Invasive Diagnosis of Advanced NAFLD Fibrosis. *Am J Gastroenterol* 2017; **112**: 740-751 [PMID: 27725647 DOI: 10.1038/ajg.2016.453]
48 **Lin Y**, Feng X, Cao X, Miao R, Sun Y, Li R, Ye J, Zhong B. Age patterns of nonalcoholic fatty liver disease incidence: heterogeneous associations with metabolic changes. *Diabetol Metab Syndr* 2022; **14**: 181 [PMID: 36443867 DOI: 10.1186/s13098-022-00930-w]
49 **Ameling S**, Kacprowski T, Chilukoti RK, Malsch C, Liebscher V, Suhre K, Pietzner M, Friedrich N, Homuth G, Hammer E, Völker U. Associations of circulating plasma microRNAs with age, body mass index and sex in a population-based study. *BMC Med Genomics* 2015; **8**: 61 [PMID: 26462558 DOI: 10.1186/s12920-015-0136-7]
50 **Marchesini G**, Bugianesi E, Forlani G, Cerrelli F, Lenzi M, Manini R, Natale S, Vanni E, Villanova N, Melchionda N, Rizzetto M. Nonalcoholic fatty liver, steatohepatitis, and the metabolic syndrome. *Hepatology* 2003; **37**: 917-923 [PMID: 12668987 DOI: 10.1053/jhep.2003.50161]
51 **Loomis AK**, Kabadi S, Preiss D, Hyde C, Bonato V, St Louis M, Desai J, Gill JM, Welsh P, Waterworth D, Sattar N. Body Mass Index and Risk of Nonalcoholic Fatty Liver Disease: Two Electronic Health Record Prospective Studies. *J Clin Endocrinol Metab* 2016; **101**: 945-952 [PMID: 26672639 DOI: 10.1210/jc.2015-3444]
52 **Lonardo A**, Suzuki A. Sexual Dimorphism of NAFLD in Adults. Focus on Clinical Aspects and Implications for Practice and Translational Research. *J Clin Med* 2020; **9** [PMID: 32354182 DOI: 10.3390/jcm9051278]
53 **Lonardo A**, Nascimbeni F, Ballestri S, Fairweather D, Win S, Than TA, Abdelmalek MF, Suzuki A. Sex Differences in Nonalcoholic Fatty Liver Disease: State of the Art and Identification of Research Gaps. *Hepatology* 2019; **70**: 1457-1469 [PMID: 30924946 DOI: 10.1002/hep.30626]
54 **Koutoukidis DA**, Astbury NM, Tudor KE, Morris E, Henry JA, Noreik M, Jebb SA, Aveyard P. Association of Weight Loss Interventions With Changes in Biomarkers of Nonalcoholic Fatty Liver Disease: A Systematic Review and Meta-analysis. *JAMA Intern Med* 2019; **179**: 1262-1271 [PMID: 31260026 DOI: 10.1001/jamainternmed.2019.2248]
55 **Brunner KT**, Henneberg CJ, Wilechansky RM, Long MT. Nonalcoholic Fatty Liver Disease and Obesity Treatment. *Curr Obes Rep* 2019; **8**: 220-228 [PMID: 30945129 DOI: 10.1007/s13679-019-00345-1]
56 **Bonacini M**, Kassamali F, Kari S, Lopez Barrera N, Kohla M. Racial differences in prevalence and severity of non-alcoholic fatty liver disease. *World J Hepatol* 2021; **13**: 763-773 [PMID: 34367497 DOI: 10.4254/wjh.v13.i7.763]
57 **Riazi K**, Swain MG, Congly SE, Kaplan GG, Shaheen AA. Race and Ethnicity in Non-Alcoholic Fatty Liver Disease (NAFLD): A Narrative Review. *Nutrients* 2022; **14** [PMID: 36364818 DOI: 10.3390/nu14214556]
58 **Tang M**, Liu M, Zhang Y, Xie R. Association of family income to poverty ratio and vibration-controlled transient elastography quantified degree of hepatic steatosis in U.S. adolescents. *Front Endocrinol (Lausanne)* 2023; **14**: 1160625 [PMID: 37033220 DOI: 10.3389/fendo.2023.1160625]
59 **Tan SY**, Georgousopoulou EN, Cardoso BR, Daly RM, George ES. Associations between nut intake, cognitive function and non-alcoholic fatty liver disease (NAFLD) in older adults in the United States: NHANES 2011-14. *BMC Geriatr* 2021; **21**: 313 [PMID: 34001034 DOI: 10.1186/s12877-021-02239-1]
60 **Krämer A**, Green J, Pollard J Jr, Tugendreich S. Causal analysis approaches in Ingenuity Pathway Analysis. *Bioinformatics* 2014; **30**: 523-530 [PMID: 24336805 DOI: 10.1093/bioinformatics/btt703]
61 **Griffiths-Jones S**, Grocock RJ, van Dongen S, Bateman A, Enright AJ. miRBase: microRNA sequences, targets and gene nomenclature. *Nucleic Acids Res* 2006; **34**: D140-D144 [PMID: 16381832 DOI: 10.1093/nar/gkj112]
62 **Kanehisa M**, Goto S. KEGG: kyoto encyclopedia of genes and genomes. *Nucleic Acids Res* 2000; **28**: 27-30 [PMID: 10592173 DOI: 10.1093/nar/28.1.27]
63 **Lloyd S**. Least squares quantization in PCM. *IEEE* 1982; **28**: 129-137 [DOI: 10.1109/TIT.1982.1056489]
64 **Marutho DHH**, Wijaya S, Muljono E. The Determination of Cluster Number at k-Mean Using Elbow Method and Purity Evaluation on Headline News. *IEEE* 2018 [DOI: 10.1109/ISEMANTIC.2018.8549751]

65 **Jain AK**. Data clustering: 50 years beyond K-means. *Pattern Recognit Lett* 2010; **31**: 651-666 [DOI: 10.1016/j.patrec.2009.09.011]

66 **Thorndike RL**. Who belongs in the family? *Psychometrika* 1953; **18**: 267-276 [DOI: 10.1007/BF02289263]

67 **Soronen J**, Yki-Järvinen H, Zhou Y, Sädevirta S, Sarin AP, Leivonen M, Sevastianova K, Perttilä J, Laurila PP, Sigruener A, Schmitz G, Olkkonen VM. Novel hepatic microRNAs upregulated in human nonalcoholic fatty liver disease. *Physiol Rep* 2016; **4** [PMID: 26733244 DOI: 10.14814/phy2.12661]

68 **Liang Q**, Chen H, Xu X, Jiang W. miR-182-5p Attenuates High-Fat -Diet-Induced Nonalcoholic Steatohepatitis in Mice. *Ann Hepatol* 2019; **18**: 116-125 [PMID: 31113580 DOI: 10.5604/01.3001.0012.7902]

69 **Katsura A**, Morishita A, Iwama H, Tani J, Sakamoto T, Tatsuta M, Toyota Y, Fujita K, Kato K, Maeda E, Nomura T, Miyoshi H, Yoneyama H, Himoto T, Fujiwara S, Kobara H, Mori H, Niki T, Ono M, Hirashima M, Masaki T. MicroRNA profiles following metformin treatment in a mouse model of non-alcoholic steatohepatitis. *Int J Mol Med* 2015; **35**: 877-884 [PMID: 25672270 DOI: 10.3892/ijmm.2015.2092]

70 **Wan Z**, Yang X, Liu X, Sun Y, Yu P, Xu F, Deng H. M2 macrophage-derived exosomal microRNA-411-5p impedes the activation of hepatic stellate cells by targeting CAMSAP1 in NASH model. *iScience* 2022; **25**: 104597 [PMID: 35789846 DOI: 10.1016/j.isci.2022.104597]

71 **Adinolfi LE**, Rinaldi L, Guerrera B, Restivo L, Marrone A, Giordano M, Zampino R. NAFLD and NASH in HCV Infection: Prevalence and Significance in Hepatic and Extrahepatic Manifestations. *Int J Mol Sci* 2016; **17** [PMID: 27231906 DOI: 10.3390/ijms17060803]

72 **Iacob DG**, Rosca A, Ruta SM. Circulating microRNAs as non-invasive biomarkers for hepatitis B virus liver fibrosis. *World J Gastroenterol* 2020; **26**: 1113-1127 [PMID: 32231417 DOI: 10.3748/wjg.v26.i11.1113]

73 **Long JK**, Dai W, Zheng YW, Zhao SP. miR-122 promotes hepatic lipogenesis *via* inhibiting the LKB1/AMPK pathway by targeting Sirt1 in non-alcoholic fatty liver disease. *Mol Med* 2019; **25**: 26 [PMID: 31195981 DOI: 10.1186/s10020-019-0085-2]

74 **Hu Y**, Peng X, Du G, Zhang Z, Zhai Y, Xiong X, Luo X. MicroRNA-122-5p Inhibition Improves Inflammation and Oxidative Stress Damage in Dietary-Induced Non-alcoholic Fatty Liver Disease Through Targeting FOXO3. *Front Physiol* 2022; **13**: 803445 [PMID: 35222075 DOI: 10.3389/fphys.2022.803445]

75 **Li K**, Zhao B, Wei D, Wang W, Cui Y, Qian L, Liu G. miR146a improves hepatic lipid and glucose metabolism by targeting MED1. *Int J Mol Med* 2020; **45**: 543-555 [PMID: 31894315 DOI: 10.3892/ijmm.2019.4443]

76 **Huang R**, Duan X, Liu X, Cao H, Wang Y, Fan J, Wang B. Upregulation of miR-181a impairs lipid metabolism by targeting PPARα expression in nonalcoholic fatty liver disease. *Biochem Biophys Res Commun* 2019; **508**: 1252-1258 [PMID: 30558790 DOI: 10.1016/j.bbrc.2018.12.061]

77 **Gjorgjieva M**, Sobolewski C, Ay AS, Abegg D, Correia de Sousa M, Portius D, Berthou F, Fournier M, Maeder C, Rantakari P, Zhang FP, Poutanen M, Picard D, Montet X, Nef S, Adibekian A, Foti M. Genetic Ablation of MiR-22 Fosters Diet-Induced Obesity and NAFLD Development. *J Pers Med* 2020; **10** [PMID: 33066497 DOI: 10.3390/jpm10040170]

78 **Yadav AK**, Sata TN, Verma D, Sah AK, Mishra AK, Mrinalini, Hossain MM, Pant K, Venugopal SK. Free fatty acid-induced miR-22 inhibits gluconeogenesis *via* SIRT-1-mediated PGC-1α expression in nonalcoholic fatty liver disease. *iLIVER* 2023; **2**: 1-9 [DOI: 10.1016/j.iliver.2023.01.002]

79 **Zhang Q**, Yu K, Cao Y, Luo Y, Liu Y, Zhao C. miR-125b promotes the NF-κB-mediated inflammatory response in NAFLD *via* directly targeting TNFAIP3. *Life Sci* 2021; **270**: 119071 [PMID: 33515562 DOI: 10.1016/j.lfs.2021.119071]

80 **Feili X**, Wu S, Ye W, Tu J, Lou L. MicroRNA-34a-5p inhibits liver fibrosis by regulating TGF-β1/Smad3 pathway in hepatic stellate cells. *Cell Biol Int* 2018; **42**: 1370-1376 [PMID: 29957876 DOI: 10.1002/cbin.11022]

81 **Liang Z**, Li J, Zhao L, Deng Y. miR-375 affects the hedgehog signaling pathway by downregulating RAC1 to inhibit hepatic stellate cell viability and epithelial-mesenchymal transition. *Mol Med Rep* 2021; **23** [PMID: 33398380 DOI: 10.3892/mmr.2020.11821]

82 **Spengler EK**, Loomba R. Recommendations for Diagnosis, Referral for Liver Biopsy, and Treatment of Nonalcoholic Fatty Liver Disease and Nonalcoholic Steatohepatitis. *Mayo Clin Proc* 2015; **90**: 1233-1246 [PMID: 26219858 DOI: 10.1016/j.mayocp.2015.06.013]

World Journal of Gastroenterology

Submit a Manuscript: https://www.f6publishing.com

World J Gastroenterol 2024 January 28; 30(4): 346-366

DOI: 10.3748/wjg.v30.i4.346

ISSN 1007-9327 (print) ISSN 2219-2840 (online)

ORIGINAL ARTICLE

Observational Study

Gastrointestinal manifestations of critical ill heatstroke patients and their associations with outcomes: A multicentre, retrospective, observational study

Yu-Cong Wang, Xin-Yang Jin, Zheng Lei, Xiao-Jiao Liu, Yu Liu, Bang-Guo Zhang, Jian Gong, Lie-Tao Wang, Lv-Yuan Shi, Ding-Yuan Wan, Xin Fu, Lu-Ping Wang, Ai-Jia Ma, Yi-Song Cheng, Jing Yang, Min He, Xiao-Dong Jin, Yan Kang, Bo Wang, Zhong-Wei Zhang, Qin Wu

Specialty type: Gastroenterology and hepatology

Provenance and peer review: Unsolicited article; Externally peer reviewed.

Peer-review model: Single blind

Peer-review report's scientific quality classification

Grade A (Excellent): 0
Grade B (Very good): B
Grade C (Good): 0
Grade D (Fair): 0
Grade E (Poor): 0

P-Reviewer: Thongon N, Thailand

Received: October 3, 2023
Peer-review started: October 3, 2023
First decision: December 6, 2023
Revised: December 17, 2023
Accepted: January 9, 2024
Article in press: January 9, 2024
Published online: January 28, 2024

Yu-Cong Wang, Lie-Tao Wang, Lv-Yuan Shi, Ding-Yuan Wan, Xin Fu, Lu-Ping Wang, Ai-Jia Ma, Yi-Song Cheng, Jing Yang, Min He, Xiao-Dong Jin, Yan Kang, Bo Wang, Zhong-Wei Zhang, Qin Wu, Department of Critical Care Medicine, West China Hospital, Sichuan University, Chengdu 610041, Sichuan Province, China

Xin-Yang Jin, School of Pharmacy, Macau University of Science and Technology, Macau 999078, China

Zheng Lei, Department of Critical Care Medicine, The First People's Hospital of Ziyang City, Ziyang 641399, Sichuan Province, China

Xiao-Jiao Liu, Department of Critical Care Medicine, The First People's Hospital of Guanghan City, Chengdu 618399, Sichuan Province, China

Yu Liu, Department of Critical Care Medicine, Lezhi County Traditional Chinese Medicine Hospital, Chengdu 641599, Sichuan Province, China

Bang-Guo Zhang, Department of Critical Care Medicine, Chengdu Qingbaijiang District People's Hospital, Chengdu 610399, Sichuan Province, China

Jian Gong, Department of Critical Care Medicine, Ziyang People's Hospital, Chengdu 641399, Sichuan Province, China

Corresponding author: Qin Wu, MD, Doctor, Professor, Department of Critical Care Medicine, West China Hospital, Sichuan University, No. 37 Guoxue Alley, Wuhou District, Chengdu 610041, Sichuan Province, China. qinwu0221@gmail.com

Abstract

BACKGROUND

Extreme heat exposure is a growing health problem, and the effects of heat on the gastrointestinal (GI) tract is unknown. This study aimed to assess the incidence of GI symptoms associated with heatstroke and its impact on outcomes.

AIM

To assess the incidence of GI symptoms associated with heatstroke and its impact on outcomes.

METHODS

Patients admitted to the intensive care unit (ICU) due to heatstroke were included from 83 centres. Patient history, laboratory results, and clinically relevant outcomes were recorded at ICU admission and daily until up to day 15, ICU discharge, or death. GI symptoms, including nausea/vomiting, diarrhoea, flatulence, and bloody stools, were recorded. The characteristics of patients with heatstroke concomitant with GI symptoms were described. Multivariable regression analyses were performed to determine significant predictors of GI symptoms.

RESULTS

A total of 713 patients were included in the final analysis, of whom 132 (18.5%) patients had at least one GI symptom during their ICU stay, while 26 (3.6%) suffered from more than one symptom. Patients with GI symptoms had a significantly higher ICU stay compared with those without. The mortality of patients who had two or more GI symptoms simultaneously was significantly higher than that in those with one GI symptom. Multivariable logistic regression analysis revealed that older patients with a lower GCS score on admission were more likely to experience GI symptoms.

CONCLUSION

The GI manifestations of heatstroke are common and appear to impact clinically relevant hospitalization outcomes.

Key Words: Extreme heat; Flatulence; Sunstroke; Intensive care units; Diarrhea

Core Tip: This study aimed to assess the incidence of gastrointestinal (GI) symptoms associated with heatstroke and its impact on outcomes. This was a retrospective, multi-center, observational cohort study that involved patients admitted to 83 intensive care unit located in 16 cities in the Sichuan Province, China between June 1 and October 31, 2022. Results showed older heatstroke patients with a lower Glasgow coma scale score on admission were more likely to experience GI symptoms, which had statistical difference. Clinicians should pay attention to the time at which heatstroke patients started manifesting GI symptoms, as well as the duration of said symptoms, to ensure that patients are timely treated with the proper enteral therapy and have the best prognosis possible.

Citation: Wang YC, Jin XY, Lei Z, Liu XJ, Liu Y, Zhang BG, Gong J, Wang LT, Shi LY, Wan DY, Fu X, Wang LP, Ma AJ, Cheng YS, Yang J, He M, Jin XD, Kang Y, Wang B, Zhang ZW, Wu Q. Gastrointestinal manifestations of critical ill heatstroke patients and their associations with outcomes: A multicentre, retrospective, observational study. *World J Gastroenterol* 2024; 30(4): 346-366
URL: https://www.wjgnet.com/1007-9327/full/v30/i4/346.htm
DOI: https://dx.doi.org/10.3748/wjg.v30.i4.346

INTRODUCTION

Owing to the effects of climate change, extreme heat is rapidly becoming a global public health concern. Direct exposure to extreme heat can cause dysregulation of body temperature, leading to heatstroke[1]. Over the past two decades, there has been a 50% increase in heat-related mortality among adults aged 65 and older. As an acute life-threatening condition manifesting an uncontrolled rise in core body temperature, heatstroke presents clinically as a systemic disorder and comprises the following symptoms: Encephalopathy, hypotension, respiratory failure, liver, muscle, coagulopathy and kidney damage[2]. In recent years, some studies have indicated that sustained high body temperature can cause structural and functional damage to the gastrointestinal (GI) tract, resulting in vomiting, diarrhoea, or intolerance to enteral nutrition (EN), which can exacerbate patients' condition[3,4]. Nevertheless, the impact of heatstroke on the GI tract remains to be elucidated.

Located in southwestern part of China, the Sichuan Province is the second largest Chinese province, with a permanent population of more than 80 million. According to the records of the Sichuan meteorological administration, as of May 2022, summer temperatures have reached a historical high since 1961, with two consecutive strong high-temperature periods. One of the most notable consequences of this phenomenon is the significant increase in the number of cases of heatstroke. Accordingly, we conducted a retrospective, multi-center study to examine the demographic characteristics of heatstroke patients admitted to the intensive care unit (ICU) in 2022. Our study primarily aimed to determine the incidence of GI disturbances among patients experiencing heatstroke from various medical centres in the Sichuan Province, with a secondary objective of identifying the risk factors for GI symptoms after heatstroke.

MATERIALS AND METHODS

This was a retrospective, multi-center, observational cohort study that involved patients admitted to 83 ICUs located in 16 cities in the Sichuan Province, China between June 1 and October 31, 2022. Ethical approval for this study was obtained from the Biomedical Ethics Review Committee of the West China Hospital of Sichuan University (approval No. SCU-2022-1542), in accordance with the principles outlined in the Declaration of Helsinki. Given the retrospective nature of this study, the requirement for informed consent was waived.

Patients and examination

Inclusion criteria comprised: (1) an age > 18 years; and (2) hospitalization in any type of ICU due to heatstroke or heatstroke-related complications. Patients with heatstroke were diagnosed by front-line medical staff in each center, and the diagnosis was made according to the corresponding clinical manifestations, as well as clinical history[5]. The exclusion criteria included an age < 18; burns; death within 24 h following ICU admission; palliative care; and simultaneous participation in any other nutrition-related interventional studies. Patients whose data is unsuitable for the analysis performed in this study were also excluded. Demographic characteristics were recorded at ICU admission, and clinical variables were recorded daily until up to day 15 of ICU stay or ICU discharge or death. Patients included in the study were managed by physicians in their respective ICUs. The treatment plan for each patient was determined by the attending physician based on the patient's individual condition.

Data collection and definitions

An electronic data capture system (Sichuan Zhikang Technology Co., Ltd, China) was implemented to gather information on heatstroke patients. Data collectors, who were primarily front-line physicians in each centre's ICU, recorded information on each patient. The data collected was determined after extensive discussion based on expert opinions and in combination with literature review. The trial filling of data was conducted twice through two extensive online meetings with experts from each center to finalize all forms. A training in which the use of the electronic data capture system and heatstroke-related knowledge are explained was conducted in each center before initiating data collection. An online meeting would be hosted every week to check the quality of the data collected during said week. The data underwent a two-step verification process to ensure its completeness and accuracy, and unqualified data was to be collected again. Four researchers (Yu-Cong Wang, Lie-Tao Wang, Lv-Yuan Shi, and Ding-Yuan Wan) reviewed all data independently for completeness and accuracy, and the data management team (Min He, Jing Yang and Qin Wu) conducted a thorough cleaning of the data, identifying any missing information.

Data comprising baseline information, laboratory test results, treatment plan, GI symptoms, nutrition support, and patient outcome were collected in the electronic data capture system. As demographic information, age, sex, body mass index (BMI), and concomitant diseases were collected. Patients' body temperature at hospital admission, including duration of exposure to heat, first symptoms according to chief complain, nutrition risk screening 2002 (NRS-2002), and Glasgow coma scale (GCS) score were also recorded. Moreover, the average, maximum, and minimum temperature data for the months of May, June, and July in 2022, which was publicly available on the website of the Sichuan meteorological administration, was also collected. The definition of fever in this study was set as a body temperature greater than 37.3 °C as determined through anal temperature measurement. High environment temperature was defined as when the maximum environment temperature reaches or exceeds 35 °C. If the high temperature lasts for more than 3 d, it was defined as a high temperature heat wave. Treatment received during the observation period, including organ support technical, antibiotics, and steroids, were recorded.

GI symptoms were defined as the presence of nausea/vomiting, diarrhoea, flatulence, or bloody stools that do not resolve with medical therapy[6-8]. Specifically, nausea/vomiting in non-intubated patients was defined as the self-reporting of epigastric discomfort followed by vomiting, self-reporting of nausea alone without vomiting, or vomiting alone without nausea. As for intubated patients, nausea/vomiting was defined as the presence of reflux or aspiration for abnormal causes. Diarrhoea was defined as frequent exclusion of loose thin faeces or even watery stools for more than 3 times daily of more than 200 mL each time. Flatulence was defined as awake patients feeling fullness in part or all of the abdomen or partial or total abdominal distention as determined by physical examination in non-awake patients. Bloody stool was defined as having a positive faecal occult blood test more than twice or dark red or black stool. Information on GI symptoms comes from the hourly nursing observation records or daily disease course records.

For patients' outcome, we collected complications during the observational period, mortality at 15 d, and length of stay in the ICU. The complications in this study included disturbance of water and electrolyte, rhabdomyolysis, myocardial damage, acute kidney injury, acute liver function impairment, and central nervous system impairment. More specifically, disturbance of water and electrolyte was defined as dehydration, oedema, hyperkalaemia, hypokalemia, hypercalcemia, hypocalcaemia, hypermagnesemia or hypomagnesemia, as determined by clinicians. Rhabdomyolysis was defined as muscle pain, tenderness, swelling, weakness, and other muscle involvement and serum creatine kinase levels being significantly elevated more than 5 times the upper limit of normal. Myocardial damage was defined as elevated myocardial enzymes with a normal electrocardiogram. Acute kidney injury was defined according to the kidney disease: Improving Global Outcomes criteria after high temperature exposure. Acute liver function impairment was defined as elevated serum aminotransferase and bilirubin levels above the normal limit after exposure to high temperature with the absence of chronic liver disease, liver failure, coagulation dysfunction, and hepatic encephalopathy. Central nervous system impairment was defined as the occurrence of seizures, motor dysfunction, or sensory dysfunction, including limb hemiplegia, immobility, numbness of the hemi limb, or spontaneous pain in a patient with no history of central nervous system disease.

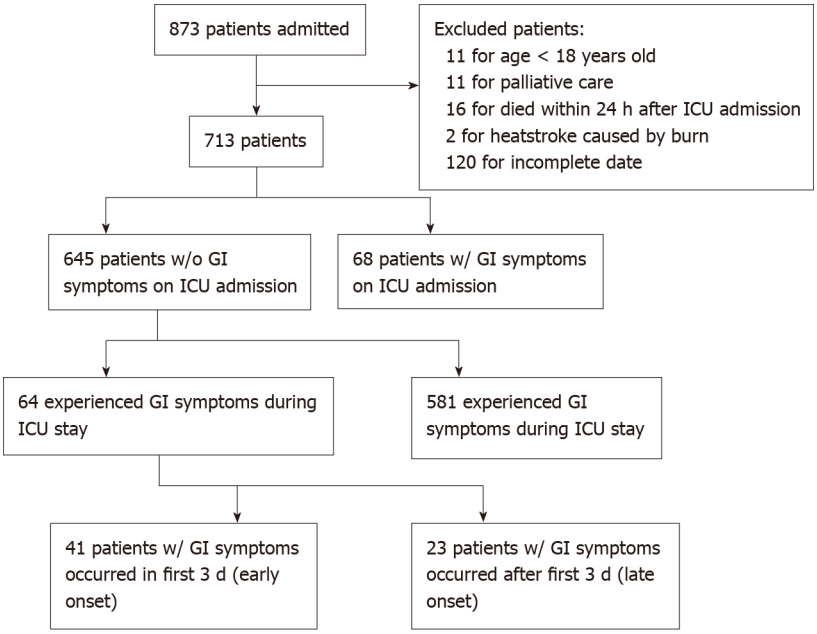

DOI: 10.3748/wjg.v30.i4.346 **Copyright** ©The Author(s) 2024.

Figure 1 Flow chart of the study. Patients were grouped according to whether gastrointestinal (GI) symptoms occurred on intensive care unit (ICU) admission, then whether GI symptoms occurred during ICU hospitalization and the onset of patients' GI symptoms. ICU: Intensive care unit; GI: Gastrointestinal; w: With; o: Without.

The primary outcome of the study was the incidence of post-heatstroke GI symptoms, as determined through data collection by trained data collectors. Secondary outcomes included the identification of risk factors for GI dysfunction following heatstroke.

Statistical analysis

Statistical analysis was performed using descriptive statistics. Continuous variables were reported as median and quartile ranges or simple ranges, while categorical variables were summarized as counts and percentages. Items missing more than 10% of their data will be excluded from the analysis, and no imputation was made for missing data. All data were analysed using SPSS Statistics version 25 software (IBM Corp., Armonk, NY, United States). Descriptive statistical analyses reflected the distribution of characteristics of the sample population across case and control groups in the form of counts and proportions. *T* tests and χ^2 tests were applied to test the association between case and control group variables. The incidence of confirmed cases was visually represented using a map created with Dychart.com (Wuhan Dysprosium Metadata Technology Co., Ltd, Wuhan, Hubei, China). We developed a logistic regression model to assess the association between the rates of GI dysfunction after heatstroke and several high-risk indicators, including age, initial temperature, initial symptoms, and comorbidities using Graphpad Prism 9 XML project (Graphpad Software Inc., San Diego, CA, United States).

RESULTS

Study population

Between June 1, 2022 and October 31, 2022, a total of 873 patients admitted from 83 ICUs across 16 cities due to heatstroke were collected. Of these patients, 160 were excluded as follows: 11 patients were excluded as they were under 18 of age; 2 for heatstroke caused by burn; 16 for mortality within 24 h after ICU admission; 11 for palliative care after ICU admission; and 120 for incomplete data (Figure 1). A total of 713 patients were enrolled in the final analysis. The number of patients enrolled each day during the trial period and daily change in average and maximum temperature in the Sichuan Province are displayed in Supplementary Figure 1. The number of centres from different cities participating in the trial and corresponding total number of patients enrolled are shown in Supplementary Figure 2.

Of the 713 analysed patients, 46.6% were female, and the median age was 72 years [interquartile range (IQR): 64–80; Table 1]. The median body temperature of patients at hospital admission was 40.7 (IQR: 40.0 to 41.3). Around 50% of patients (343/713, 48.10%) were admitted with altered mental states or behaviours. Part of the cohort had at least one underlying illness, such as hypertension (187/713, 26.20%) or diabetes (87/713, 12.20%). Upon admission, the median level of C-reactive protein was elevated (5.0 mg/L, IQR: 1.0–11.8). The same was true for the median levels of procalcitonin (2.7 mg/mL, IQR: 0.5–13.1), and median D-dimer (4.6 mg/L, IQR: 1.8–12.9). A total of 439 patients (61.7%) underwent endotracheal intubation upon ICU admission. At day 15, 349 patients (48.9%) were discharged from the hospital, while 144 (20.2%) died, 187 (26.2%) were still hospitalized, and 33 (4.6%) transferred to another hospital. During

Table 1 Clinical characteristics, laboratory findings at admission, gastrointestinal symptoms findings, complications, treatments, and clinical outcomes of the study patients, according to developed gastrointestinal symptoms or not[1]

	All Patients, (*n* = 713)	GI Symptoms whether[2]		*P* value
		Yes (*n* = 132)	No (*n* = 581)	
Characteristic				
Age, median (IQR), yr	72.0 (64.0-80.0)	70.0 (59.0-76.0)	73.0 (64.0-81.0)	0.076
Distribution, *n* (%)				
0-39 yr	13 (1.8)	1 (0.01)	12 (2.1)	–
40-59 yr	132 (18.5)	32 (24.2)	100 (17.2)	–
60-79 yr	371 (52.0)	73 (55.3)	298 (51.2)	–
≥ 80 yr	197 (27.6)	26 (19.6)	171 (29.4)	–
Female sex	332 (46.6)	60 (45.4)	272 (46.8)	0.561
BMI, median (IQR), kg/m^2	22.1 (20.3-24.2)	22.5 (20.0-24.6)	22.0 (20.3-24.1)	0.875
GCS score at ICU admission, median (IQR)	6.0 (4.0-9.0)	5.0 (3.0-7.0)	6.0 (4.0-9.0)	0.018
NRS-2002 score at ICU admission, median (IQR)	4.0 (3.0-5.0)	3.0 (3.0-5.0)	4.0 (3.0-5.0)	0.014
Body temperature on admission				
Patients, *n* (%)	710 (99.1)	132 (100.0)	578 (98.8)	0.374
Temperature, median (IQR), °C	40.7 (40.0-41.3)	41.0 (40.1-42.0)	40.5 (40.0-41.2)	< 0.001
Heat exposure duration, median (IQR), h	4.0 (2.0-6.0)	4.0 (2.0-6.0)	4.0 (2.0-6.3)	0.206
Distribution of body temperature on admission, *n* (%)				
< 37.3 °C	6 (1.0)	0 (0.0)	6 (0.1)	–
37.3–38.0 °C	13 (2.1)	1 (0.8)	12 (2.3)	–
38.1–39.0 °C	59 (9.3)	8 (6.7)	51 (9.9)	–
39.1–40.0 °C	175 (27.7)	33 (27.7)	142 (27.7)	–
> 40.0 °C	379 (60.0)	77 (64.7)	302 (58.9)	–
Number of complaints and symptoms on admission, *n* (%)				
< 2	169/672 (25.1)	27/126 (21.4)	142/546 (26.3)	0.053
2-3	348/672 (51.8)	47/126 (37.3)	301/546 (55.1)	0.094
> 3	155/672 (23.1)	52/126 (41.3)	103/546 (18.9)	< 0.001
Complaints and symptoms on admission, *n* (%)				
Fever	476 (66.8)	93 (70.5)	383 (65.9	0.272
Altered mental state or behavior	343 (48.1)	55 (41.7)	288 (49.6	0.177
Dry skin or excessive sweating	65 (9.1)	20 (15.1)	45 (7.7)	< 0.001
Rubefaction	32 (4.5)	11 (8.3)	21 (3.6)	0.035
Fast pulse	142 (19.9)	40 (30.3)	102 (17.5	< 0.001
Polypnea	175 (24.5)	38 (38.7)	137 (23.6)	0.019
Headache	15 (2.1)	3 (2.3)	12 (2.1)	0.438
Syncope	309 (43.3)	85 (64.4)	224 (38.6)	< 0.001
Other	102 (14.3)	27 (20.5)	75 (12.9)	0.013
Coexisting disorder, *n* (%)				
Diabetes	87 (12.2)	10 (7.6)	77 (13.3)	0.225
Hypertension	187 (26.2)	36 (27.3)	151 (26.0)	0.985

Chronic obstructive pulmonary disease	124 (17.4)	21 (15.9)	103 (17.7)	0.697
Chronic cardiac insufficiency	79 (11.1)	16 (12.1)	63 (10.8)	0.541
Hepatitis B infection	14 (2.0)	1 (0.8)	13 (2.2)	0.488
Cancer[3]	5 (0.7)	3 (2.3)	2 (0.3)	0.033
Chronic renal disease	17 (2.4)	2 (1.5)	15 (2.6)	0.149
Immunodeficiency	9 (1.3)	3 (2.3)	6 (1.0)	0.965
Laboratory findings, median (IQR)				
PaO_2/FiO_2 ratio	239.0 (174.0-323.0)	238.0 (185.5-300.5)	248.0 (190.0-336.0)	0.064
White-cell count, 10^9/L	11.7 (8.2-15.5	10.0 (6.6-14.4),	11.7 (8.4-15.5)	0.032
Lymphocyte count, 10^9/L	1.3 (0.7-2.4)	0.9 (0.5-2.3)	1.0 (0.6-2.1)	0.746
Platelet count, 10^9/L	108.0 (73.0-162.0)	84.0 (45.0-115.0)	110.0 (75.0-165.5)	0.147
Hemoglobin, g/L	123 (109-138)	115 (102-127)	124 (109-138)	0.014
Albumin, g/L	37.0 (33.2-40.2)	33.4 (29.1-43.8)	37.0 (33.3-40.3)	0.014
Other findings, median (IQR)				
C-reactive protein, mg/L	5.0 (1.0-11.8)	11.9 (5.1-32.1)	5.0 (1.0-12.0)	0.005
Procalcitonin, ng/mL	2.7 (0.5-13.1)	3.2 (0.4-8.9)	2.8 (0.5-12.6)	0.593
Lactate dehydrogenase, U/L	367.9 (284.8-547.5)	327.0 (273.0-507.4)	362.5 (281.8-524.0)	0.667
Aspartate aminotransferase, U/L	79.0 (40.9-191.0)	115.9 (51.3-269.8)	74.0 (39.3-168.8)	0.128
Alanine aminotransferase, U/L	38.0 (21.0-85.0)	48.0 (28.1-104.1)	36.0 (20.0-77.3)	0.479
Total bilirubin, μmol/L	17.9 (12.5-25.7)	18.2 (11.8-258.9),	17.9 (12.5-25.9)	0.186
CK-Mb, U/L	10.0 (2.8-32.0)	13.6 (4.2-74.6)	9.9 (2.7-31.7)	0.539
Creatinine, μmol/L	125.0 (89.8-169.2)	122.0 (84.0-162.	123.0 (88.4-169.2)	0.944
D-dimer, mg/L	4.6 (1.8-12.9)	4.1 (2.1-8.6)	4.7 (1.7-12.8)	0.561
Minerals, median (IQR), mmol/L				
Sodium	133.3 (129.0-139.0)	136.0 (132.0-140.0)	133.6 (129.0-139.0)	0.158
Potassium	3.2 (2.9-3.8)	3.6 (3.0-3.9)	3.2 (2.9-3.8)	0.043
Lactate	3.5 (2.1-5.1)	3.1 (1.6-4.1)	3.4 (2.0-5.1)	0.036
GI symptoms findings, *n* (%)				
Duration of GI symptoms, median (IQR), d	–	4.0 (2.0-7.0)	–	–
Diarrhea	–	99 (75.0)	–	–
Flatulence	–	36 (27.3)	–	–
Nausea/vomiting	–	21 (15.9)	–	–
Bloody stools	–	8 (6.1)	–	–
Complications, *n* (%)				
Number of complications				
< 2	263 (36.9)	28 (21.1)	235 (38.8)	0.002
2-3	133 (18.7)	12 (9.2)	121 (19.8)	0.025
> 3	317 (44.5)	92 (69.7)	225 (41.4)	< 0.001
Disturbance of water and electrolyte	412 (57.8)	95 (72.0)	317 (54.6)	0.013
Rhabdomyolysis	102 (14.3)	34 (25.8)	68 (11.7)	0.004
Myocardial damage	281 (39.4)	70 (53.0)	211 (36.3)	< 0.001
Disseminated intravascular coagulation	221 (31.0)	62 (46.9)	159 (27.4)	0.006
Acute respiratory distress syndrome	256 (35.9)	66 (50.0)	190 (32.7)	0.001

Acute kidney injury	299 (41.9)	83 (62.9)	216 (37.2)	0.003
Acute liver function impairment	305 (42.8)	81 (61.4)	224 (38.6)	< 0.001
Central nervous system damage	256 (35.9)	74 (56.1)	182 (31.9)	0.003
Treatments, *n* (%)				
Mechanical ventilation				
Invasive	439 (61.7)	108 (82.6)	331 (57.1)	< 0.001
Noninvasive	10 (1.4)	0 (0.0)	10 (1.6)	0.271
Use of continuous renal-replacement therapy	24 (3.4)	7 (9.2)	17 (2.7)	0.003
Length of ICU stay, median (IQR), d	2.0 (1.0-4.0)	4.0 (2.0-7.0)	2.0 (1.0-3.0)	0.001
Clinical outcomes at data cutoff, *n* (%)				
Hospital discharge	349 (48.9)	64 (48.5)	285 (49.1)	0.906
Death	144 (20.2)	26 (19.7)	118 (20.3)	0.874
Still hospitalization	187 (26.2)	33 (25.0)	154 (26.5)	0.723
Transferred to another hospital	33 (4.6)	9 (6.8)	24 (4.1)	< 0.001

[1]The denominators of patients who were included in the analysis are provided if they differed from the overall numbers in the group. Percentages may not total 100 because of rounding.
[2]Nausea/vomiting, diarrhea, flatulence, or bloody stools are defined as gastrointestinal symptoms.
[3]Included in this category is any type of cancer.
IQR: Interquartile range; GCS: Glasgow coma scale; NRS: Nutrition risk screening; GI: Gastrointestinal; BMI: Body mass index; ICU: Intensive care unit; CK-Mb: Creatine kinase.

hospitalization, acute liver dysfunction was observed in 42.8% (305/713) patients, 41.9% (299/713) experienced acute kidney injury, 39.4% (281/713) experienced myocardial damage, and 35.9% (256/713) experienced central nervous system damage.

Patient characteristics and outcomes according to whether gastrointestinal symptoms are present

Our study results showed that 18.5% (132/713) of heatstroke patients experienced at least one episode of GI symptoms during ICU stay. Of these patients, 8 (6.1%) experienced bloody stools, 21 (15.9%) experienced nausea/vomiting, 36 (27.3%) experienced flatulence, and 99 (75.0%) experienced diarrhoea (Table 1 and Figure 2). Patients with heatstroke were subsequently categorized into two groups: Those who experienced GI symptoms (n = 132) and those who did not (n = 581) during their ICU stay. There was no difference in the median age of patients between both groups (Table 1). Patients with GI symptoms had significantly lower GCS scores (5.0 *vs* 6.0, ^{a}P = 0.018) and lower NRS-2002 scores (3.0 *vs* 4.0, ^{b}P = 0.014) on admission. There was also no significant difference in the presence of comorbidities upon admission between the groups during the study period, except for a prior history of cancer (2.5% *vs* 0.5%, ^{c}P = 0.033; Table 1). Laboratory results on admission revealed that patients with GI symptoms had significantly lower levels of albumin (33.4 *vs* 37.0, ^{d}P = 0.014) and hemoglobin (115.0 *vs* 124.0, ^{e}P = 0.014) and a higher level of blood lactate (3.1 *vs* 3.4, ^{e}P = 0.036) and C-reactive protein (11.9 *vs* 5.0, ^{f}P = 0.043). It was observed that patients presenting with GI symptoms had an increased likelihood of developing multiple complications, including acute kidney injury (62.9%, ^{g}P = 0.003), acute liver function impairment (61.4%, ^{h}P < 0.001), and central nervous system damage (56.1%, ^{i}P = 0.003). However, the presence of GI symptoms did not have a significant impact on patient mortality. Multivariate logistic regression showed that heatstroke patients who were older than the average year of the cohort were more likely to develop GI symptoms (^{j}P = 0.001; Figure 3A). Moreover, patients with a lower GCS score were prone to have GI symptoms (^{k}P = 0.006; Figure 3A). This positive correlation of GCS score with GI symptoms persisted when we adjusted for complications (Figure 3B) and laboratory results (Figure 3C).

Relationship between GI symptoms and enteral nutrition therapy

Considering that the predominant GI symptom is diarrhoea, a total of 439 heatstroke patients with endotracheal intubation shortly after ICU admission were analysed to explore the relationship between GI symptoms and EN therapy. We found that the presence of GI symptoms was not associated with EN therapy (Table 2). There was no statistical difference in the proportion of EN support, amount of calories and proteins, and total volume received on admission between the patients who underwent EN therapy. Of note, EN therapy was initiated in only a small proportion (139/439, 31.7%) of intubated patients within 48 h after ICU admission, as shown in Table 3. Patients who did not start EN within 48 h of ICU admission had a significantly lower GCS score (5.0 *vs* 4.0, ^{l}P = 0.002), experienced more GI symptoms after ICU admission (22.3% *vs* 12.9%, ^{m}P = 0.021), and had a longer ICU stay (3.0 *vs* 2.0, ^{n}P < 0.001). Logistic regression analysis showed that GI symptoms were an independent risk factor for not initiating early EN (^{o}P = 0.037; Supplementary Figure 3). During the observational period, 266 (60.6%) patients with endotracheal intubation at admission failed

Table 2 Clinical characteristics of the heatstroke patients with endotracheal intubation, according to developed gastrointestinal symptoms or not[1]

	All intubated patients (*n* = 439)	GI symptoms whether[2]		*P* value
		Yes (*n* = 108)	No (*n* = 331)	
Characteristic				
Age, median (IQR), yr	71.0 (63.0-80.0)	72.0 (64.0-80.0)	69.5 (59.8-78.0)	0.202
Female sex, *n* (%)	197 (44.9)	49 (45.4)	148 (44.7)	0.905
GCS score at ICU admission, median (IQR)	4.0 (3.0-5.0)	4.0 (3.0-5.0)	4.0 (4.0-5.0)	0.204
NRS score at ICU admission, median (IQR)	4.0 (3.0-5.0)	3.0 (3.0-5.0)	4.0 (3.0-5.0)	0.057
Body temperature on admission				
Patients, *n* (%)	439 (100.0)	108 (100.0)	331 (100.0)	0.348
Temperature, median (IQR), °C	41.0 (40.0-41.8)	41.0 (40.0-42.0)	41.0 (40.0-41.6)	0.497
Complaints and symptoms on admission, *n* (%)				
Fever	296 (67.4)	76 (70.4)	220 (66.5)	0.452
Altered mental state or behavior	205 (46.7)	41 (38.0)	164 (49.5)	0.036
Dry skin or excessive sweating	45 (10.3	20 (18.5)	25 (7.6)	0.001
Rubefaction	17 (3.9)	9 (8.3)	8 (2.4)	0.006
Fast pulse	99 (22.6)	34 (31.5)	65 (19.6)	0.105
Polypnea	122 (27.8)	31 (28.7)	91 (27.5)	0.807
Headache	7 (1.6)	2 (18.5)	5 (1.5)	0.805
Syncope	207 (47.2)	70 (64.8)	137 (41.4)	< 0.001
Other	61 (13.9)	71 (65.7)	40 (12.1)	< 0.001
Laboratory findings, median (IQR)				
PaO_2/FiO_2 ratio	225.0 (135.5-306.5)	221.0 (148.7-308.0)	226.0 (155.0-305.5)	0.999
White-cell count, 10^9/L	11.7 (8.1-15.6)	11.8 (8.0-15.8)	11.7 (8.1-15.6)	0.405
Lymphocyte count, 10^9/L	1.7 (0.8-2.8)	1.6 (0.8-2.8)	1.8 (0.8-28)	0.279
Platelet count, 10^9/L	92.0 (56.0-138.0)	83.5 (55.5-114.5)	97.0 (59.0-141.0)	0.143
Hemoglobin, g/L	124.0 (109.0-139.0)	121.0 (108.3-135.8)	125.0 (110.0-139.0)	0.053
Albumin, g/L	35.3 (32.5-38.9)	34.5 (31.8-38.0)	35.3 (32.5-38.9)	0.028
EN support				
Early (< 48 h) EN, *n* (%)	68 (15.5)	13 (12.0)	55 (16.6)	0.253
Average EN calorie, median (IQR), kcal/d	1000.0 (750.0-1500.0)	1000.0 (750.0-1500.0)	1000.0 (750.0-1500.0)	0.559
Average EN protein, median (IQR), g/d	28.0 (17.0-56.0)	30.0 (17.0-56.0)	28.0 (20.0-56.0)	0.867
Average EN volume, median (IQR), mL/d	600.0 (150.0-1150.0)	625.0 (142.5-1200.0)	600.0 (150.0-1082.5)	0.31
Complications, *n* (%)				
Disturbance of water and electrolyte	271 (61.7)	89 (82.4)	187 (56.5)	< 0.001
Rhabdomyolysis	81 (18.5)	31 (28.7)	50 (15.1)	0.002
Myocardial damage	216 (49.2)	63 (58.0)	153 (46.2)	0.029
Disseminated intravascular coagulation	172 (39.2)	54 (50.0)	118 (35.6)	0.001
Acute respiratory distress syndrome	226 (51.5)	62 (57.4)	164 (49.5)	0.156
Acute kidney injury	233 (53.1)	77 (71.3)	156 (47.1)	< 0.001
Acute liver function impairment	332 (75.6)	73 (65.6)	159 (48.0)	< 0.001
Central nervous system damage	206 (46.9)	65 (60.2)	141 (42.6)	0.001

Clinical outcomes at data cutoff, *n* (%)				
Hospital discharge	210 (47.8)	51 (47.2)	159 (48.0)	0.234
Death	123 (28.0)	24 (22.2)	99 (29.9)	0.122
Still hospitalization	78 (17.8)	24 (22.2)	54 (16.3)	0.163
Transferred to another hospital	28 (6.4)	9 (8.3)	19 (5.7)	0.338

[1]The denominators of patients who were included in the analysis are provided if they differed from the overall numbers in the group. Percentages may not total 100 because of rounding.
[2]Nausea/vomiting, diarrhea, flatulence, or bloody stools are defined as gastrointestinal symptoms.
IQR: Interquartile range; GCS: Glasgow coma scale; NRS: Nutrition risk screening; GI: Gastrointestinal; EN: Enteral nutrition; ICU: Intensive care unit.

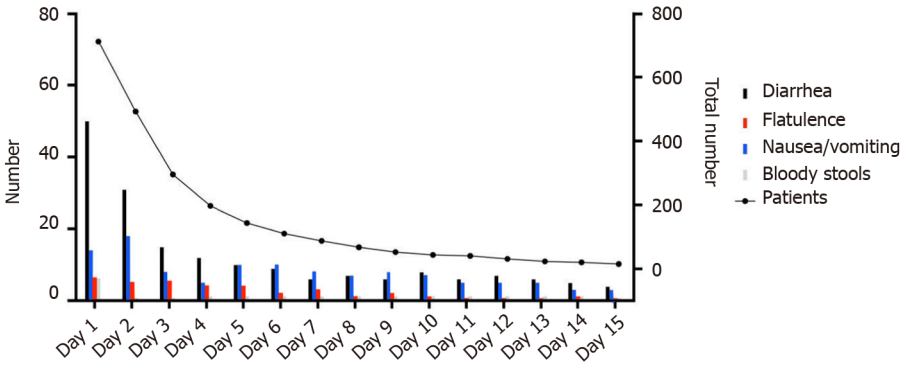

DOI: 10.3748/wjg.v30.i4.346

Figure 2 Number of patients with gastrointestinal symptoms and total number of heatstroke patients still in the intensive care unit per day.

to establish full EN (Table 4). Patients who do not receive full EN experienced more GI symptoms (22.6% *vs* 14.5%, [p]*P* = 0.036). Moreover, the mortality of patients who did not receive full EN was significantly higher than those who did (35.3% *vs* 16.8%, [q]*P* < 0.001). Moreover, rhabdomyolysis (20.7% *vs* 11.6%, [r]*P* = 0.013) and acute kidney injury (57.9% *vs* 45.7%, [s]*P* = 0.012) were more common, and ICU stay was longer in the former population (3.0 *vs* 2.0, [t]*P* < 0.001).

Subgroup analysis

Since the definition of GI manifestations was composite, we subsequently explore whether there was difference in the characteristics of patients with different symptoms. We selected patients with a single symptom and divided them into 3 groups according to different GI manifestations (Table 5). There was a statistically significant difference in temperature on admission between patients with diarrhoea, flatulence, and nausea/vomiting ([u]*P* = 0.003). Notably, there were significant differences in complications between the three subgroups, except for complications of disturbance of water and electrolyte. Although mortality was not different between subgroups, the difference in the number of patients who were still hospitalized was statistically significant ([v]*P* = 0.025).

As we observed that the onset of GI symptoms was significantly different between patients, we further divided patients with GI symptoms into two categories: Those with GI symptoms on ICU admission and those with GI symptoms developed during ICU stay. The patient characteristics of both groups are shown in Table 6. The patients who had GI symptoms on admission were younger ([v]*P* = 0.050), had a higher BMI (22.7 *vs* 21.1, [w]*P* = 0.050), and had a lower nutrition risk screening (NRS-2002) score on admission (3.0 *vs* 4.0, [x]*P* = 0.009) than had those who developed symptoms later on. Patients who had less GI symptoms on admission had a lower number of comorbidities, including diabetes (1/68, 1.5% *vs* 9/64, 14.1%, [y]*P* = 0.009), but more complications, including haemorrhage of the digestive tract (23/68, 33.8% *vs* 12/64, 18.8%) and disseminated intravascular coagulation (38/68, 55.9% *vs* 24/64, 37.5%). Nevertheless, there is no difference in mortality and ICU length of stay.

We divided patients who developed GI symptoms during their ICU stay into the early-onset (< 3 d of ICU stay) and late-onset groups (≥ 3 d of ICU stay) groups. As shown in Table 7, there was a significant statistical difference in EN support between the two groups. Fewer patients received EN support in the early-onset than in the late-onset group (29/41, 70.7 *vs* 22/23, 95.7%, [z]*P* < 0.001). The early-onset group received less EN calorie [752.0 kcal/d (IQR: 500.0–1007.5) *vs* 1292.0 kcal/d (IQR: 750.0-1560.0)], protein [20.0 g/d (IQR: 17.6–32.5) *vs* 28.0 g/d (IQR: 15.0–57.0)], and EN volume [600.0 mL/d (IQR: 147.5–1000.0) *vs* 900.0 mL/d (IQR: 461.2–1500.0)]. Moreover, patients in the early-onset group received EN support for a shorter time than did those in the late-onset group [3.0 d (IQR: 1.8–5.0) *vs* 7.0 d (IQR: 4.0–11.0)].

To further explore the relationship between the duration of GI symptoms and prognosis of heatstroke patients, we stratified patients into those who had GI symptoms for more than 4 d and those who did for had GI symptoms for less than 4 d, as shown in Table 8. Patients with GI symptoms for at least 4 d had lower albumin levels (37.0 g/L *vs* 34.4 g/L,

Table 3 Characteristics of the heatstroke patients with endotracheal intubation, according to received enteral nutrition within 48 h after intensive care unit admission or not[1]

	All intubated patients (*n* = 439)	EN therapy whether ≤ 48 h		*P* value
		Yes (*n* = 139)	No (*n* = 300)	
Characteristic				
Age, median (IQR), yr	71.0 (63.0-80.0)	72.0 (63.0-80.0)	71.0 (63.0-79.0)	0.801
Female sex, *n* (%)	197 (44.9)	62 (46.8)	135 (43.6)	0.938
GCS score at ICU admission, median (IQR)	4.0 (3.0-5.0)	5.0 (3.0-7.0)	4.0 (3.0-5 .0)	0.002
NRS score at ICU admission, median (IQR)	4.0 (3.0-5.0)	5.0 (4.0-6.0)	4.0 (3.0-5.0)	0.017
Body temperature on admission				
Patients, *n* (%)	439 (100.0)	139 (100.0)	300 (100.0)	–
Temperature, median (IQR), °C	41.0 (40.0-41.8)	41.0 (40.0-41.5)	41.0 (40.0-42.0)	0.154
Laboratory findings, median (IQR)				
PaO_2/FiO_2 ratio	225.0 (135.5-306.5)	226.0 (164.0-287.0)	223.0 (128.0-316.0)	0.825
White-cell count, 10^9/L	11.7 (8.1-15.6)	12.4 (8.6-16.8)	11.3 (8.0-15.0)	0.290
Lymphocyte count, 10^9/L	1.7 (0.8-2.8)	1.5 (0.7-2.3)	1.9 (0.9-3.0)	0.105
Platelet count, 10^9/L	92.0 (56.0-138.0)	101.0 (66.8-147.3)	88.0 (54.0-130.0)	0.039
Hemoglobin, g/L	124.0 (109.0-139.0)	122.0 (109.0-136.0)	124.5 (109.0-140.0)	0.311
Albumin, g/L	35.3 (32.5-38.9)	35.1 (32.0-38.5)	35.4 (32.5-39.0)	0.544
GI symptoms[2], *n* (%)				
Total patients	85 (19.4)	18 (12.9)	67 (22.3)	0.021
Diarrhea	60 (13.7)	13 (9.4)	47 (15.7)	0.073
Flatulence	25 (5.7)	7 (5.0)	18 (6.0)	0.685
Nausea/vomiting	14 (3.2)	7 (5.0)	7 (2.3)	0.134
Bloody stools	8 (1.8)	0 (0.0)	8 (2.6)	0.052
Complications, *n* (%)				
Disturbance of water and electrolyte	271 (61.7)	79 (56.8)	192 (64.0)	0.151
Rhabdomyolysis	81 (18.5)	20 (11.6)	61 (20.3)	0.135
Myocardial damage	216 (49.2)	65 (46.8)	151 (50.3)	0.486
Disseminated intravascular coagulation	172 (39.2)	50 (36.0)	122 (40.7)	0.349
Acute respiratory distress syndrome	226 (51.5)	74 (53.2)	152 (50.7)	0.616
Acute kidney injury	233 (53.1)	66 (47.5)	167 (55.7)	0.110
Acute liver function impairment	332 (75.6)	74 (53.2)	258 (86.0)	< 0.001
Central nervous system damage	206 (46.9)	62 (44.6)	144 (48.0)	0.507
Treatments				
Use of continuous renal-replacement therapy, *n* (%)	34 (7.7)	10 (8.1)	20 (7.5)	0.826
Length of ICU stay, median (IQR), d	2.0 (1.0-3.0)	2.0 (1.0-3.0)	3.0 (2.0-5.0)	< 0.001
Clinical outcomes at data cutoff, *n* (%)				
Hospital discharge	210 (47.8)	68 (48.9)	142 (47.3)	0.757
Death	123 (28.0)	24 (17.3)	99 (33.3)	< 0.001
Still hospitalization	78 (17.8)	36 (25.9)	42 (14.0)	0.002
Transferred to another hospital	28 (6.4)	11 (7.9)	17 (5.7)	0.370

[1]The denominators of patients who were included in the analysis are provided if they differed from the overall numbers in the group. Percentages may not total 100 because of rounding.
[2]Nausea/vomiting, diarrhea, flatulence, or bloody stools are defined as gastrointestinal symptoms.
IQR: Interquartile range; GCS: Glasgow coma scale; NRS: Nutrition risk screening; GI: Gastrointestinal; ICU: Intensive care unit.

P = 0.310) and more complications, including disseminated intravascular coagulation (27.8% *vs* 54.2%, P = 0.007) and acute respiratory distress syndrome (12.0% *vs* 54.2%, P < 0.001). They also showed higher recovery rates than did those who had symptoms for more than 4 d (56.3% *vs* 27.8%, P = 0.004).

DISCUSSION

In this retrospective, multi-center study, we reported the incidence of GI manifestations among critically ill adult patients with heatstroke admitted to ICUs in the Sichuan Province, China. Our data demonstrated that patients with GI symptoms had a significantly longer ICU stay compared with those without. As a manifestation of systemic organ damage in heatstroke, the appearance of GI symptoms affect patients' EN therapy outcomes. Patients with older age and a lower GCS score on admission were more likely to experience GI symptoms. Our study provides valuable real-world evidence regarding the associations between heatstroke and GI symptoms with, to our knowledge, the highest number of patients from multiple centres to date.

Conventionally, critically ill patients with have GI dysfunction; however, there is little evidence supporting this phenomenon among heatstroke patients. Due to the lack of standardization of the diagnostic and therapeutic approaches, in this study, we evaluated the GI tract according to its symptoms and found that 18.5% of patients with heatstroke suffered from said symptoms during their stay. Compared with other non-heat stroke critically ill patients, the incidence of GI symptoms in our cohort is relatively low[9,10]. This is partly due to the fact that our study only used symptoms to evaluate GI function, though other high-incidence studies generally included physical examination, including that for bowel sounds, for comprehensive evaluation. When comparing the same symptoms, such as vomiting, between patients with heatstroke and those in the ICU, we observed that the incidence of GI symptoms in heatstroke patients is still lower than that of patients in the general ICU. One reason behind this is that heatstroke patients do not have GI structural damage from the perspective of pathogenesis, but patients in the general ICU comprise those who underwent abdominal surgery, that is, those who already have GI structural disorders. Another reason is that our study only assessed GI symptoms without other indicators such as physical examination, which may have led to the underestimation of the incidence of GI dysfunction. Nevertheless, our research suggests that GI injury is an important high-incidence manifestation of organ failure among heatstroke patients.

Our study found that heatstroke patients with older age and lower GCS score were more likely to experience GI symptoms. Multiple clinical studies had described risk factors for GI dysfunction in critically ill patients, including older age, larger BMI, lower Acute Physiology and Chronic Health Evaluation II and Sequential Organ Failure Assessment scores, surgical laparotomy, and use of mechanical ventilation, analgesic sedation, and vasopressors[9-11]. Similar to other studies, our study also observed that older patients were more likely to experience GI symptoms after heatstroke. Of note, our study found that the degree of nervous system damage, as quantified by the GCS score, is also related to the occurrence of GI dysfunction. This may be because heat damages the enteric nervous system, as well as the central nervous system. Moreover, patients with lower GCS scores were more likely to receive mechanical ventilation and vasopressors, posing an impact on the intestinal blood supply and, consequently, possibly leading to GI failure. The causes of GI dysfunction caused by heatstroke warrant further research.

We also observed that the presence of GI symptoms may affect EN support therapy. In our study, we found heatstroke patients who did not receive EN therapy within 48 h after ICU admission experienced more GI symptoms with more complications, longer ICU stay, and higher ICU mortality. The emergence of GI symptoms is the reason why EN cannot be started. Simultaneously, the failure to start EN support is also a reason for the deterioration of GI function. We also observed that a considerable proportion of patients with heat stroke still cannot implement total EN within 2 wk, suggesting that, for patients with heatstroke, further research to develop individualized nutrition support strategies is warranted.

We also performed various subgroup analyses to discuss different GI symptoms and whether their timing and duration had an impact on patient prognosis. First, we found that patients with different GI symptoms have different clinical features. Different symptoms may indicate that the severity of heatstroke in these patients varies, and whether this reflects their prognosis to some extent requires further study. The onset of GI symptoms in patients also differed. Overall, the earlier the GI symptoms appeared, the severer the patient's condition was. At the same time, due to GI symptoms, such patients could not tolerate EN or could not meet EN standards, further impairing their GI function and forming a vicious circle. Better approaches for EN support in these patients are warranted. Finally, we discussed the duration of the patient's GI symptoms. This was the same as we previously realized: The longer the duration of GI symptoms, the worse their prognosis. These patients were unable to start EN therapy early on. In contrast, they were more likely to have GI microcirculation disorders and damage to the intestinal barrier.

Currently, the cause of GI dysfunction caused by heatstroke is not particularly clear. Several reports have documented increased intestinal permeability during exercise with and without heat stress[4,12,13]. A murine model of classic heatstroke that induced a body core temperature as high as 42.7 °C showed considerable gut histological injury[14,15].

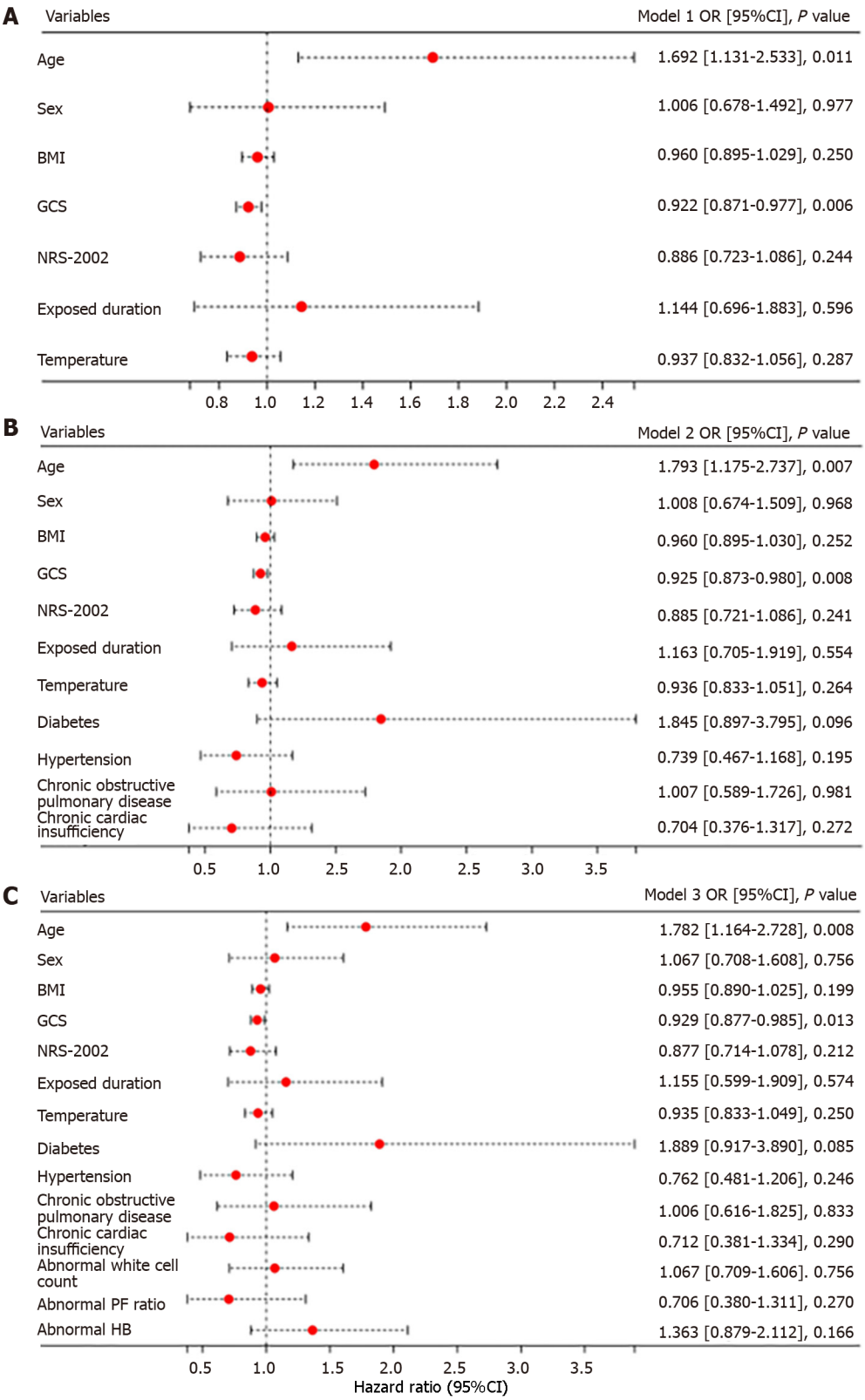

DOI: 10.3748/wjg.v30.i4.346 **Copyright** ©The Author(s) 2024.

Figure 3 Multivariable-adjusted logistic regression of risk factors with gastrointestinal symptoms. A: It showed multivariable logistic regression between heatstroke patients' gastrointestinal (GI) symptoms with age, sex, body mass index (BMI) Glasgow coma scale (GCS) score, nutrition risk screening 2002 (NRS-2002) score, high temperature exposed duration and patients' temperature; B: It is adjusted for coexisting disorder and index in Figure 3A; C: It is adjusted for laboratory results at intensive care unit admission and index in Figure 3A. Age is a categorical variable bounded by the median age of the patient, with less than the median age being compared. Sex is the categorical variable, with women being compared. BMI, GCS score, NRS-2002, exposed duration and temperature are continuous variables. Diabetes, hypertension, chronic obstructive disease, chronic cardiac insufficiency, abnormal white cell count, PaO_2/FiO_2 ratio and hemoglobin are categorical variable. BMI: Body mass index; GCS score: Glasgow coma scale score; NRS-2002 score: Nutrition risk screening-2002 score; OR: Odds ratio; PF ratio: PaO_2/FiO_2 ratio; HB: Hemoglobin.

Studies have shown that one of the important mechanisms of heatstroke is the excessive opening of intestinal tight junctions, destruction of intestinal cell structure and function, increase in intestinal mucosal permeability, and introduction of endotoxin into the blood[16,17]. One of the most frequently mentioned mechanisms of how heatstroke causes GI symptoms is the leaky gut hypothesis. Our results also suggest that while heat can cause changes in the state of consciousness caused by central nervous system damage, it may also cause damage to the enteric nervous system, thereby causing GI dysfunction. Such inferences need further research to confirm in the future.

The retrospective design of this study offers several benefits, including a high quality of data and a large number of patients. Our study provides a real-world representation of the current clinical practices for heatstroke in a mixed population of critically ill adult patients treated in ICUs in Sichuan Province, China. The patient sample size provides a robust representation of the target population, increasing the generalizability of our findings. Overall, our study provides important insights into the prevalence of GI symptoms among critically ill heatstroke patients and its relationship with risk factors and clinical outcomes. The findings of this study have important implications for the management and care of critically ill patients with heatstroke. Previous literature has demonstrated the vulnerability of the digestive tract to abnormal conditions, including hypoxia and elevated temperatures[4,12,13,18,19]. Studies have also indicated that most patients experience some form of GI symptoms during intense physical activity and elevated body temperature[20]. Our study on GI symptoms following heatstroke incorporates risk factors and provides a comprehensive understanding of the subject, thereby supplementing previous research.

Nevertheless, this study had some limitations. First, the use of GI symptoms to respond to GI dysfunction is one-sided. Another limitation is the exclusion of the most critically ill patients who had already passed away and those admitted to general wards. While this selection criterion was a necessary aspect of the research program, it is possible that the inclusion of these patients would not have greatly impacted the overall prognosis, as previously discussed. Our study was an observation of symptoms and did not address possible effects of treatment on GI function. Additionally, there is a high rate of missed diagnoses due to a lack of awareness of heatstroke in remote mountainous areas and the inadequate identification of heatstroke in a timely manner.

CONCLUSION

The incidence of GI symptoms among heatstroke patients admitted to the ICU was reportedly 18.5% in our study. Patients who are older and with a lower GCS score on admission have an increased likelihood of developing GI symptoms. Heatstroke patients with GI symptoms found it more difficult to tolerate EN therapy than did those without. Patients with GI symptoms were found to have a higher incidence of complications. The earlier the GI symptoms appeared and the longer the duration of GI symptoms, the more difficult it was for patients to tolerate EN, and the worse the predicted prognosis.

Table 4 Characteristics of the heatstroke patients with endotracheal intubation, according to received full enteral nutrition after intensive care unit admission or not[1]

	All intubated patients (*n* = 439)	Full EN whether		*P* value
		Yes (*n* = 173)	No (*n* = 266)	
Characteristic				
Age, median (IQR), yr	71.0 (63.0-80.0)	72.0 (63.0-80.0)	71.0 (63.0-79.0)	0.801
Female sex, *n* (%)	197 (44.9)	81 (46.8)	116 (43.6)	0.509
GCS score at ICU admission, median (IQR)	4.0 (3.0-5.0)	6.0 (4.0-8.0)	5.0 (3.0-7.0)	0.002
NRS score at ICU admission, median (IQR)	4.0 (3.0-5.0)	4.5 (4.0-5.0)	4.0 (3.0-5.0)	0.193
Body temperature on admission				
Patients, *n* (%)	439 (100.0)	173 (100.0)	266 (100.0)	–
Temperature, median (IQR), °C	41.0 (40.0-41.8)	41.0 (40.0-41.4)	41.0 (40.0-42.0)	0.128
Laboratory findings, median (IQR)				
PaO_2/FiO_2 ratio	225.0 (135.5-306.5)	246.0 (191.0-334.0)	222.0 (134.0-315.0)	0.226
White-cell count, 10^9/L	11.7 (8.1-15.6)	12.6 (9.4-16.7)	11.4 (8.0-15.3)	0.287
Lymphocyte count, 10^9/L	1.7 (0.8-2.8)	0.8 (0.5-1.6)	2.0 (0.9-3.0)	0.084
Platelet count, 10^9/L	92.0 (56.0-138.0)	71.5 (37.0-113.8)	89.0 (54.0-132.5)	0.011
Hemoglobin, g/L	124.0 (109.0-139.0)	119.0 (107.5-129.0)	125.0 (110.0-140.0)	0.002

Albumin, g/L	35.3 (32.5-38.9)	32.0 (29.0-35.2)	35.5 (32.5-39.2)	< 0.001
GI symptoms[2], *n* (%)				
Total patients	85 (19.4)	25 (14.5)	60 (22.6)	0.036
Diarrhea	60 (13.7)	17 (9.8)	43 (16.2)	0.059
Flatulence	25 (5.7)	8 (4.6)	17 (6.4)	0.435
Nausea/vomiting	14 (3.2)	7 (4.0)	7 (2.6)	0.409
Bloody stools	8 (1.8)	0 (0.0)	8 (3.1)	0.021
Complications, *n* (%)				
Disturbance of water and electrolyte	271 (61.7)	105 (60.7)	166 (62.4)	0.718
Rhabdomyolysis	81 (18.5)	20 (11.6)	55 (20.7)	0.013
Myocardial damage	216 (49.2)	83 (48.0)	133 (50.0)	0.678
Disseminated intravascular coagulation	172 (39.2)	60 (34.7)	112 (42.1)	0.119
Acute respiratory distress syndrome	226 (51.5)	92 (53.2)	134 (50.4)	0.566
Acute kidney injury	233 (53.1)	79 (45.7)	154 (57.9)	0.012
Acute liver function impairment	332 (75.6)	94 (54.3)	138 (51.9)	0.615
Central nervous system damage	206 (46.9)	80 (46.2)	126 (47.4)	0.817
Treatments				
Use of continuous renal-replacement therapy, *n* (%)	34 (7.7)	14 (8.1)	20 (7.5)	0.826
Length of ICU stay, median (IQR), d	2.0 (1.0-3.0)	2.0 (1.0-2.0)	3.0 (1.0-4.0)	< 0.001
Clinical outcomes at data cutoff, *n* (%)				
Hospital discharge	210 (47.8)	83 (48.0)	127 (47.7)	0.962
Death	123 (28.0)	29 (16.8)	94 (35.3)	< 0.001
Still hospitalization	78 (17.8)	46 (26.6)	82 (20.8)	0.339
Transferred to another hospital	28 (6.4)	15 (8.7)	13 (4.9)	0.113

[1]The denominators of patients who were included in the analysis are provided if they differed from the overall numbers in the group. Percentages may not total 100 because of rounding.
[2]Nausea/vomiting, diarrhea, flatulence, or bloody stools are defined as gastrointestinal symptoms.
IQR: Interquartile range; GCS: Glasgow coma scale; NRS: Nutrition risk screening; GI: Gastrointestinal; ICU: Intensive care unit.

Table 5 Clinical characteristics of the study patients, according to types of gastrointestinal symptoms[1]

	GI Symptoms[2]			*P* value
	Diarrhea (*n* = 88)	Flatulence (*n* = 27)	Nausea/vomiting (*n* = 15)	
Characteristic				
Age, median (IQR), yr	65.0 (56.0-76.0)	69.0 (56.0-79.0)	68.0 (57.5-78.0)	0.565
Female sex, *n* (%)	35.0 (39.8)	14.0 (51.8)	6 (40.0)	0.529
GCS score at ICU admission, median (IQR)	5.0 (3.0-7.0)	6.0 (3.0-9.5)	4.0 (3.0-6.0)	0.540
NRS score at ICU admission, median (IQR)	4.0 (3.0-5.0)	4.5 (4.0-5.0)	4.0 (3.0-5.0)	0.193
Body temperature admission				
Patients, *n* (%)	88.0 (100.0)	27.0 (100.0)	15.0 (100.0)	–
Temperature, median (IQR), °C	41.0 (40.0-42.0)	40.0 (39.8-41.0)	40.1 (39.8-41.0)	0.003
Complaints and symptoms, *n* (%)				
Fever	62.0 (70.5)	20.0 (74.0)	8.0 (53.3)	0.343

Altered mental state or behavior	35.0 (39.8)	13.0 (48.1)	4.0 (26.7)	0.395
Dry skin or excessive sweating	19.0 (21.6)	2.0 (7.4)	2.0 (13.3)	0.215
Rubefaction	7.0 (8.0)	2.0 (7.4)	1.0 (6.7)	0.983
Fast pulse	32.0 (36.4)	6.0 (22.2)	4.0 (26.7)	0.344
Polypnea	29.0 (33.0)	6.0 (22.2)	3.0 (20.0)	0.397
Headache	1.0 (1.1)	3.0 (11.1)	0.0 (0.0)	0.024
Syncope	63.0 (71.6)	13.0 (48.1)	8.0 (53.3)	0.052
Other	22.0 (25.0)	4.0 (14.8)	2.0 (13.3)	0.378
Laboratory findings, median (IQR)				
White-cell count, 10^9/L	13.0 (8.2-16.3)	13.0 (8.2-16.3)	13.0 (8.2-16.3)	0.210
Hemoglobin, g/L	122.0 (110.3-136.0)	125.0 (110.5-137.5)	120.0 (107.3-130.0)	0.589
Albumin, g/L	35.8 (32.9-38.8)	35.3 (32.0-39.5)	36.7 (29.3-39.5)	0.969
Complications, *n* (%)				
Disturbance of water and electrolyte	63 (71.6)	20 (74.0)	11 (73.3)	0.085
Rhabdomyolysis	24 (27.3)	6 (22.2)	4 (26.7)	0.003
Myocardial damage	49 (55.7)	11.0 (40.7)	9 (60.0)	0.008
Disseminated intravascular coagulation	40 (45.5)	9 (33.3)	6 (40.0)	0.010
Acute respiratory distress syndrome	46 (52.3)	9 (33.3)	6 (40.0)	0.012
Acute kidney injury	52 (59.1)	15 (55.6)	10 (66.7)	0.024
Acute liver function impairment	52 (59.1)	15 (55.6)	10 (66.7)	0.024
Central nervous system damage	48 (54.5)	15 (55.6)	9 (60.0)	0.019
Treatments				
Use of continuous renal-replacement therapy, *n* (%)	7 (8.0)	3 (11.1)	2 (13.3)	< 0.001
Length of ICU stay, median (IQR), d	1.0 (1.0-2.0)	1.0 (1.0-1.0)	2.0 (1.0-3.0)	0.015
Clinical outcomes at data cutoff, *n* (%)				
Hospital discharge	44.0 (50.0)	11.0 (40.7)	5.0 (33.3)	0.400
Death	16.0 (18.2)	2.0 (7.4)	4.0 (26.7)	0.240
Still hospitalization	19.0 (21.6)	13.0 (48.1)	5.0 (33.3)	0.025
Transferred to another hospital	9.0 (10.2)	1.0 (3.7)	1.0 (6.7)	0.547

[1]The denominators of patients who were included in the analysis are provided if they differed from the overall numbers in the group. Percentages may not total 100 because of rounding.
[2]Nausea/vomiting, diarrhea, flatulence, or bloody stools are defined as gastrointestinal symptoms.
IQR: Interquartile range; GCS: Glasgow coma scale; NRS: Nutrition risk screening; GI: Gastrointestinal; ICU: Intensive care unit.

Table 6 Heat stroke patient characteristics according to the time of onset of gastrointestinal symptoms

	GI symptoms[1]		*P* value
	On admission (*n* = 68)	Developed in ICU stay (*n* = 64)	
Characteristic			
Age, median (IQR), yr	67.0 (57.0-76.0)	70.0 (64.0-80.0)	0.050
Female sex, *n* (%)	28 (41.2)	32 (50.0)	0.310
BMI, median (IQR), kg/m^2	22.7 (20.2-24.8)	21.1 (20.0-23.3)	0.050
GCS score at ICU admission, median (IQR)	5.0 (3.0-8.0)	5.0 (3.0-7.0)	0.814

NRS score at ICU admission, median (IQR)	3.0 (3.0-4.5)	4.0 (3.0-6.0)	0.009
Fever on admission			
Patients, *n* (%)	68 (100.0)	64 (100.0)	–
Temperature, median (IQR), °C	41.0 (40.0-42.0)	41.0 (40.0-41.3)	0.265
Complaints and symptoms on admission, *n* (%)			
Fever	54 (79.4)	39 (60.9)	0.020
Altered mental state or behavior	25 (36.8)	30 (46.9)	0.239
Dry skin or excessive sweating	13 (19.1)	7 (10^9)	0.190
Rubefaction	5 (7.4)	6 (9.4)	0.674
Fast pulse	27 (39.7)	13 (20.3)	0.015
Polypnea	24 (35.3)	14 (21.9)	0.089
Headache	1 (1.5)	2 (3.1)	0.524
Syncope	49 (72.1)	36 (56.2)	0.058
Other	20 (29.4)	7 (10^9)	0.009
Coexisting disorder, *n* (%)			
Diabetes	1 (1.5)	9 (14.1)	0.009
Hypertension	15 (22.1)	21 (32.8)	0.166
Chronic obstructive pulmonary disease	11 (16.2)	10 (15.6)	0.931
Chronic cardiac insufficiency	5 (7.4)	11 (17.2)	0.084
Hepatitis B infection	1 (1.5)	0 (0.0)	0.330
Cancer	1 (1.5)	2 (3.1)	0.524
Chronic renal disease	0 (0.0)	2 (3.1)	0.142
Immunodeficiency	1 (1.5)	2 (3.1)	0.524
Laboratory findings			
PaO_2/FiO_2 ratio	240.0 (141.8-316.0)	217.0 (165.0-285.8)	0.775
White-cell count, 10^9/L	12.1 (7.8-16.2)	11.8 (8.2-14.2)	0.667
Lymphocyte count, 10^9/L	2.1 (1.0-3.3)	1.2 (0.6-2.0)	0.023
Platelet count, 10^9/L	90.0 (60.5-120.3)	98.5 (67.8-150.5)	0.256
Hemoglobin, g/L	126.0 (112.0-135.5)	118.5 (103.5-137.5)	0.106
Albumin, g/L	36.5 (33.3-40.0)	35.0 (32.1-38.6)	0.093
Other findings, median (IQR)			
C-reactive protein, mg/L	5.0 (0.5-10.0)	5.0 (1.0-14.9)	0.605
Procalcitonin, ng/mL	1.4 (0.4-8.2)	9.3 (2.2-29.3)	0.055
Lactate dehydrogenase, U/L	465.0 (314.3-810.3)	382.5 (282.8-537.8)	0.263
Aspartate aminotransferase, U/L	123.9 (58.3-272.3)	107.2 (44.0-268.3)	0.152
Alanine aminotransferase, U/L	46.5 (26.2-112.4)	48.0 (27.1-89.5)	0.247
Total bilirubin, μmol/L	18.5 (12.8-25.9)	15.6 (10.1-23.0)	0.211
CK-Mb, U/L	10.1 (2.9-33.1)	8.7 (3.3-41.0)	0.214
Creatinine, μmol/L	131.1 (105.3-182.8)	137.0 (97.5-171.0)	0.628
D-dimer, mg/L	3.9 (2.5-11.5)	4.6 (1.9-12.7)	0.524
Minerals, median (IQR), mmol/L			
Sodium	132.0 (129.0-137.0)	133.9 (128.5-136.8)	0.959
Potassium	3.3 (3.0-3.9)	3.5 (2.9-3.8)	0.849

Lactate	4.2 (3.1-5.5)	3.6 (2.4-5.3)	0.649
Complication, *n* (%)			
Disturbance of water and electrolyte	51 (75.0)	44 (68.8)	0.424
Rhabdomyolysis	21 (30.9)	13 (20.3)	0.165
Myocardial damage	40 (58.8)	30 (46.9)	0.122
Disseminated intravascular coagulation	38 (55.9)	24 (37.5)	0.034
Acute respiratory distress syndrome	39 (57.4)	27 (42.2)	0.082
Acute kidney injury	45 (66.2)	38 (59.4)	0.419
Acute liver function impairment	41 (60.3)	40 (62.5)	0.795
Central nervous system damage	42 (61.8)	30 (46.9)	0.086
Clinical outcomes at data cutoff, *n* (%)			
Hospital discharge	35 (51.5)	29 (45.3)	0.479
Death	17 (25.0)	9 (14.1)	0.114
Still hospitalization	13 (19.1)	20 (31.3)	0.108
Transferred to another hospital	3 (4.4)	6 (9.4)	0.258

[1]Nausea/vomiting, diarrhea, flatulence, or bloody stools are defined as gastrointestinal symptoms.
IQR: Interquartile range; CK-Mb: Creatine kinase; GI: Gastrointestinal; ICU: Intensive care unit; BMI: Body mass index.

Table 7 Heat stroke patient characteristics according to the time of onset of gastrointestinal symptoms[1]

	Early onset, *n* = 41	Late onset, *n* = 23	*P* value
Characteristic[2]			
Age, median (IQR), yr	69.0 (62.3-79.0)	64.0 (56.0-76.0)	0.856
Female sex, *n* (%)	23 (56.1)	8 (34.8)	0.102
Fever on admission			
Patients, *n* (%)	41 (100.0)	23 (100.0)	–
Temperature, median (IQR), °C	41.0 (40.0-42.0)	40.7 (39.6-41.3)	0.338
Body temperature on admission, *n* (%)			
Fever	23 (56.1)	15 (65.2)	0.475
Altered mental state or behavior	19 (46.3)	11 (47.8)	0.909
Dry skin or excessive sweating	4 (9.8)	3 (13.0)	0.686
Rubefaction	4 (9.8)	2 (8.7)	0.889
Fast pulse	11 (26.8)	2 (8.7)	0.084
Polypnea	9 (22.0)	5 (21.7)	0.984
Headache	2 (4.9)	0 (0.0)	0.282
Syncope	21 (51.2)	13 (56.5)	0.683
Other	3 (7.3)	4 (17.4)	0.215
EN support			
EN, *n* (%)	29 (70.7)	22 (95.7)	< 0.001
Average EN calorie, median (IQR), kcal/d	752.0 (500.0-1007.5)	1292.0 (750.0-1560.0)	< 0.001
Average EN protein, median (IQR), g/d	20.0 (17.6-32.5)	28.0 (15.0-57.0)	0.003
Average EN volume, median (IQR), ml/d	600.0 (147.5-1000.0)	900.0 (461.2-1500.0)	< 0.001
Duration of EN, median (IQR), d	3.0 (1.8-5.0)	7.0 (4.0-11.0)	0.011

Laboratory findings, median (IQR)			
White-cell count, 10^9/L	10.6 (7.8-13.5)	13.5 (8.6-15.8)	0.351
Hemoglobin, g/L	117.0 (106.0-128.0)	128.5 (105.3-141.5)	0.187
Albumin, g/L	35.4 (33.7-39.2)	34.4 (30.8-36.8)	0.239
Complications, *n* (%)			
Disturbance of water and electrolyte	26 (63.4)	17 (73.9)	0.391
Rhabdomyolysis	6 (14.6)	6 (26.1)	0.261
Hemorrhage of digestive tract	8 (19.5)	3 (13.1)	0.511
Myocardial damage	17 (41.5)	12 (52.2)	0.409
Disseminated intravascular coagulation	14 (34.1)	9 (39.1)	0.691
Acute respiratory distress syndrome	17 (41.5)	6 (26.1)	0.855
Clinical outcomes at data cutoff, *n* (%)			
Hospital discharge	17 (41.5)	11 (47.8)	0.622
Death	7 (17.1)	2 (8.7)	0.355
Still hospitalization	12 (29.3)	8 (34.8)	0.648
Transferred to another hospital	4 (9.8)	2 (8.7)	0.889

[1]Nausea/vomiting, diarrhea, flatulence, or bloody stools are defined as gastrointestinal symptoms.
[2]The denominators of patients who were included in the analysis are provided if they differed from the overall numbers in the group. Percentages may not total 100 because of rounding.
IQR: Interquartile range; EN: Enteral nutrition.

Table 8 Heat stroke patient characteristics according to duration of gastrointestinal symptoms[1]

	Last < 4 d, *n* = 96	Last ≥ 4 d, *n* = 36	*P* value
Characteristic			
Age, median (IQR), yr	70.0 (61.5-78.3)	67.0 (59.0-76.0)	0.659
Female sex, *n* (%)	43 (44.8)	17 (47.2)	0.803
Body temperature on admission			
Patients, *n* (%)	96 (100.0)	36 (100.0)	-
Temperature, median (IQR), °C	41.0 (40.0-41.5)	41.0 (40.0-42.0)	0.948
Complaints and symptoms on admission, *n* (%)			
Fever	69 (71.9)	24 (66.7)	0.559
Altered mental state or behavior	39 (40.6)	16 (44.4)	0.692
Dry skin or excessive sweating	16 (16.7)	4 (11.1)	0.428
Rubefaction	9 (9.4)	2 (5.6)	0.889
Fast pulse	32 (33.3)	8 (22.2)	0.767
Polypnea	31 (32.3)	7 (19.4)	0.147
Headache	2 (2.1)	1 (2.8)	0.811
Syncope	67 (69.8)	18 (50.0)	0.034
Other	19 (19.8)	8 (22.2)	0.758
Laboratory findings, median (IQR)			
White-cell count, 10^9/L	11.0 (7.5-14.2)	7.3 (9.2-16.3)	0.062
Hemoglobin, g/L	122.0 (110.5-135.5)	118.0 (106.0-132.5)	0.941
Albumin, g/L	37.0 (33.3-39.7)	34.4 (31.1-36.4)	0.031

Complications, *n* (%)			
Disturbance of water and electrolyte	69 (71.9)	20 (55.6)	0.075
Rhabdomyolysis	28 (29.2)	6 (16.7)	0.144
Hemorrhage of digestive tract	28 (29.2)	7 (19.4)	0.26
Myocardial damage	50 (52.1)	20 (55.6)	0.722
Disseminated intravascular coagulation	27 (27.8)	20 (54.2)	0.007
Acute respiratory distress syndrome	12 (12.0)	20 (54.2)	< 0.001
Clinical outcomes at data cutoff, *n* (%)			
Hospital discharge	54 (56.3)	10 (27.8)	0.004
Death	17 (17.7)	9 (25.0)	0.348
Still hospitalization	21 (21.9)	12 (33.3)	0.176
Transferred to another hospital	4 (4.2)	5 (13.9)	0.048

[1]Nausea/vomiting, diarrhea, flatulence, or bloody stools are defined as gastrointestinal symptoms.
IQR: Interquartile range.

ARTICLE HIGHLIGHTS

Research background
Extreme heat exposure is a growing health problem. The effects of heat on the gastrointestinal tract is unknown.

Research motivation
It was intended to summarize the effects of heat on the gastrointestinal (GI) tract of intensive care unit (ICU) patients.

Research objectives
This study aimed to assess the incidence of GI symptoms associated with heatstroke and its impact on outcomes.

Research methods
We conducted a retrospective, multi-center, observational cohort study to analyze outcomes between patients.

Research results
The timing and duration of gastrointestinal symptoms affects heatstroke patient's prognosis and enteral nutrition (EN) therapy. The status of EN therapy is related to heatstroke patients' outcomes. Advanced age and low Glasgow coma scale (GCS) scores are risk factors for gastrointestinal symptoms in heatstroke patients.

Research conclusions
The GI manifestations of heatstroke are common and appear to impact clinically relevant hospitalization outcomes.

Research perspectives
This was a retrospective, multi-center, observational cohort study that involved patients admitted to 83 ICUs located in 16 cities in the Sichuan Province, China between June 1 and October 31, 2022. Results showed older heatstroke patients with a lower GCS score on admission were more likely to experience GI symptoms, which had statistical difference. Clinicians should pay attention to the time at which heatstroke patients started manifesting gastrointestinal symptoms, as well as the duration of said symptoms, to ensure that patients are timely treated with the proper EN therapy and have the best prognosis possible.

ACKNOWLEDGEMENTS

The authors would like to acknowledge all investigators who participated in this trial. A full list of members who participated in this study from the Heatstroke Research Group in Southwest China: Wei Tang (Dazhou Central Hospital), Yi-Song Ren (Chengdu Pidu District Traditional Chinese Medicine Hospital), Qiong-Lan Dong (The Third People's Hospital of Mianyang), Mao-Juan Wang (Deyang People's Hospital), Liang-Hai Cao (Yibin Second People's Hospital), Xian-JunWang (The Second People's Hospital of Jiangyou City), Lang Tu (Shehong People's Hospital), Guang-Hong Ye (Anyue County Hospital of Traditional Chinese Medicine), Li Chen (Guang'an District People's Hospital, Guang'an City), An-Qin Li (The Fourth People's Hospital of Jiangyou City), Zhi-Fu Liu (Jingyan County People's Hospital), Xiao-Lin Han

(Pengzhou Traditional Chinese Medicine Hospital), Yu Dai (Mianyang Anzhou District People's Hospital), Xiong Yang (Langzhong People's Hospital), Jun Chen (Jianyang People's Hospital), Xian-Peng Qiu (The Fourth People's Hospital of Zigong City), Sen-Zhong Cheng (Zhongjiang County People's Hospital), Bo Qi (Sichuan Jiangyou 903 Hospital), Pan Yang (Meishan Cancer Hospital), Xu-Ting Deng (Luxian People's Hospital), Qin-Ya Ding (Linshui County Traditional Chinese Medicine Hospital), Chun-Mei Huang (Nanjiang County Traditional Chinese Medicine Hospital), Fang-Pei Zhang (Hejiang County Hospital of Traditional Chinese Medicine), Hong-Yu Yang (Mianyang Fulin Hospital), Xiao-Cui Wang (Deyang Hospital of Integrated Traditional Chinese and Medicine), Jia-Jin Li (Mianyang People's Hospital), Xiao-Jiao Liu (Guanghan People's Hospital), Xue-Mei Ye (Meishan People's Hospital), Fang Wu (Ziyang Lezhi County People's Hospital), Tao Ye (Leshan Traditional Chinese Medicine Hospital), Zhuo Tang (Zizhong County Traditional Chinese Medicine Hospital), Liang He (Pyeongchang County Traditional Chinese Medicine Hospital), Jian Gong (Ziyang People's Hospital), Hong-Xu Chen (Leshan Traditional Chinese Medicine Hospital); Qiong-Hua Hu (Mianyang Central Hospital); Zhen Wang (Shifang Second Hospital); Rong Hu (Xingwen County People's Hospital); You-Wei Li (The Third People's Hospital of Anyue County); Lin Hou (Bazhong Enyang District People's Hospital); Zhuo Chen (The Third People's Hospital of Yibin); Hua-Qiang Shen (Bazhong Central Hospital); Jian Wang (Guang'an People's Hospital); Ping Fang (Neijiang Second People's Hospital); Yu Liu (Lezhi County Traditional Chinese Medicine Hospital in Sichuan Province); Yan Luo (Luzhou Traditional Chinese Medicine Hospital); Wei-Peng Xu (Fushun County People's Hospital); Chun-Lin Zhang (Yibin Traditional Chinese Medicine Hospital); Xiao-Qi Tang (Ziyang Yanjiang District People's Hospital); Yu-Liu (Lezhi County People's Hospital); Jing-Mei Yang (Qingshen County People's Hospital); Xin-Pin Yang (Pyeongchang County People's Hospital, Bazhong City); Liang Chen (Gaoxian People's Hospital); Guang-Wei Yang (Huaying People's Hospital); Chun-Hong Tang (Jintang County First People's Hospital); Shi-Hao Ren (Zitong County People's Hospital); Jie Zhao (Ziyang People's Hospital); Pin Li (Shehong Hospital of Traditional Chinese Medicine); Ya Qiang (Mianyang Traditional Chinese Medicine Hospital); Hong-Zhou Wang (Sichuan Science City Hospital); Sen-Zhong Cheng (Sichuan Mianyang 404 Hospital); Song-Lin Wu (Affiliated Hospital of Southwest Medical University); Lu Liu (Luzhou Xuyong County People's Hospital); Xue-Cha Li (Neijiang Dongxing District People's Hospital); Shi-Hu Zhang (Ya'an Yucheng District People's Hospital); He Lin (Zizhong County People's Hospital); Xiao-Dong Feng (Mianzhu People's Hospital); Jun Liang (Zitong County People's Hospital of Mianyang City).

FOOTNOTES

Co-first authors: Yu-Cong Wang and Xin-Yang Jin.

Co-corresponding authors: Zhong-Wei Zhang and Qin Wu.

Author contributions: Kang Y, Jin XD, Wang B, Zhang ZW, Wu Q, Yang J, He M, Cheng YS, Wang YC, Gong J, Jin XY, Lei Z contributed to the conception and design of the study, Wang YC, Wang LT, Shi LY, Wan DY, Fu X, Wang LP, Ma AJ, Liu XJ, Jin XY, Lei Z contributed to the acquisition of data, Wang YC, Wang LT, Shi LY, Wan DY, Gong J, Zhang BG, Liu Y, Jin XY, Lei Z contributed to the analysis and interpretation of the data. Kang Y, Jin XD, Wang B, Zhang ZW, Wu Q, Yang J, He M, Cheng YS, Wang YC, Wang LT, Shi LY, Wan DY, Fu X, Wang LP, Ma AJ, Gong J, Zhang BG, Liu Y, Jin XY, Lei Z drafted or provided critical revision of the article. Kang Y, Jin XD, Wang B, Zhang ZW, Wu Q, Yang J, He M, Cheng YS, Wang YC, Wang LT, Shi LY, Wan DY, Fu X, Wang LP, Ma AJ, Gong J, Zhang BG, Liu Y, Jin XY, Lei Z read and approved the final manuscript. The reasons for designating Wang YC and Jin XY as co-first authors, and Wu Q and Zhang ZW as co-corresponding authors are threefold. First, the research was performed as a collaborative effort, and the designation of co-corresponding authorship accurately reflects the distribution of responsibilities and burdens associated with the time and effort required to complete the study and the resultant paper. This also ensures effective communication and management of post-submission matters, ultimately enhancing the paper's quality and reliability. Second, the overall research team encompassed authors with a variety of expertise and skills from different fields, and the designation of co-corresponding authors best reflects this diversity. This also promotes the most comprehensive and in-depth examination of the research topic, ultimately enriching readers' understanding by offering various expert perspectives. Third, Wang YC and Jin XY contributed efforts of equal substance throughout the research process. The choice of these researchers as co-corresponding authors acknowledges and respects this equal contribution, while recognizing the spirit of teamwork and collaboration of this study. In summary, we believe that designating Zhang ZW and Wu Q as co-corresponding authors of is fitting for our manuscript as it accurately reflects our team's collaborative spirit, equal contributions, and diversity.

Supported by National Key R&D Program of China, No. 2022YFC2504500; and 1.3.5 Project for Disciplines of Excellence, West China Hospital, Sichuan University, No. ZYGD23012.

Institutional review board statement: Ethical approval for this study was obtained from the Biomedical Ethics Review Committee of the West China Hospital of Sichuan University (approval No. SCU-2022-1542), in accordance with the principles outlined in the Declaration of Helsinki.

Informed consent statement: Given the retrospective nature of this study, the requirement for informed consent was waived.

Conflict-of-interest statement: All the authors report no relevant conflicts of interest for this article.

Data sharing statement: The datasets used and/or analyzed during the current study are available from the corresponding author on reasonable request at 716461751@qq.com or qinwu0221@gmail.com.

STROBE statement: The authors have read the STROBE Statement—checklist of items, and the manuscript was prepared and revised according to the STROBE Statement—checklist of items.

Country/Territory of origin: China

ORCID number: Yan Kang 0000-0002-5715-3900; Zhong-Wei Zhang 0000-0002-5759-2487; Qin Wu 0000-0002-7470-8429.

S-Editor: Li L
L-Editor: A
P-Editor: Li L

REFERENCES

1 **Bouchama A**, Abuyassin B, Lehe C, Laitano O, Jay O, O'Connor FG, Leon LR. Classic and exertional heatstroke. *Nat Rev Dis Primers* 2022; **8**: 8 [PMID: 35115565 DOI: 10.1038/s41572-021-00334-6]
2 **Bouchama A**, Cafege A, Devol EB, Labdi O, el-Assil K, Seraj M. Ineffectiveness of dantrolene sodium in the treatment of heatstroke. *Crit Care Med* 1991; **19**: 176-180 [PMID: 1989755 DOI: 10.1097/00003246-199102000-00011]
3 **Pires W**, Wanner SP, Soares DD, Coimbra CC. Author's Reply to Kitic: Comment on: "Association Between Exercise-Induced Hyperthermia and Intestinal Permeability: A Systematic Review". *Sports Med* 2018; **48**: 2887-2889 [PMID: 30014333 DOI: 10.1007/s40279-018-0954-9]
4 **Soares AD**, Costa KA, Wanner SP, Santos RG, Fernandes SO, Martins FS, Nicoli JR, Coimbra CC, Cardoso VN. Dietary glutamine prevents the loss of intestinal barrier function and attenuates the increase in core body temperature induced by acute heat exposure. *Br J Nutr* 2014; **112**: 1601-1610 [PMID: 25322775 DOI: 10.1017/S0007114514002608]
5 **Epstein Y**, Yanovich R. Heatstroke. *N Engl J Med* 2019; **380**: 2449-2459 [PMID: 31216400 DOI: 10.1056/NEJMra1810762]
6 **Razzak JA**, Agrawal P, Chand Z, Quraishy S, Ghaffar A, Hyder AA. Impact of community education on heat-related health outcomes and heat literacy among low-income communities in Karachi, Pakistan: a randomised controlled trial. *BMJ Glob Health* 2022; **7** [PMID: 35101860 DOI: 10.1136/bmjgh-2021-006845]
7 **Grimaldi D**, Legriel S, Pichon N, Colardelle P, Leblanc S, Canouï-Poitrine F, Ben Hadj Salem O, Muller G, de Prost N, Herrmann S, Marque S, Baron A, Sauneuf B, Messika J, Dior M, Creteur J, Bedos JP, Boutin E, Cariou A. Ischemic injury of the upper gastrointestinal tract after out-of-hospital cardiac arrest: a prospective, multicenter study. *Crit Care* 2022; **26**: 59 [PMID: 35287719 DOI: 10.1186/s13054-022-03939-9]
8 **Guan WJ**, Ni ZY, Hu Y, Liang WH, Ou CQ, He JX, Liu L, Shan H, Lei CL, Hui DSC, Du B, Li LJ, Zeng G, Yuen KY, Chen RC, Tang CL, Wang T, Chen PY, Xiang J, Li SY, Wang JL, Liang ZJ, Peng YX, Wei L, Liu Y, Hu YH, Peng P, Wang JM, Liu JY, Chen Z, Li G, Zheng ZJ, Qiu SQ, Luo J, Ye CJ, Zhu SY, Zhong NS; China Medical Treatment Expert Group for Covid-19. Clinical Characteristics of Coronavirus Disease 2019 in China. *N Engl J Med* 2020; **382**: 1708-1720 [PMID: 32109013 DOI: 10.1056/NEJMoa2002032]
9 **Mutlu GM**, Mutlu EA, Factor P. GI complications in patients receiving mechanical ventilation. *Chest* 2001; **119**: 1222-1241 [PMID: 11296191 DOI: 10.1378/chest.119.4.1222]
10 **Reintam A**, Parm P, Kitus R, Kern H, Starkopf J. Gastrointestinal symptoms in intensive care patients. *Acta Anaesthesiol Scand* 2009; **53**: 318-324 [PMID: 19243317 DOI: 10.1111/j.1399-6576.2008.01860.x]
11 **Spohn SN**, Mawe GM. Non-conventional features of peripheral serotonin signalling - the gut and beyond. *Nat Rev Gastroenterol Hepatol* 2017; **14**: 412-420 [PMID: 28487547 DOI: 10.1038/nrgastro.2017.51]
12 **Pires W**, Veneroso CE, Wanner SP, Pacheco DAS, Vaz GC, Amorim FT, Tonoli C, Soares DD, Coimbra CC. Association Between Exercise-Induced Hyperthermia and Intestinal Permeability: A Systematic Review. *Sports Med* 2017; **47**: 1389-1403 [PMID: 27943148 DOI: 10.1007/s40279-016-0654-2]
13 **Walter E**, W Watt P, Gibson OR, Wilmott AGB, Mitchell D, Moreton R, Maxwell NS. Exercise hyperthermia induces greater changes in gastrointestinal permeability than equivalent passive hyperthermia. *Physiol Rep* 2021; **9**: e14945 [PMID: 34409760 DOI: 10.14814/phy2.14945]
14 **Leon LR**, DuBose DA, Mason CW. Heat stress induces a biphasic thermoregulatory response in mice. *Am J Physiol Regul Integr Comp Physiol* 2005; **288**: R197-R204 [PMID: 15331376 DOI: 10.1152/ajpregu.00046.2004]
15 **Leon LR**, Blaha MD, DuBose DA. Time course of cytokine, corticosterone, and tissue injury responses in mice during heat strain recovery. *J Appl Physiol (1985)* 2006; **100**: 1400-1409 [PMID: 16239608 DOI: 10.1152/japplphysiol.01040.2005]
16 **Camus G**, Deby-Dupont G, Duchateau J, Deby C, Pincemail J, Lamy M. Are similar inflammatory factors involved in strenuous exercise and sepsis? *Intensive Care Med* 1994; **20**: 602-610 [PMID: 7706577 DOI: 10.1007/BF01705731]
17 **Garcin JM**, Bronstein JA, Cremades S, Courbin P, Cointet F. Acute liver failure is frequent during heat stroke. *World J Gastroenterol* 2008; **14**: 158-159 [PMID: 18176983 DOI: 10.3748/wjg.14.158]
18 **Costa RJS**, Snipe RMJ, Kitic CM, Gibson PR. Systematic review: exercise-induced gastrointestinal syndrome-implications for health and intestinal disease. *Aliment Pharmacol Ther* 2017; **46**: 246-265 [PMID: 28589631 DOI: 10.1111/apt.14157]
19 **Rowell LB**. Human cardiovascular adjustments to exercise and thermal stress. *Physiol Rev* 1974; **54**: 75-159 [PMID: 4587247 DOI: 10.1152/physrev.1974.54.1.75]
20 **Graber CD**, Reinhold RB, Breman JG, Harley RA, Hennigar GR. Fatal heat stroke. Circulating endotoxin and gram-negative sepsis as complications. *JAMA* 1971; **216**: 1195-1196 [PMID: 5314093 DOI: 10.1001/jama.216.7.1195]

World Journal of Gastroenterology

Submit a Manuscript: https://www.f6publishing.com

World J Gastroenterol 2024 January 28; 30(4): 367-380

DOI: 10.3748/wjg.v30.i4.367

ISSN 1007-9327 (print) ISSN 2219-2840 (online)

ORIGINAL ARTICLE

Basic Study

Amlodipine inhibits the proliferation and migration of esophageal carcinoma cells through the induction of endoplasmic reticulum stress

Yan-Min Chen, Wen-Qian Yang, Cheng-Wei Gu, Ying-Ying Fan, Yu-Zhen Liu, Bao-Sheng Zhao

Specialty type: Gastroenterology & hepatology

Provenance and peer review: Unsolicited article; Externally peer reviewed.

Peer-review model: Single blind

Peer-review report's scientific quality classification

Grade A (Excellent): 0
Grade B (Very good): B
Grade C (Good): 0
Grade D (Fair): 0
Grade E (Poor): 0

P-Reviewer: Suresh Kumar VC, United States

Received: December 12, 2023
Peer-review started: December 12, 2023
First decision: December 19, 2023
Revised: December 21, 2023
Accepted: January 3, 2024
Article in press: January 3, 2024
Published online: January 28, 2024

Yan-Min Chen, Wen-Qian Yang, Cheng-Wei Gu, Yu-Zhen Liu, Bao-Sheng Zhao, Department of Thoracic Surgery, The First Affiliated Hospital of Xinxiang Medical University, Weihui 453100, Henan Province, China

Yan-Min Chen, Department of Oncology, The Affiliated Hospital, Henan Polytechnic University, Jiaozuo 454000, Henan Province, China

Wen-Qian Yang, Yu-Zhen Liu, Life Science Research Center, The First Affiliated Hospital of Xinxiang Medical University, Weihui 453100, Henan Province, China

Ying-Ying Fan, Department of Gastroenterology, The First Affiliated Hospital of Xinxiang Medical University, Weihui 453100, Henan Province, China

Corresponding author: Bao-Sheng Zhao, BMed, Chief Physician, Professor, Department of Thoracic Surgery, The First Affiliated Hospital of Xinxiang Medical University, No. 88 Jiankang Road, Weihui 453100, Henan Province, China. drbszhao@xxmu.edu.cn

Abstract

BACKGROUND

L-type calcium channels are the only protein channels sensitive to calcium channel blockers, and are expressed in various cancer types. The Cancer Genome Atlas database shows that the mRNA levels of multiple L-type calcium channel subunits in esophageal squamous cell carcinoma tumor tissue are significantly higher than those in normal esophageal epithelial tissue. Therefore, we hypothesized that amlodipine, a long-acting dihydropyridine L-type calcium channel blocker, may inhibit the occurrence and development of esophageal cancer (EC).

AIM

To investigate the inhibitory effects of amlodipine on EC through endoplasmic reticulum (ER) stress.

METHODS

Cav1.3 protein expression levels in 50 pairs of EC tissues and corresponding paracancerous tissues were examined. Subsequently, the inhibitory effects of amlodipine on proliferation and migration of EC cells *in vitro* were detected using

3-(4,5-dimethyl-2-thiazolyl)-2,5-diphenyl-2-H-tetrazolium bromide and Transwell assays. *In vivo* experiments were performed using murine xenograft model. To elucidate the underlying mechanisms, *in vitro* cell studies were performed to confirm that ER stress plays a role in inhibition proliferation and migration of EC cells treated with amlodipine.

RESULTS

The expression level of Cav1.3 in esophageal carcinoma was 1.6 times higher than that in paracancerous tissues. Amlodipine treatment decreased the viability of esophageal carcinoma cells in a dose- and time-dependent manner. *In vivo* animal experiments also clearly indicated that amlodipine inhibited the growth of EC tumors in mice. Additionally, amlodipine reduces the migration of tumor cells by inhibiting epithelial-mesenchymal transition (EMT). Mechanistic studies have demonstrated that amlodipine induces ER stress-mediated apoptosis and suppresses EMT. Moreover, amlodipine-induced autophagy was characterized by an increase in autophagy lysosomes and the accumulation of light chain 3B protein. The combination of amlodipine with the ER stress inhibitor 4-phenylbutyric acid further confirmed the role of the ER stress response in amlodipine-induced apoptosis, EMT, and autophagy. Furthermore, blocking autophagy increases the ratio of apoptosis and migration.

CONCLUSION

Collectively, we demonstrate for the first time that amlodipine promotes apoptosis, induces autophagy, and inhibits migration through ER stress, thereby exerting anti-tumor effects in EC.

Key Words: L-type calcium channel; Amlodipine; Esophageal cancer; Autophagy; Endoplasmic reticulum stress

Core Tip: L-type calcium channel blockers have been shown to inhibit the growth of various tumors. We observed a higher expression of the L-type calcium channel Cav1.3 in esophageal cancer (EC) tissue than in paracancerous tissues. Subsequently, we confirmed that amlodipine inhibited the development of EC both *in vivo* and *in vitro*. Finally, we established that this inhibitory effect is related to the activation of endoplasmic reticulum stress.

Citation: Chen YM, Yang WQ, Gu CW, Fan YY, Liu YZ, Zhao BS. Amlodipine inhibits the proliferation and migration of esophageal carcinoma cells through the induction of endoplasmic reticulum stress. *World J Gastroenterol* 2024; 30(4): 367-380
URL: https://www.wjgnet.com/1007-9327/full/v30/i4/367.htm
DOI: https://dx.doi.org/10.3748/wjg.v30.i4.367

INTRODUCTION

Esophageal cancer (EC) is a common malignant tumor of digestive system, the eighth of incidence and the sixth leading cause of cancer-related mortality in the world and consists of two subtypes: Esophageal squamous cell carcinoma (ESCC) and esophageal adenocarcinoma (EAC)[1]. Data from relevant organizations suggests that more than half of all EC cases worldwide are occur in China, with over 90% being squamous cell carcinoma subtypes[2]. Despite significant advances in medical technology and surgical techniques in recent years, patients with late-stage EC still face challenges regarding effective treatment. In China, the 5-year overall survival rate for EC is currently < 20%[3], highlighting the urgent need to identify new biological markers and therapeutic strategies for EC.

Voltage-gated calcium channels comprise a major group of cell membrane potential transducers, with L-type calcium channels being the only subtype. These channels are responsible for altering intracellular calcium ion transit, which triggers various physiological processes[4]. Conventional studies on L-type calcium channels have primarily focused on the excitation-contraction coupling of skeletal and cardiac muscles[5], regulation of hormone secretion from endocrine cells, and neurotransmitter release from nerve cells[6]. Previous research has shown that L-type calcium channels play a critical role in various biological processes, such as cell proliferation, differentiation, and migration[7]. Current research suggests that the expression levels of L-type calcium channels are closely related to potential biomarkers off certain types of cancer, such as those found in the prostate, breast, and uterine cervix[8]. Previous studies have found that amlodipine, a dihydropyridine L-type calcium channel blocker, significantly suppresses the proliferation of human colon carcinoma cells[9]. Similarly, amlodipine, another dihydropyridine L-type calcium channel blocker inhibited the growth of breast cancer[10], gastric cancer[11], and melanoma cells[12].

The endoplasmic reticulum (ER) is a fundamental organelle found in eukaryotic cells that fulfills several key functions such as protein synthesis and folding, calcium ion storage, and lipid and carbohydrate metabolism[13]. ER plays a vital role in maintaining the homeostasis of intracellular Ca^{2+} by acting as a major storage site. Disturbance of this balance results in the activation of the unfolded protein response (UPR) signaling pathway, which leads to the ER stress response. This leads to the expression of molecular chaperones within the ER, restoring normal cellular homeostasis[14]. In mammals, the UPR activation begins with three primary ER stress sensors: PKR-like ER kinase (PERK), inositol-requiring

enzyme 1 (IRE1), and activating transcription factor 6 (ATF6)[15]. These sensors remain inactive by binding to the chaperone glucose-regulated protein 78-kDa (GRP78) under normal conditions. However, when ER stress occurs, un/misfolded proteins bind to GRP78, leading to the dissociation of PERK, IRE1, and ATF6 from GRP78. This initiates downstream signaling molecules in the UPR pathway[16]. ER stress initiates multiple signals, including activation of PERK, which induces phosphorylation of the eukaryotic translation initiation factor-2 alpha subunit (eIF2a). This phosphorylation inhibits the synthesis of most proteins, reducing the accumulation of proteins in the ER, and promoting UPR-related protein expression, including ATF4, which induces the transcription of C/EBP homologous protein (CHOP)[17]. These responses either restore normal ER function or induce apoptosis and autophagy as self-protective mechanisms to maintain normal cell functions. When the ER stress response persists for an extended period without resolution, the UPR triggers specific cellular apoptosis programs designed to eliminate cells that have suffered significant damage. ER stress-induced apoptosis mainly involves two processes. One process activates signaling pathways, such as PERK/eIF2a/CHOP, where increased expression levels of the CHOP protein effectively suppress sustained increases in Bcl-2 levels. The ER stress response produces a molecule called caspase-12, which is another factor contributing to apoptosis in cells[18]. Other studies have also shown that ER stress may be closely related to the cellular autophagy process. Activation of PERK/eIF2a/CHOP signaling can lead to increased expression of the autophagy marker light chain 3 (LC3)[19]. ER stress is a common cellular response to anti-cancer treatments. Several studies have suggested that certain natural bioactive compounds induce prolonged ER stress and activate pro-death signaling pathways in different types of cancer[20]. However, some reports have indicated that ER stress plays a protective role against cisplatin resistance in lung cancer patients[21].

The Cancer Genome Atlas database showed that the mRNA levels of multiple L-type calcium channel subunits (such as CACNA1C and CACNA1D) in ESCC tumor tissues were significantly higher than those in normal controls. Although L-type calcium channel blockers such as amlodipine have been effective in blocking certain types of cancer, their effects on EC have not yet been reported. Therefore, in this study, we first hypothesized that amlodipine could effectively act on EC cells and then investigated the associated ER stress processes and UPR activation results in detail. We found that amlodipine inhibited the cell proliferation *in vitro* and *in vivo*, amlodipine also suppressed the migration of EC cells. Moreover, we demonstrated that one mechanism by which amlodipine plays an anti-EC role involves autophagic cell death initiated by the activation of ER stress signaling.

MATERIALS AND METHODS

Reagents and antibodies

Amlodipine was obtained from the Shihuida Pharma Group (Jilin Province, China). 3-(4,5-dimethyl-2-thiazolyl)-2,5-diphenyl tetrazolium bromide (MTT) and the ER stress inhibitor 4-phenylbutyric acid (4-PBA) were purchased from Sigma-Aldrich (St. Louis, MO, United States). The autophagy inhibitor 3-methyladenine (3-MA) was ordered from APEXBIO (Houston, TX, United States). Annexin V-FITC/propidium iodide Apoptosis Detection Kit was procured from Beyotime Technology (Shanghai, China). The primary antibodies against Cav1.3, E-cadherin, N-cadherin, Vimentin, β-catenin, ATF6, CHOP, GRP78, p-eIF2α, Bax, Bcl-2, cytochrome C, cleaved-PARP, cleaved caspase 3, cleaved caspase 9, cleaved caspase 12, beclin-1, light chain 3 B (LC3B), GAPDH, and goat anti-rabbit secondary antibody were all purchased from Cell Signal Technologies (Danvers, MA, United States). Hanbio Biotechnology (Shanghai, China) supplied the mRFP-GFP-LC3 adenovirus particles. All the other chemicals were purchased from Boster (Wuhan, Hubei Province, China).

Patients and tissue specimens

This study enrolled 50 patients diagnosed with ESCC based on pathological analyses. All patients had undergone surgery at The First Affiliated Hospital of Xinxiang Medical University between 2017 and 2018, and none had received neo-adjuvant radiotherapy or chemotherapy. The collected tissue specimens included both the tumor tissue and paired paracancerous esophageal mucous membranes obtained from 5 cm beyond the edge of the tumor tissue. All participants were required to sign informed consent forms, and the research plan was approved by the committee of The First Affiliated Hospital of Xinxiang Medical University before the commencement of the study.

Cell culture and treatments

Human EC cell lines were procured from Cobioer Biosciences (Nanjing, Jiangsu Province, China). These cells were cultured in PRMI-1640 medium supplemented with 10% heated fetal bovine serum (FBS; Biological Industries, Israel), maintaining a constant temperature of 37 °C in a 5% CO_2 humidified incubator. Amlodipine was prepared in a PBS solution and diluted in the culture medium, with PBS serving as the control. Cells underwent various treatments as follows: amlodipine at concentrations ranging from 4 to 10 μg/mL, 4 μg/mL amlodipine treatment in the presence and absence of 3-MA, or 0.2 μM 4-PBA treatment 24 h prior to the application of 4 μg/mL amlodipine.

Cell viability assay

The KYSE-450, Eca109, SKGT-4 (seeded at 4 × 10^3 cells/well), and TE-1 cells (seeded at 5 × 10^3 cells/well) were plated overnight in 96-well plates. Subsequently, cells were subjected to treatment with various concentrations (4 μg/mL, 6 μg/mL, 8 μg/mL, and 10 μg/mL) and doses of amlodipine. Control and experimental groups were established for each concentration. After one, two, and three days of culture, 10 μL of 0.5 mg/mL MTT dye was added to each well. Following

a further 4-h incubation, the resulting blue MTT formazan crystals were dissolved in 100 μL/well of DMSO. Absorbance was measured at 490 nm using a Multisken Spectrum microplate reader (Thermo Fisher Scientific, Carlsbad, CA, United States). OD values were used to calculate cell viability. The percentage of live cells was determined using the following formula: Percentage of live cells in each well = the average absorbance value per well from five tests divided by the average absorbance value from the control wells, multiplied by 100%. The percentage of live cells treated with each concentration was calculated as the average percentage of live cells obtained from five replicate experiments.

Transwell migration assay

Cell migration was assessed using a Transwell assay. Specifically, 1×10^5 of KYSE-450 or Eca109 cell suspension in 200 μL serum-free medium was added directly to the upper chamber with 8 μm micro-pores (Corning Costar, Manassas, Virginia, United States). Subsequently, 600 μL of complete culture medium was added to the lower chamber of the insert. Amlodipine was administered at specified doses to both the upper and lower compartments of the insert. After the migration period, non-migrating cells on the upper side of the membrane were removed using a cotton swab. Cells that migrated to the underside of the Transwell were fixed in a 4% paraformaldehyde solution and stained with 0.1% crystal violet. Five randomly selected fields on each membrane were observed under a phase-contrast microscope (Nikon, Tokyo, Japan) to determine the number of migrated cells.

Flow cytometric assay of apoptosis

KYSE-450 or Eca109 cells at a density of 8×10^4 cells were seeded in 6-mm culture dishes with a complete culture medium. After a 12-h incubation period, cells were treated with amlodipine at concentrations of 6 μg/mL and 8 μg/mL. Cells were harvested after 48 h of treatment. Cell apoptosis was assessed using membrane-associated protein V-FETC or propidium iodide staining. This allowed for the detection of cells undergoing apoptosis. The apoptosis rate was calculated using the BD FACS Calibur™.

Autophagic flux measurement

Autophagic flux was examined by infecting cells with the mRFP-GFP-LC3 adenovirus. Briefly, the mRFP-GFP-LC3 adenoviral infection was induced according to the manufacturer's instructions. After 24 h of infection, the cells were transferred onto glass coverslips in 12-well plates at a density of 1×10^4 cells/well and incubated overnight. Subsequently, these cells were treated with 4 μg/mL of amlodipine for 24 h. Finally, the cells were meticulously observed under an Axio Observer A1 microscope (Carl Zeiss, Germany), and the images were acquired with a Nikon digital camera DS-U3 (Nikon, Tokyo, Japan).

Western blot analysis

RIPA lysis buffer supplemented with 1 mmol/L PMSF, 2 μg/mL aprotinin, and 100 μM leupeptin was used to lyse cells. Equal amounts of 30 μg protein extracts were separated using SDS-polyacrylamide gel and transferred to nitrocellulose membranes. After blocking with a 5% non-fat dry milk solution, the membranes were incubated at 4°C overnight with primary antibodies targeting various proteins, including Cav1.3, cyclin B1, p21, Bax, Bcl-2, cleaved-PARP, cytochrome C, E-cadherin, N-cadherin, Vimentin, β-catenin, ATF6, CHOP, GRP78, cleaved caspase-3, cleaved caspase-9, cleaved caspase-12, beclin-1, or LC3B. Subsequently, the samples were washed with PBS-T and incubated with a secondary antibody conjugated with horseradish peroxidase. Following three washes with PBS-T, the samples were treated with chemiluminescent substrates using an UltraSignal West Pico kit (Thermo Fisher Scientific, Waltham, MA, United States). Finally, all blots were analyzed using the Amersham™ Imager 600 System (GE Healthcare Bio-Sciences, Pittsburgh, PA, United States), and quantitative analysis was performed using ImageJ (Version 1.53c).

Anti-tumor activity in murine xenograft model

A total of 16 female BALB/c nude mice were procured from Beijing Vital River Laboratory Animal Technology (Beijing, China) and maintained under specific pathogen-free conditions (12-h light/dark cycle, 21 °C ± 2 °C, humidity 50% ± 10%). Mice were cared for in accordance with the guidelines approved by the Ethics Committee of the First Affiliated Hospital of Xinxiang Medical University. A tumor xenograft mouse model was successfully established by injecting 1×10^6 Eca109 cells into the left hind limb of BALB/c mice. Tumor size was calculated using the formula $V = L \times W^2/2$, where L and W represent the maximum and minimum diameters, respectively. Once the tumor volume reached approximately 50 mm^3, the mice were randomly divided into two groups of eight mice each, and gavage administration was initiated. One group was treated with the vehicle control PBS, whereas the other group was treated with amlodipine at a concentration of 13 mg/kg per day for 15 d. Daily weight and tumor size were measured and recorded throughout the procedure. At the end of the 15-d treatment period with amlodipine, the experimental mice were euthanized, and the tumor was removed, weighed, and measured.

Statistical analysis

The data were analyzed using the SPSS 26 statistical software, and the mean and standard deviation were calculated. The Student's *t*-test was used to assess the differences between two sets of data to determine statistical significance. For comparisons involving multiple groups, an analysis of variance (ANOVA) was conducted, followed by post hoc least significant difference testing, where appropriate. Statistical significance was set at $P < 0.05$.

Table 1 Clinicopathological characteristics of the esophageal squamous cell carcinoma patients

Parameters	*n*	Cav1.3 expression		*P* value
		High, *n* = 28	Low, *n* = 22	
Age				0.833
< 65	33	17	16	
≥ 65	17	11	6	
Gender				0.231
Male	34	21	13	
Female	16	7	9	
Tumor location				0.485
Middle	30	18	12	
Lower	20	10	10	
Differentiation				0.102
Low	16	8	8	
Moderate	21	12	9	
High	13	8	5	
TNM staging				0.435
I	10	6	4	
II	27	13	14	
III	13	9	4	
Lymphatic metastasis				0.854
Yes	22	12	10	
No	28	16	12	
Hypertension				0.284
Yes	14	7	7	
No	36	21	15	

RESULTS

Expression of Cav1.3 in EC tissue and cells

Evidence indicates that abnormal expression of L-type calcium channels is associated with cancer progression. To investigate the protein levels of Cav1.3, a crucial subunit of the L-type calcium ion channel, in patients with ESCC, tumor tissues and paired adjacent tissues from 50 patients with ESCC, whose clinical features are detailed in Table 1, were subjected to Western blot analysis. The representative results are shown in Figure 1A. Quantitative analysis revealed that the levels of Cav1.3 in ESCC tumor tissues were 1.60 times higher than those in the adjacent tissues (Figure 1B). Subsequent examination of Cav1.3 protein levels in various EC cell lines revealed that they were higher than those in normal human esophageal epithelial cells (Figure 1C). Consequently, we hypothesized that elevated levels of Cav1.3 promote the occurrence and development of ESCC and that L-type calcium ion channel blockers may play an inhibitory role against ESCC. Amlodipine, a third-generation dihydropyridine long-acting calcium channel blocker, is commonly used to treat cardiovascular diseases because of its minimal side effects. Therefore, we used amlodipine in follow-up experiments to explore the effect of L-type calcium channel blockers on progression of EC.

Amlodipine inhibits EC cell growth through mitochondria-mediated apoptosis

To investigate the anti-tumor effect of amlodipine on EC cells, an MTT assay was initially conducted to assess its effect on cell proliferation in both ESCC and EAC cells. Various concentrations of amlodipine (ranging from 4 μg/mL to 10 μg/mL) were applied to the cells, with different treatment durations ranging from 24 h to 72 h. Figure 2A illustrates the effects of amlodipine concentration and treatment duration on cell viability, which indicated a significant inhibitory effect on ESCC cell proliferation.

To explore the potential mechanisms underlying the inhibition of ESCC cell proliferation by amlodipine, its effects on apoptosis in KYSE-450 and Eca109 cells were investigated. After treatment with amlodipine for 48 h, flow cytometry revealed an increase in the apoptotic index (Figure 2B), establishing a correlation between the dose of amlodipine and the

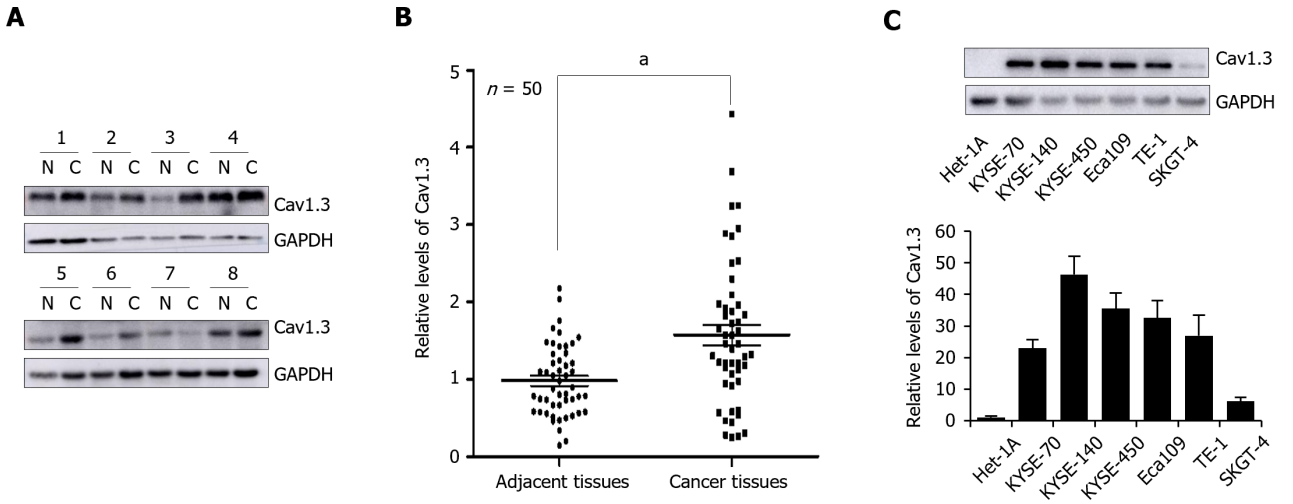

DOI: 10.3748/wjg.v30.i4.367

Figure 1 Levels of Cav1.3 expression in esophageal cancer cell tissues. A: Representative detection of Cav1.3 level in esophageal squamous cell carcinoma (ESCC) by Western blot, N means adjacent tissues and C means cancer tissues; B: Statistical analysis of 50 cases of esophageal squamous cell carcinoma showed that level of Cav1.3 in ESCC tumor tissue was 1.60 times higher than that in adjacent tissue. $^{a}P < 0.05$ *vs* the adjacent tissues; C: Western blot detection showed that the level of Cav1.3 in ESCC cells KYSE-70, KYSE-140, KYSE-450, Eca109, TE-1, and esophageal adenocarcinoma cell SKGT-4 was higher than that in esophageal squamous cell Het-1A.

induction of apoptosis in KYSE-450 and Eca109 cells. To delve deeper into the molecular signals involved in amlodipine-induced apoptosis, we examined apoptosis-related proteins, specifically focusing on mitochondrial apoptosis markers, including Bax, Bcl-2, cytochrome C, and cleaved-PARP, by Western blotting (Figure 2C). The results indicated that amlodipine reduced the levels of Bcl-2 and induced the levels of Bax, cytochrome C, and cleaved-PARP. Overall, our findings suggest that the amlodipine-induced inhibition of ESCC cell viability is associated with the induction of mitochondrial apoptosis.

Amlodipine inhibited migration of EC Cells by restraining epithelial-mesenchymal transition

To identify the effect of amlodipine on EC cell migration, a Transwell assay was performed. Based on the MTT assay results described in Figure 1A, doses of amlodipine at 4 μg/mL, 6 μg/mL, and 8 μg/mL were selected, and cells were allowed to migrate for 24 h post-amlodipine treatment. Notably, the inhibitory effect of amlodipine on ESCC cell migration was more potent than that observed on EAC cells (Figure 3A), which was consistent with the cell proliferation data presented in Figure 1A. Cell migration involves multiple steps, including epithelial-mesenchymal transition (EMT). To clarify whether amlodipine inhibits EMT, the levels of EMT markers, including β-catenin, E-cadherin, N-cadherin, and Vimentin were measured. The results demonstrated that amlodipine significantly reduced the expression levels of β-catenin, Vimentin, and N-cadherin, while increasing the protein content of E-cadherin, as depicted in Figure 3B. These findings suggest that the inhibitory effect of amlodipine on EC cell migration is primarily due to its inhibitory effect on EMT.

Amlodipine inhibited the viability and migration of EC cell through the induction of ER stress

Given that amlodipine is an L-type calcium channel blocker that can induce changes in intracellular calcium homeostasis by triggering ER stress, the protein levels of ER stress molecules in patients after amlodipine treatment were systematically investigated. As shown in Figure 4A, the levels of UPR sensors, including GRP78, ATF-6, p-eIF2α, and CHOP, increased after amlodipine treatment in KYSE-450 and EC-109 cell lines, indicating that amlodipine induces ER stress. Studies have suggested that CHOP, which is elevated in response to excessive ER stress, activates the caspase cascade. Therefore, the effect of amlodipine on apoptosis-related caspase cleavage was investigated. Amlodipine upregulated the levels of cleaved caspase-12, cleaved caspase-9, and cleaved caspase-3 (Figure 4A). To further explore whether the effects of amlodipine on ESCC cell viability and migration were mediated by ER stress, the inhibitor 4-PBA was applied to ESCC cells before amlodipine treatment. Pretreatment with 4-PBA significantly blocked the amlodipine-induced inhibitory effects on ESCC cell viability (Figure 4B), and migration (Figure 4C) exhibiting a definite reversal effect on amlodipine-induced alterations in ATF-6, p-eIF2α, and CHOP proteins related to ER stress, cleaved caspase-3 proteins related to apoptosis, and E-cadherin proteins related to EMT (Figure 4D). Collectively, these results suggest that amlodipine reduces ESCC cell viability and migration by inducing ER stress.

Amlodipine-induced autophagy in EC cells

The Ca^{2+} signaling pathway plays a critical role in various cellular activities, and its impact on autophagy can either facilitate or inhibit[22]. Given that the blockade of L-type calcium channels leads to an imbalance in intracellular calcium homeostasis, whether amlodipine promotes autophagy in ESCC cells was investigated. Autophagy dual-fluorescent LC3 adenoviruses were introduced into ESCC cells and alterations in autophagic flux in response to amlodipine treatment

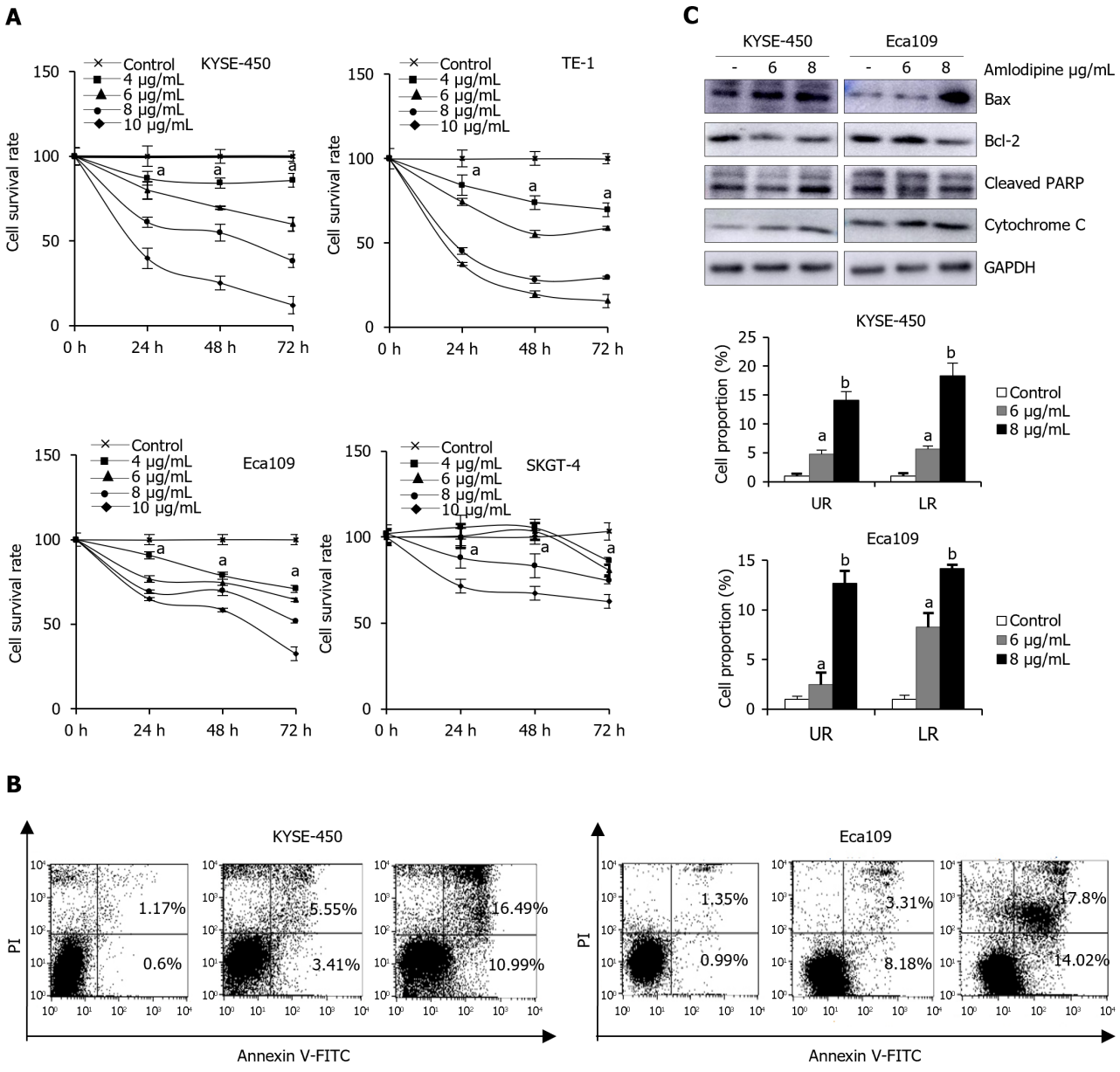

DOI: 10.3748/wjg.v30.i4.367

Figure 2 Amlodipine suppressed esophageal carcinoma cell growth through mitochondria-mediated apoptosis. A: For human esophageal cancer cells, treatment with different concentrations of amlodipine solution at 4-10 μg/mL, increasing by 2 μg/mL, was performed. Cell viability was measured using the 3-(4,5-dimethyl-2-thiazolyl)-2,5-diphenyl tetrazolium bromide (MTT) assay to observe the state of cells after treatment for one, two, and three days $^{a}P < 0.05$ *vs* Control; B: KYSE-450 and Eca109 cells were exposed to amlodipine at a concentration of either 6 or 8 μg/mL for 48 h, following which the percentage of apoptotic cells was measured using flow cytometry or propidium iodide staining $^{a}P < 0.05$ *vs* Control, $^{b}P < 0.01$ *vs* Control; C: In addition, after two days of treatment with amlodipine, changes in the levels of various apoptosis-related proteins including Bcl-2, Bax, cleaved PARP, and cytochrome C were detected using Western blotting techniques. UR: Upper right quadrant LR: Lower right quadrant.

were examined. In control cells (left lane in Figure 5A), both green (GFP-LC3) and red (RFP-LC3) fluorescence were dispersed in the cytoplasm. However, after amlodipine treatment (right lane in Figure 5A), green fluorescent spots (autophagosomes) and red fluorescent spots (autophagolysosomes) were observed, suggesting that amlodipine promotes autophagy. Microtubule-associated protein 1 LC3B, an autophagosome membrane-type LC3 converted from cytoplasmic LC3-I, and beclin-1, a key regulator required for the initiation of autophagosome formation, were examined. The results demonstrated that amlodipine increased the levels of LC3B and beclin-1 in a dose-dependent manner (Figure 5B), further confirming the role of amlodipine in promoting autophagy. To investigate whether autophagy is mediated by amlodipine-induced ER stress, the cells were treated with an ER stress inhibitor 4-PBA. As shown in Figure 5C, 4-treatment reduced the amlodipine-induced upregulation of LC3B. These data suggest that amlodipine promotes autophagy *via* activation of ER stress in ESCC cells.

Inhibition of autophagy enhanced amlodipine-induced apoptosis and migration

Autophagy is induced when ER stress occurs and serves as a crucial compensatory protective mechanism in cells. When

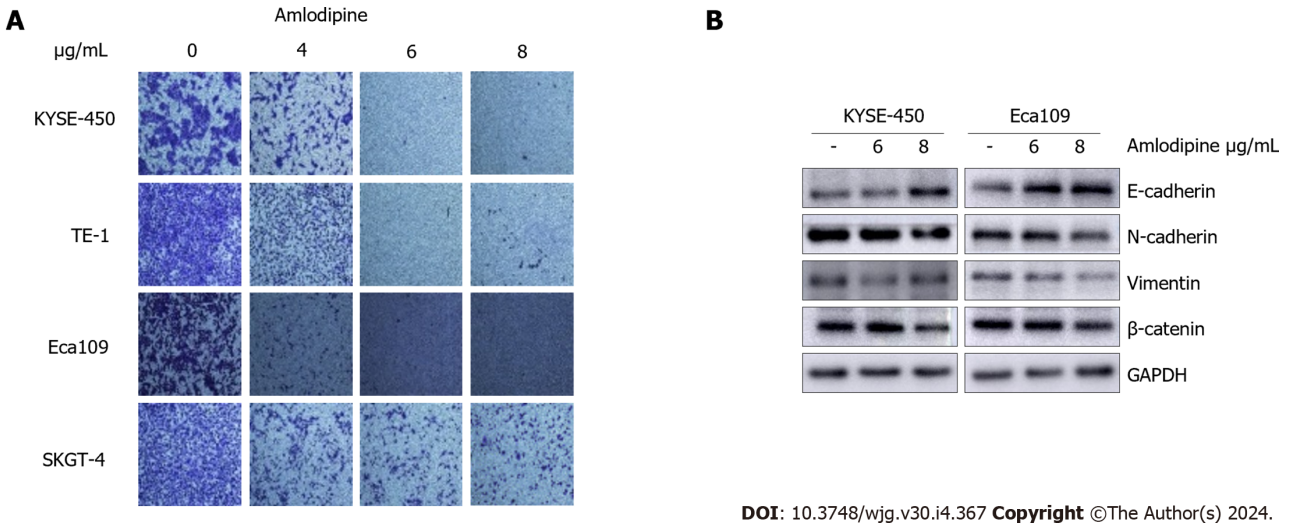

DOI: 10.3748/wjg.v30.i4.367 **Copyright** ©The Author(s) 2024.

Figure 3 Amlodipine inhibited esophageal carcinoma cells migration by restraining epithelial-mesenchymal transition. A: Human esophageal carcinoma cells (KYSE-450, TE-1, Eca109, and SKGT-4) were treated with increasing doses of amlodipine (4 μg/mL, 6 μg/mL, and 8 μg/mL) and assessed cell migration at 24 h *via* Transwell migration assay; B: The Western blot results clearly showed the percentage of mesenchymal marker N-cadherin, epithelial marker E-cadherin, and β-catenin protein in KYSE-450 and Eca109 cells after treatment with amlodipine.

autophagy is insufficient to counteract damaging factors, apoptosis can occur. Therefore, we investigated whether amlodipine-induced autophagy functions as a compensatory protective mechanism in ESCC cells and whether it promotes cell apoptosis. To verify this hypothesis, the autophagy inhibitor 3-MA was used. Compared to amlodipine treatment alone, the combination of 3-MA and amlodipine resulted in more pronounced inhibitory effects on cell viability and migration (Figure 6A and B), indicating that the inhibition of autophagy enhances amlodipine-induced apoptosis and migration. Western blot analysis revealed that the combination treatment blocked amlodipine-induced LC3B formation and promoted amlodipine-induced upregulation of E-cadherin, while cleaved caspase-3 decreased (Figure 6C). In summary, the results of these experiments demonstrate the efficacy of amlodipine and suggest that inhibiting autophagy increases amlodipine-induced cell death.

Amlodipine inhibited growth of human EC cell line-derived xenograft tumor in vivo

To further determine whether amlodipine exhibits an anti-tumor role against ESCC *in vivo*, a study was conducted in BALB/c nude mice, wherein these mice were implanted with Eca109 cells to establish a tumor xenograft model. The mice were then divided into the amlodipine treatment and vehicle groups. Compared to the vehicle group, the amlodipine group exhibited a dynamically significant reduction in tumor size without affecting body weight (Figure 7A and B). At the end of the experiment, the tumor tissues (Figure 7C) were photographed, and their average weight (Figure 7D) was calculated. Images and results showed that, compared to the vehicle group, the tumors had a smaller volume and reduced tumor weight in the amlodipine-treated group, further supporting the anti-tumor role of amlodipine in ESCC. The amlodipine-induced tumor inhibition rate was 30.95% (Figure 7E). Taken together, these data indicated that amlodipine inhibited EC growth *in vivo*.

DISCUSSION

Cytosolic free Ca^{2+} is a ubiquitous secondary messenger that controls various fundamental cellular processes, including muscle contraction, cell motility, neurotransmitter release, exocytosis, and endocytosis. It also has been well documented that cytosolic free Ca^{2+} plays essential roles in cell proliferation, migration, cell cycle control, and apoptosis, which are general features that malignant cells possess[23]. Intracellular Ca^{2+} homeostasis is regulated by calcium channels on the cell membrane, ER, and mitochondrial surface[24]. One type of calcium channel on the cell membrane is the voltage-gated calcium channel (VGCC), the activation of which causes Ca^{2+} influx into the cells. Previous research and available public datasets have demonstrated that L-type calcium channels, which constitute a major type of VGCCs, are functionally expressed in various cancer cells and tissue samples from diverse cancer types[8]. Therefore, the extent to which L-type calcium channels are expressed in ESCC is unclear. In this study, we measured the levels of Cav1.3, an essential subunit of the L-type calcium ion channel, in 50 cases of paired EC and adjacent tissues from patients with ESCC and discovered that the average level of Cav1.3 in cancerous tissue was 1.60 times higher than that seen in adjacent tissues. Higher levels of Cav1.3 were detected in both ESCC and EAC cells compared to those in the esophageal epithelial cell line Het-1A. These results suggest that L-type calcium channels possibly function as potential targets for anti-EC therapies.

Dihydropyridine calcium channel blockers are the best-known class of L-type calcium channel blockers and are widely used to treat hypertension, angina pectoris, and atherosclerosis[25]. Many studies have demonstrated that dihydropyridine calcium channel blockers effectively suppress cancer cell growth[26]. Amlodipine, a third-generation calcium

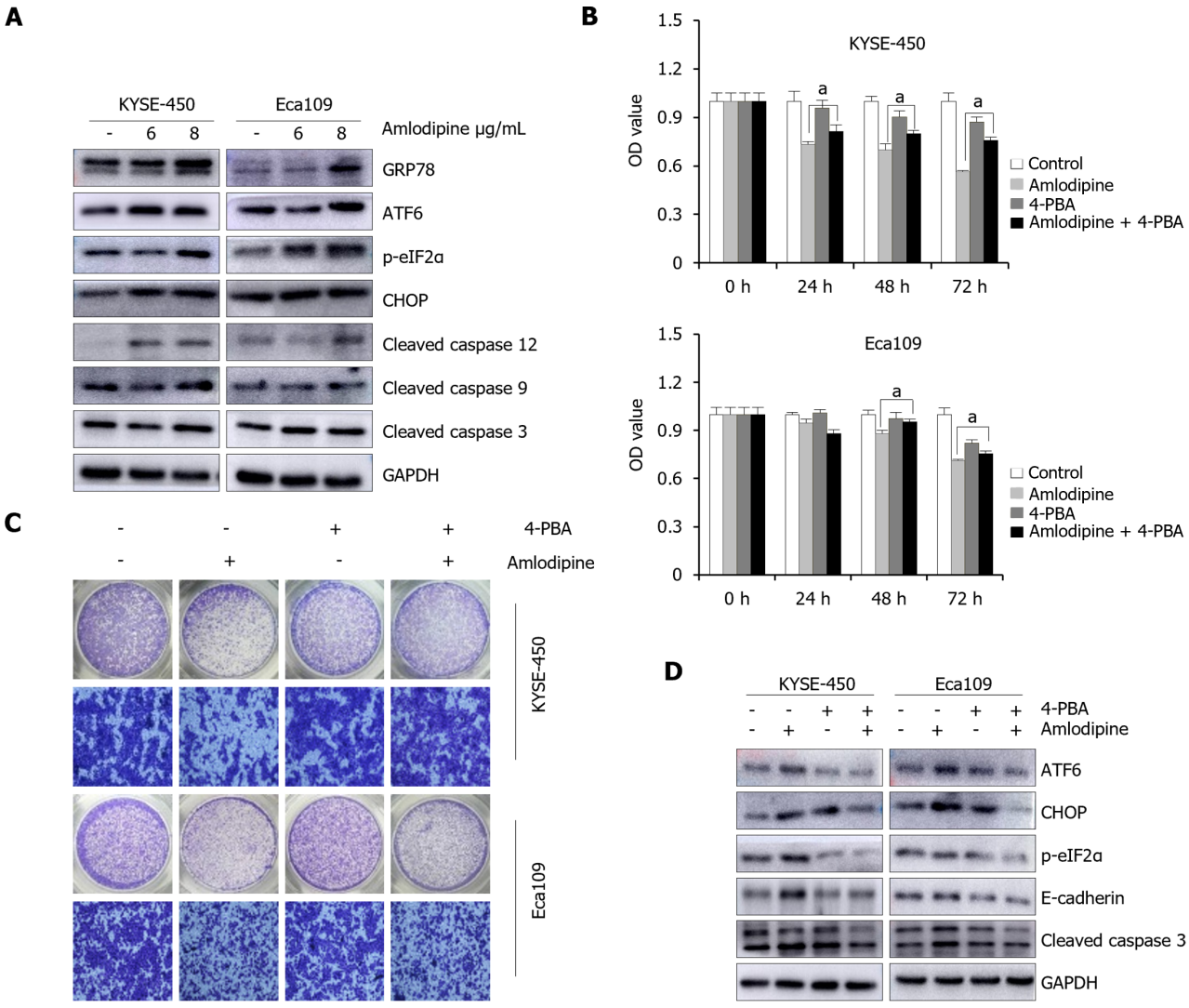

DOI: 10.3748/wjg.v30.i4.367

Figure 4 Amlodipine repressed esophageal carcinoma proliferation and migration *via* induction of endoplasmic reticulum stress. A: KYSE-450 and Eca109 cells were treated with amlodipine at different concentrations for two days. According to the Western blot results, the protein levels of CHOP, p-eIF2α, GRP78, cleaved caspase-12, ATF6, cleaved caspase-9, and cleaved caspase-3 could be observed; B: With a concentration of 4 μg/mL amlodipine drug, 0.2 μM of 4-phenylbutyric acid (4-PBA), mixed treatment, then placed into KYSE-450 and Eca109 cells, with the help of 3-(4,5-dimethyl-2-thiazolyl)-2,5-diphenyl tetrazolium bromide (MTT) assay to test the cell activity presented by these cells in 1 d to 3 d $^{a}P < 0.05$ *vs* amlodipine; C: Transwell migration assay was conducted to examine cell migration of KYSE-450 and Eca109 when treatment with amlodipine (4 μg/mL), 4-PBA (0.2 μM) or both combination for 24 h; D: Western blot analysis showed the levels of ATF6, CHOP, p-eIF2α, E-cadherin, and cleaved caspase-3 in KYSE-450 and Eca109 cells after treatment with amlodipine (4 μg/mL), 4-PBA (0.2 μM) or both combination for 48 h. All amlodipine and 4-PBA combination treatment was applying 4-PBA in advance for 1 h then amlodipine.

antagonist, suppresses the proliferation and migration of various cancer cell types. For example, this drug can utilize ERK1 or ERK2, integrin-β1, Bcl-2, and other inhibitors of the proliferation of breast cancer cells in the body, resulting in the formation of colonies, which are vulnerable to invasion[10]. Amlodipine also suppresses the growth of gastric cancer stem cells and exerts an anti-tumor effect mainly by affecting the stability of Ca^{2+} concentrations within the cells[27].

When the intracellular Ca^{2+} concentration is out of balance, it often destroys Ca^{2+} homeostasis in the ER, consequently leading to ER stress, which maintains ER homeostasis and ensures cell survival *via* the UPR[14]. The UPR mainly includes three protein signal transduction pathways: PERK, IRE1, and ATF6. The UPR mechanism activated during ER stress reduces the accumulation of misfolded or unfolded proteins in the ER, thereby minimizing the damage caused by protein accumulation, restoring ER homeostasis, and ultimately promoting the survival of stressed cells. These effects are mediated through the activation of three signaling pathways described previously[16]. However, when persistent and severe ER stress occurs, the survival mode of UPR changes to a mode that promotes apoptosis. CHOP is a marker gene for apoptosis induced by ER stress[28]. ER stress-mediated apoptosis involves several cellular mechanisms, including the regulation of CHOP gene expression and the subsequent activation of downstream targets, such as members of the Bcl-2 protein family. Continuous activation of CHOP can lead to the downregulation of the anti-apoptotic protein Bcl-2, ultimately leading to the activation of mitochondrial apoptosis regulated by Bax[29]. Moreover, caspase-12 is also recognized as a key factor in ER stress-induced apoptosis. IRE1α, located on the ER membrane, can induce apoptosis during periods of ER stress. Activation of caspase-12 induced by ER stress leads to the cleavage and activation of caspase-

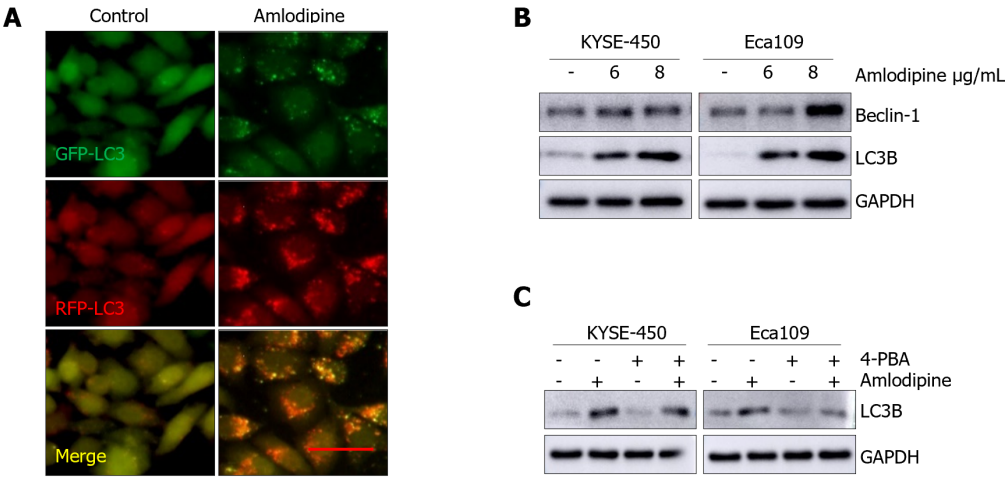

DOI: 10.3748/wjg.v30.i4.367 **Copyright** ©The Author(s) 2024.

Figure 5 Amlodipine induced autophagy in esophageal carcinoma cells. A: Eca109 cells after transient infection with GFP-RFP-LC3 virus were treated with vehicle control PBS or amlodipine (6 μg/mL) for 24 h and representative fluorescence images were captured. Bar = 20 μm; B: Protein trajectory results were measured using PBS or different concentrations of amlodipine, and the levels of beclin-1 and light chain 3 B (LC3B) in KYSE-450 and Eca109 cells after two days of treatment were detected; C: Western blot analysis revealed the level of LC3B in KYSE-450 and Eca109 after 48 h treatment with amlodipine (4 μg/mL), 4-phenylbutyric acid (4-PBA) (0.2 μM) or both combination (applying 4-PBA in advance for 1 h then amlodipine). GAPDH served as a loading control.

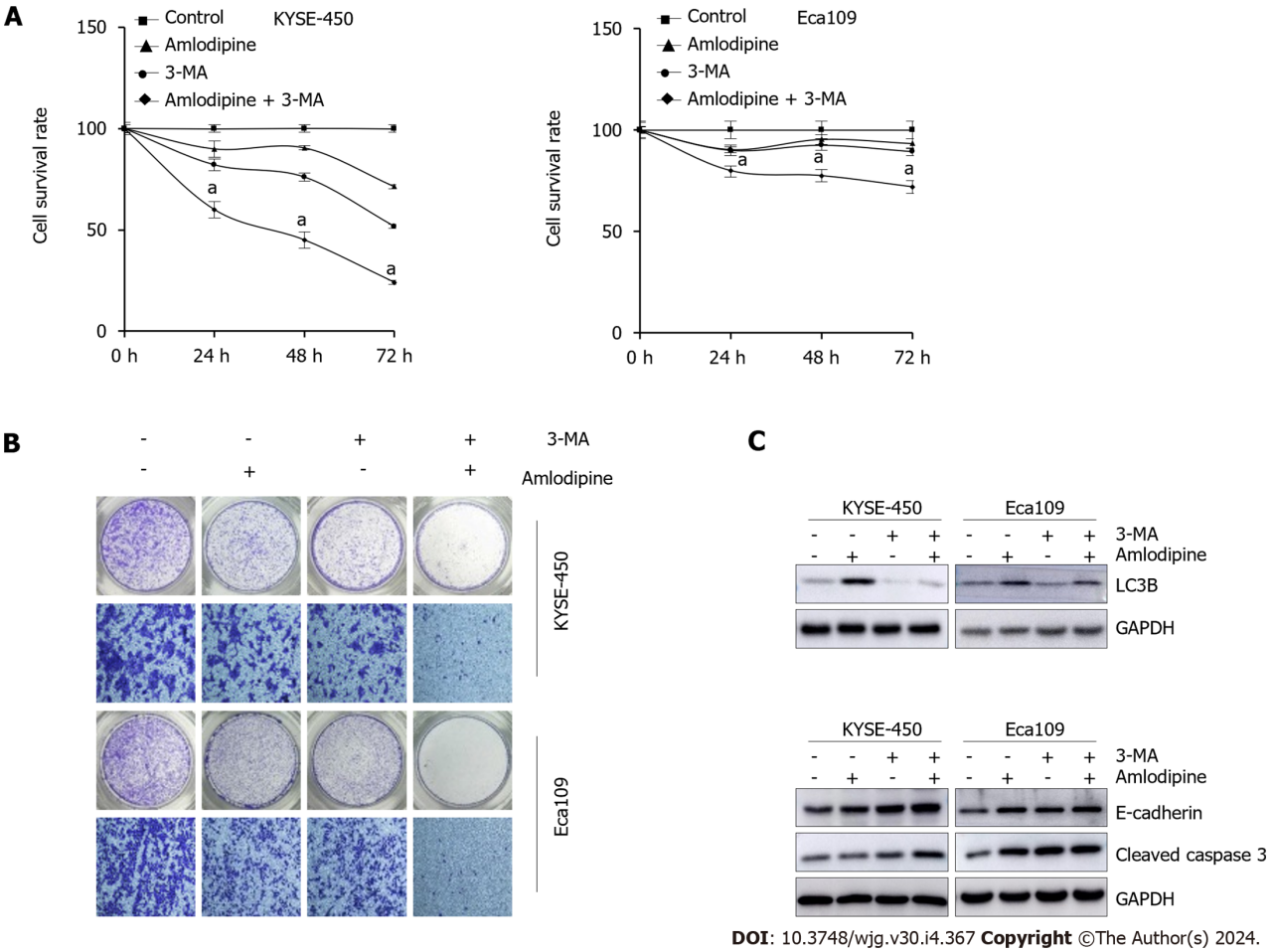

DOI: 10.3748/wjg.v30.i4.367 **Copyright** ©The Author(s) 2024.

Figure 6 Inhibition of autophagy enhanced amlodipine-induced apoptosis and migration. A and B: To investigate the effects of amlodipine, 3-methyladenine (3-MA), or their combination on cell proliferation and migration of KYSE-450 and Eca109 cells, 3-(4,5-dimethyl-2-thiazolyl)-2,5-diphenyl tetrazolium bromide (MTT) and Transwell migration assay were carried out, and significant results were observed with $^{a}P < 0.05$ *vs* Control; C: LC3B, as well as E-cadherin content and levels, were tested in detail by means of western blot analysis, cleaved caspase 3 in KYSE-450 and Eca109 cells after treatment with amlodipine (4 μg/mL), 3-MA (3 mmol/L), or their combination. GAPDH served as a loading control. 3-MA: 3-methyladenine.

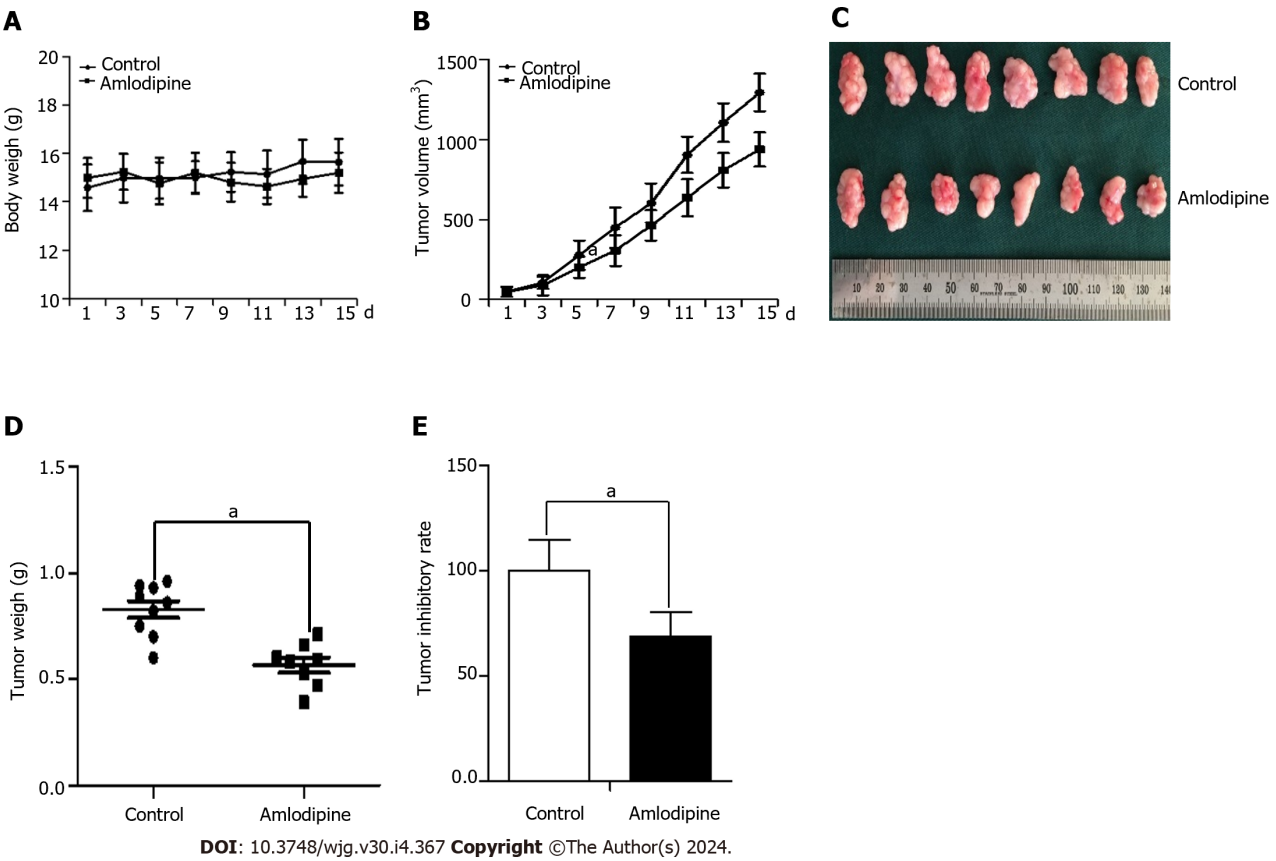

DOI: 10.3748/wjg.v30.i4.367 **Copyright** ©The Author(s) 2024.

Figure 7 *In vivo* studies revealed that amlodipine was able to impede Eca109 tumor xenografts. Initially, 1 × 10^6 Eca109 cells were subcutaneously implanted into the left hind limb of female BALB/c nude mice. After five days, when tumors reached an approximate size of 50 mm^3, the mice were orally administered with amlodipine (13 mg/kg/d) or PBS control vehicle once daily *via* gavage. Following treatment for fifteen days, the mice were euthanized and their respective tumors were excised for further analysis. A and B: Body weight (A) and the growth curves (B) of tumors were compared between the control group and amlodipine group with significant differences observed at $^aP < 0.05$ *vs* Control; C: Physical images of tumor xenografts in each group; D: The xenogeneic tumor weights in each group $^aP < 0.05$ *vs* Control; E: Inhibitory rate of amlodipine on Eca109 xenografts in athymic nude mice $^aP < 0.05$ *vs* Control.

9, which then activates a series of effector caspases and induces apoptosis[30]. This experiment demonstrates that the drug effect of amlodipine increases the content of ER stress-related proteins in ESCC cells, the most important ones being GRP78, ATF6 and p-eIF2α. This causes the process of Bcl-2 expression, regulated by CHOP signaling, to decrease. Consequently, the expression levels of both cytochrome c and the pro-apoptotic protein Bax in cells are increased. These phenomena provide strong evidence that amlodipine causes an ER stress response and apoptosis in the mitochondria. At the same time, we detected an increase in the expression of ER stress-specific apoptotic molecules, including cleaved caspase-12, whose expression was elevated. This further activated cleaved caspase-9 and cleaved caspase-3 to promote cell apoptosis.

Recent studies have found that ER stress/UPR are not only related to tumor survival and apoptosis, but are also related to tumor metastasis. Research has indicated that molecules associated with ER stress signaling can impact the EMT process in tumor cells, mainly by regulating the transcriptional changes of EMT-induced transcription factors[31]. For example, the activation of IRE1 α/XBP1 signal pathway can induce Snail transcription in breast cancer cells, promote EMT in these cells, and enhance their migration and invasion ability[32,33]. It has also been reported that the activation of ER stress inhibits the metastasis of gastric and lung cancers by inhibiting EMT[34,35]. This study provides valuable evidence that amlodipine inhibits EMT, which ultimately affects the migration of ESCC cells. To further confirm that amlodipine induces ER stress to promote apoptosis and inhibit EMT, we used 4-PBA, an inhibitor of ER stress, and observed the reversal of ER stress, apoptosis, and EMT-related protein functions. In *in vivo* experiments, we demonstrated that amlodipine has an anti-tumor effect, although its internal mechanism could not be clarified. These data suggested that the anti-cancer effects of amlodipine against ESCC cells may be attributed to the activation of ER stress.

The proteasome-regulated degradation system cannot handle excessive amounts of un/misfolded proteins during ER stress. Consequently, autophagy is induced to remove these proteins[36]. It has been proven that ER stress and autophagy induced by it are closely related to tumors and have double-edged sword effects[37]. Therefore, it is particularly important to utilize different conditions to clarify the effects and related mechanisms of autophagy in tumor cells, to provide a valuable basis for the development of treatments involving cellular autophagy. In this study, 4-PBA combined with amlodipine downregulated LC3B levels. The results of this study indicate that amlodipine-induced autophagy may be due to ER stress. To further elucidate the role of autophagy in amlodipine-induced ER stress, the autophagy inhibitor 3-MA was used. Amlodipine combined with 3-MA significantly enhanced amlodipine-induced cell death and inhibited cell migration. Amlodipine promotes autophagy through ER stress, and autophagy plays a role in protecting tumor cells,

providing a basis for the combined application of amlodipine and autophagy inhibitors in clinical setting.

CONCLUSION

In conclusion, we have demonstrated for the first time that amlodipine inhibits cell proliferation *in vitro* and *in vivo*, promotes apoptosis and inhibits EMT through ER stress in EC. Moreover, amlodipine induces autophagy, which alleviates ER stress and may play a cytoprotective role. Our findings provide essential evidence supporting amlodipine, and the combined use of amlodipine with an autophagy inhibitor, as potential therapeutic options for patients with ESCC.

ARTICLE HIGHLIGHTS

Research background

Esophageal cancer (EC) is the sixth most common tumor worldwide and has a poor prognosis. Although L-type calcium channel blockers have demonstrated efficacy in inhibiting the occurrence and development of various tumors, their impact on EC remains unclear.

Research motivation

Patients with EC have a poor prognosis owing to a lack of effective treatments and prognostic indicators. This study aimed to explore a novel approach for treating EC and improving patient survival rates.

Research objectives

To elucidate the mechanism by which the L-type calcium channel blocker, amlodipine, inhibits the proliferation and migration of EC cells, thereby offering a potential new avenue for the treatment of EC.

Research methods

Western blot analysis was used to assess the expression of relevant proteins. Cell migration was evaluated using Transwell assays and apoptosis was measured using flow cytometry. The endoplasmic reticulum (ER) stress inhibitor 4-phenylbutyric acid was used to prevent ER stress. Transduction of EC cells with GFP-RFP-LC3 adenovirus confirmed that amlodipine-mediated ER stress functions through downstream autophagy. In addition, a murine xenograft model constructed using Eca109 cells was used to validate the anti-tumor effects of amlodipine *in vivo*.

Research results

This study revealed that the Cav1.3 level in EC tissues was higher than that in adjacent tissues. The L-type calcium channel blocker, amlodipine, inhibits the proliferation and migration of EC cells while promoting apoptosis. Mechanistic investigations have indicated that these effects are associated with the induction of cellular ER stress. Further studies using GFP-RFP-LC3 adenovirus-transfected cells treated with amlodipine demonstrated that autophagy, mediated by ER stress, played a protective role in this process. In addition, amlodipine inhibited EC cell growth and presented an antitumor effect *in vivo*.

Research conclusions

L-type calcium channels are highly expressed in EC tissues. Both *in vivo* and *in vitro* experiments revealed that amlodipine inhibited the proliferation and migration of EC cells through ER stress.

Research perspectives

The expression levels of L-type calcium channels in EC may serve as an index of prognosis, and the combination of amlodipine with autophagy inhibitors holds promise as a novel treatment approach. Future endeavors should involve large-sample multicenter clinical studies to further validate its reliability.

ACKNOWLEDGEMENTS

We thank Chen-Fang Qi (Intensive Care Unit, Cedars-Sinai Medical Center, 8700 Beverly Blvd, Los Angeles, CA 90048, United States) for providing language editorial assistance.

FOOTNOTES

Author contributions: Chen YM, Liu YZ, and Zhao BS made substantial contributions to conception and design of the study; Chen YM and Yang WQ conducted the experiments, acquired and analyzed data; Chen YM, Yang WQ, Liu YZ, and Zhao BS interpreted the data;

Gu CW and Fan YY were responsible for clinical sample collection; Chen YM and Liu YZ wrote the manuscript drift; Liu YZ and Zhao BS revised the manuscript; and all authors approved the final version of the manuscript.

Supported by the Key Medical Scientific and Technological Project of Henan Province, No. SBGJ202102188; Henan Provincial Medical Science and Technology Project, No. LHGJ20221012; and the Key Project of Science and Technology of Xinxiang, No. GG2020027.

Institutional review board statement: This study was reviewed and approved by the First Affiliated Hospital of Xinxiang Medical University Institutional Review Board (Approval No. EC-023-487).

Institutional animal care and use committee statement: All procedures involving animals were reviewed and approved by the First Affiliated Hospital of Xinxiang Medical University Institutional Review Board (Approval No. EC-023-488).

Conflict-of-interest statement: The authors declare that no conflict of interest exists in this study.

Data sharing statement: No additional data are available.

ARRIVE guidelines statement: The authors have read the ARRIVE guidelines, and the manuscript was prepared and revised according to the ARRIVE guidelines.

Country/Territory of origin: China

ORCID number: Wen-Qian Yang 0000-0001-7940-0637; Cheng-Wei Gu 0000-0001-7908-4603; Yu-Zhen Liu 0000-0001-8329-1795; Bao-Sheng Zhao 0000-0002-7854-111X.

S-Editor: Chen YL
L-Editor: A
P-Editor: Chen YX

REFERENCES

1 **Dias F**, Morais M, Teixeira AL, Medeiros R. Involving the microRNA Targetome in Esophageal-Cancer Development and Behavior. *Cancers (Basel)* 2018; **10** [PMID: 30322005 DOI: 10.3390/cancers10100381]
2 **Song Y**, Li L, Ou Y, Gao Z, Li E, Li X, Zhang W, Wang J, Xu L, Zhou Y, Ma X, Liu L, Zhao Z, Huang X, Fan J, Dong L, Chen G, Ma L, Yang J, Chen L, He M, Li M, Zhuang X, Huang K, Qiu K, Yin G, Guo G, Feng Q, Chen P, Wu Z, Wu J, Zhao J, Luo L, Fu M, Xu B, Chen B, Li Y, Tong T, Wang M, Liu Z, Lin D, Zhang X, Yang H, Zhan Q. Identification of genomic alterations in oesophageal squamous cell cancer. *Nature* 2014; **509**: 91-95 [PMID: 24670651 DOI: 10.1038/nature13176]
3 **Lv J**, Guo L, Liu JJ, Zhao HP, Zhang J, Wang JH. Alteration of the esophageal microbiota in Barrett's esophagus and esophageal adenocarcinoma. *World J Gastroenterol* 2019; **25**: 2149-2161 [PMID: 31143067 DOI: 10.3748/wjg.v25.i18.2149]
4 **Xu L**, Sun L, Xie L, Mou S, Zhang D, Zhu J, Xu P. Advances in L-Type Calcium Channel Structures, Functions and Molecular Modeling. *Curr Med Chem* 2021; **28**: 514-524 [PMID: 32664834 DOI: 10.2174/0929867327666200714154059]
5 **Ednie AR**, Bennett ES. Intracellular O-linked glycosylation directly regulates cardiomyocyte L-type Ca(2+) channel activity and excitation-contraction coupling. *Basic Res Cardiol* 2020; **115**: 59 [PMID: 32910282 DOI: 10.1007/s00395-020-00820-0]
6 **Dickerson MT**, Dadi PK, Butterworth RB, Nakhe AY, Graff SM, Zaborska KE, Schaub CM, Jacobson DA. Tetraspanin-7 regulation of L-type voltage-dependent calcium channels controls pancreatic β-cell insulin secretion. *J Physiol* 2020; **598**: 4887-4905 [PMID: 32790176 DOI: 10.1113/JP279941]
7 **Phan NN**, Wang CY, Chen CF, Sun Z, Lai MD, Lin YC. Voltage-gated calcium channels: Novel targets for cancer therapy. *Oncol Lett* 2017; **14**: 2059-2074 [PMID: 28781648 DOI: 10.3892/ol.2017.6457]
8 **Jacquemet G**, Baghirov H, Georgiadou M, Sihto H, Peuhu E, Cettour-Janet P, He T, Perälä M, Kronqvist P, Joensuu H, Ivaska J. L-type calcium channels regulate filopodia stability and cancer cell invasion downstream of integrin signalling. *Nat Commun* 2016; **7**: 13297 [PMID: 27910855 DOI: 10.1038/ncomms13297]
9 **Floersheim GL**, Racine C. Calcium antagonist radioprotectors do not reduce radiotherapeutic efficacy in three human tumor xenografts. *Strahlenther Onkol* 1995; **171**: 403-407 [PMID: 7631262]
10 **Alqudah MAY**, Al-Samman R, Azaizeh M, Alzoubi KH. Amlodipine inhibits proliferation, invasion, and colony formation of breast cancer cells. *Biomed Rep* 2022; **16**: 50 [PMID: 35620309 DOI: 10.3892/br.2022.1533]
11 **Panneerpandian P**, Rao DB, Ganesan K. Calcium channel blockers lercanidipine and amlodipine inhibit YY1/ERK/TGF-β mediated transcription and sensitize the gastric cancer cells to doxorubicin. *Toxicol In Vitro* 2021; **74**: 105152 [PMID: 33771646 DOI: 10.1016/j.tiv.2021.105152]
12 **Shaughnessy M**, Lamuraglia G, Klebanov N, Ji Z, Rajadurai A, Kumar R, Flaherty K, Tsao H. Selective uveal melanoma inhibition with calcium channel blockade. *Int J Oncol* 2019; **55**: 1090-1096 [PMID: 31545410 DOI: 10.3892/ijo.2019.4873]
13 **Schwarz DS**, Blower MD. The endoplasmic reticulum: structure, function and response to cellular signaling. *Cell Mol Life Sci* 2016; **73**: 79-94 [PMID: 26433683 DOI: 10.1007/s00018-015-2052-6]

14 **Groenendyk J**, Agellon LB, Michalak M. Calcium signaling and endoplasmic reticulum stress. *Int Rev Cell Mol Biol* 2021; **363**: 1-20 [PMID: 34392927 DOI: 10.1016/bs.ircmb.2021.03.003]

15 **Di Conza G**, Ho PC. ER Stress Responses: An Emerging Modulator for Innate Immunity. *Cells* 2020; **9** [PMID: 32178254 DOI: 10.3390/cells9030695]

16 **Zhu L**, Zhou Q, He L, Chen L. Mitochondrial unfolded protein response: An emerging pathway in human diseases. *Free Radic Biol Med* 2021; **163**: 125-134 [PMID: 33347985 DOI: 10.1016/j.freeradbiomed.2020.12.013]

17 **Yin Y**, Sun G, Li E, Kiselyov K, Sun D. ER stress and impaired autophagy flux in neuronal degeneration and brain injury. *Ageing Res Rev* 2017; **34**: 3-14 [PMID: 27594375 DOI: 10.1016/j.arr.2016.08.008]

18 **Hetz C**, Zhang K, Kaufman RJ. Mechanisms, regulation and functions of the unfolded protein response. *Nat Rev Mol Cell Biol* 2020; **21**: 421-438 [PMID: 32457508 DOI: 10.1038/s41580-020-0250-z]

19 **Lee WS**, Yoo WH, Chae HJ. ER Stress and Autophagy. *Curr Mol Med* 2015; **15**: 735-745 [PMID: 26391548 DOI: 10.2174/1566524015666150921105453]

20 **Limonta P**, Moretti RM, Marzagalli M, Fontana F, Raimondi M, Montagnani Marelli M. Role of Endoplasmic Reticulum Stress in the Anticancer Activity of Natural Compounds. *Int J Mol Sci* 2019; **20** [PMID: 30813301 DOI: 10.3390/ijms20040961]

21 **Lai ST**, Wang Y, Peng F. Astragaloside IV sensitizes non-small cell lung cancer cells to cisplatin by suppressing endoplasmic reticulum stress and autophagy. *J Thorac Dis* 2020; **12**: 3715-3724 [PMID: 32802451 DOI: 10.21037/jtd-20-2098]

22 **Sukumaran P**, Nascimento Da Conceicao V, Sun Y, Ahamad N, Saraiva LR, Selvaraj S, Singh BB. Calcium Signaling Regulates Autophagy and Apoptosis. *Cells* 2021; **10** [PMID: 34440894 DOI: 10.3390/cells10082125]

23 **Patergnani S**, Danese A, Bouhamida E, Aguiari G, Previati M, Pinton P, Giorgi C. Various Aspects of Calcium Signaling in the Regulation of Apoptosis, Autophagy, Cell Proliferation, and Cancer. *Int J Mol Sci* 2020; **21** [PMID: 33171939 DOI: 10.3390/ijms21218323]

24 **Ye L**, Zeng Q, Ling M, Ma R, Chen H, Lin F, Li Z, Pan L. Inhibition of IP3R/Ca2+ Dysregulation Protects Mice From Ventilator-Induced Lung Injury *via* Endoplasmic Reticulum and Mitochondrial Pathways. *Front Immunol* 2021; **12**: 729094 [PMID: 34603302 DOI: 10.3389/fimmu.2021.729094]

25 **Santa-Helena E**, Cabrera DDC, D'Oca MGM, Scaini JLR, de Oliveira MWB, Werhli AV, Machado KDS, Gonçalves CAN, Nery LEM. Long-chain fatty dihydropyridines: Docking calcium channel studies and antihypertensive activity. *Life Sci* 2020; **259**: 118210 [PMID: 32763289 DOI: 10.1016/j.lfs.2020.118210]

26 **Wu L**, Lin W, Liao Q, Wang H, Lin C, Tang L, Lian W, Chen Z, Li K, Xu L, Zhou R, Ding Y, Zhao L. Calcium Channel Blocker Nifedipine Suppresses Colorectal Cancer Progression and Immune Escape by Preventing NFAT2 Nuclear Translocation. *Cell Rep* 2020; **33**: 108582 [PMID: 33378684 DOI: 10.1016/j.celrep.2020.108582]

27 **Shiozaki A**, Katsurahara K, Kudou M, Shimizu H, Kosuga T, Ito H, Arita T, Konishi H, Komatsu S, Kubota T, Fujiwara H, Okamoto K, Otsuji E. Amlodipine and Verapamil, Voltage-Gated Ca(2+) Channel Inhibitors, Suppressed the Growth of Gastric Cancer Stem Cells. *Ann Surg Oncol* 2021; **28**: 5400-5411 [PMID: 33566246 DOI: 10.1245/s10434-021-09645-0]

28 **Delbrel E**, Soumare A, Naguez A, Label R, Bernard O, Bruhat A, Fafournoux P, Tremblais G, Marchant D, Gille T, Bernaudin JF, Callard P, Kambouchner M, Martinod E, Valeyre D, Uzunhan Y, Planès C, Boncoeur E. HIF-1α triggers ER stress and CHOP-mediated apoptosis in alveolar epithelial cells, a key event in pulmonary fibrosis. *Sci Rep* 2018; **8**: 17939 [PMID: 30560874 DOI: 10.1038/s41598-018-36063-2]

29 **Hu H**, Tian M, Ding C, Yu S. The C/EBP Homologous Protein (CHOP) Transcription Factor Functions in Endoplasmic Reticulum Stress-Induced Apoptosis and Microbial Infection. *Front Immunol* 2018; **9**: 3083 [PMID: 30662442 DOI: 10.3389/fimmu.2018.03083]

30 **Imran M**, Rauf A, Abu-Izneid T, Nadeem M, Shariati MA, Khan IA, Imran A, Orhan IE, Rizwan M, Atif M, Gondal TA, Mubarak MS. Luteolin, a flavonoid, as an anticancer agent: A review. *Biomed Pharmacother* 2019; **112**: 108612 [PMID: 30798142 DOI: 10.1016/j.biopha.2019.108612]

31 **Han CC**, Wan FS. New Insights into the Role of Endoplasmic Reticulum Stress in Breast Cancer Metastasis. *J Breast Cancer* 2018; **21**: 354-362 [PMID: 30607156 DOI: 10.4048/jbc.2018.21.e51]

32 **Li H**, Chen X, Gao Y, Wu J, Zeng F, Song F. XBP1 induces snail expression to promote epithelial- to-mesenchymal transition and invasion of breast cancer cells. *Cell Signal* 2015; **27**: 82-89 [PMID: 25280941 DOI: 10.1016/j.cellsig.2014.09.018]

33 **Cuevas EP**, Eraso P, Mazón MJ, Santos V, Moreno-Bueno G, Cano A, Portillo F. LOXL2 drives epithelial-mesenchymal transition *via* activation of IRE1-XBP1 signalling pathway. *Sci Rep* 2017; **7**: 44988 [PMID: 28332555 DOI: 10.1038/srep44988]

34 **Liu SH**, Lee WJ, Lai DW, Wu SM, Liu CY, Tien HR, Chiu CS, Peng YC, Jan YJ, Chao TH, Pan HC, Sheu ML. Honokiol confers immunogenicity by dictating calreticulin exposure, activating ER stress and inhibiting epithelial-to-mesenchymal transition. *Mol Oncol* 2015; **9**: 834-849 [PMID: 25619450 DOI: 10.1016/j.molonc.2014.12.009]

35 **Markov AV**, Odarenko KV, Sen'kova AV, Salomatina OV, Salakhutdinov NF, Zenkova MA. Cyano Enone-Bearing Triterpenoid Soloxolone Methyl Inhibits Epithelial-Mesenchymal Transition of Human Lung Adenocarcinoma Cells In Vitro and Metastasis of Murine Melanoma In Vivo. *Molecules* 2020; **25** [PMID: 33327637 DOI: 10.3390/molecules25245925]

36 **Adacan K**, Obakan-Yerlikaya P, Arisan ED, Coker-Gurkan A, Kaya RI, Palavan-Unsal N. Epibrassinolide-induced autophagy occurs in an Atg5-independent manner due to endoplasmic stress induction in MEF cells. *Amino Acids* 2020; **52**: 871-891 [PMID: 32449072 DOI: 10.1007/s00726-020-02857-w]

37 **Zhou B**, Lu Q, Liu J, Fan L, Wang Y, Wei W, Wang H, Sun G. Melatonin Increases the Sensitivity of Hepatocellular Carcinoma to Sorafenib through the PERK-ATF4-Beclin1 Pathway. *Int J Biol Sci* 2019; **15**: 1905-1920 [PMID: 31523192 DOI: 10.7150/ijbs.32550]

World Journal of Gastroenterology

Submit a Manuscript: https://www.f6publishing.com

World J Gastroenterol 2024 January 28; 30(4): 381-417

DOI: 10.3748/wjg.v30.i4.381

ISSN 1007-9327 (print) ISSN 2219-2840 (online)

SYSTEMATIC REVIEWS

Current status of magnetic resonance imaging radiomics in hepatocellular carcinoma: A quantitative review with Radiomics Quality Score

Valentina Brancato, Marco Cerrone, Nunzia Garbino, Marco Salvatore, Carlo Cavaliere

Specialty type: Gastroenterology and hepatology

Provenance and peer review: Invited article; Externally peer reviewed.

Peer-review model: Single blind

Peer-review report's scientific quality classification

Grade A (Excellent): 0
Grade B (Very good): B, B
Grade C (Good): 0
Grade D (Fair): 0
Grade E (Poor): 0

P-Reviewer: Wang W, China; Wang SM, China

Received: October 31, 2023
Peer-review started: October 31, 2023
First decision: November 24, 2023
Revised: December 5, 2023
Accepted: January 10, 2024
Article in press: January 10, 2024
Published online: January 28, 2024

Valentina Brancato, Department of Information Technology, IRCCS SYNLAB SDN, Naples 80143, Italy

Marco Cerrone, Nunzia Garbino, Marco Salvatore, Carlo Cavaliere, Department of Radiology, IRCCS SYNLAB SDN, Naples 80143, Italy

Corresponding author: Marco Cerrone, BSc, Researcher, Department of Radiology, IRCCS SYNLAB SDN, Via E. Gianturco 113, Naples 80143, Italy. marco.cerrone@synlab.it

Abstract

BACKGROUND

Radiomics is a promising tool that may increase the value of magnetic resonance imaging (MRI) for different tasks related to the management of patients with hepatocellular carcinoma (HCC). However, its implementation in clinical practice is still far, with many issues related to the methodological quality of radiomic studies.

AIM

To systematically review the current status of MRI radiomic studies concerning HCC using the Radiomics Quality Score (RQS).

METHODS

A systematic literature search of PubMed, Google Scholar, and Web of Science databases was performed to identify original articles focusing on the use of MRI radiomics for HCC management published between 2017 and 2023. The methodological quality of radiomic studies was assessed using the RQS tool. Spearman's correlation (ρ) analysis was performed to explore if RQS was correlated with journal metrics and characteristics of the studies. The level of statistical significance was set at $P < 0.05$.

RESULTS

One hundred and twenty-seven articles were included, of which 43 focused on HCC prognosis, 39 on prediction of pathological findings, 16 on prediction of the expression of molecular markers outcomes, 18 had a diagnostic purpose, and 11 had multiple purposes. The mean RQS was 8 ± 6.22, and the corresponding percentage was 24.15% ± 15.25% (ranging from 0.0% to 58.33%). RQS was positively correlated with journal impact factor (IF; ρ = 0.36, $P = 2.98 \times 10^{-5}$), 5-

years IF ($\rho = 0.33$, $P = 1.56 \times 10^{-4}$), number of patients included in the study ($\rho = 0.51$, $P < 9.37 \times 10^{-10}$) and number of radiomics features extracted in the study ($\rho = 0.59$, $P < 4.59 \times 10^{-13}$), and time of publication ($\rho = -0.23$, $P < 0.0072$).

CONCLUSION

Although MRI radiomics in HCC represents a promising tool to develop adequate personalized treatment as a noninvasive approach in HCC patients, our study revealed that studies in this field still lack the quality required to allow its introduction into clinical practice.

Key Words: Hepatocellular carcinoma; Systematic review; Magnetic resonance imaging; Radiomics; Radiomics quality score

Core Tip: This systematic review aimed at evaluating the status of magnetic resonance imaging (MRI) radiomic studies related to hepatocellular carcinoma (HCC) using the Radiomics Quality Score (RQS) to assess methodological quality. A systematic literature search identified 127 articles covering various steps of HCC management. The mean RQS was 8 ± 6.22, with significant variation. RQS was significantly correlated with journal impact factor (IF), 5-year IF, the number of patients involved, the number of radiomic features extracted, and the publication year. Despite the potential of MRI radiomics in HCC, its clinical implementation is hindered by a lack of quality in studies in this field.

Citation: Brancato V, Cerrone M, Garbino N, Salvatore M, Cavaliere C. Current status of magnetic resonance imaging radiomics in hepatocellular carcinoma: A quantitative review with Radiomics Quality Score. *World J Gastroenterol* 2024; 30(4): 381-417
URL: https://www.wjgnet.com/1007-9327/full/v30/i4/381.htm
DOI: https://dx.doi.org/10.3748/wjg.v30.i4.381

INTRODUCTION

Medical imaging has progressed over the last few decades from a simple diagnostic tool for diseases to a massive supply of quantitative data free of the normal subjective interpretation that characterizes conventional clinical practice. The introduction of technological advances and the quest for precision medicine have given rise to a new potential branch of research known as "radiomics". Radiomics is a quantitative technique that turns digitized medical pictures into high-dimensional mineable features that may be correlated with clinical endpoints such as pathological findings, treatment response, and survival. Radiomics can also be integrated with other quantitative data, such as genomics and pathomics data, to provide a comprehensive approach to disease[1-4]. As a quantitative analysis of digital images, radiomics has the potential to reveal specific disease characteristics that are otherwise inaccessible to the naked eye using conventional imaging modalities. This method may increase the quantity of clinically relevant data that may be extracted from medical images, offering the possibility of discovering innovative imaging biomarkers for the diagnosis, characterization, and prediction of outcomes in a wide range of diseases, including oncologic diseases[5]. In the field of oncology, the rationale behind radiomics is that biological tumor characteristics might be mirrored by quantifying medical image heterogeneity using extracted radiomic features, encompassing aspects of tumor progression, response to therapeutic interventions, and clinical outcomes. Quantitative imaging has garnered significant interest in the non-invasive detection of tumor heterogeneity, and recent radiomics studies across various oncological fields have shown a strong association between imaging heterogeneity and the characteristics of solid tumors[6].

Hepatocellular carcinoma (HCC) is one of the leading causes of cancer-related deaths worldwide and poses serious challenges for screening, early diagnosis and treatment firstly because most HCC is diagnosed at an advanced stage when curative treatment options are limited, and also because of its complex heterogeneity at multiple levels: heterogeneity between tumor nodules from the same patient (intertumor heterogeneity), within the same tumor nodule (intratumor heterogeneity) and between patients (interpatient heterogeneity)[7,8]. Furthermore, current clinical practice based on single bioptic or tumor tissue section fails to discover useful biomarkers, and many existing staging systems for HCC are based on postoperative pathological examinations, which cannot aid in preoperative decision-making[9]. In contrast to numerous other solid tumors, HCC can be diagnosed by using distinctive enhancement patterns on dynamic multiphasic CT or magnetic resonance imaging (MRI), without additional histopathologic confirmation[10,11]. Although imaging plays an important role in the screening, early identification, and management of HCC patients, the imaging evaluation of HCC is still based on subjective interpretation of qualitative imaging descriptors and tumor size estimate, both of which are prone to variability[10,12,13]. Of note, although CT is more generally available, faster, and needs less experience to administer and interpret pictures than MRI, its downsides include radiation exposure and low soft tissue contrast, which demands the use of iodinated contrast agents. The increased soft tissue contrast of MRI, on the other hand, enables for the examination of a range of tissue features that may be relevant in HCC therapy[14,15]. In this context, recent advantages in MRI radiomics can potentially address the urgent need for noninvasive, radiation-free strategies that can aid in the early detection of HCC and preoperative prediction of tumor behavior, as well as address the inherent variability of qualitative imaging descriptors and provide previously unavailable information to obtain a better

stratification of HCC patients for a more precise treatment decision making.

Over the last decade, there has been a significant increase in radiomics studies in the field of HCC. Many of these studies have demonstrated the effectiveness of radiomic features for differential diagnosis, grading, predicting microvascular invasion, overall survival, recurrence, and treatment response[16-19]. Nevertheless, radiomics is presently limited to academic literature in the context of HCC, as physicians question its utility due to the absence of a translation from research studies to clinical application. This is attributed, at least in part, to the overall deficiency of streamlined and productive methods for integrating imaging biomarkers into clinical practice[20-22]. Lambin *et al*[2] developed the Radiomics Quality Score (RQS) to provide a standardized evaluation of the radiomics performance, reproducibility, and clinical. The RQS metric system determines the validity and comprehensiveness of radiomics investigations. This tool is modality-independent tool and was designed to assess the methodological quality of radiomics studies. The methodology and analyses of a radiomics study are evaluated based on 16 criteria that reward or penalize, promoting the best scientific practice[2]. Recent research tried to examine the current state of the art in HCC radiomics, stressing the major concepts, clinical applications, and limitations[23-25]. However, it is clear from these research that the bulk of radiomic investigations on HCC have been conducted on CT, with only a few looking into MRI. Furthermore, the quality of science and reporting in HCC MRI radiomics research investigations is mainly unknown.

Hence, the objective of this study was to provide a comprehensive overview of the existing state of MRI radiomic investigations related to HCC. Simultaneously, we aimed to evaluate the methodological quality of each study using the RQS to assess the radiomics analyses conducted in prior publications. The study's goal is to promote the quality of MRI radiomics research studies in HCC as a diagnostic, prognostic, and/or predictive tool, to allow radiomics to become an appropriate medical decision-making tool by facilitating the combined analysis of clinical data and high-throughput imaging features, while taking advantage of the benefits arising from the MRI technique.

MATERIALS AND METHODS

Search strategy and selection criteria

A systematic search was conducted for all published studies exploring the role of MRI radiomics in the field of HCC. PubMed, Web of Science and Google Scholar electronic databases were comprehensively explored and used to build the search. Only studies published in the last six years were selected. The last search was performed on June 1, 2023. The search terms consisted in: ("radiomics" OR "texture" OR "histogram") AND ("MRI" OR "Magnetic Resonance Imaging") AND ("Hepatocellular Carcinoma" OR "HCC"). The literature search was limited to English language publications and studies of human subjects. Two reviewers, after having independently screened the identified titles and abstracts, assessed the full text of articles aiming at exploring MRI radiomics in the field of HCC and that were not review articles. For articles meeting these criteria with full text available, the following further selection criteria had to be fulfilled: Involvement of adult patients (age > 18 years); involvement of patients with HCC confirmed by pathology and/or surgery and/or overall analysis combined with medical history, clinical symptoms, and imaging data; presence of information about MRI protocol. Moreover, studies were excluded if they performed analyses on mixed patients (*e.g.*, groups of patients with multiple hepatic malignant diseases) that did not allow conclusions to be drawn only about HCC patients; if they did not evaluate an outcome measure; if they were focused only on semantic imaging features (radiologist-dependent). After selecting the studies that met the inclusion and exclusion criteria, reference lists of these studies were also searched in order to recruit any potential eligible studies. In addition, pre-existing reviews/systematic reviews/meta-analyses were also searched in order to recruit any other potentially eligible studies from their reference lists.

Planning and conducting the review

After the above-mentioned selection procedure, selected articles were analysed by two reviewers, and data useful for conducting the systematic review were collected in a predesigned sheet. Extracted data will include the following: first author name, publication year, Journal name, scientometric indexes [impact factor (IF), 5-years IF, CiteScore, H-index, first author IF with and without self-citations], study design, in particular prospective/retrospective, clinical purpose, specific output measured in the study, number and type of patients, imaging modalities used for radiomic feature extraction, information on region of interest (ROI)/volume of interest (VOI) placement (segmentation technique and ROI/VOI type), software used for radiomic feature extraction, number and features type, feature selection methods (if used), classification methods, information on if models were applied to a separate dataset, highest accuracy/most important results and main findings.

This systematic review was conducted according to the PRISMA statement[26].

Quality assessment with RQS

The methodological quality of each radiomics study was assessed by two reviewers using the RQS tool[2]. The assessment was performed independently, and any disagreement was resolved by consensus. RQS tool is composed of 16 items structured to assess various crucial steps in the workflow of radiomics analyses (see Supplementary Table 1). In particular, a maximum of 36 points can be assigned to each study: up to 2 points for the first RQS checkpoint (a single item, namely "Image protocol quality"), up to 3 points for the second RQS checkpoint (3 items, specifically on multiple segmentation strategies, the use of phantoms and multiple imaging time points) and up to 31 points for the third RQS checkpoint (12 items, encompassing feature extraction, exploratory analysis design as well as model building and validation). The total score ranges between −8 and 36 and can be translated into a final 0–100 RQS percentage, with −8 to

0 defined as 0%, indicating the lowest quality, and 36 as 100%, indicating the highest quality in terms of the methodology and reporting standards of the radiomics study[2].

Correlation analysis between RQS and journal metrics

Spearman's correlation (ρ) analysis was performed to explore if there was a correlation between RQS and journal metrics, comprising IF of the journal at the year of publication, 5-year IF, CiteScore, and H-index at the year of publication. Additionally, Spearman's correlation was used to explore the correlation between RQS and H-index of the first author at the year of publication of the study (both with and without self-citations), time of publication (calculated as time between the publication date and the date of last literature research, in months), as well as the association with the number of patients involved and the number of radiomic features extracted in the study. Finally, to explore if there was a difference in RQS according to clinical purpose of the study, a subgroup analysis using Kruskal-Wallis H test was performed. In case of significance, Wilcoxon rank-sum post hoc tests with Bonferroni correction were carried out on each pair of groups. The significance level was set at 0.05. All statistical analysis was performed using SPSS (version 27).

RESULTS

Study selection

A total of 537 articles were identified from scientific electronic scientific databases. Only 211 articles were retained after the removal of duplicates.

We reviewed the titles and abstracts of these records, excluding 59 due to non-compliance with inclusion criteria (29 unrelated to the topic, 16 were reviews, 5 conducted analyses on mixed patients, and 9 did not assess an outcome measure). The full text of 149 articles was assessed, leading to the exclusion of 16 off-topic articles. Additionally, four studies were excluded for not evaluating an outcome measure, and two for analyzing mixed patients. Thirteen more articles were found through references in selected articles or existing reviews/systematic reviews/meta-analyses, and seven of these were incorporated into the review. A total of 127 data sets were included in the review. Figure 1 shows the PRISMA flow diagram of the included studies based on the inclusion and exclusion criteria.

Characteristics of included studies

The details regarding the characteristics of the 127 studies chosen for this review are presented in Table 1. Approximately half of these studies (51 out of 127) were published in the last two years, and only 9 studies deviated from a retrospective design. Most of the selected studies (43 out of 127) explored radiomic approaches for HCC prognosis after surgical, radiofrequency ablation and/or trans-arterial chemo embolization treatment. Forty studies investigated the ability of radiomics in predicting pathological findings [*e.g.*, microvascular invasion (MVI), vessels encapsulating tumor clusters, histologic grade], of which 27 aimed at investigating the performance of radiomics analysis for MVI prediction. Sixteen studies aimed at exploring if MRI radiomics could infer the expression of molecular markers (*e.g.*, CK19, Ki67, GPC3) outcomes. Among the remaining studies, 24/127 aimed to evaluate the power of radiomics for distinguishing HCC from other solid hepatic lesions, while 11 had multiple aims.

The number of total included patients was 18.949, with a sample size varying from 17 to 602 patients (median: 309.5). Most studies (96 out of 127) explored more than one phase/sequence to perform radiomic analysis. Most studies (106 out of 127) performed 3D segmentation. In 114 of them, segmentation was manually performed, while in the remaining studies was used a semiautomatic (12 studies) or automatic (2 study) segmentation approach. Concerning software used for feature extraction, PyRadiomics was the most popular (used in 42 out of 127 studies), followed by AK software (used in 23 out of 127 studies) and Matlab (used in 19 out of 127studies). The number of radiomics features extracted from each phase/sequence ranged from 3 to 3144 (mean: 68 ± 206). Shape features were extracted in 55 out of 127 studies, first-order features in all but three studies, textural features in 82/127 studies, and features from filtered images (*e.g.*, wavelet, Laplacian of gaussian) in 34 out of 127 studies. Concerning feature selection algorithms, the Least Absolute Shrinkage and Selection Operator regression was the most widely used (used in 55 out of 127 studies). Other frequently used algorithms for feature selection were intra-class correlation coefficient (used in 25 studies), correlation (used in 12 studies) and minimum redundancy maximum relevancy (used in 9 studies). The performance metrics of the studies, when present, corresponded to accuracy in 9 out of 127 studies, area under the receiver operating characteristic curve (AUC) in 99 out of 127 studies and to C-index in 12 out of 127 studies. Most studies involved machine learning techniques for radiomic analysis, of which 51 splitted the subjects into training and test cohort to test the prediction models performance. Further details on these characteristics can be found in Table 1 and Supplementary Table 2.

Quality assessment with RQS

Supplementary Table 3 provides the RQS details of all included studies. The average total RQS score was 8 ± 6.22, corresponding to a percentage of 24.15% ± 15.25%, with a range from 0.0% to 58.33% (Figure 2). Concerning the first RQS checkpoint, nearly all studies, excluding ten, provided thorough documentation of the imaging protocol, yet none achieved the maximum points for utilizing a public protocol. In relation to the second RQS checkpoint (items 2 to 4), a majority of studies (84.25%, 107 out of 127) employed multiple segmentation, mainly by different radiologists, but none of the articles met the requirement for 'imaging at multiple time points' and only one article met the requirement for a 'phantom study'. With respect to the third RQS checkpoint (items 5 to 16), feature reduction techniques were applied in all but 15 studies (88.28%). Multivariable analysis with non-radiomics features was performed in 85 studies (66.92%) of

Table 1 Characteristics of included studies

Ref.	ST	CP	Specific outcome	NP (type)	Modalities used for feature extraction	Seg	Software used for feature extraction	Features number (type)	FS	CM	Model applied to a separate dataset?	Most important result	Main findings
Liu *et al* [42], 2023	R	PPF	MVI	104 (HCC)	T2WI	M, 3D	AK SOFTWARE	851 (first order, shape, GLCM, GLSZM, GLRLM, NGTDM, and GLDM)	LASSO, LR	LR	Yes	AUC = 0.867 in the TS, 0.820 in the VS	A prediction model using radiomic features from single T2WI can predict MVI in HCC
Wang *et al* [43], 2023	R	PR	LRT	100 (HCC)	AP, PVP, T2WI	M, 3D	3D SLICER	851 (first-order, shape, GLCM, GLDM, GLSZM, GLRLM, NGTDM and wavelet)	*t*-test/Mann Whitney, LASSO	ROC	Yes	AUC = 0.867	MRI-based radiomics analysis may serve as a promising and noninvasive tool to predict outcome of locoregional treatment in HCC patients
Gong *et al* [44], 2023	R	MC	PD-1/PD-L1	108 (HCC)	T2WI FS, AP, PVP	M, 3D	NS	352 (GLCM, GLRLM, intensity histogram, and shape)	ICC, *t*-test/ MANN WHYTNEY, LASSO	LR	Yes	AUC = 0.946 in the TS and 0.815 in the VS	A radiomics model based on multisequence MRI has the potential to predict the preoperative expression of PD-1 and PD-L1 in HCC
Zhang *et al* [45], 2023	R	MC	CK 19+/-HCC	311 (HCC)	T1WI, T2WI, DWI, AP, VP, and DP	M, 3D	uRP	2286 (first order, wavelet)	ICC, LASSO	LR	Yes	in the TS (C-index, 0.914), internal (C-index, 0.855), and external VS (C-index, 0.795)	The combined model based on clinic-radiological radiomics features can be used for predicting CK19+ HCC preoperatively
Zhang *et al* [46], 2023	R	PPF	MTM HCC	232 (HCC)	DCE-MRI	M, 3D	Pyradiomics	1037 (first order, shape GLRLM, GLSZM, NGTDM, GLCM, GLDM LoG and wavelet)	ICC, GBDT	LR, KNN, Naive-Bayes, Decision Tree, SVM	Yes	AUCs of 0.896 and 0.805 in the TS e VS	The nomogram containing radiomics, age, alpha-fetoprotein, tumour size, and tumour-to-liver ADC ratio revealed excellent predictive ability in preoperatively identifying the MTM-HCC Subtype
Dong *et al* [47], 2024	R	D, PR	VETC	221 (HCC)	DCE-MRI	M, 3D	Pyradiomics	1218 (FIRST ORDER)	ICC	LR, decision tree, RF, SVM, KNN, and Bayes	Yes	AUC = 0.844	The DLR model provides a noninvasive method

												to discriminate VETC status and prognosis of HCC patients preoperatively
Tabari *et al* [48], 2023	R	PPF	Pre-ablation tumor radiomics	97 (HCC)	AP, DCE-MRI	M, 3D	NS	112 first-order, (GLCM, GLDM, GLRLM, GLSZM, NGTDM)	mRMR	RF	Yes	AUC = 0.83	Pre-ablation MRI radiomics could act as a valuable imaging biomarker for the prediction of tumor pathologic response in patients with HCC
Cao *et al* [49], 2023	R	PR	RFS	249 (HCC)	T2WI FS, T1WI FS, DCE-MRI	M, 3D	Pyradiomics	NS (first-order, shape, and texture, wavelet, Laplacian)	LASSO	Cox regression	Yes	C-index = 0.893 TS, 0.851 (test set), 0.797 (external)	The combined radiomic model provides superior ability to discern the possibility of recurrence-free survival in HCC over the total radiomic and the clinical–radiological models
İnce *et al* [50], 2023	R	PPF	TARE	82 (HCC)	DCE-MRI	S, 3D	Pyradiomics	1128 (first-order, GLCM, GLDM, GLRLM, GLSZM, and NGTDM)	ICC, PCA, SFS	SVM, LR, RM, LightGBM	No	AUC = 0.94	Machine learning–based clinicoradiomic models demonstrated potential to predict response to TARE
Chen *et al* [51], 2023	R	PR	TACE	144 (HCC)	T2WI, AP, PVP, DP	M, 3D	Pyradiomics	110 (NS)	mRMR, LASSO, DNN	SVM, LR	Yes	AUC = 0.974	DNN model performs better than other classifiers in predicting TACE response. Integrating with clinically significant factors, the CD model may be valuable in pre-treatment counseling of HCC patients who may benefit the most from TACE intervention
Jiang *et al* [52], 2023	R	PPF	MVI	102 (HCC)	T1_in, T1_A, T2W, DWI	M, 3D	Pyradiomics	1967 (first-order, shapes, textures, GLCM, GLSZM, GLDM, GLRLM, and filter-transformed)	LASSO	ULR	Yes	AUC = 0.901, 0.923 for TS and VS	The multiparametric MRI-based radiomics nomogram is a promising tool for the preoperative diagnosis of peritumoral MVI in

												HCCs
Hu *et al* [53], 2023	R	D, MC	CK19+	110 (HCC)	AP, VP, HBP	M, 3D	PyRadiomics	1130 (shape, first order, GLCOM, GLRLM, GLSZ, GLDM)	ICC	RFE	No	AUC = 0.92	The established radiomics signature based on preoperative gadoxetic acid-enhanced MRI could be an accurate and potential imaging biomarker for HCC CK19 (+) prediction
Chong *et al* [54], 2023	R	MC, PR	Glypican 3-Positive HCC	259 (HCC)	T2WI, DWI, PRE, AP, PVP, TP and HBP	M, 3D	PyRadiomics	749 (first order statistics, shape and size) and textural property types (GLSZM, GLCM, GLDM, GLRLM, and NGTDM)	Test-retest procedure, ICC, LASSO, RF, SVM	LR, RF, SVM	Yes	AUC = 0.943 *vs* 0.931 TS and VS respectively	Preoperative EOB-MRI radiomics-based nomogram satisfactorily distinguished GPC3 status and outcomes of solitary HCC 5 cm
Hu *et al* [55], 2023	R	D, PPF	Functional liver reserve	403 (HCC)	DCE MRI	M, 3D	Pyradiomics	851 (shape, first-order GLCM, GLRLM, GLSZ, GLDM, NGTDM, wavelet)	ICC, Spearman's correlation	LR, SVM	No	AUC = 0.71	A radiomics model based on gadoxetic acid-enhanced MRI was constructed in this study to discriminate HCC with different histopathologic grades
Tao Y *et al* [56], 2023	R	MC	PD-L2	108 (HCC)	T2WI, AP, PV	M, 3D	R	1130	ICC, LASSO	ROC	No	AUC = 0.871	Prediction based on the radiomic characteristics of MRI could noninvasively predict the expression of PD-L2 in HCC
Yang *et al* [57], 2022	R	PR	ER	181 (HCC)	T1WI, T2WI	M, 3D	LIFEx	34 (Histogram, Shape)	LASSO	ROC	Yes	AUC = 0.79	The model for early recurrence of HCC after ablation based on the clinical, imaging, and radiomics features presented good predictive performance
Liu *et al* [58], 2023	R	PPF	MVI	161 (HCC)	AP, PVP, DP	M, 3D	3D Slicer, Pyradiomics	321 (shape, first-order histogram, GLCM, GLDM, GLRLM, GLSZM, NGTDM)	LASSO, ICC	LR	Yes	AUC = 0.87	The nomogram model can effectively predict MVI in patients with HCC
Zhang *et al* [59], 2022	R	PPF	MVI	189 (HCC)	HBP	M, 3D	IBEX SOFTWARE	1768	LASSO, ICC	nomogram	Yes	AUC = 0.884	Depending on the clinicoradiological factors and

												radiological features, nomograms can effectively predict MVI status in HCC patients
Sim *et al* [60], 2022	R	PPF	MVI	50 (HCC)	T1 AP, T1PVP	M, 2D	MaZda	290 (area, histogram, gradient, GLCM, GLRLM, autoregressive, and wavelet)	Mutual Information, recursive pruning	SVM	No	Accuracy = 0.878	Texture analysis of tumours on pre-operative MRI can predict presence of MVI in HCC
Zhang *et al* [61], 2022	R	PR	RFA, ER	90 (HCC)	T1WI, T2WI, CE-MRI	M, 2D	AK Software	1316 (first-order histogram, shape, texture, GLCM, GLRLM, GLSZM, NGTDM, GLDM, and local binary pattern, high-order, and wavelet)	ANOVA	RF, LASSO	Yes	AUC of 0.822 in the TS and 0.812 in the VS	The multi-parametric MRI-based radiomics nomogram has a high predictive value for ER of small HCC after RFA
Zhao *et al* [62], 2023	R	PR	HAIC	112 (HCC)	T2WI	M, 3D	AK software	396 (histogram, form factor, texture, GLZSM, GLCM, GLRLM, and Haralick)	LASSO	ROC	Yes	Accuracy = 0.81	The nomogram based on the combined model consisting of MRI radiomics and ALBI score could be used as a biomarker to predict the therapeutic response of unresectable HCC after HAIC
Lu *et al* [63], 2022	R	PPF	MVI	165 (HCC)	T2WI, DWI (b = 800 s/mm^2), T1WI, AP, PP, TP, and HBP	M, 3D	Pyradiomics	1227 (shape, first-order, texture, GLSZM, GLRLM, GLCM, NGTDM, and GLDM)	LASSO	multivariate LR	Yes	AUC = 0.826	The combined model based on radiomics features of Gd-EOB-DTPA enhanced MRI, tumour margin, and peritumoural hypointensity was valuable for predicting HCC MVI
Yang *et al* [64], 2022	R	PPF	MVI	110 (HCC)	DCE-MRI	M, 3D	A.K. Software	11 (Grey Histogram, GLCM)	NO	ROC	No	AUC = 0.797	The combination of MR image features and texture analysis may improve the efficiency in prediction of MVI
Ameli *et al* [65], 2022	R	D	Degree of tumor differentiation	129 (HCC)	ADC, VE MAPS	S, 3D	MATLAB R2017B	95 (global, histogram, GLCM, GLRLM, GLSZM, NGTDM)	multi-class classification algorithm	RF	Yes	AUC = 0.832	The addition of radiomics-based texture analysis improved HCC grading over that of

												ADC or venous enhancement values alone
Li *et al*[66], 2022	R	PR	ER	302 (HCC)	T2WI, DWI (800 s/mm^2), AP, and PVP	M, 3D	Pyradiomics	853 (shape, first order, texture, and wavelet)	SPSS, LASSO, ICC	ROC	Yes	AUCs of 0.91 and 0.87 in the TS and VS	The proposed predictive model incorporating clinico-radiological factors and the fusion radiomics signature derived from multiparametric MR images may be an effective tool for the individualized prediction of postoperative ER in patients with HCC
Zeng *et al* [67], 2022	R	PPF	BETA-CATENIN MUTATION	98 (HCC)	AP, PVP, DP, HBP	M, 3D	Pyradiomics	1674 (first order, GLCOM, GLSZM, GLRLM, GLDM)	T-test, fisher's exact test	LSVC	Yes	AUC = 0.86	The RHBP radiomics model may be used as an effective model indicative of HCCs with b-catenin mutation preoper-atively
Aujay *et al* [68], 2022	R	PR	TARE	22 (HCC)	AP, PVP	M, 3D	Pyradiomics	107 (Shape, first- and second- order)	Mann-Whitney U test	LR	No	AUC = 0.92	Radiomics could aid in the prediction of early treatment response following TARE in patients with HCC
Chen *et al* [69], 2022	R	PPF	MVI	415 (HCC)	T1WI, T2WI, DWI, AP, PVP, HBP	M, 3D	R	1409 (First order, shape, two order texture, Laplacian, wavelet, logarithmic, and exponential filters)	LASSO	SVM, XGBoost, RF, LR	Yes	AUC = 0.979	Machine learning with an LR classifier yielded the best radiomics score for HBP and DWI. The radiomics nomogram developed as a noninvasive preoperative prediction method showed favorable predictive accuracy for evaluating MVI in sHCC
Wu *et al* [70], 2023	R	D	DP-HCC	179 (DPHCC, non DPHCC)	DCE-MRI	M, 3D	PyRadiomics	1781 (first-order statistics, shape, and texture)	PCC, RFE	SVM, LR, LR-LASSO	Yes	AUC = 0.908	MRI radiomics models may be useful for discriminating DPHCC from non-DPHCC before

												surgery
Li *et al*[71], 2022	R	PPF	MVI	113 (HCC)	T2WI, T1WI, DCE MRI	M, 2D	MaZda	101 (histogram, GLCOM, GLRLM)	*t*-test, Mann-whitney *U* test	ROC	No	AUC = 0.939	Noninvasive MRI radiomic model based on MDF values and imaging biomarkers may be useful to make preoperative prediction of MVI in patients with primary HCC
Wang *et al* [72], 2022	R	PR	ER	190 (HCC)	T2WI, T2WI FS, DCE MRI	M, 3D	PyRadiomics	1316 (first-order histogram, texture, shape, GLZSM, GLRLM, GLCM, GLDM, and NGTDM, wavelet, local binary pattern, and Laplacian of Gaussian)	ICC, LASSO	LASSO, ICC, LR	Yes	AUC = 0.90	The predictive model incorporated the clinical–radiological risk factors and radiomics features that could adequately predict the individualized ER risk in patients with solitary HCC ≤ 5 cm
Zhang *et al* [73], 2023	P	PPF	MVI	602 (HCC)	T1WI, T2WI, AP, VP, HBP and ADC	M, 3D	Radcloud platform	1409 (First order, second order, shape, texture)	LASSO	LR, RF, SVM	Yes	AUC = 0.824 E 0.821 in the TS and VS	The combination of clinicoradiological factors and fusion radiomics signature of AP and VP images based on Gd-EOB-DTPA-enhanced MRI can effectively predict MVI
Brancato *et al*[74], 2022	R	PPF	IABR	38 (HCC)	T2WI, DCE-MRI	M, 3D	Pyradiomics	386 (shape, first-order, and texture)	correlation filter, Wilcoxon-rank sum test, MI	LR	No	AUC = 0.96	Radiomics MRI based on T2 and DCE-MRI revealed promising results concerning both HCC detection and grading
Fan *et al* [75], 2022	R	PR	VEGF	202 (HCC)	AP, PV, HBP, BP, DP	M, 3D	PyRadiomics	1906 (first order, shape)	ICC, ANOVA	LR	Yes	AUC = 0.892 in the TS, 0.800 in the VS	The combined model acquired from Gd-EOB-DTPA enhanced MRI could be considered as a credible prognostic marker for the level of VEGF in HCC
Gao *et al* [76], 2022	R	PPF	MVI	115 (HCC)	T2WI, T1WI, AP, PVP, DP, and HBP	M, 3D	Pyradiomics	107 (shape, first-order, and textural)	LR, SVC, RFC, and AdaBoost	LR	Yes	AUCs of 0.866 in the TS and 0.855 in the VS	The fusion model of multi-region radiomics achieves an enhanced prediction of the individualized

												risk estimation of MVI in HCC patients
Hu *et al* [77], 2022	R	PPF	MVI	501 (HCC)	T1WI, AP, PVP, HBP	M, 3D	Pyradiomics	2600 (first order, shape, GLCM, GLRLM, GLSZM, GLDM and NGTDM)	LASSO	ROC	Yes	AUC = 0.962	The radiomics signatures of the dual regions for tumor and peritumor on AP and PVP images are of significance to predict MVI
He *et al* [78], 2022	R	PR	DFS, OS	103 (HCC)	DCE MRI	M, 2D	AK software	1217 (First order, Morphological, GLCM, GLRLM, GLSZM, GLDM, LOG)	ICC, Lasso, cox regression	LASSO	Yes	AUC = 0.884	Multimodal radiomics models can serve as effective visual tools for predicting prognosis in patients with liver cancer
Ren *et al* [79], 2023	R	PR	HCC grade	270 (HCC)	T2WI	M, 3D	Pyradiomics	1197 (first-order and shape, GLCM, GLRLM, GLRM, and spatial gray scale corre-lation matrix)	MIC, Spearman's correlation, LR	LR	Yes	AUC = 0.864	The clinical–radiomics model integrating radiomics features and clinical factors can improve recurrence predictions beyond predictions made using clinical factors or radiomics features alone
Luo *et al* [80], 2022	R	PR	TACE	61 (HCC)	T1WI, T1WI AP, T1WI PP, T2WI, DWI (b = 800), ADC	M, 3D	Pyradiomics	1782 (shape, GLCM, GLRLM, GLSZM, NGTDM)	RF, single cox regression	ROC	No	AUC = 0.71	Radiomic signatures derived from pretreatment MRIs could predict response to combined Lenvatinib and TACE therapy. Furthermore, it can increase the accuracy of a combined model for predicting disease progression
Wang *et al* [81], 2022	R	PPF	MVI	113 (HCC)	AP	M, 3D	MATLAB	12 (first order)	NO	Mann-Whitney *U* test, LR	No	AUC = 0.741	Peritumoral AP enhanced degree on MRI showed an encouraging predictive performance for preoperative prediction of MVI
Mao *et al* [82], 2022	R	PPF	HCC GRADE	122 (HCC)	T2WI (AP, HBP phases)	M, 3D	Image Analyzer	121 (histogram, shape, texture, GLRLM and GLCM)	ICC	ANN, LR	Yes	AUC = 0.889	Prediction models consisting of clinical parameters and Gd-

												EOB-DTPA-enhanced MRI radiomic features could distinguish between high-grade HCCs and low-grade HCCs
Anderson *et al*[83], 2023	P	PR	IVIM	17 (HCC)	DWI-MRI	M, 2D	Matlab	3 (10^{th}, 50^{th}, and 90^{th} percentiles)	NO	Wilcoxon signed-rank test	No	NS	DW-MRI with IVIM and histogram analysis revealed significant reductions of D* early after treatment as well as an association between D at baseline and smaller tumor growth at three months
Li *et al*[84], 2022	R	PPF	SEV, MVI	43 (HCC)	DWI, DCE-MRI	M, 2D	Matlab, SPSS, Medcalc	8 (Histogram)	NO	ROC	No	AUC = 0.863	Histogram parameters DDC and ADC, but not the α value, are useful predictors of MVI. The fifth percentile of DDC was the most useful value to predict MVI of HCC
Li *et al*[85], 2022	R	PPF	MVI	301 (HCC)	T1WI, T2WI	M, 3D	MITK SOFTWARE	328 (first-order, GLCM, GLRLM, form factor)	LASSO, ANOVA, MANN-WHITNEY TEST	LASSO	Yes	AUC = 0.914	The preoperative MRI-based radiomic-clinical model predicted the MVI of HCC effectively and was more efficient compared with the radiomic model or clinical model alone
Wang *et al* [86], 2022	R	D	DD (cCC-HCC, HCC, CC)	196 (33 cHCC-CC, 88 HCC and 75 CC)	DCE (ART, PVP, DP)	M; 3D	Pyradiomics	1316 (shape, first-order, texture - GLCM, GLSZM, GLRLM, GLDM, NGTDM- from original, LoG and wavelet filtered images)	MI, F-test, Chi2-test, LASSO	SVM	No	AUC = 0.91	The classification ability of cHCC-CC, HCC and CC can be further improved by extracting MRI high-order features and using a two-level feature selection method
Yang *et al* [87], 2021	R	PPF	MVI	201 (HCC)	DCE (Pre-T1WI, AP, PVP, DP and HBP)	S; 3D	AK software	851 (shape, first-order, texture-GLCM, GLSZM, GLRLM, GLDM, NGTDM-, wavelet-	mRMR, LASSO	ROC; LR	Yes	Radiomics: AUC = 0.896 (TS), 0.788 (VS); Radiomics + clinical: AUC = 0.932 (TS), 0.917	The preoperative nomogram integrating clinicoradiological risk factors and the MR radiomics signature

								transformed)				(VS)	showed favourable predictive efficiency for predicting MVI
Lv *et al*[88], 2021	R	PR	AIR of RFA-treated HCC	58 (HCC)	DCE	S; 3D	AK software	396 (histogram, GLCM, GRLM, GLSZM, formfactor)	LASSO	LASSO, ROC	Yes	AUC = 0.941 and 0.818 in the TS and VS	The predictive nomogram integrated with clinical factors and CE-T1WI -based radiomics signature could accurately predict the occurrence of AIR after RFA
Yu *et al* [89], 2022	R	PPF, PR	VECT, PFS in VETC + and VETC-patients	182 (HCC)	HBP	M; 3D	Pyradiomics	1316 (shape, first-order, texture-GLCM, GLRLM, GLSZM, GLDM, NGTDM-)	LASSO	Multivariate LR; forest, SVM; DT	Yes	AUC = 0.972 (peritumoral radiomics model), AUC = 0.91 (intratumoral model)	The intratumoral or peritumoral radiomics model may be useful in predicting VETC and patient prognosis preoperatively. The peritumoral radiomics model may yield an incremental value over intratumoral model
Fang *et al* [90], 2021	R	PR	PFS of TACE + RFA treated HCC	113 (HCC)	DCE (HAP, PVP, SPP, and DP)	S; 3D	AK software	396 (histogram, GLCM, GLSZM GRLM)	LASSO	Cox regression; ROC	Yes	C-index radiomics: 0.646 and 0.669 in TS and VS; C-index combined model: 0.772 and 0.821 in TS and VS	A nomogram combining radiomics and clinical factors predicted the PFS of intermediate and advanced HCC treated with TACE plus RFA
Yang *et al* [91], 2021	R	MC	CK19+ HCC	257 (HCC)	T2WI; DWI	M; 3D	MATLAB	968 (shape, first-order, texture-GLCM, GLRLM, GLSZM, NGTDM-, wavelet)	Univariate analysis, mRMR	Multiple LR; SVM; RF; ANN	Yes	ANN-model: AUROCs = 0.857, 0.726, and 0.790 in the TS and VS A and B	The combined model based on mpMRI-radiomics accurately classify CK19+ HCC
Chen *et al* [92], 2021	R	MC	CK19+ HCC	141 (HCC)	HBP	S; 3D	Python (U-Net)	1024 (Deep semantic)	grid search	GBDT	Yes	AUC = 0.820 and 0.781 in TS and VS	DCE-MRI-based radiomics DLR model can preoperatively predict CK19-positive HCCs
Horvat *et al* [93], 2021	R	PR	Sustained complete response in RFA-treated HCC	34 (HCC)	DCE (AP and EP)	M; 3D	Pyradiomics	107 (shape, first-order, texture-GLDM, NGTDM, GLSZM, GLCM-)	NO	ROC	No	AUC > 0.7	Second-order features extracted from equilibrium phase obtained highest discriminatory performance
Alksas *et al*	R	D	DD (types and	95 (38 benign	DCE (Pre-	M; 3D	NS	249 (morphological,	Wrapper approach,	RF; SVM; NB,	No	Accuracy = 0.88	The identified

[94], 2021			grades of liver tumors)	tumors, 19 intermediate tumors, 38 HCC)	T1WI, LAP, PVP, and DP)			functional, first-order, texture-GLCM, GLRLM-)	and Gini impurity-based selection	KNN; LDA			imaging markers and CAD system can early and accurately detect and grade liver cancer
Chong *et al* [95], 2021	R	PR	2 yr RFS after hepatectomy	23 (HCC)	DCE (AP, PVP, TP, HBP)	M; 3D	Pyradiomics	2950 (shape, first-order, texture-GLCM, GLRLM, GLSZM, GLDM, NGTDM- from original and filtered images -Wavelets, Gaussian, Laplacian Sharpening-)	Inter-correlation, LASSO	LR, RF, SVM	Yes	AUC = 0.93 and 0.84 in TS and VS	DCE-MRI-based peritumoral dilation radiomics is a potential preoperative biomarker for early recurrence of HCC patients without MVI
Ding *et al* [96], 2021	R	D	DD (HCC *vs* FNH)	224 (149 HCC, 75 FNH)	AP and PVP	M; 3D	Pyradiomics	2260 (shape, first-order, texture - GLDM, GLCM, GLRLM, GLSZM, NGTDM-, from original LoG and wavelet filtered images)	mRMR, RF, correlation, LASSO	LR	Yes	AUC combined model = 0.984 and 0.972 in TS and VS	The combined model can differentiate HCC from FNH in non-cirrhotic liver with higher accuracy than the clinical model
Fan *et al* [97], 2021	R	MC	Ki67+ HCC	51 (HCC)	DCE (AP, PVP, HPB); T2WI	M; 3D	Pyradiomics	1300 (shape, first-order, texture - GLCM, GLSZM, GLRLM, GLDM, NGTDM- from original, LoG and wavelet filtered images)	LASSO	LR	Yes	Combined model: AUC = 0.922 (TS) and 0.863 (VS)	Combined AP-Rad-score-serum AFP model can preoperatively predict Ki-67 expression in HCC and outperforms AP-based radiomics model
Gao *et al* [98], 2021	R	PPF	MVI	225 (HCC)	T2WI	M; 3D	Matlab, SE-DenseNet	180 low level (intensity, shape, GLCM, GLRLM) + high-level semantic with CNN	LASSO	LR, KNN, RF, SVM, CNNs	Yes	AUC = 0.826	The proposed ensemble learning algorithm is proved to be an effective method for MVI prediction
Li *et al*[99], 2022	R	MC	GOLM1, SETD7, and RND1 expression levels	92 (HCC)	T2WI	M; 2D	MATLAB	307 (first-order statistics, GLCM, GLRLM, GLSZM, NGTDM), with five, LBP, fractal analysis, shape metrics, FOS, variance, power)	Correlation, RELIEFF	SVM	Yes	$r = 0.67$	MRI radiomics features could help quantify GOLM1, SETD7, and RND1 expression levels and predict the recurrence risk for early-stage HCC patients
Shi *et al* [100], 2022	R	PR	Functional liver reserve	60 (HCC)	HBP	M; 3D	QTIELAB	165 (shape, histogram, texture-GLCM, GLRLM, GLZSM-)	Boruta algorithm	RF	No	AUC = 0.90, 0.95, 0.99 for ICG R15 < 10%, < 15%, and < 20%	Radiomics analysis of Gd-EOB-DTPA enhanced hepatic MRI can be used for assessment of functional liver

												reserve in HCC patients
Dai *et al* [101], 2021	R	PPF	MVI	69 (HCC)	DCE (Pre-T1WI, AP, PVP or HBP)	M; 3D	Matlab	106 (texture -GLCM, GLRLM, GLSZM, SGLDM, NGTDM, and NGLDS-)	LASSO, SVM-RFE, mRMR, LASSO-RFE	GBDT; SVM; LR; RF	No	AUC = 0.792 for HBP model	The radiomics model based on the HBP had better predictive performance than those based on the AP, PVP, and pre-enhanced T1W
Fan *et al* [102], 2021	R	PPF	VECT+ HCC	81 (HCC)	DCE (AP and HBP)	M; 3D	Pyradiomics	1316 (first-order, texture -GLCM, GLSZM, GLRLM, GLDM, NGTDM- from original, wavelet and LoG filtered images)	ICC, LASSO	ROC; LR	No	AUC = 0.84	Texture analysis based on Gd-EOB-DTPA-enhanced MRI can help identify VETC-positive HCC
Yang *et al* [103], 2021	R	PPF	Poorly differentiated HCC	188 (HCC)	T1WI, T2WI, DCE (AP, PP and DP)	M; 3D	LIFEx	200 (shape, histogram, texture -GLCM, NGLDM, GLRLM, GLZLM-)	LASSO	LASSO	Yes	Model1: AUC = 0.623 and 0.576 in TS and VS, while it is 0.576 in the validation cohort. Model2: AUC = 0.721, and 0.681 in TS and VS	The MRI-based radiomics signature and clinical model can distinguish HCC patients that belong in a low differentiation group fromother patients
Chen *et al* [104], 2021	R	PPF	MVI	269 (HCC)	T2WI; DWI, DCE (AP, PVP, and HBP)	M; 3D	Pyradiomics	1395 (first-order, GLRLM, GLCM from original, Laplacian, logarithmic, exponential, and wavelet filtered images)	Variance threshold, LASSO	KNN SVM, XGBoost, RF, LR, DT	Yes	For HBP model: AUC = 0.942 (SVM), 0.938 (XGBoost), and 0.936 (LR)	Radiomics signatures with machine learning can further improve the ability to predict MVI and are best modeled during HBP
Kong *et al* [16], 2021	R	PR	Response to TACE	99 (HCC)	T2WI	M; 3D	AK software	396 (histogram, texture-GLSZM, GLCM, GLRLM-)	LASSO, correlation	ROC	Yes	AUC = 0.861 and 0.884 in TS and VS	The radiomics and clinical-based nomogram can well predict TR in intermediate-advanced HCC
Zhao *et al* [105], 2021	R	MC	GPC3	143 (HCC)	DCE-MRI, DWI	M; 3D	MedCalc, R	6 (Histogram)	NO	Mann-Whitney *U* test	No	C-INDEX = 0.804	Elevated serum AFP levels and lower 75th percentile ADC values were helpful in differentiating GPC3-positive and GPC3-negative HCCs. The combined nomogram achieved satisfactory preoperative risk

													prediction of GPC3 expression in HCC patients
Song *et al* [106], 2021	R	PPF	MVI	601 (HCC)	T2WI FS; DWI; ADC; DCE (AP, PVP, and DP)	M; 3D	PyRadiomics	110 (shape, first-order, texture)	PCA, ANOVA	SVM, AE, LDA, RF, LR, LASSO, AdaBoost, DT, Gaussian process, NB, DL	Yes	DLC model: AUC = 0.931 for MVI prediction; AUC = 0.793 for MVI-grade stratification	DLC model predicts and grades MVI better than DL model
Zhong *et al* [107], 2021	R	D	DD (small HCC 3 cm *vs* benign nodules)	150 (112 HCC, 44 benign nodules)	in phase sequence; T2WI FS; ADC	M; 2D	MaZda	837 (histogram, GLCM, RLM, wavelet, absolute gradient, autoregressive model)	ICC, Mann-Whitney, LASSO	LR; ROC	No	AUC = 0.917	MRI-based radiomics analysis showed additive value to the LI-RADS v 2018 algorithm for differentiating small HCCs from benign nodules in the cirrhotic liver
Zhao *et al* [105], 2021	R	MC	GPC3 expression	143 (HCC)	ADC	M;3D	MR Multiparametric Analysis software	6 (histogram)	Univariate analysis (*t*-test, Mann-Whitney, Pearson, χ^2, Fisher)	LR	No	C-index = 0.804	The combined nomogram achieved satisfactory preoperative risk prediction of GPC3 expression in HCC patients
Chen *et al* [108], 2021	R	PR	Post hepatectomy liver failure	144 (HCC)	HBP	M; 2D	AK software	1,044 (shape, first-order, texture-GLSZM, GLCM, GLRLM-)	Correlation, RFE	LR; ROC; liver failure model	Yes	AUC = 0.956 and 0.844 in TS and VS	The LF model is able to predict PHLF in HCC patients
Liang *et al* [109], 2021	R	PPF	MVD	30 (HCC)	DCE	M; 2D	AK software	376 (histogram, texture-GLSZM, GLCM, GLRLM-)	Mann-Whitney	LR	No	AUC = 0.83 and 0.94	DITET model provides a better indication of the microcirculation of HCC than SITET
Zhang *et al* [110], 2021	R	PR	RFS of HCC patients treated with surgical resection	153 (HCC)	T2WI FS; DCE (AP, PVP, and HBP)	M; 3D	Pyradiomics	107 (shape, first-order, texture - GLCM, GLSZM, GLRLM, GLDM, NGTDM-)	LASSO	LASSO Cox regression	Yes	C-index 0.725	The prediction model combining MRI radiomics signatures with clinical factors predicts the prognosis of surgically resected HCC patients
Zhang *et al* [111], 2021	R	PR	RFS after curative ablation	132 (HCC)	T2WI FS; T1WI FS; DCE (AP, PVP, and HBP)	M; 3D	Pyradiomics	1316 (shape, first-order, texture - GLCM, GLSZM, GLRLM, GLDM, NGTDM-, LoG, wavelet)	RandomForestSRC	Cox regression; random survival forest; ROC	Yes	C-index = 0.706	The radiomics model combining DCE-MRI with clinical characteristics could predict HCC recurrence after curative ablation
Zhang *et al*	R	PPF	MVI	195 (HCC)	T2WI FS;	M; 3D	AK software	396 (histogram,	ANOVA, Mann-	Multivariate LR	Yes	AUC = 0.901 and	The combined

[112], 2021					DWI; ADC; DCE (AP, PP, DP)			GLCM, GLSZM, RLM, formfactor, haralick)	Whitney U-test, correlation, LASSO			0.840 in the TS and VS	radiomics-clinical model can preoperatively and noninvasively predict MVI in HCC
Zhao *et al* [113], 2021	R	PR	Response to TACE	122 (HCC)	DCE (AP, PVP, and DP)	M; 3D	AK software	789 (histogram,GLCM, GLRLM, GLZSM, Haralick,Gaussian transform)	ICC, Spearman's correlation, univariate LR, LASSO	LR; ROC	Yes	AUC = 0.838 and 0.833 in TS and VS	The combined model (radiomics score + clinical-radiological risk factors) showed better performance than the clinical-radiological model in predicting TACE efficacy in HCC patients
Kuang *et al* [114], 2021	R	PR	Predict short-term response after TACE in HCC	153 (HCC)	T2WI; DCE (AP)	A; 3D	AK software	396 (shape, histogram, GLSZM, GLCM, RLM)	mRMR, LASSO	LR	Yes	AUC = 0.83 and 0.81 in TS and VS	MRI-based nomogram has greater predictive efficacy to predict the response after TACE than radiomics and clinics models alone
Meng *et al* [115], 2021	R	PPF	MVI	402 (HCC)	T1WI, T2WI, DWI, CE-CT	M, 3D	Pyradiomics	1288	ICC, MANN-WHITNEY, LASSO	LR	Yes	AUC = 0.804	CT and MRI had a comparable predictive performance for MVI in solitary HCC. The RS of MRI only hadsignificant added value for predicting MVI in HCC of 2–5 cm
Zhu *et al* [116], 2021	R	D	DD (MTM-HCC *vs* HCC)	88 (32 MTM-HCCs, 56 Non-MTM-HCC)	T2WI FS; in-phase and out-of-phase sequences; DCE (AP, PVP, and DP)	M; 2D	MaZda	101 (histogram, the absolute gradient, GLRLM, GLCM, autoregressive model and wavelet transform)	Fisher, MI, POE + ACC, LASSO	LR; ROC	No	AUC = 0.785	A DCE-MRI-based radiomics nomogram can predict MTM-HCC
Liu *et al* [117], 2021	R	PR	TACE, MWA	102 (HCC)	T1WI, T2WI, PVP	M, 2D	MaZda	20 (First order, GLCM)	NS	ROC	No	AUC = 0.876	MR imaging texture features may be used to predict the prognosis of HCC treated with TACE combined with MWA
Chong *et al* [118], 2021	R	PR	MVI, RFS after curative surgery (HCC≤ 5 cm)	356 (HCC)	DWI, DCE (Pre-T1WI, AP, PVP, TP, HBP)	M; 3D	Pyradiomics	854 (shape, first-order, texture - GLCM, GLDM, GLRLM, NGTDM, GLSZLM- from original and wavelet	LASSO	RF; LR	Yes	AUC = 0.920 with RF, 0.879 with LR in validation cohort	Preoperative radiomics-based nomogram using random forest is a potential biomarker of MVI and RFS

								filtered images)					prediction for solitary HCC ≤ 5 cm
Gu *et al* [119], 2020	R	MC	GPC3+ HCC	293 (HCC)	DCE (DP)	M; 3D	Pyradiomics	853 (shape, histogram, texture - GLCM, GLSZM, GLRLM, GLDM, NGTDM-, wavelet)	ICC, Mann-Whitney, Fisher	LR; SVM	Yes	AUC = 0.926 and 0.914 in TS and VS	The combined AFP + radiomics nomogram may provide an effective tool for noninvasive and individualized prediction of GPC3-positive in HCC patients
Zhao *et al* [120], 2021	R	PR	ER after partial hepatectomy	113 (HCC)	T2WI; in-phase and out-of-phase sequences; DWI; DCE (AP, PVP, and DP)	M; 3D	AK software	1146 (shape, histogram, texture - GLCM, GLRLM, GLSZM-)	Spearman's correlation, LASSO, stepwise LR	Multivariate LR	Yes	Radiomics: AUC = 0.771 in the VS. Combined nomogram: AUC = 0.873	A combined nomogram incorporating the mpMRI radiomics score and clinicopathologic-radiologic characteristics can predict ER (≤ 2 yr) in HCC
Ai *et al* [121], 2020	R	D	DD (HCC, HH, HC)	89 (33 HH, 22 HC, 34 HCC)	IVIM	M; 3D	MITK-DI	13 (histogram)	Kruskal-Wallis	ROC	No	AUC = 0.883	A multiparametric histogram from IVIM is an effective means of identifying HH, HC, and HCC
Shaghaghi *et al*[122], 2021	R	PR	Post-TACE OS and TFS	104 (HCC)	ADC	S; 3D	NS	3 (mean, skewness, and kurtosis)	NO	NO	No	Significant results for changes in ADC mean and Kurtosis	Changes in mean ADC and ADC kurtosis can be used to predict post-TACE OS and TFS in well-circumscribed HCC
Li *et al* [123], 2020	R	D	DD (HCC *vs* HMRC)	75 (41 HCC, 34 HMRC)	DCE	M; 2D	OmniKinetic	67 (First order, histogram, GLCM, Haralick, RLM)	*t*-test, ROC	FDA	No	AUC = 0.86 (radiomics + pharmacokinetic) and 0.89 (DA based on radiomics)	A model based on DCEMRI radiomics and pharmacokinetic parameters was useful for differentiating HCC from HMRC
Geng *et al* [124], 2021	R	PPF, MC	MVI; GRADE; CK-7, CK-19, GPC3 expression status	53 (HCC)	SWI	M;3D	PyRadiomics	107 (first-order, shape, GLCM, GLRLM, GLSZM, NGTDM)	ICC	LR	No	AUC = 0.905 (CK-19+), 0.837 (CK-7+), 0.800 (high histopathologic grade) and 0.760 (GPC-3+)	Extracting the radiomics features from SWI images was feasible to evaluate multiple histo-pathologic indexes of HCC
Zhang *et al* [125], 2020	R	PR	OS after surgical resection	136 (44 MCC, 59 HCC, 33 CHCC)	DCE (EP); DWI	M; 3D	AK software	384 (histogram, GLCM, GLSZM, RLM, formfactor,	mRMR method and the elastic network algorithm	Multivariable cox regression	No	Parameters independently associated with OS	Clinicopathological and radiomics features are

							haralick)				($P < 0.05$)	independently associated with the OS of patients with primary liver cancer
Zhang *et al* [126], 2020	P	PR	OS after surgical resection	120 (HCC)	T2WI FS; DCE (AP, PVP, TP, and HBP)	S; 2D	AK software	350 (histogram, form factor, GLCM, GLRLM)	ICC, LASSO	LASSO Cox regression	Yes	C-index = 0.92	Radiomics + clinic-radiological predictors can efficiently aid in preoperative HCC prognosis prediction after surgical resection with respect to clinic-radiological model
Hectors *et al*[127], 2020	P	PR	6- and 12- week response to 90 yr	24 (HCC)	DCE-MRI, IVIM-DWI	M; 3D	Matlab	40 DCE MRI histogram parameters and 20 IVIM DWI histo-gram parameters	Stepwise feature selection	LR	No	AUC = 0.92	Diffusion and perfusion MRI can be combied to evaluate the response of HCC to radioembolization
Shi *et al* [128], 2020	P	PPF, MC	HCC GRADE, KI67+ HCC, CAPSULE FORMATION+	52 (HCC)	IVIM	M; 3D	ImageJ, Mazda	15 (histogram)	*t*-test	LR	No	AUC = 0.92 (grading), 0.86 (Ki67+) and 0.84 (capsule formation)	Multiple prognostic factors can be accurately predicted with assistance of histogram metrics sourced from a single IVIM scan
Feng *et al* [129], 2020	R	D, MC	DD	104 (HCC)	Gd-EOB-DTPA-enhanced MRI and T2WI	M, 3D	Mazda	262 (Histogram, GLCOM, GLRLM, WAVELET TRANSFORM)	PCA, LDA, NDA, RDA	ROC	No	AUC = 0.879	Texture analysis of Gd-EOB-DTPA-enhanced MRI and T2WI was valuable and might be a promising method in identifying the HCC grade
Nebbia *et al* [130], 2020	R	PPF	MVI	99 (HCC)	T2WI; DCE (AP and PP); DWI	M; 3D	Pyradiomics	100 (shape, first-order, texture - GLCM, GLDM, GLSZM-)	LASSO	SVM; DT; KNN, NB	No	AUC = 0.867	Information from mpMRI sequences is complementary in identifying MVI
Schobert *et al*[131], 2020	R	PR	Response to DEB-TACE, PFS	46 (HCC)	DCE (HAP, PVP, and DP)	M; 3D	Pyradiomics	14 (shape, first-order)	Univariate analysis, stepwise forward selection	LinearRegression; Cox regression; Kaplan–Meier analysis	No	High NLR and PLR correlated with non-spherical tumor growth ($P = 0.001$ and $P < 0.001$)	This study establishes the prognostic value of quantitative inflam-matory biomarkers associated with aggressive nonspherical tumor growth and predictive of poorer tumor response and shorter PFS after DEB-TACE

Sun *et al* [132], 2020	R	PR	Early progression of unresectable HCC after TACE	84 (HCC)	T2WI; DWI; ADC	M; 3D	Pyradiomics	1597 (first-order, shape, texture - GLCM, GLRLM, GLSZM, NGTDM, GLDM-)	Variance threshold, Pearson's correlation, LASSO	LR	Yes	AUC = 0.800	mpMRI-based radiomic model predicts the outcome of TACE therapy for unresectable HCC outperforms monomodality radiomic models
Wilson *et al* [133], 2020	R	PPF, PR	MVI, OS, DFS after surgery	38 (HCC)	T2WI; in-phase and out-of-phase sequences; DCE (HAP, and PVP)	M; 2D	TexRAD	7 (histogram)	NO	LR	No	AUC = 0.83	Tumor entropy and mean are both associated with MVI. Texture analysis on preoperative imaging correlates with microscopic features of HCC
Hectors *et al*[134], 2020	R	MC, PR	Immuno-oncological markers (CD3, CD68, CD31), recurrence at 12 m	48 (HCC)	DCE (Pre-T1WI, AP, PVP, LVP, and HBP); ADC	M; 2D	MATLAB	36 (Haralick, qualitative and quantitative)	NO	LR	No	AUC = 0.76–0.80	MRI radiomics features may serve as noninvasive predictors of HCC immuno-oncological characteristics and tumour recurrence
Wang *et al* [135], 2020	R	MC	CK19+ HCC	227 (HCC)	DWI; ADC; T2WI; DCE (Pre-T1WI, AP, PVP, DP, and HBP)	M; 3D	Pyradiomics	647 (shape, histogram, texture, wavelet)	ICC, LASSO	Logistic model; ROC	Yes	AUC = 0.95	The combined model based on a fusion radiomics signature derived from AP and HBP can be a reliable biomarker for CK19 status of HCC
Wang *et al* [136], 2020	R	PR	5 yr survival after curative hepatectomy	201 (HCC)	T1WI; T2WI; DWI; ADC; DCE (AP, PVP, and EP)	S; 3D	Precision Medicine Open Platform	3144 (histogram, texture, wavelet, statistical)	Gini index	Random Forest	Yes	AUC = 0.9804 and 0.7578 in the TS and VS	This radiomics model is a valid method to predict 5-year survival in HCC patients
Song *et al* [137], 2020	R	PR	RFS after c-TACE	184 (HCC)	DCE (AP, and PVP)	S; 3D	AK software	396 (histogram, GLCM, GRLM, GLSZM)	ICC, LASSO	LASSO Cox regression	Yes	C-index = 0.802	The combined model is more valuable than the clinical-radiological model or radiomics model alone for evaluating the RFS of HCC patients after c-TACE
Zhang *et al* [138], 2019	R	PR	ER (1 yr after hepatectomy)	100 (HCC)	DCE (AP, PVP, and DP)	S; 3D	Omni Kinetic	6 (skewness, kurtosis, uniformity, energy, entropy, and correlation)	NO	LR	No	AUC = 0.867	Texture analysis based on preoperative MRI are potential quantitative predictors of ER in HCC patients after

													hepatectomy
Huang *al* [139], 2019	R	D, PR	DD (HCC *vs* DPHCC), DFS, OS after surgery	100 (HCC)	DCE (AP, PVP, DP, and HBP)	M; 3D	Huiying Medical Technology	1029 (First-order, shape, texture - GLCM, GLRLM, GLSZM-)	LASSO	Multi-layer perceptron; SVM; LR; K-nearest-neighbor; ROC	No	Accuracy of LR in PVP (0.77), DP (0.798), HBP (0.756) and of multi-layer perceptron in PVP (0.798)	The radiomics features extracted from DCE-MRI can be used to diagnose preoperative DPHCC
Ye *et al* [140], 2019	P	MC	Ki67 expression	89 (HCC)	T2WI FS; DCE (Pre-T1WI, AP, PVP, TP, and HBP)	M; 3D	AK software	396 (histogram, texture, GLCM, GLRLM)	LASSO	LR	No	C-index = 0.936	The combination of DCE-MRI texture signature and clinical factors demonstrated the potential to preoperatively predict Ki-67 status of HCC after curative resection
Zhang *et al* [141] 2019	R	PPF	MVI	267 (HCC)	T2WI FS; in-phase and out-of-phase sequences; T1WI; DWI; DCE (AP, PVP, and EP)	M; 3D	MATLAB	484 (intensity, texture, wavelet)	mRMR	LR	Yes	AUC = 0.784 and 0.820 in TS and VS	The radiomics nomogram can serve as a visual predictive tool for MVI in HCC and outperformed clinico-radiological model
Chen *et al* [142], 2020	R	MC	CK19+, EpCAM	115 (HCC)	T2WI, pre-T1WI, DCE (AP, PVP, HBP), ADC	M; 3D	AK software	23 (histogram)	Univariate analysis	LR	No	Accuracy = 0.86, C-index = 0.94	Noninvasive prediction of HCCs with progenitor phenotype can be achieved with high accuracy by integrated interpretation of biochemical and radiological information
Xu *et al* [143], 2019	R	PPF	HCC GRADE	51 (HCC)	ADC	M; 3D	SPSS	27 (histogram)	NO	NO	No	$\rho = -0.397$ for ADC 25^{th} percentile; AUC = 0.76 for ADC min	The 25^{th} percentile ADC showed a stronger correlation with the histological grade of HCC than other ADC parameters, and the minimum ADC value might be an optimal metric for determining poor and fair diferentiations of HCC in DWI
Li *et al* [144], 2019	R	MC	Ki67 expression	83 (HCC)	DCE (HAP, PVP, EP, and	M; 3D	MaZda	30 (histogram, GLCM, GLRLM,	Fisher coefficient, MI, POE + ACC,	ROC (accuracy)	No	Lowest misclassification rates: PCA-	Texture analysis of HBP, arterial phase,

					HBP); T2WI FS			absolute gradient, the autoregressive model, wavelet transform)	correlation			PVP = 40.96%; LDA-PVP = 9.64%; NDA-AP = 6.02%.	and portal venous phase are helpful for predicting Ki67 expression
Oyama *et al* [145], 2019	R	D	DD (HCC, MT, HH)	93 (50 HCCs, 50 MTs, 50 HHs)	T1WI	M; 3D	MATLAB	43 (GLCM, GLRLM, GLSZM, NGTDM)	correlation	LDA	No	Accuracy = 92% (texture analysis) and 85% (persistence imges analyses)	Texture analysis or topological data analysis support the classifcation of HCC, MT, and HH with considerable accuracy, solely based on non-contrast-enhanced T1WI 3D
Wang *et al* [146], 2019	R	MC	CK19+ HCC	48 (HCC)	T2WI FS; in-phase and out-of-phase sequences; DCE (AP, PVP, DP); DWI (b values 0 and 500 s/mm^2); ADC	M; 2D	In-house software	2415 (intensity, gradient, Gabor wavelet, local binary pattern histogram Fourier, GLCM, GLGCM)	LDA (AUC)	LR	No	AUC = 0.765	The StdSeparation 3D texture character may be a reliable imaging biomarker which can improve the diagnostic performance.
Zhu *et al* [147], 2019	R	PPF	MVI	142 (HCC)	DCE (AP, PVP)	M; 3D	Omni-kinetics software	58 (histogram, GLCM, Haralick, GRLM)	Kruskal-Wallis, univariate LR, Pearson's correlation	LR	Yes	AUC = 0.81	The combined model of arterial phase radiomic features with clinical-radiological features could improve MVI prediction ability
Zhang *et al* [148], 2019	P	PR	ER (1 yr after surgical resection)	155 (HCC)	T2WI FS, DCE (AP, PVP, TP, and HBP)	M; 3D	AK software	385 (histogram, texture, GLCM, GLRLM)	LASSO	LR; ROC	Yes	AUC = 0.844	The radiomics nomogram integrating the radiomics score with clinical-radiological risk factors showed better discriminative performance than the clinical-radiological nomogram
Gordic *et al* [149], 2019	R	PR	CR, PR, SD	22 (HCC)	volumetric ADC	M; 3D	MATLAB	7 (histogram)	Wald test	LR	No	AUC = 0.91	Diffusion histogram parameters obtained at 6w and early changes in ADC from baseline are predictive of subsequent response of HCCs treated with RE

Jansen *et al* [150], 2019	R	D	DD (adenomas, cysts, hemangiomas, HCC, metastases)	211 (40 adenomas, 29 cysts, 56 hemangiomas, 30 HCC, 56 metastases)	DCE-MRI, T2WI	M; 2D	NS	164 (contrast curve, histogram, and GLCM texture)	ANOVA F-SCORE	Randomized tree classifier	No	Accuracy = 0.77	The proposed classification system using features derived from clinical DCE-MR and T2WI, with additional risk factors is able to differentiate five common types of lesions and is a step forward to a clinically useful aid for focal liver lesion diagnosis
Ma *et al* [151], 2019	R	PR	Post RFA progression	64 (HCC)	ADC	M; 3D	Volume View	8 (histogram)	NO	Cox-regression	No	C-index = 0.62	Pre-RFA ADC histogram analysis might serve as a useful biomarker for predicting tumor progression and survival in patients with HCC treated with RFA
Wu *et al* [152], 2019	R	D	DD (HCC, HH)	369 (222 HCCs, 224 HHs)	In-phase and out-of-phase sequences; T2WI; DWI	M; 3D	PyRadiomics	1029 (shape, first-order, texture - GLCM, GLRLM, GLSZM-, exponential, square, square root, logarithm, and wavelet)	Variance threshold, select k best, LASSO	Decision tree; random forest; K nearest neighbours; LR; ROC	Yes	AUC = 0.86 and 0.89 in TS and VS	mpMRI radiomics signature is an adjunct tool to distinguish HCC and HH, outperformed a less experienced radiologist, and is nearly equal to an experienced radiologist
Kim *et al* [153], 2019	R	PR	ER (< = 2 yr), LR (> 2 yr) after curative resection	167 (HCC)	DCE (AP, PP, HBP, AP-PP, AP-HBP, PP-HBP, and AP-PP-HBP)	S; 3D	PyRadiomics	1301 (first-order, shape, texture - GLCM, GLRLM, GLSZM, NGTDM, GLDM-, LoG, wavelet)	RF minimal depth algorithm	random survival forest	Yes	C-index = 0.716	The clinicopathologic-radiomic model showed best performances, suggesting the importance of including clinicopathologic information in the radiomic analysis of HCC
Lewis *et al* [154], 2019	R	D	DD (HCC, ICC, HCC-ICC)	63 (36 HCC; 17 ICC; 12 HCC-ICC)	ADC	M; 3D	MATLAB	11 (histogram)	Wald criteria	Binary LR and AUROC	No	AUC = 0.9	The combination of quantitative ADC histogram parameters and LI-RADS categorization yielded the best prediction accuracy for distinction of HCC vs ICC and combined

													HCC-ICC
Chen *et al* [155], 2019	R	MC	Immunoscore (CD3+ and CD8+)	207 (HCC)	HBP	M; 3D	AK software	1044 (histogram, texture, factor parameters, GLCM, GLRLM, GLSZM)	Recursive elimination	LR	Yes	AUC = 0.92	The combined MRI-radiomics-based clinical nomogram is effective in predicting immunoscore in HCC
Feng *et al* [156], 2019	R	PPF	MVI	160 (HCC)	HBP	M; 3D	AK software	1044 (histogram, texture, wavelet transformed, filter transformed texture)	LASSO	LR	Yes	AUC = 0.85 and 0.83 in TS and VS	A combined intrat-umoural and peritu-moural radiomics model based on DCE-MRI is able to pre-operatively predict MVI in primary HCC patients
Wu *et al* [157], 2019	R	PPF	HCC grade	170 (HCC)	T1WI; T2WI FS	M; 3D	MATLAB	656 (histogram, shape, GLCM, wavelet)	LASSO	LR	Yes	AUC = 0.8	The combination of the radiomics signatures with clinical factors may be helpful for the preoperative prediction of HCC grade
Yang *et al* [158], 2019	R	PPF	MVI	208 (HCC)	T2WI FS; DWI; DCE (AP, PVP, DP, and HBP)	M; 3D	MATLAB	647 (shape, intensity, textur-GLCM, GLRLM, GLZLM, NGLDS-)	LASSO, AIC	LR	Yes	AUC = 0.94 and 0.86	The nomogram incorporating clinicoradiological risk factors and radiomic features derived from HBP images achieved satisfactory preoperative prediction of the individualized risk of MVI in HCC patients
Stocker *et al* [159], 2018	R	D	DD (HCC *vs* FNH *vs* HA)	108 (55 HCC, 24 HA, 29 FNH)	T1WI FS; T2WI; DCE (AP, PVP, and HBP)	M; 2D	MATLAB	19 (histogram, GLCM, GLRLM)	LR	LR; ROC	No	AUC = 0.92	2D-TA of MR images may help to distinguish HCC from benign hepatocellular tumors in the non-cirrhotic liver, with most promising results were found in TA features in the AP images
Ahn *et al* [160], 2019	R	PR	ER (1y after surgical resection)	179 (HCC)	HBP	M; 3D	In-house software program	13 (histogram, GLCM)	Univariate analysis	LR	No	AUC = 0.83	When added texture variables to MRI findings, the diagnostic performance for

													predicting early recurrence is improved
Hui *et al* [161], 2018	R	PR	ER (1yr), LNR (late or no recurrence) after surgery	50 (HCC)	T2WI; DCE (AP, PVP and EP)	M; 2D	MaZda	290 (histogram, texture, autoregressive model, GRLM, GLCM, wavelet)	PRTools	ROC	No	Accuracy 78%-84%	Texture analysis of preoperative MRI has the potential to predict ER of HCC with up to 84% accuracy using an appropriate, single texture analysis parameter
Zou *et al* [162], 2019	R	D	DD (IMCC and HCC)	33 IMCC, 98 HCC	volumetric ADC, DCE-MRI	M; 3D	SPSS	9 (histogram)	NO	ROC	No	AUC = 0.79	Volumetric ADC histogram analysis provides additional value to dynamic enhanced MRI in differentiating IMCC from HCC
Li *et al* [163], 2018	P	PPF	MVI	41 (HCC)	IVIM-DWI	M; 3D	MATLAB	10 (histogram)	Univariate analysis	ROC	No	AUC = 0.87	Histogram analysis of IVIM based on whole tumor volume can be useful for predicting MVI. The 5th percentile of D was most useful value to predict MVI of HCC
Wu *et al* [164], 2019	P	PR	TTP after TACE	55 (HCC)	IVIM-DWI	S; 3D	MR OncoTreat	8 histogram parameters	NO	Cox-regression	No	AUC = 0.82	Pre-TACE kurtosis of ADCtotal is the best independent predictor for TTP
Li *et al* [165], 2017	R	D	DD (HH *vs* HM *vs* HCC)	162 (55 HH, 67 HM, 40 HCC)	SPAIR T2WI	M; 2D	MATLAB	233 (histogram, GLCM, GLGCM, GLRLM, GWTF, ISZM)	CCC, DR, R2	ROC, KNN, BP-ANN, SVM, LR	Yes	Misclassification rates: 11.7% (HH *vs* HM), 9.6% (HM *vs* HCC) and 9.7% (HH *vs* HCC)	Texture features of T2WI SPAIR can classify HH, HM and HCC
Moriya *et al* [166], 2017	R	D	HCC grade	53 (HCC)	DWI, ADC	A; 3D	SPSS	11 (First Level)	ANOVA	ROC	No	sensitivity: 100%, specificity: 54%	Minimum ADC was most useful to differentiate poorly differentiated HCC in 3D analysis of ADC histograms

ST: Study type; R: Retrospective; P: Prospective; CP: Clinical purpose; D: Diagnosis; PPF: Prediction of pathological findings; PR: Prognosis; MC: Molecular characterization; NP: Number of patients; Seg: Segmentation; FS: Feature selection; CM: Classification method; DD: Differential diagnosis; cCC-HCC: Combined hepatocellular cholangiocarcinoma; HCC: Hepatocellular carcinoma; CC: Cholangiocarcinoma; MVI: Microvascular invasion; AIR: Aggressive intrasegmental recurrence; RFA: Radiofrequency ablation; VECT: Vessels encapsulating tumor clusters; PFS: Progression-free survival; TACE: Transcatheter arterial chemoembolization; CK19: Cytokeratin19; RFS: Recurrence-free survival; FNH: Focal nodular hyperplasia; GOLM1: Golgi membrane protein 1; SETD7: SET domain containing 7; RND1: Rho family GTPase 1; GPC3: Glypican-3; MVD: Microvessel density; MTM-HCC: Macrotrabecular-massive

hepatocellular carcinoma; ER: Early recurrence; HH: Hepatic hemangioma; HC: Hepatic cysts; OS: Overall survival; TFS: Transplant-free survival; HMRC: Hepatic metastasis of rectal cancer; CK7: Cytokeratin7; DEB-TACE: Drug-eluting bead-transcatheter arterial chemoembolization; DFS: Disease-free survival; DPHCC: Dual-phenotype HCC; EpCAM: Epithelial Cell Adhesion Molecule; MT: Metastatic tumor; CR: Complete response; PR: Partial response; SD: Stable disease; LR: Logistic regression; LRec: Late Recurrence; ICC: Intrahepatic cholangiocarcinoma; HA: Hepatic adenoma; LNR: Late regional recurrence; IMCC: Mass-forming cholangiocarcinoma; TTP: Time to progression; HM: Hepatic metastases; DCE: Dynamic contrast-enhanced; ART: Arterial phase; PVP: Portal venous phase; DP: Delayed phase; T1WI: T1-weighted imaging; AP: Arterial phase; HBP: Hepatobiliary phase; HAP: Hepatic arterial phase; SPP: Substantial period phase; T2WI: T2-weighted imaging; DWI: Diffusion-weighted imaging; EP: Equilibrium phase; LAP: Late arterial phase; TP: Transitional phase; PP: Portal phase; FS: Fat saturation; ADC: Apparent diffusion coefficient; DCE-MRI: DCE-Magnetic Resonance Imaging; IVIM: Intravoxel incoherent motion; SWI: Susceptibility weighted imaging; LVP: Late venous phase; SPAIR T2WI: Spectral attenuated inversion-recovery T2WI; M: Manually; S: Semi-automatic; A: Automatic; GLCM: Gray-level co-occurrence matrix; GLSZM: Grey Level Size Zone Matrix; GLRLM: Gray-level run-length; GLDM: Gray level dependence matrix; NGTDM: Neighboring gray tone difference matrix; CNN: Convolutional neural network; LBP: Local binary patterns; FOS: First-order statistics; NGLDS: Neighborhood gray-level difference statistics; RLM: Run-length matrix; GWTF: Gabor wavelet transform; ISZM: Intensity-size-zone matrix; MI: Mutual information; LASSO: Least absolute shrinkage and selection operator; mRMR: Minimum redundancy maximum relevance; RF: random forests; SVM-RFE: Support vector machine-recursive feature elimination; ICC: Intra-class correlation coefficient; PCA: Principal component analysis; RandomForestSRC: Random Forests for Survival, Regression, and Classification; LR: Logistic regression; POE + ACC: Classification error probability combined with average correlation coefficients; ROC: Receiver operating characteristic; LDA: Linesar discriminant analysis; AUC: Area under the curve; AIC: Akaike information criteria; CCC: Concordance correlation coefficient; DR: Dynamic range; ANN: Artificial neural network; GBDT: Gradient Boosting Tree; KNN: K-nearest Neighbours; XGBoost: Extreme gradient boosting; DT: Decision trees; DL: Deep learning; FDA: Fisher discriminant analysis; AUROC: Area under the receiver operating characteristic; BP-ANN: Back propagation artificial neural network; TS: Training sets; VS: Validation sets; ICG: Indocyanine green retention rate; NLR: Neutrophil-to-lymphocyte ratio; PLR: Platelet-to-lymphocyte ratio; CAD: Computer-aided diagnostic; TR: Transcatheter arterial chemoembolization response; SITET: Single-input two-compartment extended Tofts; DITET: Dual-input two-compartment extended Tofts; c-TACE: Conventional-transcatheter arterial chemoembolization; TA: Texture analysis; RE: Radioembolization.

the 128 included articles. However, only 40 (31.25%) identified and discussed biological correlates and only 50 (39.06%) provided cut-off analysis.

Of the 127 studies included, almost all (123) reported discrimination statistics and their statistical significance. About a quarter of these studies used resampling techniques. However, only 58 studies reported calibration statistics, and none of them applied resampling techniques.

A significant proportion (39.37%) of the studies (50 out of 127) did not provide any validation of their results. Only three studies validated their results using one external validation cohort and five studies used two external validation cohorts. Furthermore, only 47 out of 127 research examined the clinical utility of the produced model using decision curve analysis, while 42 out of 127 studies compared radiomics models with the particular gold standard (based on the study purpose).

Lastly, no study disclosed code and data to the public or performed a cost-effectiveness analysis.

Correlation analysis between RQS and journal metrics

A significant positive correlation was found between RQS and journal IF ($\rho = 0.36$, $P = 2.98 \times 10^{-5}$), 5-years IF ($\rho = 0.33$, $P = 1.56 \times 10^{-4}$), number of patients involved ($\rho = 0.51$, $P < 9.37 \times 10^{-10}$) and number of radiomics features ($\rho = 0.59$, $P < 4.59 \times 10^{-13}$) extracted in the study. On the other hand, there was a significant negative correlation between RQS and time between the publication and the performed literature research ($\rho = -0.23$, $P = 0.0072$) and there were no statistically significant differences identified in the RQS among studies with different objectives. Scatterplots with regression lines showing significant correlations between RQS and journal metrics are shown in Figure 3.

DISCUSSION

In this systematic review, we aimed at summarizing the current status of the fast-growing research on MRI radiomics for the management of HCC. We explored whether it could offer diagnostic, prognostic, and predictive information about pathological outcomes and molecular expression. Additionally, we assessed the quality of the science and reporting

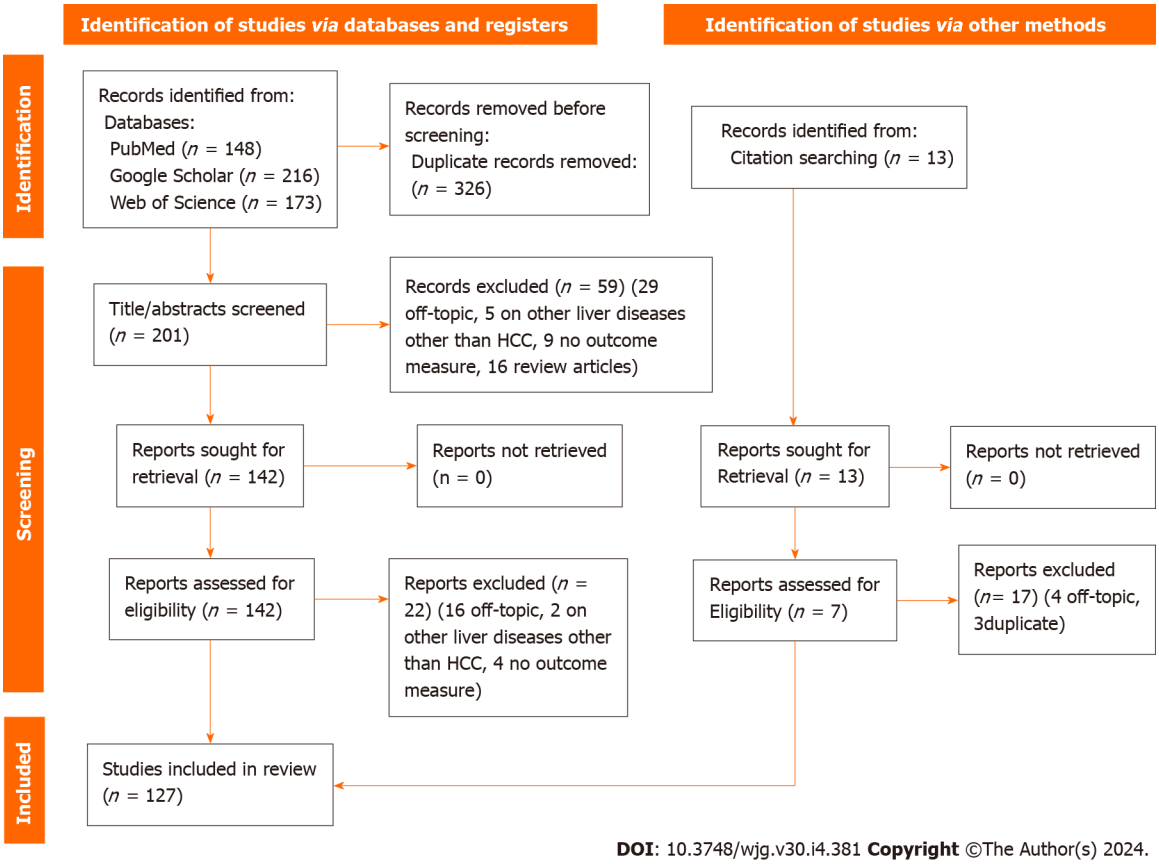

DOI: 10.3748/wjg.v30.i4.381 **Copyright** ©The Author(s) 2024.

Figure 1 PRISMA flow diagram of included studies. HCC: Hepatocellular carcinoma.

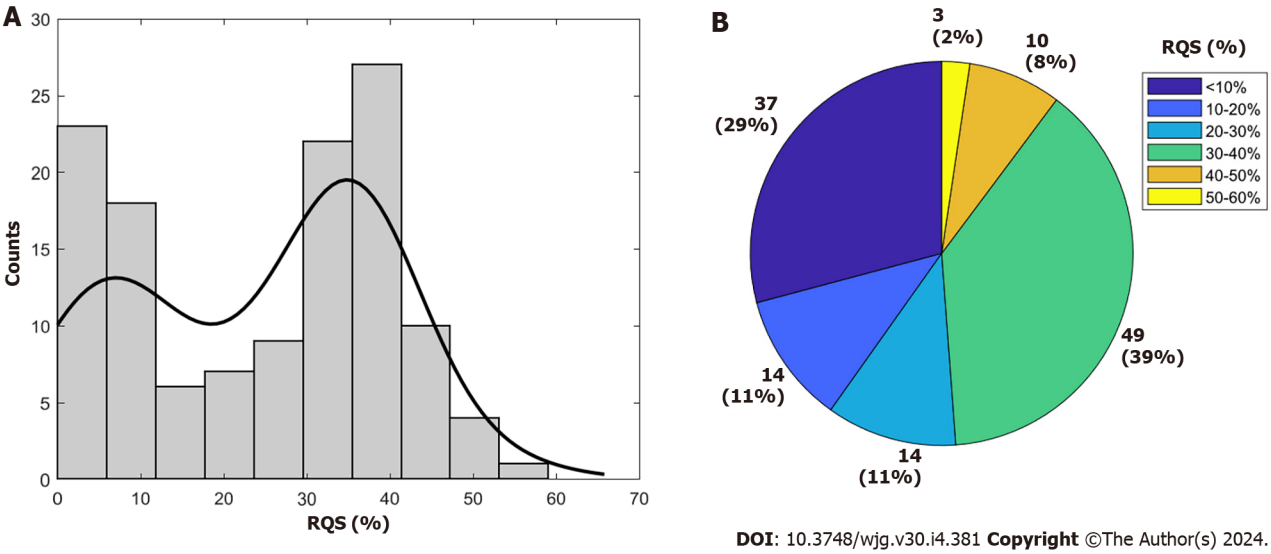

DOI: 10.3748/wjg.v30.i4.381 **Copyright** ©The Author(s) 2024.

Figure 2 Results of Radiomics Quality Score assessment. A: Histogram plot of row counts of included studies according to Results of Radiomics Quality Score (RQS) percentage; B: Pie chart of the mean RQS of included studies. RQS: Radiomics Quality Score.

across the studies using the RQS tools. 127 studies from November 2017 onwards were examined in our study. Despite promising results obtained from each of them (with best AUC and C-indexes reaching 0.98 and 0.94, respectively), our study revealed that the methodological variability of the research is considerable, and the reporting quality is insufficient.

Mean RQS was 8 out of 36, with a mean percentage RQS of 24.15%. These results are consistent with previously published data on a variety of tumors, including prostate, breast, lung, renal, and brain cancer[27-31]. Recent studies evaluating research quality in HCC radiomics also align with our findings[25,32]. However, direct comparison with our study is not possible due to differences in purpose and inclusion criteria.

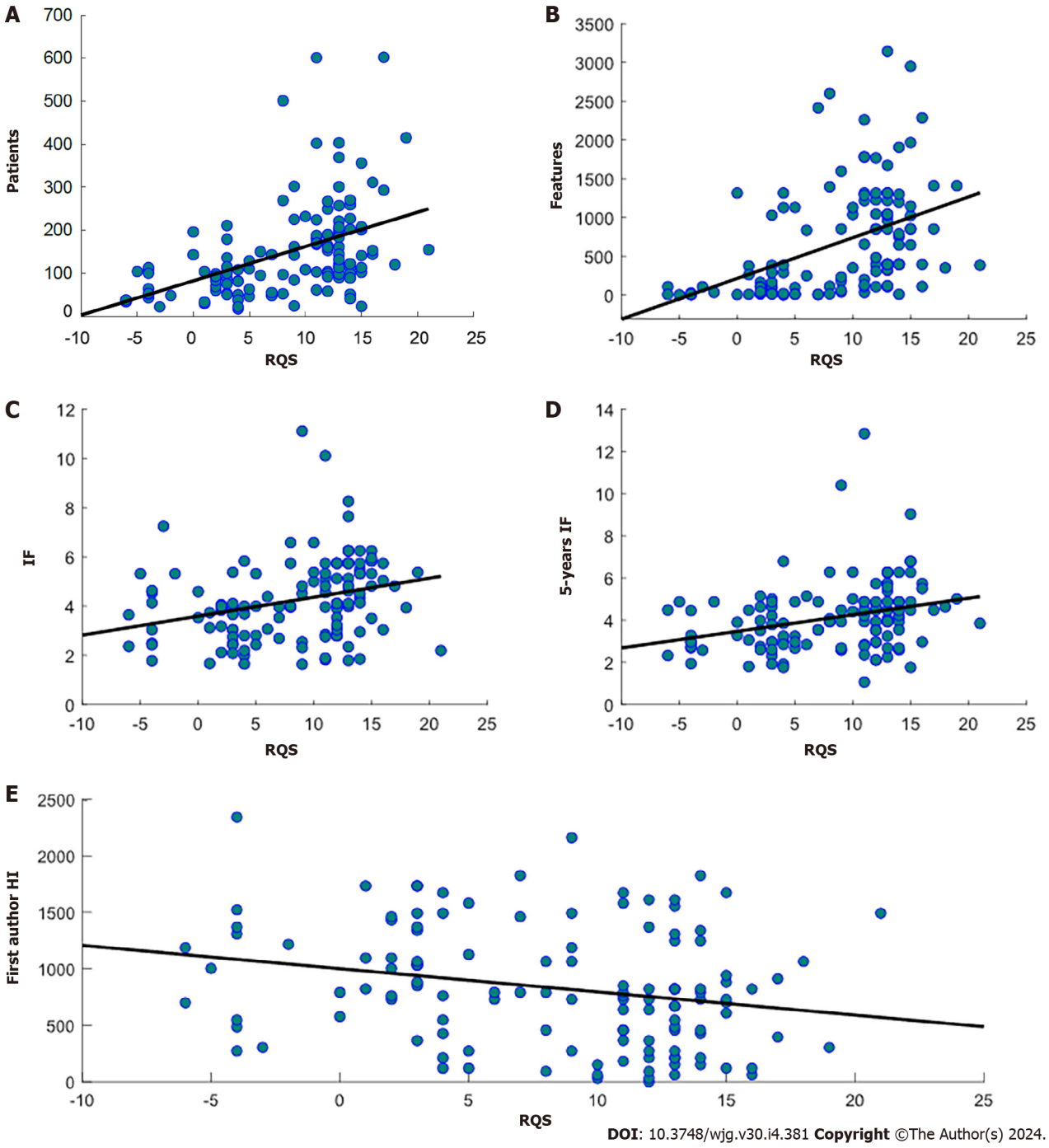

DOI: 10.3748/wjg.v30.i4.381

Figure 3 Scatterplots with regression lines showing correlations between Radiomics Quality Score and journal metrics. A: Correlation between Radiomics Quality Score (RQS) and number of included patients; B: Correlation between RQS and number of radiomic features extracted; C: Correlation between RQS and impact factor (IF); D: Correlation between RQS and 5-years IF; E: Correlation between RQS and first author. Each point corresponds to a study. RQS: Radiomics Quality Score; IF: Impact factor; HI: H-Index.

The results of our analysis showed that the poor RQS scores of the included studies were mostly caused by the absence of rigorous procedures pertaining to radiomics workflow.

Regarding RQS checkpoint 1, practically all investigations have a thorough documentation of the imaging methodology. Nevertheless, the lack of public image methods in the investigations negatively impacts the radiomic studies' repeatability and reproducibility. Notably, the CE-T1WI MRI sequence emerged as the most extensively explored, given its primary role in preoperative HCC assessment. Nevertheless, there exists variability in MRI acquisition due to differences in manufacturers, scanning protocols, contrast media, and phases employed. A significant diversity across the included studies was also noted in terms of RQS checkpoint 2. Specifically, 108 out of 127 studies adopted multiple segmentations to mitigate bias arising from segmentation variability. It's crucial to highlight, however, the lack of consistency among studies regarding the type of ROI (2D/3D) and the segmentation method used (manual, semi-automatic, automatic). It is worth mentioning that the majority of studies used manual or semi-automated image segmentation with manual correction, which restricts the studies included. Both manual and semi-automatic

segmentation can introduce significant observation bias, which may affect studies on intra- and interobserver variation in ROI/VOI delineation[1].

None of the studies determined scanner/manufacturer variability or collected images at multiple time points, making it difficult to detect potential feature variability between scanners and manufacturers, as well as temporal variability. Positively, all but twelve studies performed feature reduction, which is consistent with the third RQS checkpoint. In fact, excessive dimensionality of features can negatively affect model performance and lead to overfitting[33]. The RQS showed high variability in items 6, 7 and 8. However, it is important to note that these items are highly dependent on the aim of the study.

Another notable finding from our review was that only nine of the studies in the review were prospective studies, which is the highest weighting in the RQS tool. This constitutes a significant drawback in radiological studies since a meticulously planned prospective trial serves to diminish and control potential confounding factors, thereby offering a superior level of evidence regarding the trial's quality. This elucidates the rationale behind assigning the highest weight (7 points) to studies with a prospective design in the RQS tool, representing approximately 20% of the total score. Thus, this limitation highlights the importance of conducting well-designed prospective studies.

It is noteworthy that nearly half of the examined papers lacked outcome validation which increases the risk of false-positive results and hinders the implementation of radiomics in clinical practice. However, approximately half of the studies that did not validate their results with an independent cohort chose to perform cross-validation.

The majority of the studies did not provide open access to their data sets, segmentations or codes, which limits the ability to verify and reproduce their results[34,35].

Cost-effectiveness analyses that evaluate radiomic prediction models from a health economic perspective when applied in clinical practice have the same limitation. The assumption is that a new predictor should be no more costly than existing predictors, given comparable accuracy. In addition, the health impact of a radiomics predictor is compared to a condition in which no radiomic predictor[2,32]. However, this criterion of RQS is not as important as the need to standardize and validate the models.

As far as we are aware, this is the first systematic review that looks into the possibility of employing MRI radiomics to gather information regarding the management of HCC and to assess studies using the RQS tool.

Previous studies evaluated the quality of radiomic analysis in different studies for different oncologic applications[27-31,36]. Similar to our study, Wakabayashi *et al*[25] assessed whether radiomics is a valuable and reproducible method for clinical management of HCC using RQS. However, their work included studies up to 2018 and was not focused on MRI modality. In addition, Wang *et al*[32] also aimed to assess the methodological quality of radiomics studies for HCC management. However, although similar findings with respect to our study were found (mean RQS of 10), their study was focused on the prediction of MVI in HCC patients and also included studies involving other imaging modalities than MRI.

I contrast to most studies that focus on assessing the quality of radiomic studies by means of RQS, our approach involved exploring the potential correlation between RQS and scientometric indixes. Our findings revealed that publications that have higher RQS were published in journals with higher IF and 5-years IF. However, studies with high/low RQS and low/high IF and 5-years IF were also found. Moreover, although no significant correlation was found, it was observed that RQS tended to increase with time (decreasing number of months passed from literature research). Interestingly, we discovered that the quality of included studies increased as the number of included patients and extracted attributes grew.

It is crucial to underscore that only 45 out of 127 studies referenced the Image Biomarker Standardization Initiative (IBSI) guidelines or utilized software for radiomic feature extraction compliant with IBSI standards (*e.g.*, PyRadiomics). Emphasizing the importance of adhering to standardized radiomic features nomenclature and calculation according to IBSI, our study highlights the need for future research to align with these standards, thus enhancing the reproducibility of scientific researches[37].

Despite the insights gained, our study is not without limitations. The RQS scoring system, as acknowledged in prior research, is not a definitive standard for evaluating radiomics studies and requires ongoing refinement for widespread acceptance in radiology. The existing research is limited by issues including conducting phantom studies across all scanners, applying imaging at multiple time points, and lacking definition for a particular study purpose[38,39]. Additionally, the predominantly retrospective nature of the included studies introduces bias, compounded by the absence of external validation cohorts and comparisons with reference standards, hindering conclusive remarks on the efficacy of MRI radiomics in HCC[40,41]. Variability in sample size, inclusion criteria, and methodological settings across studies precluded a meta-analysis aligned with study objectives. Furthermore, the study did not explore specific shared radiomic features among different studies, considering the wide-ranging variability in imaging protocols and software for feature extraction.

CONCLUSION

In summary, despite the potential of recent developments in MRI radiomics to fulfill the urgent requirement for noninvasive, radiation-free, and quantitative approaches to support decision-making in HCC treatment, the current studies in this domain lack the requisite quality for integration into clinical practice. Emphasizing the significance of external validation, addressing concerns related to feature reproducibility, conducting clinical utility analyses, and fostering scientific openness are crucial steps that need to be addressed. This endeavor aims to provide fresh perspectives and contribute to the establishment of a consensus regarding the application of the radiomic method in assessing HCC.

ARTICLE HIGHLIGHTS

Research background

Radiomics is a promising tool that may increase the value of Magnetic Resonance Imaging (MRI) for different tasks linked to the management of patients with hepatocellular carcinoma (HCC).

Research motivation

Over the last decade, there has been a substantial increase in radiomics studies in the field of HCC. Many of these studies have demonstrated the power of radiomic features for differential diagnosis, grading, predicting microvascular invasion, overall survival, recurrence, and treatment response. However, the use of radiomics in HCC is currently limited to academic literature, and no studies have yet been translated into clinical applications. This has led to doubts among clinicians about the radiomics validity. This is in part due to many issues related to the methodological quality of radiomic studies.

Research objectives

To summarize the status of MRI radiomic studies concerning HCC, using the radiomics quality score (RQS) to assess the quality of the methodology used in each study.

Research methods

We systematically reviewed PubMed, Google Scholar, and Web of Science databases to identify original articles focused on using MRI radiomics for HCC management published between 2017 and 2023. The RQS tool was employed to evaluate the methodological quality of radiomic studies. Spearman's correlation (ρ) analysis was conducted to investigate the association between RQS and journal metrics, as well as the characteristics of the studies. The threshold for statistical significance was established at $P < 0.05$.

Research results

127 articles were included, of which 43 focused on HCC prognosis, 39 on prediction of pathological findings, 16 on prediction of the expression of molecular markers outcomes, 18 had a diagnostic purpose, and 11 had multiple aims. Mean RQS was 8 ± 6.22, with the corresponding percentage of 24.15% ± 15.25% (ranging from 0.0 to 58.33%). RQS was positively correlated with journal impact factor (IF; $\rho = 0.36$, $P = 2.98 \times 10^{-5}$), 5-years IF ($\rho = 0.33$, $P = 1.56 \times 10^{-4}$), number of patients involved ($\rho = 0.51$, $P < 9.37 \times 10^{-10}$) and number of radiomics features ($\rho = 0.59$, $P < 4.59 \times 10^{-13}$) extracted in the study, and time of publication ($\rho = -0.23$, $P = 0.0072$).

Research conclusions

Although the MRI radiomics in HCC represents an auspicious tool for developing adequate personalized treatment as a noninvasive approach in HCC patients, our study revealed that studies in this field still lack the quality required to allow its introduction in clinical practice.

Research perspectives

Although recent advantages in MRI radiomics can potentially satisfy the urgent need for noninvasive, radiation-free and quantitative strategies that can aid in HCC treatment decision making, studies in this field still lack the quality required to allow its introduction in clinical practice. Future studies including external validation and adhering to the standardization of radiomics features are necessary. Moreover, limitations and challenges related to feature reproducibility, analysis of the clinical utility, and openness of science need to be addressed. This work may provide new insights and contribute to a common understanding of the use of radiomics in the assessment of HCC.

FOOTNOTES

Author contributions: Brancato V, Cerrone M and Cavaliere C conceptualized the problem determined the review scope and strategies; Cerrone M, Garbino N, and Cavaliere C conducted the searching and screening of the literature and reviewed the selected articles; Brancato V performed statistical analyses and drafted statistical sections; Cerrone M and Brancato V wrote the manuscript; Brancato V, Cerrone M, Salvatore M and Cavaliere C reviewed and edited the manuscript draft; all authors contributed to the article and approved the submitted version.

Supported by the "Ricerca Corrente" Grant from Italian Ministry of Health, No. IRCCS SYNLAB SDN.

Conflict-of-interest statement: Authors have no conflict of interest to declare.

PRISMA 2009 Checklist statement: The authors have read the PRISMA 2009 Checklist, and the manuscript was prepared and revised according to the PRISMA 2009 Checklist.

Country/Territory of origin: Italy

ORCID number: Valentina Brancato 0000-0002-6232-7645; Marco Cerrone 0000-0001-7448-5766; Nunzia Garbino 0000-0001-6863-7313; Marco Salvatore 0000-0001-9734-7702; Carlo Cavaliere 0000-0002-3297-2213.

S-Editor: Lin C
L-Editor: A
P-Editor: Yu HG

REFERENCES

1 **van Timmeren JE**, Cester D, Tanadini-Lang S, Alkadhi H, Baessler B. Radiomics in medical imaging-"how-to" guide and critical reflection. *Insights Imaging* 2020; **11**: 91 [PMID: 32785796 DOI: 10.1186/s13244-020-00887-2]

2 **Lambin P**, Leijenaar RTH, Deist TM, Peerlings J, de Jong EEC, van Timmeren J, Sanduleanu S, Larue RTHM, Even AJG, Jochems A, van Wijk Y, Woodruff H, van Soest J, Lustberg T, Roelofs E, van Elmpt W, Dekker A, Mottaghy FM, Wildberger JE, Walsh S. Radiomics: the bridge between medical imaging and personalized medicine. *Nat Rev Clin Oncol* 2017; **14**: 749-762 [PMID: 28975929 DOI: 10.1038/nrclinonc.2017.141]

3 **Lu C**, Shiradkar R, Liu Z. Integrating pathomics with radiomics and genomics for cancer prognosis: A brief review. *Chin J Cancer Res* 2021; **33**: 563-573 [PMID: 34815630 DOI: 10.21147/j.issn.1000-9604.2021.05.03]

4 **Bodalal Z**, Trebeschi S, Nguyen-Kim TDL, Schats W, Beets-Tan R. Radiogenomics: bridging imaging and genomics. *Abdom Radiol (NY)* 2019; **44**: 1960-1984 [PMID: 31049614 DOI: 10.1007/s00261-019-02028-w]

5 **Gillies RJ**, Kinahan PE, Hricak H. Radiomics: Images Are More than Pictures, They Are Data. *Radiology* 2016; **278**: 563-577 [PMID: 26579733 DOI: 10.1148/radiol.2015151169]

6 **Limkin EJ**, Sun R, Dercle L, Zacharaki EI, Robert C, Reuzé S, Schernberg A, Paragios N, Deutsch E, Ferté C. Promises and challenges for the implementation of computational medical imaging (radiomics) in oncology. *Ann Oncol* 2017; **28**: 1191-1206 [PMID: 28168275 DOI: 10.1093/annonc/mdx034]

7 **Barcena-Varela M**, Lujambio A. The Endless Sources of Hepatocellular Carcinoma Heterogeneity. *Cancers (Basel)* 2021; **13** [PMID: 34073538 DOI: 10.3390/cancers13112621]

8 **Sung H**, Ferlay J, Siegel RL, Laversanne M, Soerjomataram I, Jemal A, Bray F. Global Cancer Statistics 2020: GLOBOCAN Estimates of Incidence and Mortality Worldwide for 36 Cancers in 185 Countries. *CA Cancer J Clin* 2021; **71**: 209-249 [PMID: 33538338 DOI: 10.3322/caac.21660]

9 **Vogel A**, Cervantes A, Chau I, Daniele B, Llovet JM, Meyer T, Nault JC, Neumann U, Ricke J, Sangro B, Schirmacher P, Verslype C, Zech CJ, Arnold D, Martinelli E; ESMO Guidelines Committee. Hepatocellular carcinoma: ESMO Clinical Practice Guidelines for diagnosis, treatment and follow-up. *Ann Oncol* 2018; **29**: iv238-iv255 [PMID: 30285213 DOI: 10.1093/annonc/mdy308]

10 **Osho A**, Rich NE, Singal AG. Role of imaging in management of hepatocellular carcinoma: surveillance, diagnosis, and treatment response. *Hepatoma Res* 2020; **6** [PMID: 32944652 DOI: 10.20517/2394-5079.2020.42]

11 **European Association For The Study Of The Liver**; European Organisation For Research And Treatment Of Cancer. EASL-EORTC clinical practice guidelines: management of hepatocellular carcinoma. *J Hepatol* 2012; **56**: 908-943 [PMID: 22424438 DOI: 10.1016/j.jhep.2011.12.001]

12 **Navin PJ**, Venkatesh SK. Hepatocellular Carcinoma: State of the Art Imaging and Recent Advances. *J Clin Transl Hepatol* 2019; **7**: 72-85 [PMID: 30944823 DOI: 10.14218/JCTH.2018.00032]

13 **Chernyak V**, Fowler KJ, Kamaya A, Kielar AZ, Elsayes KM, Bashir MR, Kono Y, Do RK, Mitchell DG, Singal AG, Tang A, Sirlin CB. Liver Imaging Reporting and Data System (LI-RADS) Version 2018: Imaging of Hepatocellular Carcinoma in At-Risk Patients. *Radiology* 2018; **289**: 816-830 [PMID: 30251931 DOI: 10.1148/radiol.2018181494]

14 **Choi JY**, Lee JM, Sirlin CB. CT and MR imaging diagnosis and staging of hepatocellular carcinoma: part I. Development, growth, and spread: key pathologic and imaging aspects. *Radiology* 2014; **272**: 635-654 [PMID: 25153274 DOI: 10.1148/radiol.14132361]

15 **Choi JY**, Lee JM, Sirlin CB. CT and MR imaging diagnosis and staging of hepatocellular carcinoma: part II. Extracellular agents, hepatobiliary agents, and ancillary imaging features. *Radiology* 2014; **273**: 30-50 [PMID: 25247563 DOI: 10.1148/radiol.14132362]

16 **Kong C**, Zhao Z, Chen W, Lv X, Shu G, Ye M, Song J, Ying X, Weng Q, Weng W, Fang S, Chen M, Tu J, Ji J. Prediction of tumor response *via* a pretreatment MRI radiomics-based nomogram in HCC treated with TACE. *Eur Radiol* 2021; **31**: 7500-7511 [PMID: 33860832 DOI: 10.1007/s00330-021-07910-0]

17 **Harding-Theobald E**, Louissaint J, Maraj B, Cuaresma E, Townsend W, Mendiratta-Lala M, Singal AG, Su GL, Lok AS, Parikh ND. Systematic review: radiomics for the diagnosis and prognosis of hepatocellular carcinoma. *Aliment Pharmacol Ther* 2021; **54**: 890-901 [PMID: 34390014 DOI: 10.1111/apt.16563]

18 **Tang YY**, Zhao YN, Zhang T, Chen ZY, Ma XL. Comprehensive radiomics nomogram for predicting survival of patients with combined hepatocellular carcinoma and cholangiocarcinoma. *World J Gastroenterol* 2021; **27**: 7173-7189 [PMID: 34887636 DOI: 10.3748/wjg.v27.i41.7173]

19 **Chen W**, Zhang T, Xu L, Zhao L, Liu H, Gu LR, Wang DZ, Zhang M. Radiomics Analysis of Contrast-Enhanced CT for Hepatocellular Carcinoma Grading. *Front Oncol* 2021; **11**: 660509 [PMID: 34150628 DOI: 10.3389/fonc.2021.660509]

20 **Vallières M**, Zwanenburg A, Badic B, Cheze Le Rest C, Visvikis D, Hatt M. Responsible Radiomics Research for Faster Clinical Translation. *J Nucl Med* 2018; **59**: 189-193 [PMID: 29175982 DOI: 10.2967/jnumed.117.200501]

21 **Shaikh F**, Franc B, Allen E, Sala E, Awan O, Hendrata K, Halabi S, Mohiuddin S, Malik S, Hadley D, Shrestha R. Translational Radiomics: Defining the Strategy Pipeline and Considerations for Application-Part 2: From Clinical Implementation to Enterprise. *J Am Coll Radiol* 2018;

15: 543-549 [PMID: 29366598 DOI: 10.1016/j.jacr.2017.12.006]
22 **Shaikh F**, Franc B, Allen E, Sala E, Awan O, Hendrata K, Halabi S, Mohiuddin S, Malik S, Hadley D, Shrestha R. Translational Radiomics: Defining the Strategy Pipeline and Considerations for Application-Part 1: From Methodology to Clinical Implementation. *J Am Coll Radiol* 2018; **15**: 538-542 [PMID: 29366600 DOI: 10.1016/j.jacr.2017.12.008]
23 **Sagir Kahraman A**. Radiomics in Hepatocellular Carcinoma. *J Gastrointest Cancer* 2020; **51**: 1165-1168 [PMID: 32844349 DOI: 10.1007/s12029-020-00493-x]
24 **Miranda Magalhaes Santos JM**, Clemente Oliveira B, Araujo-Filho JAB, Assuncao-Jr AN, de M Machado FA, Carlos Tavares Rocha C, Horvat JV, Menezes MR, Horvat N. State-of-the-art in radiomics of hepatocellular carcinoma: a review of basic principles, applications, and limitations. *Abdom Radiol (NY)* 2020; **45**: 342-353 [PMID: 31707435 DOI: 10.1007/s00261-019-02299-3]
25 **Wakabayashi T**, Ouhmich F, Gonzalez-Cabrera C, Felli E, Saviano A, Agnus V, Savadjiev P, Baumert TF, Pessaux P, Marescaux J, Gallix B. Radiomics in hepatocellular carcinoma: a quantitative review. *Hepatol Int* 2019; **13**: 546-559 [PMID: 31473947 DOI: 10.1007/s12072-019-09973-0]
26 **Page MJ**, McKenzie JE, Bossuyt PM, Boutron I, Hoffmann TC, Mulrow CD, Shamseer L, Tetzlaff JM, Akl EA, Brennan SE, Chou R, Glanville J, Grimshaw JM, Hróbjartsson A, Lalu MM, Li T, Loder EW, Mayo-Wilson E, McDonald S, McGuinness LA, Stewart LA, Thomas J, Tricco AC, Welch VA, Whiting P, Moher D. The PRISMA 2020 statement: an updated guideline for reporting systematic reviews. *BMJ* 2021; **372**: n71 [PMID: 33782057 DOI: 10.1136/bmj.n71]
27 **Stanzione A**, Gambardella M, Cuocolo R, Ponsiglione A, Romeo V, Imbriaco M. Prostate MRI radiomics: A systematic review and radiomic quality score assessment. *Eur J Radiol* 2020; **129**: 109095 [PMID: 32531722 DOI: 10.1016/j.ejrad.2020.109095]
28 **Granzier RWY**, van Nijnatten TJA, Woodruff HC, Smidt ML, Lobbes MBI. Exploring breast cancer response prediction to neoadjuvant systemic therapy using MRI-based radiomics: A systematic review. *Eur J Radiol* 2019; **121**: 108736 [PMID: 31734639 DOI: 10.1016/j.ejrad.2019.108736]
29 **Ursprung S**, Beer L, Bruining A, Woitek R, Stewart GD, Gallagher FA, Sala E. Radiomics of computed tomography and magnetic resonance imaging in renal cell carcinoma-a systematic review and meta-analysis. *Eur Radiol* 2020; **30**: 3558-3566 [PMID: 32060715 DOI: 10.1007/s00330-020-06666-3]
30 **Park JE**, Kim HS, Kim D, Park SY, Kim JY, Cho SJ, Kim JH. A systematic review reporting quality of radiomics research in neuro-oncology: toward clinical utility and quality improvement using high-dimensional imaging features. *BMC Cancer* 2020; **20**: 29 [PMID: 31924170 DOI: 10.1186/s12885-019-6504-5]
31 **Chen Q**, Zhang L, Mo X, You J, Chen L, Fang J, Wang F, Jin Z, Zhang B, Zhang S. Current status and quality of radiomic studies for predicting immunotherapy response and outcome in patients with non-small cell lung cancer: a systematic review and meta-analysis. *Eur J Nucl Med Mol Imaging* 2021; **49**: 345-360 [PMID: 34402924 DOI: 10.1007/s00259-021-05509-7]
32 **Wang Q**, Li C, Zhang J, Hu X, Fan Y, Ma K, Sparrelid E, Brismar TB. Radiomics Models for Predicting Microvascular Invasion in Hepatocellular Carcinoma: A Systematic Review and Radiomics Quality Score Assessment. *Cancers (Basel)* 2021; **13** [PMID: 34831018 DOI: 10.3390/cancers13225864]
33 **Park JE**, Park SY, Kim HJ, Kim HS. Reproducibility and Generalizability in Radiomics Modeling: Possible Strategies in Radiologic and Statistical Perspectives. *Korean J Radiol* 2019; **20**: 1124-1137 [PMID: 31270976 DOI: 10.3348/kjr.2018.0070]
34 **Vesteghem C**, Brøndum RF, Sønderkær M, Sommer M, Schmitz A, Bødker JS, Dybkær K, El-Galaly TC, Bøgsted M. Implementing the FAIR Data Principles in precision oncology: review of supporting initiatives. *Brief Bioinform* 2020; **21**: 936-945 [PMID: 31263868 DOI: 10.1093/bib/bbz044]
35 **Hasselbring W**, Carr L, Hettrick S, Packer H, Tiropanis T. From FAIR research data toward FAIR and open research software. *it – Inf Technol* 2020; **62**: 39-47 [DOI: 10.1515/itit-2019-0040]
36 **Wang H**, Zhou Y, Li L, Hou W, Ma X, Tian R. Current status and quality of radiomics studies in lymphoma: a systematic review. *Eur Radiol* 2020; **30**: 6228-6240 [PMID: 32472274 DOI: 10.1007/s00330-020-06927-1]
37 **Zwanenburg A**, Vallières M, Abdalah MA, Aerts HJWL, Andrearczyk V, Apte A, Ashrafinia S, Bakas S, Beukinga RJ, Boellaard R, Bogowicz M, Boldrini L, Buvat I, Cook GJR, Davatzikos C, Depeursinge A, Desseroit MC, Dinapoli N, Dinh CV, Echegaray S, El Naqa I, Fedorov AY, Gatta R, Gillies RJ, Goh V, Götz M, Guckenberger M, Ha SM, Hatt M, Isensee F, Lambin P, Leger S, Leijenaar RTH, Lenkowicz J, Lippert F, Losnegård A, Maier-Hein KH, Morin O, Müller H, Napel S, Nioche C, Orlhac F, Pati S, Pfaehler EAG, Rahmim A, Rao AUK, Scherer J, Siddique MM, Sijtsema NM, Socarras Fernandez J, Spezi E, Steenbakkers RJHM, Tanadini-Lang S, Thorwarth D, Troost EGC, Upadhaya T, Valentini V, van Dijk LV, van Griethuysen J, van Velden FHP, Whybra P, Richter C, Löck S. The Image Biomarker Standardization Initiative: Standardized Quantitative Radiomics for High-Throughput Image-based Phenotyping. *Radiology* 2020; **295**: 328-338 [PMID: 32154773 DOI: 10.1148/radiol.2020191145]
38 **Sanduleanu S**, Woodruff HC, de Jong EEC, van Timmeren JE, Jochems A, Dubois L, Lambin P. Tracking tumor biology with radiomics: A systematic review utilizing a radiomics quality score. *Radiother Oncol* 2018; **127**: 349-360 [PMID: 29779918 DOI: 10.1016/j.radonc.2018.03.033]
39 **Park JE**, Kim D, Kim HS, Park SY, Kim JY, Cho SJ, Shin JH, Kim JH. Quality of science and reporting of radiomics in oncologic studies: room for improvement according to radiomics quality score and TRIPOD statement. *Eur Radiol* 2020; **30**: 523-536 [PMID: 31350588 DOI: 10.1007/s00330-019-06360-z]
40 **Norvell DC**. Study types and bias-Don't judge a study by the abstract's conclusion alone. *Evid Based Spine Care J* 2010; **1**: 7-10 [PMID: 23637661 DOI: 10.1055/s-0028-1100908]
41 **Tripepi G**, Jager KJ, Dekker FW, Zoccali C. Selection bias and information bias in clinical research. *Nephron Clin Pract* 2010; **115**: c94-c99 [PMID: 20407272 DOI: 10.1159/000312871]
42 **Liu J**, Cheng D, Liao Y, Luo C, Lei Q, Zhang X, Wang L, Wen Z, Gao M. Development of a magnetic resonance imaging-derived radiomics model to predict microvascular invasion in patients with hepatocellular carcinoma. *Quant Imaging Med Surg* 2023; **13**: 3948-3961 [PMID: 37284095 DOI: 10.21037/qims-22-1011]
43 **Wang Y**, Liu Z, Xu H, Yang D, Jiang J, Asayo H, Yang Z. MRI-based radiomics model and nomogram for predicting the outcome of locoregional treatment in patients with hepatocellular carcinoma. *BMC Med Imaging* 2023; **23**: 67 [PMID: 37254089 DOI: 10.1186/s12880-023-01030-5]
44 **Gong XQ**, Liu N, Tao YY, Li L, Li ZM, Yang L, Zhang XM. Radiomics models based on multisequence MRI for predicting PD-1/PD-L1 expression in hepatocellular carcinoma. *Sci Rep* 2023; **13**: 7710 [PMID: 37173350 DOI: 10.1038/s41598-023-34763-y]
45 **Zhang L**, Zhou H, Zhang X, Ding Z, Xu J. A radiomics nomogram for predicting cytokeratin 19-positive hepatocellular carcinoma: a two-

center study. *Front Oncol* 2023; **13**: 1174069 [PMID: 37182122 DOI: 10.3389/fonc.2023.1174069]
46 **Zhang Y**, He D, Liu J, Wei YG, Shi LL. Preoperative prediction of macrotrabecular-massive hepatocellular carcinoma through dynamic contrast-enhanced magnetic resonance imaging-based radiomics. *World J Gastroenterol* 2023; **29**: 2001-2014 [PMID: 37155523 DOI: 10.3748/wjg.v29.i13.2001]
47 **Dong X**, Yang J, Zhang B, Li Y, Wang G, Chen J, Wei Y, Zhang H, Chen Q, Jin S, Wang L, He H, Gan M, Ji W. Deep Learning Radiomics Model of Dynamic Contrast-Enhanced MRI for Evaluating Vessels Encapsulating Tumor Clusters and Prognosis in Hepatocellular Carcinoma. *J Magn Reson Imaging* 2024; **59**: 108-119 [PMID: 37078470 DOI: 10.1002/jmri.28745]
48 **Tabari A**, D'Amore B, Cox M, Brito S, Gee MS, Wehrenberg-Klee E, Uppot RN, Daye D. Machine Learning-Based Radiomic Features on Pre-Ablation MRI as Predictors of Pathologic Response in Patients with Hepatocellular Carcinoma Who Underwent Hepatic Transplant. *Cancers (Basel)* 2023; **15** [PMID: 37046718 DOI: 10.3390/cancers15072058]
49 **Cao X**, Yang H, Luo X, Zou L, Zhang Q, Li Q, Zhang J, Li X, Shi Y, Jin C. A Cox Nomogram for Assessing Recurrence Free Survival in Hepatocellular Carcinoma Following Surgical Resection Using Dynamic Contrast-Enhanced MRI Radiomics. *J Magn Reson Imaging* 2023; **58**: 1930-1941 [PMID: 37177868 DOI: 10.1002/jmri.28725]
50 **İnce O**, Önder H, Gençtürk M, Cebeci H, Golzarian J, Young S. Prediction of Response of Hepatocellular Carcinoma to Radioembolization: Machine Learning Using Preprocedural Clinical Factors and MR Imaging Radiomics. *J Vasc Interv Radiol* 2023; **34**: 235-243.e3 [PMID: 36384224 DOI: 10.1016/j.jvir.2022.11.004]
51 **Chen M**, Kong C, Qiao E, Chen Y, Chen W, Jiang X, Fang S, Zhang D, Chen M, Ji J. Multi-algorithms analysis for pre-treatment prediction of response to transarterial chemoembolization in hepatocellular carcinoma on multiphase MRI. *Insights Imaging* 2023; **14**: 38 [PMID: 36854872 DOI: 10.1186/s13244-023-01380-2]
52 **Jiang T**, He S, Yang H, Dong Y, Yu T, Luo Y, Jiang X. Multiparametric MRI-based radiomics for the prediction of microvascular invasion in hepatocellular carcinoma. *Acta Radiol* 2023; **64**: 456-466 [PMID: 35354318 DOI: 10.1177/02841851221080830]
53 **Hu X**, Wang Q, Huang G, He X, Sparrelid E, Brismar TB, Fan Y. Gadoxetic Acid-Enhanced MRI-Based Radiomics Signature: A Potential Imaging Biomarker for Identifying Cytokeratin 19-Positive Hepatocellular Carcinoma. *Comput Math Methods Med* 2023; **2023**: 5424204 [PMID: 36814805 DOI: 10.1155/2023/5424204]
54 **Chong H**, Gong Y, Zhang Y, Dai Y, Sheng R, Zeng M. Radiomics on Gadoxetate Disodium-enhanced MRI: Non-invasively Identifying Glypican 3-Positive Hepatocellular Carcinoma and Postoperative Recurrence. *Acad Radiol* 2023; **30**: 49-63 [PMID: 35562264 DOI: 10.1016/j.acra.2022.04.006]
55 **Hu X**, Li C, Wang Q, Wu X, Chen Z, Xia F, Cai P, Zhang L, Fan Y, Ma K. Development and External Validation of a Radiomics Model Derived from Preoperative Gadoxetic Acid-Enhanced MRI for Predicting Histopathologic Grade of Hepatocellular Carcinoma. *Diagnostics (Basel)* 2023; **13** [PMID: 36766518 DOI: 10.3390/diagnostics13030413]
56 **Tao YY**, Shi Y, Gong XQ, Li L, Li ZM, Yang L, Zhang XM. Radiomic Analysis Based on Magnetic Resonance Imaging for Predicting PD-L2 Expression in Hepatocellular Carcinoma. *Cancers (Basel)* 2023; **15** [PMID: 36672315 DOI: 10.3390/cancers15020365]
57 **Yang X**, Yuan C, Zhang Y, Li K, Wang Z. Predicting hepatocellular carcinoma early recurrence after ablation based on magnetic resonance imaging radiomics nomogram. *Medicine (Baltimore)* 2022; **101**: e32584 [PMID: 36596081 DOI: 10.1097/MD.0000000000032584]
58 **Liu HF**, Zhang YZ, Wang Q, Zhu ZH, Xing W. A nomogram model integrating LI-RADS features and radiomics based on contrast-enhanced magnetic resonance imaging for predicting microvascular invasion in hepatocellular carcinoma falling the Milan criteria. *Transl Oncol* 2023; **27**: 101597 [PMID: 36502701 DOI: 10.1016/j.tranon.2022.101597]
59 **Zhang S**, Duan C, Zhou X, Liu F, Wang X, Shao Q, Gao Y, Duan F, Zhao R, Wang G. Radiomics nomogram for prediction of microvascular invasion in hepatocellular carcinoma based on MR imaging with Gd-EOB-DTPA. *Front Oncol* 2022; **12**: 1034519 [PMID: 36387156 DOI: 10.3389/fonc.2022.1034519]
60 **Sim JZT**, Hui TCH, Chuah TK, Low HM, Tan CH, Shelat VG. Efficacy of texture analysis of pre-operative magnetic resonance imaging in predicting microvascular invasion in hepatocellular carcinoma. *World J Clin Oncol* 2022; **13**: 918-928 [PMID: 36483976 DOI: 10.5306/wjco.v13.i11.918]
61 **Zhang X**, Wang C, Zheng D, Liao Y, Wang X, Huang Z, Zhong Q. Radiomics nomogram based on multi-parametric magnetic resonance imaging for predicting early recurrence in small hepatocellular carcinoma after radiofrequency ablation. *Front Oncol* 2022; **12**: 1013770 [PMID: 36439458 DOI: 10.3389/fonc.2022.1013770]
62 **Zhao Y**, Huang F, Liu S, Jian L, Xia X, Lin H, Liu J. Prediction of therapeutic response of unresectable hepatocellular carcinoma to hepatic arterial infusion chemotherapy based on pretherapeutic MRI radiomics and Albumin-Bilirubin score. *J Cancer Res Clin Oncol* 2023; **149**: 5181-5192 [PMID: 36369395 DOI: 10.1007/s00432-022-04467-3]
63 **Lu XY**, Zhang JY, Zhang T, Zhang XQ, Lu J, Miao XF, Chen WB, Jiang JF, Ding D, Du S. Using pre-operative radiomics to predict microvascular invasion of hepatocellular carcinoma based on Gd-EOB-DTPA enhanced MRI. *BMC Med Imaging* 2022; **22**: 157 [PMID: 36057576 DOI: 10.1186/s12880-022-00855-w]
64 **Yang WL**, Zhu F, Chen WX. Texture analysis of contrast-enhanced magnetic resonance imaging predicts microvascular invasion in hepatocellular carcinoma. *Eur J Radiol* 2022; **156**: 110528 [PMID: 36162156 DOI: 10.1016/j.ejrad.2022.110528]
65 **Ameli S**, Venkatesh BA, Shaghaghi M, Ghadimi M, Hazhirkarzar B, Rezvani Habibabadi R, Aliyari Ghasabeh M, Khoshpouri P, Pandey A, Pandey P, Pan L, Grimm R, Kamel IR. Role of MRI-Derived Radiomics Features in Determining Degree of Tumor Differentiation of Hepatocellular Carcinoma. *Diagnostics (Basel)* 2022; **12** [PMID: 36292074 DOI: 10.3390/diagnostics12102386]
66 **Li W**, Shen H, Han L, Liu J, Xiao B, Li X, Ye Z. A Multiparametric Fusion Radiomics Signature Based on Contrast-Enhanced MRI for Predicting Early Recurrence of Hepatocellular Carcinoma. *J Oncol* 2022; **2022**: 3704987 [PMID: 36213823 DOI: 10.1155/2022/3704987]
67 **Zeng F**, Dai H, Li X, Guo L, Jia N, Yang J, Huang D, Zeng H, Chen W, Zhang L, Qin G. Preoperative radiomics model using gadobenate dimeglumine-enhanced magnetic resonance imaging for predicting β-catenin mutation in patients with hepatocellular carcinoma: A retrospective study. *Front Oncol* 2022; **12**: 916126 [PMID: 36185240 DOI: 10.3389/fonc.2022.916126]
68 **Aujay G**, Etchegaray C, Blanc JF, Lapuyade B, Papadopoulos P, Pey MA, Bordenave L, Trillaud H, Saut O, Pinaquy JB. Comparison of MRI-based response criteria and radiomics for the prediction of early response to transarterial radioembolization in patients with hepatocellular carcinoma. *Diagn Interv Imaging* 2022; **103**: 360-366 [PMID: 35183483 DOI: 10.1016/j.diii.2022.01.009]
69 **Chen YD**, Zhang L, Zhou ZP, Lin B, Jiang ZJ, Tang C, Dang YW, Xia YW, Song B, Long LL. Radiomics and nomogram of magnetic resonance imaging for preoperative prediction of microvascular invasion in small hepatocellular carcinoma. *World J Gastroenterol* 2022; **28**: 4399-4416 [PMID: 36159011 DOI: 10.3748/wjg.v28.i31.4399]
70 **Wu Q**, Yu YX, Zhang T, Zhu WJ, Fan YF, Wang XM, Hu CH. Preoperative Diagnosis of Dual-Phenotype Hepatocellular Carcinoma Using

Enhanced MRI Radiomics Models. *J Magn Reson Imaging* 2023; **57**: 1185-1196 [PMID: 36190656 DOI: 10.1002/jmri.28391]
71 **Li YM**, Zhu YM, Gao LM, Han ZW, Chen XJ, Yan C, Ye RP, Cao DR. Radiomic analysis based on multi-phase magnetic resonance imaging to predict preoperatively microvascular invasion in hepatocellular carcinoma. *World J Gastroenterol* 2022; **28**: 2733-2747 [PMID: 35979164 DOI: 10.3748/wjg.v28.i24.2733]
72 **Wang L**, Ma X, Feng B, Wang S, Liang M, Li D, Zhao X. Multi-Sequence MR-Based Radiomics Signature for Predicting Early Recurrence in Solitary Hepatocellular Carcinoma ≤5 cm. *Front Oncol* 2022; **12**: 899404 [PMID: 35756618 DOI: 10.3389/fonc.2022.899404]
73 **Zhang HD**, Li XM, Zhang YH, Hu F, Tan L, Wang F, Jing Y, Guo DJ, Xu Y, Hu XL, Liu C, Wang J. Evaluation of Preoperative Microvascular Invasion in Hepatocellular Carcinoma Through Multidimensional Parameter Combination Modeling Based on Gd-EOB-DTPA MRI. *J Clin Transl Hepatol* 2023; **11**: 350-359 [PMID: 36643030 DOI: 10.14218/JCTH.2021.00546]
74 **Brancato V**, Garbino N, Salvatore M, Cavaliere C. MRI-Based Radiomic Features Help Identify Lesions and Predict Histopathological Grade of Hepatocellular Carcinoma. *Diagnostics (Basel)* 2022; **12** [PMID: 35626241 DOI: 10.3390/diagnostics12051085]
75 **Fan T**, Li S, Li K, Xu J, Zhao S, Li J, Zhou X, Jiang H. A Potential Prognostic Marker for Recognizing VEGF-Positive Hepatocellular Carcinoma Based on Magnetic Resonance Radiomics Signature. *Front Oncol* 2022; **12**: 857715 [PMID: 35444942 DOI: 10.3389/fonc.2022.857715]
76 **Gao L**, Xiong M, Chen X, Han Z, Yan C, Ye R, Zhou L, Li Y. Multi-Region Radiomic Analysis Based on Multi-Sequence MRI Can Preoperatively Predict Microvascular Invasion in Hepatocellular Carcinoma. *Front Oncol* 2022; **12**: 818681 [PMID: 35574328 DOI: 10.3389/fonc.2022.818681]
77 **Hu F**, Zhang Y, Li M, Liu C, Zhang H, Li X, Liu S, Hu X, Wang J. Preoperative Prediction of Microvascular Invasion Risk Grades in Hepatocellular Carcinoma Based on Tumor and Peritumor Dual-Region Radiomics Signatures. *Front Oncol* 2022; **12**: 853336 [PMID: 35392229 DOI: 10.3389/fonc.2022.853336]
78 **He Y**, Hu B, Zhu C, Xu W, Ge Y, Hao X, Dong B, Chen X, Dong Q, Zhou X. A Novel Multimodal Radiomics Model for Predicting Prognosis of Resected Hepatocellular Carcinoma. *Front Oncol* 2022; **12**: 745258 [PMID: 35321432 DOI: 10.3389/fonc.2022.745258]
79 **Ren Y**, Bo L, Shen B, Yang J, Xu S, Shen W, Chen H, Wang X, Cai X. Development and validation of a clinical-radiomics model to predict recurrence for patients with hepatocellular carcinoma after curative resection. *Med Phys* 2023; **50**: 778-790 [PMID: 36269204 DOI: 10.1002/mp.16061]
80 **Luo J**, Huang Z, Wang M, Li T, Huang J. Prognostic role of multiparameter MRI and radiomics in progression of advanced unresectable hepatocellular carcinoma following combined transcatheter arterial chemoembolization and lenvatinib therapy. *BMC Gastroenterol* 2022; **22**: 108 [PMID: 35260095 DOI: 10.1186/s12876-022-02129-9]
81 **Wang X**, Sun Y, Zhou X, Shen Z, Zhang H, Xing J, Zhou Y. Histogram peritumoral enhanced features on MRI arterial phase with extracellular contrast agent can improve prediction of microvascular invasion of hepatocellular carcinoma. *Quant Imaging Med Surg* 2022; **12**: 1372-1384 [PMID: 35111631 DOI: 10.21037/qims-21-499]
82 **Mao Y**, Wang J, Zhu Y, Chen J, Mao L, Kong W, Qiu Y, Wu X, Guan Y, He J. Gd-EOB-DTPA-enhanced MRI radiomic features for predicting histological grade of hepatocellular carcinoma. *Hepatobiliary Surg Nutr* 2022; **11**: 13-24 [PMID: 35284527 DOI: 10.21037/hbsn-19-870]
83 **Andersson M**, Jalnefjord O, Montelius M, Rizell M, Sternby Eilard M, Ljungberg M. Evaluation of response in patients with hepatocellular carcinoma treated with intratumoral dendritic cell vaccination using intravoxel incoherent motion (IVIM) MRI and histogram analysis. *Acta Radiol* 2023; **64**: 32-41 [PMID: 34904868 DOI: 10.1177/02841851211065935]
84 **Li H**, Wang L, Zhang J, Duan Q, Xu Y, Xue Y. Evaluation of microvascular invasion of hepatocellular carcinoma using whole-lesion histogram analysis with the stretched-exponential diffusion model. *Br J Radiol* 2022; **95**: 20210631 [PMID: 34928172 DOI: 10.1259/bjr.20210631]
85 **Li L**, Su Q, Yang H. Preoperative prediction of microvascular invasion in hepatocellular carcinoma: a radiomic nomogram based on MRI. *Clin Radiol* 2022; **77**: e269-e279 [PMID: 34980458 DOI: 10.1016/j.crad.2021.12.008]
86 **Wang X**, Wang S, Yin X, Zheng Y. MRI-based radiomics distinguish different pathological types of hepatocellular carcinoma. *Comput Biol Med* 2022; **141**: 105058 [PMID: 34836622 DOI: 10.1016/j.compbiomed.2021.105058]
87 **Yang Y**, Fan W, Gu T, Yu L, Chen H, Lv Y, Liu H, Wang G, Zhang D. Radiomic Features of Multi-ROI and Multi-Phase MRI for the Prediction of Microvascular Invasion in Solitary Hepatocellular Carcinoma. *Front Oncol* 2021; **11**: 756216 [PMID: 34692547 DOI: 10.3389/fonc.2021.756216]
88 **Lv X**, Chen M, Kong C, Shu G, Meng M, Ye W, Cheng S, Zheng L, Fang S, Chen C, Wu F, Weng Q, Tu J, Zhao Z, Ji J. Construction of a novel radiomics nomogram for the prediction of aggressive intrasegmental recurrence of HCC after radiofrequency ablation. *Eur J Radiol* 2021; **144**: 109955 [PMID: 34600237 DOI: 10.1016/j.ejrad.2021.109955]
89 **Yu Y**, Fan Y, Wang X, Zhu M, Hu M, Shi C, Hu C. Gd-EOB-DTPA-enhanced MRI radiomics to predict vessels encapsulating tumor clusters (VETC) and patient prognosis in hepatocellular carcinoma. *Eur Radiol* 2022; **32**: 959-970 [PMID: 34480625 DOI: 10.1007/s00330-021-08250-9]
90 **Fang S**, Lai L, Zhu J, Zheng L, Xu Y, Chen W, Wu F, Wu X, Chen M, Weng Q, Ji J, Zhao Z, Tu J. A Radiomics Signature-Based Nomogram to Predict the Progression-Free Survival of Patients With Hepatocellular Carcinoma After Transcatheter Arterial Chemoembolization Plus Radiofrequency Ablation. *Front Mol Biosci* 2021; **8**: 662366 [PMID: 34532340 DOI: 10.3389/fmolb.2021.662366]
91 **Yang F**, Wan Y, Xu L, Wu Y, Shen X, Wang J, Lu D, Shao C, Zheng S, Niu T, Xu X. MRI-Radiomics Prediction for Cytokeratin 19-Positive Hepatocellular Carcinoma: A Multicenter Study. *Front Oncol* 2021; **11**: 672126 [PMID: 34476208 DOI: 10.3389/fonc.2021.672126]
92 **Chen Y**, Chen J, Zhang Y, Lin Z, Wang M, Huang L, Huang M, Tang M, Zhou X, Peng Z, Huang B, Feng ST. Preoperative Prediction of Cytokeratin 19 Expression for Hepatocellular Carcinoma with Deep Learning Radiomics Based on Gadoxetic Acid-Enhanced Magnetic Resonance Imaging. *J Hepatocell Carcinoma* 2021; **8**: 795-808 [PMID: 34327180 DOI: 10.2147/JHC.S313879]
93 **Horvat N**, Araujo-Filho JAB, Assuncao-Jr AN, Machado FAM, Sims JA, Rocha CCT, Oliveira BC, Horvat JV, Maccali C, Puga ALBL, Chagas AL, Menezes MR, Cerri GG. Radiomic analysis of MRI to Predict Sustained Complete Response after Radiofrequency Ablation in Patients with Hepatocellular Carcinoma - A Pilot Study. *Clinics (Sao Paulo)* 2021; **76**: e2888 [PMID: 34287480 DOI: 10.6061/clinics/2021/e2888]
94 **Alksas A**, Shehata M, Saleh GA, Shaffie A, Soliman A, Ghazal M, Khelifi A, Khalifeh HA, Razek AA, Giridharan GA, El-Baz A. A novel computer-aided diagnostic system for accurate detection and grading of liver tumors. *Sci Rep* 2021; **11**: 13148 [PMID: 34162893 DOI: 10.1038/s41598-021-91634-0]
95 **Chong H**, Gong Y, Pan X, Liu A, Chen L, Yang C, Zeng M. Peritumoral Dilation Radiomics of Gadoxetate Disodium-Enhanced MRI

Excellently Predicts Early Recurrence of Hepatocellular Carcinoma without Macrovascular Invasion After Hepatectomy. *J Hepatocell Carcinoma* 2021; **8**: 545-563 [PMID: 34136422 DOI: 10.2147/JHC.S309570]

96 **Ding Z**, Lin K, Fu J, Huang Q, Fang G, Tang Y, You W, Lin Z, Pan X, Zeng Y. An MR-based radiomics model for differentiation between hepatocellular carcinoma and focal nodular hyperplasia in non-cirrhotic liver. *World J Surg Oncol* 2021; **19**: 181 [PMID: 34154624 DOI: 10.1186/s12957-021-02266-7]

97 **Fan Y**, Yu Y, Wang X, Hu M, Hu C. Radiomic analysis of Gd-EOB-DTPA-enhanced MRI predicts Ki-67 expression in hepatocellular carcinoma. *BMC Med Imaging* 2021; **21**: 100 [PMID: 34130644 DOI: 10.1186/s12880-021-00633-0]

98 **Gao F**, Qiao K, Yan B, Wu M, Wang L, Chen J, Shi D. Hybrid network with difference degree and attention mechanism combined with radiomics (H-DARnet) for MVI prediction in HCC. *Magn Reson Imaging* 2021; **83**: 27-40 [PMID: 34147593 DOI: 10.1016/j.mri.2021.06.018]

99 **Li X**, Cheng L, Li C, Hu X, Tan L, Li Q, Liu C, Wang J. Associating Preoperative MRI Features and Gene Expression Signatures of Early-stage Hepatocellular Carcinoma Patients using Machine Learning. *J Clin Transl Hepatol* 2022; **10**: 63-71 [PMID: 35233374 DOI: 10.14218/JCTH.2021.00023]

100 **Shi Z**, Cai W, Feng X, Cai J, Liang Y, Xu J, Zhen J, Liang X. Radiomics Analysis of Gd-EOB-DTPA Enhanced Hepatic MRI for Assessment of Functional Liver Reserve. *Acad Radiol* 2022; **29**: 213-218 [PMID: 34183230 DOI: 10.1016/j.acra.2021.04.019]

101 **Dai H**, Lu M, Huang B, Tang M, Pang T, Liao B, Cai H, Huang M, Zhou Y, Chen X, Ding H, Feng ST. Considerable effects of imaging sequences, feature extraction, feature selection, and classifiers on radiomics-based prediction of microvascular invasion in hepatocellular carcinoma using magnetic resonance imaging. *Quant Imaging Med Surg* 2021; **11**: 1836-1853 [PMID: 33936969 DOI: 10.21037/qims-20-218]

102 **Fan Y**, Yu Y, Wang X, Hu M, Du M, Guo L, Sun S, Hu C. Texture Analysis Based on Gd-EOB-DTPA-Enhanced MRI for Identifying Vessels Encapsulating Tumor Clusters (VETC)-Positive Hepatocellular Carcinoma. *J Hepatocell Carcinoma* 2021; **8**: 349-359 [PMID: 33981636 DOI: 10.2147/JHC.S293755]

103 **Yang X**, Yuan C, Zhang Y, Wang Z. Magnetic resonance radiomics signatures for predicting poorly differentiated hepatocellular carcinoma: A SQUIRE-compliant study. *Medicine (Baltimore)* 2021; **100**: e25838 [PMID: 34106622 DOI: 10.1097/MD.0000000000025838]

104 **Chen Y**, Xia Y, Tolat PP, Long L, Jiang Z, Huang Z, Tang Q. Comparison of Conventional Gadoxetate Disodium-Enhanced MRI Features and Radiomics Signatures With Machine Learning for Diagnosing Microvascular Invasion. *AJR Am J Roentgenol* 2021; **216**: 1510-1520 [PMID: 33826360 DOI: 10.2214/AJR.20.23255]

105 **Zhao J**, Gao S, Sun W, Grimm R, Fu C, Han J, Sheng R, Zeng M. Magnetic resonance imaging and diffusion-weighted imaging-based histogram analyses in predicting glypican 3-positive hepatocellular carcinoma. *Eur J Radiol* 2021; **139**: 109732 [PMID: 33905978 DOI: 10.1016/j.ejrad.2021.109732]

106 **Song D**, Wang Y, Wang W, Cai J, Zhu K, Lv M, Gao Q, Zhou J, Fan J, Rao S, Wang M, Wang X. Using deep learning to predict microvascular invasion in hepatocellular carcinoma based on dynamic contrast-enhanced MRI combined with clinical parameters. *J Cancer Res Clin Oncol* 2021; **147**: 3757-3767 [PMID: 33839938 DOI: 10.1007/s00432-021-03617-3]

107 **Zhong X**, Guan T, Tang D, Li J, Lu B, Cui S, Tang H. Differentiation of small (≤ 3 cm) hepatocellular carcinomas from benign nodules in cirrhotic liver: the added additive value of MRI-based radiomics analysis to LI-RADS version 2018 algorithm. *BMC Gastroenterol* 2021; **21**: 155 [PMID: 33827440 DOI: 10.1186/s12876-021-01710-y]

108 **Chen Y**, Liu Z, Mo Y, Li B, Zhou Q, Peng S, Li S, Kuang M. Prediction of Post-hepatectomy Liver Failure in Patients With Hepatocellular Carcinoma Based on Radiomics Using Gd-EOB-DTPA-Enhanced MRI: The Liver Failure Model. *Front Oncol* 2021; **11**: 605296 [PMID: 33777748 DOI: 10.3389/fonc.2021.605296]

109 **Liang H**, Hu C, Lu J, Zhang T, Jiang J, Ding D, Du S, Duan S. Correlation of radiomic features on dynamic contrast-enhanced magnetic resonance with microvessel density in hepatocellular carcinoma based on different models. *J Int Med Res* 2021; **49**: 300060521997586 [PMID: 33682491 DOI: 10.1177/0300060521997586]

110 **Zhang L**, Hu J, Hou J, Jiang X, Guo L, Tian L. Radiomics-based model using gadoxetic acid disodium-enhanced MR images: associations with recurrence-free survival of patients with hepatocellular carcinoma treated by surgical resection. *Abdom Radiol (NY)* 2021; **46**: 3845-3854 [PMID: 33733337 DOI: 10.1007/s00261-021-03034-7]

111 **Zhang L**, Cai P, Hou J, Luo M, Li Y, Jiang X. Radiomics Model Based on Gadoxetic Acid Disodium-Enhanced MR Imaging to Predict Hepatocellular Carcinoma Recurrence After Curative Ablation. *Cancer Manag Res* 2021; **13**: 2785-2796 [PMID: 33790652 DOI: 10.2147/CMAR.S300627]

112 **Zhang Y**, Shu Z, Ye Q, Chen J, Zhong J, Jiang H, Wu C, Yu T, Pang P, Ma T, Lin C. Preoperative Prediction of Microvascular Invasion in Hepatocellular Carcinoma *via* Multi-Parametric MRI Radiomics. *Front Oncol* 2021; **11**: 633596 [PMID: 33747956 DOI: 10.3389/fonc.2021.633596]

113 **Zhao Y**, Wang N, Wu J, Zhang Q, Lin T, Yao Y, Chen Z, Wang M, Sheng L, Liu J, Song Q, Wang F, An X, Guo Y, Li X, Wu T, Liu AL. Radiomics Analysis Based on Contrast-Enhanced MRI for Prediction of Therapeutic Response to Transarterial Chemoembolization in Hepatocellular Carcinoma. *Front Oncol* 2021; **11**: 582788 [PMID: 33868988 DOI: 10.3389/fonc.2021.582788]

114 **Kuang Y**, Li R, Jia P, Ye W, Zhou R, Zhu R, Wang J, Lin S, Pang P, Ji W. MRI-Based Radiomics: Nomograms predicting the short-term response after transcatheter arterial chemoembolization (TACE) in hepatocellular carcinoma patients with diameter less than 5 cm. *Abdom Radiol (NY)* 2021; **46**: 3772-3789 [PMID: 33713159 DOI: 10.1007/s00261-021-02992-2]

115 **Meng XP**, Wang YC, Zhou JY, Yu Q, Lu CQ, Xia C, Tang TY, Xu J, Sun K, Xiao W, Ju S. Comparison of MRI and CT for the Prediction of Microvascular Invasion in Solitary Hepatocellular Carcinoma Based on a Non-Radiomics and Radiomics Method: Which Imaging Modality Is Better? *J Magn Reson Imaging* 2021; **54**: 526-536 [PMID: 33622022 DOI: 10.1002/jmri.27575]

116 **Zhu Y**, Weng S, Li Y, Yan C, Ye R, Wen L, Zhou L, Gao L. A radiomics nomogram based on contrast-enhanced MRI for preoperative prediction of macrotrabecular-massive hepatocellular carcinoma. *Abdom Radiol (NY)* 2021; **46**: 3139-3148 [PMID: 33641018 DOI: 10.1007/s00261-021-02989-x]

117 **Liu J**, Pei Y, Zhang Y, Wu Y, Liu F, Gu S. Predicting the prognosis of hepatocellular carcinoma with the treatment of transcatheter arterial chemoembolization combined with microwave ablation using pretreatment MR imaging texture features. *Abdom Radiol (NY)* 2021; **46**: 3748-3757 [PMID: 33386449 DOI: 10.1007/s00261-020-02891-y]

118 **Chong HH**, Yang L, Sheng RF, Yu YL, Wu DJ, Rao SX, Yang C, Zeng MS. Multi-scale and multi-parametric radiomics of gadoxetate disodium-enhanced MRI predicts microvascular invasion and outcome in patients with solitary hepatocellular carcinoma ≤ 5 cm. *Eur Radiol* 2021; **31**: 4824-4838 [PMID: 33447861 DOI: 10.1007/s00330-020-07601-2]

119 **Gu D**, Xie Y, Wei J, Li W, Ye Z, Zhu Z, Tian J, Li X. MRI-Based Radiomics Signature: A Potential Biomarker for Identifying Glypican 3-Positive Hepatocellular Carcinoma. *J Magn Reson Imaging* 2020; **52**: 1679-1687 [PMID: 32491239 DOI: 10.1002/jmri.27199]

120 **Zhao Y**, Wu J, Zhang Q, Hua Z, Qi W, Wang N, Lin T, Sheng L, Cui D, Liu J, Song Q, Li X, Wu T, Guo Y, Cui J, Liu A. Radiomics Analysis Based on Multiparametric MRI for Predicting Early Recurrence in Hepatocellular Carcinoma After Partial Hepatectomy. *J Magn Reson Imaging* 2021; **53**: 1066-1079 [PMID: 33217114 DOI: 10.1002/jmri.27424]

121 **Ai Z**, Han Q, Huang Z, Wu J, Xiang Z. The value of multiparametric histogram features based on intravoxel incoherent motion diffusion-weighted imaging (IVIM-DWI) for the differential diagnosis of liver lesions. *Ann Transl Med* 2020; **8**: 1128 [PMID: 33240977 DOI: 10.21037/atm-20-5109]

122 **Shaghaghi M**, Aliyari Ghasabeh M, Ameli S, Ghadimi M, Hazhirkarzar B, Rezvani Habibabadi R, Khoshpouri P, Pandey A, Pandey P, Kamel IR. Post-TACE changes in ADC histogram predict overall and transplant-free survival in patients with well-defined HCC: a retrospective cohort with up to 10 years follow-up. *Eur Radiol* 2021; **31**: 1378-1390 [PMID: 32894356 DOI: 10.1007/s00330-020-07237-2]

123 **Li J**, Xue F, Xu X, Wang Q, Zhang X. Dynamic contrast-enhanced MRI differentiates hepatocellular carcinoma from hepatic metastasis of rectal cancer by extracting pharmacokinetic parameters and radiomic features. *Exp Ther Med* 2020; **20**: 3643-3652 [PMID: 32855716 DOI: 10.3892/etm.2020.9115]

124 **Geng Z**, Zhang Y, Wang S, Li H, Zhang C, Yin S, Xie C, Dai Y. Radiomics Analysis of Susceptibility Weighted Imaging for Hepatocellular Carcinoma: Exploring the Correlation between Histopathology and Radiomics Features. *Magn Reson Med Sci* 2021; **20**: 253-263 [PMID: 32788505 DOI: 10.2463/mrms.mp.2020-0060]

125 **Zhang J**, Wang X, Zhang L, Yao L, Xue X, Zhang S, Li X, Chen Y, Pang P, Sun D, Xu J, Shi Y, Chen F. Radiomics predict postoperative survival of patients with primary liver cancer with different pathological types. *Ann Transl Med* 2020; **8**: 820 [PMID: 32793665 DOI: 10.21037/atm-19-4668]

126 **Zhang Z**, Chen J, Jiang H, Wei Y, Zhang X, Cao L, Duan T, Ye Z, Yao S, Pan X, Song B. Gadoxetic acid-enhanced MRI radiomics signature: prediction of clinical outcome in hepatocellular carcinoma after surgical resection. *Ann Transl Med* 2020; **8**: 870 [PMID: 32793714 DOI: 10.21037/atm-20-3041]

127 **Hectors SJ**, Lewis S, Kennedy P, Bane O, Said D, Segall M, Schwartz M, Kim E, Taouli B. Assessment of Hepatocellular Carcinoma Response to (90)Y Radioembolization Using Dynamic Contrast Material-enhanced MRI and Intravoxel Incoherent Motion Diffusion-weighted Imaging. *Radiol Imaging Cancer* 2020; **2**: e190094 [PMID: 32803165 DOI: 10.1148/rycan.2020190094]

128 **Shi G**, Han X, Wang Q, Ding Y, Liu H, Zhang Y, Dai Y. Evaluation of Multiple Prognostic Factors of Hepatocellular Carcinoma with Intra-Voxel Incoherent Motions Imaging by Extracting the Histogram Metrics. *Cancer Manag Res* 2020; **12**: 6019-6031 [PMID: 32765101 DOI: 10.2147/CMAR.S262973]

129 **Feng M**, Zhang M, Liu Y, Jiang N, Meng Q, Wang J, Yao Z, Gan W, Dai H. Texture analysis of MR images to identify the differentiated degree in hepatocellular carcinoma: a retrospective study. *BMC Cancer* 2020; **20**: 611 [PMID: 32605628 DOI: 10.1186/s12885-020-07094-8]

130 **Nebbia G**, Zhang Q, Arefan D, Zhao X, Wu S. Pre-operative Microvascular Invasion Prediction Using Multi-parametric Liver MRI Radiomics. *J Digit Imaging* 2020; **33**: 1376-1386 [PMID: 32495126 DOI: 10.1007/s10278-020-00353-x]

131 **Schobert IT**, Savic LJ, Chapiro J, Bousabarah K, Chen E, Laage-Gaupp F, Tefera J, Nezami N, Lin M, Pollak J, Schlachter T. Neutrophil-to-lymphocyte and platelet-to-lymphocyte ratios as predictors of tumor response in hepatocellular carcinoma after DEB-TACE. *Eur Radiol* 2020; **30**: 5663-5673 [PMID: 32424595 DOI: 10.1007/s00330-020-06931-5]

132 **Sun Y**, Bai H, Xia W, Wang D, Zhou B, Zhao X, Yang G, Xu L, Zhang W, Liu P, Xu J, Meng S, Liu R, Gao X. Predicting the Outcome of Transcatheter Arterial Embolization Therapy for Unresectable Hepatocellular Carcinoma Based on Radiomics of Preoperative Multiparameter MRI. *J Magn Reson Imaging* 2020; **52**: 1083-1090 [PMID: 32233054 DOI: 10.1002/jmri.27143]

133 **Wilson GC**, Cannella R, Fiorentini G, Shen C, Borhani A, Furlan A, Tsung A. Texture analysis on preoperative contrast-enhanced magnetic resonance imaging identifies microvascular invasion in hepatocellular carcinoma. *HPB (Oxford)* 2020; **22**: 1622-1630 [PMID: 32229091 DOI: 10.1016/j.hpb.2020.03.001]

134 **Hectors SJ**, Lewis S, Besa C, King MJ, Said D, Putra J, Ward S, Higashi T, Thung S, Yao S, Laface I, Schwartz M, Gnjatic S, Merad M, Hoshida Y, Taouli B. MRI radiomics features predict immuno-oncological characteristics of hepatocellular carcinoma. *Eur Radiol* 2020; **30**: 3759-3769 [PMID: 32086577 DOI: 10.1007/s00330-020-06675-2]

135 **Wang W**, Gu D, Wei J, Ding Y, Yang L, Zhu K, Luo R, Rao SX, Tian J, Zeng M. A radiomics-based biomarker for cytokeratin 19 status of hepatocellular carcinoma with gadoxetic acid-enhanced MRI. *Eur Radiol* 2020; **30**: 3004-3014 [PMID: 32002645 DOI: 10.1007/s00330-019-06585-y]

136 **Wang XH**, Long LH, Cui Y, Jia AY, Zhu XG, Wang HZ, Wang Z, Zhan CM, Wang ZH, Wang WH. MRI-based radiomics model for preoperative prediction of 5-year survival in patients with hepatocellular carcinoma. *Br J Cancer* 2020; **122**: 978-985 [PMID: 31937925 DOI: 10.1038/s41416-019-0706-0]

137 **Song W**, Yu X, Guo D, Liu H, Tang Z, Liu X, Zhou J, Zhang H, Liu Y. MRI-Based Radiomics: Associations With the Recurrence-Free Survival of Patients With Hepatocellular Carcinoma Treated With Conventional Transcatheter Arterial Chemoembolization. *J Magn Reson Imaging* 2020; **52**: 461-473 [PMID: 31675174 DOI: 10.1002/jmri.26977]

138 **Zhang J**, Liu X, Zhang H, He X, Liu Y, Zhou J, Guo D. Texture Analysis Based on Preoperative Magnetic Resonance Imaging (MRI) and Conventional MRI Features for Predicting the Early Recurrence of Single Hepatocellular Carcinoma after Hepatectomy. *Acad Radiol* 2019; **26**: 1164-1173 [PMID: 30425000 DOI: 10.1016/j.acra.2018.10.011]

139 **Huang X**, Long L, Wei J, Li Y, Xia Y, Zuo P, Chai X. Radiomics for diagnosis of dual-phenotype hepatocellular carcinoma using Gd-EOB-DTPA-enhanced MRI and patient prognosis. *J Cancer Res Clin Oncol* 2019; **145**: 2995-3003 [PMID: 31664520 DOI: 10.1007/s00432-019-03062-3]

140 **Ye Z**, Jiang H, Chen J, Liu X, Wei Y, Xia C, Duan T, Cao L, Zhang Z, Song B. Texture analysis on gadoxetic acid enhanced-MRI for predicting Ki-67 status in hepatocellular carcinoma: A prospective study. *Chin J Cancer Res* 2019; **31**: 806-817 [PMID: 31814684 DOI: 10.21147/j.issn.1000-9604.2019.05.10]

141 **Zhang R**, Xu L, Wen X, Zhang J, Yang P, Zhang L, Xue X, Wang X, Huang Q, Guo C, Shi Y, Niu T, Chen F. A nomogram based on bi-regional radiomics features from multimodal magnetic resonance imaging for preoperative prediction of microvascular invasion in hepatocellular carcinoma. *Quant Imaging Med Surg* 2019; **9**: 1503-1515 [PMID: 31667137 DOI: 10.21037/qims.2019.09.07]

142 **Chen J**, Wu Z, Xia C, Jiang H, Liu X, Duan T, Cao L, Ye Z, Zhang Z, Ma L, Song B, Shi Y. Noninvasive prediction of HCC with progenitor phenotype based on gadoxetic acid-enhanced MRI. *Eur Radiol* 2020; **30**: 1232-1242 [PMID: 31529254 DOI: 10.1007/s00330-019-06414-2]

143 **Xu YS**, Liu HF, Xi DL, Li JK, Liu Z, Yan RF, Lei JQ. Whole-lesion histogram analysis metrics of the apparent diffusion coefficient: a correlation study with histological grade of hepatocellular carcinoma. *Abdom Radiol (NY)* 2019; **44**: 3089-3098 [PMID: 31256226 DOI: 10.1007/s00261-019-02109-w]

144 **Li Y**, Yan C, Weng S, Shi Z, Sun H, Chen J, Xu X, Ye R, Hong J. Texture analysis of multi-phase MRI images to detect expression of Ki67 in hepatocellular carcinoma. *Clin Radiol* 2019; **74**: 813.e19-813.e27 [PMID: 31362887 DOI: 10.1016/j.crad.2019.06.024]

145 **Oyama A**, Hiraoka Y, Obayashi I, Saikawa Y, Furui S, Shiraishi K, Kumagai S, Hayashi T, Kotoku J. Hepatic tumor classification using texture and topology analysis of non-contrast-enhanced three-dimensional T1-weighted MR images with a radiomics approach. *Sci Rep* 2019; **9**: 8764 [PMID: 31217445 DOI: 10.1038/s41598-019-45283-z]

146 **Wang HQ**, Yang C, Zeng MS, Rao SX, Ji Y, Weng X, Wang JY, Sheng RF. Magnetic resonance texture analysis for the identification of cytokeratin 19-positive hepatocellular carcinoma. *Eur J Radiol* 2019; **117**: 164-170 [PMID: 31307643 DOI: 10.1016/j.ejrad.2019.06.016]

147 **Zhu YJ**, Feng B, Wang S, Wang LM, Wu JF, Ma XH, Zhao XM. Model-based three-dimensional texture analysis of contrast-enhanced magnetic resonance imaging as a potential tool for preoperative prediction of microvascular invasion in hepatocellular carcinoma. *Oncol Lett* 2019; **18**: 720-732 [PMID: 31289547 DOI: 10.3892/ol.2019.10378]

148 **Zhang Z**, Jiang H, Chen J, Wei Y, Cao L, Ye Z, Li X, Ma L, Song B. Hepatocellular carcinoma: radiomics nomogram on gadoxetic acid-enhanced MR imaging for early postoperative recurrence prediction. *Cancer Imaging* 2019; **19**: 22 [PMID: 31088553 DOI: 10.1186/s40644-019-0209-5]

149 **Gordic S**, Wagner M, Zanato R, Hectors S, Besa C, Kihira S, Kim E, Taouli B. Prediction of hepatocellular carcinoma response to (90)Yttrium radioembolization using volumetric ADC histogram quantification: preliminary results. *Cancer Imaging* 2019; **19**: 29 [PMID: 31142363 DOI: 10.1186/s40644-019-0216-6]

150 **Jansen MJA**, Kuijf HJ, Veldhuis WB, Wessels FJ, Viergever MA, Pluim JPW. Automatic classification of focal liver lesions based on MRI and risk factors. *PLoS One* 2019; **14**: e0217053 [PMID: 31095624 DOI: 10.1371/journal.pone.0217053]

151 **Ma X**, Ouyang H, Wang S, Wang M, Zhou C, Zhao X. Histogram analysis of apparent diffusion coefficient predicts response to radiofrequency ablation in hepatocellular carcinoma. *Chin J Cancer Res* 2019; **31**: 366-374 [PMID: 31156307 DOI: 10.21147/j.issn.1000-9604.2019.02.11]

152 **Wu J**, Liu A, Cui J, Chen A, Song Q, Xie L. Radiomics-based classification of hepatocellular carcinoma and hepatic haemangioma on precontrast magnetic resonance images. *BMC Med Imaging* 2019; **19**: 23 [PMID: 30866850 DOI: 10.1186/s12880-019-0321-9]

153 **Kim S**, Shin J, Kim DY, Choi GH, Kim MJ, Choi JY. Radiomics on Gadoxetic Acid-Enhanced Magnetic Resonance Imaging for Prediction of Postoperative Early and Late Recurrence of Single Hepatocellular Carcinoma. *Clin Cancer Res* 2019; **25**: 3847-3855 [PMID: 30808773 DOI: 10.1158/1078-0432.CCR-18-2861]

154 **Lewis S**, Peti S, Hectors SJ, King M, Rosen A, Kamath A, Putra J, Thung S, Taouli B. Volumetric quantitative histogram analysis using diffusion-weighted magnetic resonance imaging to differentiate HCC from other primary liver cancers. *Abdom Radiol (NY)* 2019; **44**: 912-922 [PMID: 30712136 DOI: 10.1007/s00261-019-01906-7]

155 **Chen S**, Feng S, Wei J, Liu F, Li B, Li X, Hou Y, Gu D, Tang M, Xiao H, Jia Y, Peng S, Tian J, Kuang M. Pretreatment prediction of immunoscore in hepatocellular cancer: a radiomics-based clinical model based on Gd-EOB-DTPA-enhanced MRI imaging. *Eur Radiol* 2019; **29**: 4177-4187 [PMID: 30666445 DOI: 10.1007/s00330-018-5986-x]

156 **Feng ST**, Jia Y, Liao B, Huang B, Zhou Q, Li X, Wei K, Chen L, Li B, Wang W, Chen S, He X, Wang H, Peng S, Chen ZB, Tang M, Chen Z, Hou Y, Peng Z, Kuang M. Preoperative prediction of microvascular invasion in hepatocellular cancer: a radiomics model using Gd-EOB-DTPA-enhanced MRI. *Eur Radiol* 2019; **29**: 4648-4659 [PMID: 30689032 DOI: 10.1007/s00330-018-5935-8]

157 **Wu M**, Tan H, Gao F, Hai J, Ning P, Chen J, Zhu S, Wang M, Dou S, Shi D. Predicting the grade of hepatocellular carcinoma based on non-contrast-enhanced MRI radiomics signature. *Eur Radiol* 2019; **29**: 2802-2811 [PMID: 30406313 DOI: 10.1007/s00330-018-5787-2]

158 **Yang L**, Gu D, Wei J, Yang C, Rao S, Wang W, Chen C, Ding Y, Tian J, Zeng M. A Radiomics Nomogram for Preoperative Prediction of Microvascular Invasion in Hepatocellular Carcinoma. *Liver Cancer* 2019; **8**: 373-386 [PMID: 31768346 DOI: 10.1159/000494099]

159 **Stocker D**, Marquez HP, Wagner MW, Raptis DA, Clavien PA, Boss A, Fischer MA, Wurnig MC. MRI texture analysis for differentiation of malignant and benign hepatocellular tumors in the non-cirrhotic liver. *Heliyon* 2018; **4**: e00987 [PMID: 30761374 DOI: 10.1016/j.heliyon.2018.e00987]

160 **Ahn SJ**, Kim JH, Park SJ, Kim ST, Han JK. Hepatocellular carcinoma: preoperative gadoxetic acid-enhanced MR imaging can predict early recurrence after curative resection using image features and texture analysis. *Abdom Radiol (NY)* 2019; **44**: 539-548 [PMID: 30229421 DOI: 10.1007/s00261-018-1768-9]

161 **Hui TCH**, Chuah TK, Low HM, Tan CH. Predicting early recurrence of hepatocellular carcinoma with texture analysis of preoperative MRI: a radiomics study. *Clin Radiol* 2018; **73**: 1056.e11-1056.e16 [PMID: 30213434 DOI: 10.1016/j.crad.2018.07.109]

162 **Zou X**, Luo Y, Li Z, Hu Y, Li H, Tang H, Shen Y, Hu D, Kamel IR. Volumetric Apparent Diffusion Coefficient Histogram Analysis in Differentiating Intrahepatic Mass-Forming Cholangiocarcinoma From Hepatocellular Carcinoma. *J Magn Reson Imaging* 2019; **49**: 975-983 [PMID: 30277628 DOI: 10.1002/jmri.26253]

163 **Li H**, Zhang J, Zheng Z, Guo Y, Chen M, Xie C, Zhang Z, Mei Y, Feng Y, Xu Y. Preoperative histogram analysis of intravoxel incoherent motion (IVIM) for predicting microvascular invasion in patients with single hepatocellular carcinoma. *Eur J Radiol* 2018; **105**: 65-71 [PMID: 30017300 DOI: 10.1016/j.ejrad.2018.05.032]

164 **Wu LF**, Rao SX, Xu PJ, Yang L, Chen CZ, Liu H, Huang JF, Fu CX, Halim A, Zeng MS. Pre-TACE kurtosis of ADC(total) derived from histogram analysis for diffusion-weighted imaging is the best independent predictor of prognosis in hepatocellular carcinoma. *Eur Radiol* 2019; **29**: 213-223 [PMID: 29922932 DOI: 10.1007/s00330-018-5482-3]

165 **Li Z**, Mao Y, Huang W, Li H, Zhu J, Li W, Li B. Texture-based classification of different single liver lesion based on SPAIR T2W MRI images. *BMC Med Imaging* 2017; **17**: 42 [PMID: 28705145 DOI: 10.1186/s12880-017-0212-x]

166 **Moriya T**, Saito K, Tajima Y, Harada TL, Araki Y, Sugimoto K, Tokuuye K. 3D analysis of apparent diffusion coefficient histograms in hepatocellular carcinoma: correlation with histological grade. *Cancer Imaging* 2017; **17**: 1 [PMID: 28057085 DOI: 10.1186/s40644-016-0103-3]

World Journal of Gastroenterology

Submit a Manuscript: https://www.f6publishing.com

World J Gastroenterol 2024 January 28; 30(4): 418-420

DOI: 10.3748/wjg.v30.i4.418

ISSN 1007-9327 (print) ISSN 2219-2840 (online)

LETTER TO THE EDITOR

Antiviral treatment standards for hepatitis B: An urgent need for expansion

Zi-Hong Bao, Zhi-Kun Dai, Hao-Xian Tang

Specialty type: Gastroenterology and hepatology

Provenance and peer review: Unsolicited article; Externally peer reviewed.

Peer-review model: Single blind

Peer-review report's scientific quality classification
Grade A (Excellent): 0
Grade B (Very good): B
Grade C (Good): C
Grade D (Fair): 0
Grade E (Poor): 0

P-Reviewer: Kishida Y, Japan; Liakina V, Lithuania

Received: September 27, 2023
Peer-review started: September 27, 2023
First decision: December 4, 2023
Revised: December 16, 2023
Accepted: January 8, 2024
Article in press: January 8, 2024
Published online: January 28, 2024

Zi-Hong Bao, Zhi-Kun Dai, Department of Infectious Diseases, The First Affiliated Hospital of Shantou University Medical College, Shantou 515041, Guangdong Province, China

Hao-Xian Tang, Medical College, Shantou University Medical College, Shantou 515041, Guangdong Province, China

Hao-Xian Tang, Department of Cardiology, The First Affiliated Hospital of Shantou University Medical College, Shantou 515041, Guangdong Province, China

Corresponding author: Hao-Xian Tang, MD, Doctor, Medical College, Shantou University Medical College, No. 22 Xinling Road, Jinping District, Shantou 515041, Guangdong Province, China. 19hxtang@stu.edu.cn

Abstract

The present letter to the editor is related to the review with the title "Past, present, and future of long-term treatment for hepatitis B virus." Chronic hepatitis B (CHB) represents an important and pressing public health concern. Timely identification and effective antiviral therapy hold the potential to reduce liver-related mortality attributable to chronic infection with hepatitis B virus (HBV) substantially. However, the current global treatment rates for CHB remain conspicuously low, with the excessively stringent treatment criteria advocated by national CHB guidelines being a contributing factor to these low rates. Nevertheless, recent strides in comprehending this malady and the emergence of novel antiviral agents prompt the imperative re-evaluation of treatment standards to extend the sphere of potential beneficiaries. An impending need arises for a novel paradigm for the classification of patients with CHB, the expansion of antiviral treatment eligibility for HBV-infected individuals, and even the streamlining of the diagnostic process for CHB to amplify cost-effectiveness and augment survival prospects.

Key Words: Hepatitis B virus; Chronic hepatitis B; Antiviral treatment criteria; Serum alanine aminotransferase; Liver-related mortality; Letter to the Editor

Core Tip: Chronic hepatitis B (CHB) is a serious public health problem. Early detection and effective antiviral treatment can remarkably reduce liver-related mortality caused by CHB. However, the global diagnosis and treatment rates of CHB are only 10% and 2%, respectively. Expanding the standard of antiviral treatment for patients with hepatitis B is urgently needed to improve cost-effectiveness and survival further.

Citation: Bao ZH, Dai ZK, Tang HX. Antiviral treatment standards for hepatitis B: An urgent need for expansion. *World J Gastroenterol* 2024; 30(4): 418-420
URL: https://www.wjgnet.com/1007-9327/full/v30/i4/418.htm
DOI: https://dx.doi.org/10.3748/wjg.v30.i4.418

TO THE EDITOR

We read with great interest the review by Broquetas and Carrión[1]. This review discusses the need to expand the antiviral treatment criteria for patients with hepatitis B to improve cost-effectiveness and overall survival in the future.

We strongly concur with the proposition that a new paradigm is required for classifying patients with chronic hepatitis B (CHB). Such a paradigm includes streamlining the diagnostic process to enhance diagnosis and treatment accessibility. Presently, treatment guidelines for CHB primarily emphasize antiviral therapy for individuals exhibiting high viral loads and liver inflammation. However, recent advancements in our understanding of CHB and the availability of novel antiviral agents necessitate a reassessment of treatment criteria to benefit a broadened range of patients potentially. Research conducted by Professor Lim *et al*[2] has demonstrated that expanding the treatment criteria to encompass individuals meeting the conditions for CHB treatment can reduce hepatitis B virus (HBV)–related mortality rates and improve cost-effectiveness[2]. Similar conclusions have been drawn by Professor Zhang *et al*[3]. Moreover, Professor Li *et al*[4] have utilized modeling to investigate HBV clearance in different diagnostic and treatment scenarios, proposing that achieving 90% diagnostic coverage and 80% standardized treatment coverage, as opposed to the current situation, could prevent approximately two million HBV-related deaths[4]. These findings underscore the remarkable potential of early detection and effective antiviral treatment in reducing liver-related mortality associated with CHB. However, a recent review has highlighted that the global diagnostic and cure rates for CHB are currently only 10% and 2%, respectively[5]. The primary issue lies in the existing CHB guidelines that recommend overly stringent treatment criteria, thereby resulting in the ineligibility of a substantial number of HBV-infected individuals for antiviral therapy. This situation could potentially contribute to disease progression.

As a country burdened heavily by chronic HBV, China may consider expanding the antiviral treatment criteria to meet the World Health Organization's (WHO) goal of reducing mortality by 65% by 2030. Serum alanine aminotransferase (ALT) is currently used as the initial indicator for commencing antiviral treatment for chronic HBV infection, with varying thresholds utilized globally. A multicenter cohort study has demonstrated that ALT levels and liver inflammation are closely correlated with histological progression[6]. The European Association for the Study of the Liver (EASL) suggests that the upper limit of normal of ALT is 40 U/L. The current ALT threshold may be unsuitable as an indicator for initiating antiviral treatment for chronic infection with HBV because a notable proportion of HBV-infected patients with normal ALT levels exhibit remarkable liver inflammation and fibrosis[7-9]. Therefore, lowering the threshold for ALT can improve the identification of considerable liver damage in patients with CHB[10]. The American Hepatitis B Foundation organized a report meeting with the title "Expanding Hepatitis B Treatment Guidelines" to propose a strategy for the antiviral treatment of all HBV DNA–positive individuals. The primary goal of antiviral therapy is to suppress HBV DNA levels to undetectable levels given that this end point is associated with an improvement in liver inflammation and fibrosis, cirrhosis reversal, and reductions in HCC risk and liver-related mortality.

The in-progress development of the new WHO guidelines for hepatitis B was introduced at the 2023 EASL Congress. These guidelines aim to expand simplified treatment standards, improve service provision, and provide innovative diagnostic approaches.

Consequently, the expansion of antiviral treatment criteria for patients with hepatitis B and simplification of diagnostic standards for hepatitis B are imminent. However, the expansion of treatment criteria necessitates the consideration of long-term outcomes, including assessing the risk of hepatocellular carcinoma, liver-related complications, and improvements in quality of life, alongside evaluating the cost-effectiveness of interventions to ensure broadened treatment access in resource-limited settings. As a result, future research will require increased sample sizes and multicenter randomized controlled trials.

ACKNOWLEDGEMENTS

We acknowledge all the authors whose publications are used as references in our article.

FOOTNOTES

Co-first authors: Zi-Hong Bao and Zhi-Kun Dai.

Author contributions: Bao ZH and Dai ZK contributed equally to the manuscript; Tang HX designed research; Bao ZH and Dai ZK performed research; Bao ZH and Dai ZK wrote the letter; Tang HX revised the letter; All authors approved the final version of the article.

Conflict-of-interest statement: All the authors report no relevant conflicts of interest for this article.

Country/Territory of origin: China

ORCID number: Zi-Hong Bao 0000-0002-2857-5370; Zhi-Kun Dai 0000-0002-7258-0134; Hao-Xian Tang 0000-0002-4346-7159.

S-Editor: Li L
L-Editor: A
P-Editor: Li L

REFERENCES

1 **Broquetas T**, Carrión JA. Past, present, and future of long-term treatment for hepatitis B virus. *World J Gastroenterol* 2023; **29**: 3964-3983 [PMID: 37476586 DOI: 10.3748/wjg.v29.i25.3964]
2 **Lim YS**, Ahn SH, Shim JJ, Razavi H, Razavi-Shearer D, Sinn DH. Impact of expanding hepatitis B treatment guidelines: A modelling and economic impact analysis. *Aliment Pharmacol Ther* 2022; **56**: 519-528 [PMID: 35614532 DOI: 10.1111/apt.17052]
3 **Zhang S**, Wang C, Liu B, Lu QB, Shang J, Zhou Y, Jia J, Xu X, Rao H, Han B, Zhao T, Chen L, Xie M, Cui J, Du J, Zeng J, Huang N, Liu Y, Zhang L, Zhuang H, Cui F. Cost-effectiveness of expanded antiviral treatment for chronic hepatitis B virus infection in China: an economic evaluation. *Lancet Reg Health West Pac* 2023; **35**: 100738 [PMID: 37424693 DOI: 10.1016/j.lanwpc.2023.100738]
4 **Li R**, Shen M, Ong JJ, Cui F, Hu W, Chan P, Zou Z, Su S, Liu H, Zhang L, Seto WK, Wong WCW. Blueprint to hepatitis B elimination in China: A modelling analysis of clinical strategies. *JHEP Rep* 2023; **5**: 100833 [PMID: 37675271 DOI: 10.1016/j.jhepr.2023.100833]
5 **Hsu YC**, Huang DQ, Nguyen MH. Global burden of hepatitis B virus: current status, missed opportunities and a call for action. *Nat Rev Gastroenterol Hepatol* 2023; **20**: 524-537 [PMID: 37024566 DOI: 10.1038/s41575-023-00760-9]
6 **Sonneveld MJ**, Brouwer WP, Hansen BE, Chan HL, Piratvisuth T, Jia JD, Zeuzem S, Chien RN, Choi H, de Knegt RJ, Wat C, Pavlovic V, Gaggar A, Xie Q, Buti M, de Man RA, Janssen HLA; SONIC-B Study Group. Very low probability of significant liver inflammation in chronic hepatitis B patients with low ALT levels in the absence of liver fibrosis. *Aliment Pharmacol Ther* 2020; **52**: 1399-1406 [PMID: 32886813 DOI: 10.1111/apt.16067]
7 **Terrault NA**, Lok ASF, McMahon BJ, Chang KM, Hwang JP, Jonas MM, Brown RS Jr, Bzowej NH, Wong JB. Update on prevention, diagnosis, and treatment of chronic hepatitis B: AASLD 2018 hepatitis B guidance. *Hepatology* 2018; **67**: 1560-1599 [PMID: 29405329 DOI: 10.1002/hep.29800]
8 **European Association for the Study of the Liver**. EASL 2017 Clinical Practice Guidelines on the management of hepatitis B virus infection. *J Hepatol* 2017; **67**: 370-398 [PMID: 28427875 DOI: 10.1016/j.jhep.2017.03.021]
9 **Chao DT**, Lim JK, Ayoub WS, Nguyen LH, Nguyen MH. Systematic review with meta-analysis: the proportion of chronic hepatitis B patients with normal alanine transaminase ≤ 40 IU/L and significant hepatic fibrosis. *Aliment Pharmacol Ther* 2014; **39**: 349-358 [PMID: 24387289 DOI: 10.1111/apt.12590]
10 **Yu HS**, Jiang H, Li MK, Yang BL, Smayi A, Chen JN, Wu B, Yang YD. Lowering the threshold of alanine aminotransferase for enhanced identification of significant hepatic injury in chronic hepatitis B patients. *World J Gastroenterol* 2023; **29**: 5166-5177 [PMID: 37744292 DOI: 10.3748/wjg.v29.i35.5166]

World Journal of Gastroenterology

Submit a Manuscript: https://www.f6publishing.com

World J Gastroenterol 2024 January 28; 30(4): 421-423

DOI: 10.3748/wjg.v30.i4.421

ISSN 1007-9327 (print) ISSN 2219-2840 (online)

LETTER TO THE EDITOR

Leukocyte immunoglobulin-like receptor B2: A promising biomarker for colorectal cancer

Wen-Zhuo Zhao, Hong-Gang Wang, Xiao-Zhong Yang

Specialty type: Gastroenterology and hepatology

Provenance and peer review: Unsolicited article; Externally peer reviewed.

Peer-review model: Single blind

Peer-review report's scientific quality classification

Grade A (Excellent): 0
Grade B (Very good): 0
Grade C (Good): C
Grade D (Fair): 0
Grade E (Poor): 0

P-Reviewer: Maida M, Italy

Received: October 17, 2023
Peer-review started: October 17, 2023
First decision: December 6, 2023
Revised: December 15, 2023
Accepted: January 10, 2024
Article in press: January 10, 2024
Published online: January 28, 2024

Wen-Zhuo Zhao, Hong-Gang Wang, Xiao-Zhong Yang, Department of Gastroenterology, The Affiliated Huai'an No. 1 People's Hospital of Nanjing Medical University, Huai'an 223300, Jiangsu Province, China

Corresponding author: Xiao-Zhong Yang, MD, PhD, Chief Doctor, Doctor, Professor, Department of Gastroenterology, The Affiliated Huaian No. 1 People's Hospital of Nanjing Medical University, No. 1 Huanghe Road, Huai'an 223300, Jiangsu Province, China. hayyyxzh@njmu.edu.cn

Abstract

According to the latest global cancer statistics, colorectal cancer (CRC) has emerged as the third most prevalent malignant tumor across the globe. In recent decades, the medical field has implemented several levels of CRC screening tests, encompassing fecal tests, endoscopic examinations, radiological examinations and blood tests. Previous studies have shown that leukocyte immunoglobulin-like receptor B2 (LILRB2) is involved in inhibiting immune cell function, immune evasion, and promoting tumor progression in acute myeloid leukemia and non-small cell lung cancer. However, its interaction with CRC has not been reported yet. Recently, a study published in the *World Journal of Gastroenterology* revealed that LILRB2 and its ligand, angiopoietin-like protein 2, are markedly overexpressed in CRC. This overexpression is closely linked to tumor progression and is indicative of a poor prognosis. The study highlights the potential of utilizing the concentration of LILRB2 in serum as a promising biomarker for tumors. However, there is still room for discussion regarding the data processing and analysis in this research.

Key Words: Colorectal cancer; Leukocyte immunoglobulin-like receptor B2; Angiopoietin-like protein 2; Therapeutic target; Noninvasive screening biomarker

Core Tip: In this study, it has been extensively demonstrated that there is an overexpression of leukocyte immunoglobulin-like receptor B2 (LILRB2) and its ligand angiopoietin-like protein 2 in colorectal cancer tissues. Furthermore, these proteins have been found to be closely associated with tumor progression and poor prognosis. The author conducted an analysis of LILRB2 serum concentration using 313 serum samples and compared its advantages and disadvantages with traditional tumor markers such as carcinoembryonic antigen and carbohydrate antigen 199. However, we believe that certain aspects of data collection and analysis in the article warrant further consideration. Therefore, we would like to discuss our perspective on this intriguing research.

Citation: Zhao WZ, Wang HG, Yang XZ. Leukocyte immunoglobulin-like receptor B2: A promising biomarker for colorectal cancer. *World J Gastroenterol* 2024; 30(4): 421-423
URL: https://www.wjgnet.com/1007-9327/full/v30/i4/421.htm
DOI: https://dx.doi.org/10.3748/wjg.v30.i4.421

TO THE EDITOR

According to the most recent global cancer statistics, colorectal cancer (CRC) is now the third most common malignant tumor worldwide. It has a notably high incidence rate, a poor prognosis at advanced stages, and ranks as the second leading cause of cancer-related deaths[1,2]. However, the implementation of population-based CRC screening, such as fecal occult blood tests and endoscopy, has significantly improved overall survival rates and brought about promising prospects for the cure of CRC[3]. We have carefully read the case-control study written by Wang *et al*[4]. This study commences by introducing the worldwide incidence and prognosis of CRC while emphasizing the challenges associated with its current treatment. Subsequently, the research team discovered the leukocyte immunoglobulin-like receptor B2 (LILRB2) protein through prior proteomic investigations[5]. The study postulates that LILRB2 could potentially serve as both a therapeutic target and a screening biomarker for CRC. Within the experimental section, the research team collected pathological specimens and medical records from a substantial number of patients who had undergone curative surgery for CRC. The expression levels of LILRB2 were compared across various populations using serological tests, immunohistochemistry, enzyme-linked immunosorbent assay, and other experimental methods. They also compared the differences in detection between this tumor marker and traditional tumor markers. Lastly, the study summarizes the experimental results and offers recommendations for further comprehensive research.

This study employed an innovative flow cytometry analysis method in combination with traditional immunohistochemical staining methods to mutually validate the results obtained from both approaches. This approach effectively confirms the reliability of the experimental findings. Moreover, the research team utilized gene platforms for online analysis of differentially expressed genes or mRNAs between normal and cancer tissues, which complemented the protein-level experiments. The team compared the expression levels of the LILRB2 protein in CRC tissues and adjacent tissues. They also analyzed the correlation between LILRB2 mRNA expression and angiopoietin-like protein 2 (ANGPTL2) mRNA expression in CRC tissues, as well as the correlation between LILRB2 protein expression and ANGPTL2 protein expression. Furthermore, they compared the diagnostic efficiency of LILRB2 with traditional tumor markers (carcinoembryonic antigen and carbohydrate antigen 199) using serum samples.

We would like to congratulate the research team on their compelling findings. They conducted a comprehensive investigation into the expression changes of the LILRB2 protein and its ligand ANGPTL2 in the occurrence and development of colorectal tumors. However, there are some questions that require further consideration by the researchers regarding this article.

The researchers collected a total of 313 serum samples between February 2021 and October 2022. Among these, there were 117 preoperative serum samples from CRC patients, 85 postoperative serum samples, 93 serum samples from adenoma patients, and 18 serum samples from healthy controls. They then compared the differences in serum LILRB2 concentrations among CRC patients, adenoma patients, and healthy controls, and discovered statistically significant variations in LILRB2 concentrations among the three groups. However, we would like to point out that there is a significant disparity in the number of serum samples between the CRC patient group (202 samples) and the healthy control group (18 samples). This raises concerns about potential data bias in the research results. Additionally, the criteria for including patients with normal colonoscopy findings in the healthy control group may be too broad. We believe it is necessary to establish detailed inclusion criteria for the healthy control group.

It is intriguing that the research findings in this article suggest that LILRB2 mRNA expression does not correlate with overall survival or progression-free survival in CRC patients. However, the overexpression of the LILRB2 protein is significantly associated with reduced overall survival, indicating a poor prognosis in CRC patients and suggesting a pro-cancer role of the LILRB2 protein in CRC progression. These results warrant further in-depth studies to elucidate the mechanisms behind these intriguing findings.

During our review of the research results in the article, we noticed the absence of any mention regarding baseline data processing for the participants' data. This omission raises concerns about the potential introduction of bias into the research results, which could impact the accurate assessment of the findings and diminish the reliability and validity of the study.

Previous studies on LILRB2 have primarily focused on hematopoietic stem cells and bone marrow immune cells, with limited attention given to CRC. LILRB2 has been found to play a significant role in inflammatory response and cell proliferation processes in these cells[6,7]. However, LILRB2 enrichment has also been observed in several malignant tumors, such as acute myeloid leukemia, chronic lymphocytic leukemia, esophageal cancer, pancreatic cancer, non-small cell lung cancer, and breast cancer[8]. It is premature to consider LILRB2 as a specific tumor marker for CRC since elevated serum levels of LILRB2 can occur in various solid tumors. Additionally, the differential effects of LILRB2 mRNA and protein expression on CRC prognosis warrant further investigation. Moreover, LILRB2 inhibitors are currently in phase I clinical trials[9], and their efficacy in treating CRC requires further observation.

This study offers preliminary evidence supporting the potential of the LILRB2 protein as a novel therapeutic target and non-invasive screening biomarker for CRC. Its implications are particularly beneficial for clinical practitioners, as it enables early screening, precise treatment and accurate prognostic evaluation of CRC.

FOOTNOTES

Author contributions: Zhao WZ wrote the letter; Wang HG revised the letter; and Yang XZ contributed to the study design, manuscript revision, supervision of the study.

Conflict-of-interest statement: All the authors report no relevant conflicts of interest for this article.

Country/Territory of origin: China

ORCID number: Hong-Gang Wang 0000-0003-4761-0407; Xiao-Zhong Yang 0000-0003-2036-5878.

S-Editor: Li L
L-Editor: A
P-Editor: Li L

REFERENCES

1 **Siegel RL**, Miller KD, Jemal A. Cancer statistics, 2020. *CA Cancer J Clin* 2020; **70**: 7-30 [PMID: 31912902 DOI: 10.3322/caac.21590]
2 **Sung H**, Ferlay J, Siegel RL, Laversanne M, Soerjomataram I, Jemal A, Bray F. Global Cancer Statistics 2020: GLOBOCAN Estimates of Incidence and Mortality Worldwide for 36 Cancers in 185 Countries. *CA Cancer J Clin* 2021; **71**: 209-249 [PMID: 33538338 DOI: 10.3322/caac.21660]
3 **Maida M**, Macaluso FS, Ianiro G, Mangiola F, Sinagra E, Hold G, Maida C, Cammarota G, Gasbarrini A, Scarpulla G. Screening of colorectal cancer: present and future. *Expert Rev Anticancer Ther* 2017; **17**: 1131-1146 [PMID: 29022408 DOI: 10.1080/14737140.2017.1392243]
4 **Wang QQ**, Zhou L, Qin G, Tan C, Zhou YC, Yao SK. Leukocyte immunoglobulin-like receptor B2 overexpression as a promising therapeutic target and noninvasive screening biomarker for colorectal cancer. *World J Gastroenterol* 2023; **29**: 5313-5326 [PMID: 37899785 DOI: 10.3748/wjg.v29.i37.5313]
5 **Wang Q**, Zhou Y, Zhou G, Qin G, Tan C, Yin T, Zhao D, Yao S. Age-stratified proteomic characteristics and identification of promising precise clinical treatment targets of colorectal cancer. *J Proteomics* 2023; **277**: 104863 [PMID: 36870673 DOI: 10.1016/j.jprot.2023.104863]
6 **Colonna M**, Samaridis J, Cella M, Angman L, Allen RL, O'Callaghan CA, Dunbar R, Ogg GS, Cerundolo V, Rolink A. Human myelomonocytic cells express an inhibitory receptor for classical and nonclassical MHC class I molecules. *J Immunol* 1998; **160**: 3096-3100 [PMID: 9531263 DOI: 10.4049/jimmunol.160.7.3096]
7 **Zheng J**, Umikawa M, Cui C, Li J, Chen X, Zhang C, Huynh H, Kang X, Silvany R, Wan X, Ye J, Cantó AP, Chen SH, Wang HY, Ward ES, Zhang CC. Inhibitory receptors bind ANGPTLs and support blood stem cells and leukaemia development. *Nature* 2012; **485**: 656-660 [PMID: 22660330 DOI: 10.1038/nature11095]
8 **Zhang Y**, Zheng J. Functions of Immune Checkpoint Molecules Beyond Immune Evasion. *Adv Exp Med Biol* 2020; **1248**: 201-226 [PMID: 32185712 DOI: 10.1007/978-981-15-3266-5_9]
9 **Siu LL**, Wang D, Hilton J, Geva R, Rasco D, Perets R, Abraham AK, Wilson DC, Markensohn JF, Lunceford J, Suttner L, Siddiqi S, Altura RA, Maurice-Dror C. First-in-Class Anti-immunoglobulin-like Transcript 4 Myeloid-Specific Antibody MK-4830 Abrogates a PD-1 Resistance Mechanism in Patients with Advanced Solid Tumors. *Clin Cancer Res* 2022; **28**: 57-70 [PMID: 34598945 DOI: 10.1158/1078-0432.CCR-21-2160]

Published by **Baishideng Publishing Group Inc**
7041 Koll Center Parkway, Suite 160, Pleasanton, CA 94566, USA
Telephone: +1-925-3991568
E-mail: office@baishideng.com
Help Desk: https://www.f6publishing.com/helpdesk
https://www.wjgnet.com